U.PORTO

FEUP FACULDADE DE ENGENHARIA
UNIVERSIDADE DO PORTO

Development of a gripper for a robotic bending cell for the production of boat hulls

Gonçalo Carneiro Martins

Dissertation submitted to
Faculdade de Engenharia da Universidade do Porto
for the degree of:

Mestre em Engenharia Mecânica

Supervisor at FEUP:
Carlos Miguel da Costa Gomes Fernandes

Supervisor at ADIRA - Metal Forming Solutions, S.A:
Jorge Borges Almeida

Porto, 2024

Abstract

This dissertation, made within the scope of the course unit Dissertation of the Master's Degree in Mechanical Engineering during the second semester of 2023/2024 at the Faculty of Engineering of the University of Porto, is the result of the project developed at ADIRA - Metal Forming Solutions, S.A.

The project involves a real case of process optimization in the manufacture of aluminium fishing boat hulls. The goal is to automate and simplify the manufacturing process of the hulls, converting the current manual production line into an automatic one by implementing a robotic bending cell. The challenge of gripping a sheet metal for a boat hull comes mainly due to the part size, weight and geometry. The sheet plate weights 109 kg and has the following dimensions: 7416.8 x 1663.7 x 3.2 [mm] - (length x width x thickness). It is imperative to design a customize gripper that is able not only to withstand the weight of the plate but also to hold and manipulate the part through all of the bending operations. Besides that, another request is to guarantee that the deflection presented by the sheet plate while being manipulated is between acceptable values. High deflection values will compromise the bending process.

The final goal was the development and design of a manipulation system for the robotic bending cell and the elaboration of all the final technical drawings and assembly drawings.

Firstly, a theoretical analytical calculation model was created to comprehend the distribution of forces exerted on the sheet metal by the vacuum cups to ensure a successful manipulation and avoid any dangerous scenarios. At the end, the vacuum cup and its respective characteristics and accessories were chosen, and the pneumatic system designed.

Then, the position of the vacuum cups throughout the flatten boat hull and its deflection were studied for both bending operations. For that, it was used finite element analysis to study the deflection of the flatten boat hull with different vacuum cups arrangement positions.

Finally, the gripper structural design was addressed. All the structural calculations, design of components, design of the coupling interface system, and manufacturing processes used. At the end, all technical drawings and assembly drawings relative to the gripper design were completed. The gripper cost was determined and some solutions implemented also considered the cost minimization.

Keywords: *Robotic bending cell*, *Sheet metal bending*, *End effector*, *Vacuum gripper*, *Vacuum system*, *Gripper design*, *Structural calculations*, *Finite element analysis*, *Technical drawings*

Resumo

O presente relatório, realizado no âmbito da unidade curricular Dissertação de Mestrado em Engenharia Mecânica durante o segundo semestre de 2023/2024 na Faculdade de Engenharia da Universidade do Porto, é o resultado do projeto desenvolvido durante este semestre na ADIRA - Metal Forming Solutions, S.A,.

O desafio proposto envolve um caso real de otimização do processo de fabrico de cascos de barcos em alumínio. O cliente pretende automatizar e simplificar a sua linha de produção dos cascos, convertendo a atual linha de produção manual em automática através da implementação de uma célula robótica de quinagem. O desafio de manipular o planificado do casco de barcos deve-se principalmente ao tamanho, peso e geometria da peça. O planificado em alumínio pesa 109 kg e tem as seguintes dimensões: 7416.8 x 1663.7 x 3.2 [mm] - (comprimento x largura x espessura). É imperativo desenvolver um gripper personalizado que seja capaz não só de suportar o peso do planificado, mas também de segurar e manipular a peça durante todas as operações de quinagem. Para além disso, outra tarefa crucial é garantir que a deflexão apresentada pela chapa enquanto é manipulada encontra-se entre valores aceitáveis. Valores de deflexão elevados irão comprometer o processo de quinagem.

O objetivo final foi o desenvolvimento de um sistema de manipulação para a célula robótica de quinagem e a elaboração de todos os desenhos técnicos finais e desenhos de conjunto relativos ao gripper.

Em primeiro lugar, foi criado um modelo teórico de cálculo analítico para compreender a distribuição das forças exercidas sobre a chapa metálica pelas ventosas, de modo a garantir uma manipulação bem sucedida e evitar qualquer cenário perigoso. No final, foram escolhidas as ventosas a ser usadas, as suas respectivas características e acessórios, e o sistema pneumático foi também desenvolvido.

De seguida, foi estudada a posição das ventosas ao longo do planificado e a sua deflexão para ambas as operações de quinagem. Para o efeito, foi utilizada a análise de elementos finitos para estudar a deformação do planificado com diferentes posições de disposição das ventosas.

Finalmente, o projeto do desenvolvimento e modelação do gripper foi abordado. Todos os cálculos estruturais, modelação e desenvolvimento dos componentes, estudo e desenvolvimento do sistema de interface de acoplamento ao robô, os processos de fabrico utilizados, e o custo final da solução económica foram analisados. No final, foram elaborados todos os desenhos técnicos e desenhos de conjunto.

Palavras-chave: *Célula robótica de quinagem*, *Quinagem*, *End effector*, *Gripper a vácuo*, *Sistema pneumático*, *Projeto do gripper*, *Cálculos estruturais*, *Análise de elementos finitos*, *Desenhos técnicos*

Acknowledgments

I would like to express my gratitude to all those who showed themselves available to to assist me, help me and share knowledge, which was essential for the development of this dissertation.

Firstly, thank you to my supervisor at FEUP, Carlos Fernandes, whose guidance was crucial. I greatly appreciate the time and effort you invested in mentoring me and in addressing my questions and concerns.

I would like to thank ADIRA - Metal Forming Solutions, S.A, for giving me the opportunity to to work on this project and for always welcoming me so well, in particular the engineering department. To Jorge Almeida, my supervisor at the company, who was always available to answer any questions I might have and to guide me throughout my internship. I would like to thank Joaquim, Miguel, and Paulo for sharing their knowledge on machine design and for giving me a practical view of mechanical engineering, whose help was crucial to the success of the project. I would like to thank João who was always available for helping me and for the way he welcomed and integrated me into the company. Finally, to Guilherme and Francisco, my internship colleagues, for all the motivation you provided during the project.

I would like to thank Abílio from SMC for always being available to help me in the development of the pneumatic system and vacuum system design.

To all my friends, your support and companionship have meant the world to me. A special thanks to 'Tortos' for all the good times over these past five years and for sharing unforgettable moments. Thank you to my friends from the Machine Design specialization, Daniel, Gonçalo, and Francisco. Completing the course in time wouldn't have been possible without you.

A special thank you to my girlfriend Daniela for her unwavering support and love.

Finally, I extend my heartfelt gratitude to all my family for their constant support and encouragement throughout this journey. To my uncle, your guidance and mentorship have been invaluable to my growth and development in this field during this last five years. To my parents and my sister, your understanding, patience, and belief in my abilities have been a source of strength and inspiration. Thank you for always being there for me.

To my grandparents

Contents

Abstract i

Resumo iii

Table of Contents viii

List of Figures xiii

List of Tables xvii

Nomenclature xix

1. Introduction 1
- 1.1. Framework and motivation . . . 1
- 1.2. Objectives . . . 2
- 1.3. Company background . . . 2
- 1.4. Methodology . . . 3
- 1.5. Thesis structure . . . 4

2. Characterization of robotic bending cells and gripper's 7
- 2.1. Introduction . . . 7
- 2.2. Robotic press brake bending cell . . . 7
  - 2.2.1. Robotic bending cell layout . . . 9
  - 2.2.2. Robotic bending cell solutions in the industry . . . 11
- 2.3. Sheet metal bending manufacturing process . . . 12
  - 2.3.1. Structure and components of a press brake . . . 13
  - 2.3.2. Sheet metal bending techniques . . . 16
    - 2.3.2.1. Sheet metal air bending . . . 17
    - 2.3.2.2. Sheet metal bottoming bending . . . 17
    - 2.3.2.3. Sheet metal coining Bending . . . 18
    - 2.3.2.4. Sheet Metal Three-Point Bending . . . 19
  - 2.3.3. Typical defects on the bending results . . . 20
    - 2.3.3.1. Spring back . . . 21
    - 2.3.3.2. Press brake deformation . . . 22
  - 2.3.4. Bending machine classification . . . 23
    - 2.3.4.1. Mechanical actuation . . . 23
    - 2.3.4.2. Hydraulic actuation . . . 23
    - 2.3.4.3. Electric actuation . . . 24
    - 2.3.4.4. Hybrid actuation . . . 24
- 2.4. End effector's design . . . 25
  - 2.4.1. End effector safety design standard . . . 26
    - 2.4.1.1. Vocabulary about end effectors . . . 26
    - 2.4.1.2. Initial design considerations . . . 27
    - 2.4.1.3. Hazard identification and risk reduction measures . . . 28
    - 2.4.1.4. Instructions for general use . . . 29

2.4.2. Gripper types . . . 29
2.4.2.1. Vacuum gripper . . . 30
2.4.2.2. Magnetic gripper . . . 34
2.4.2.3. Parallel and angular gripper . . . 36
2.4.3. Grippers solutions used in robotic bending cells available in industry 40
2.4.3.1. Small parts manipulation . . . 40
2.4.3.2. Medium parts manipulation . . . 43
2.4.3.3. Large parts manipulation . . . 45
2.4.4. Coupling interface between gripper and robot . . . 46
2.4.4.1. ISO standard for mechanical interfaces - plates . . . 46
2.4.4.2. Manual coupling solution . . . 48
2.4.4.3. Automatic coupling solution . . . 50

3. Problem characterization and proposed solution 53
3.1. Introduction . . . 53
3.2. Flatten boat hull . . . 54
3.3. Bending manufacture operations . . . 56
3.4. Robotic bending cell implementation . . . 58
3.5. Initial robot selection . . . 58
3.6. Proposed gripper design solution . . . 60
3.6.1. Gripper subassemblies . . . 64
3.6.2. Economic analysis . . . 66

4. Vacuum system 69
4.1. Introduction . . . 69
4.2. Vacuum cup selection procedure and result . . . 69
4.3. Total theoretical holding force . . . 70
4.3.1. Parameters . . . 71
4.3.2. Static free body diagram analysis . . . 72
4.3.3. Dynamic free body diagram analysis . . . 74
4.3.4. Safety factor . . . 76
4.4. Vacuum cup suction force . . . 77
4.5. Vacuum cup selection . . . 79
4.5.1. Number of vacuum cups . . . 80
4.5.2. Accessories: adapter and buffer . . . 80
4.6. How to study the deflection of the workpiece . . . 83
4.7. First bending process analysis . . . 84
4.8. Second bending process analysis . . . 88
4.9. Finite element analysis of the workpiece manipulation . . . 89
4.9.1. Constituent parts . . . 89
4.9.2. Material . . . 90
4.9.3. Constraints and boundary conditions . . . 91
4.9.4. Load . . . 91
4.9.5. Mesh creation and refinement study . . . 91
4.9.6. First bending process simulation . . . 94
4.9.7. Second bending process simulation . . . 96
4.10. Vacuum cup subassembly . . . 98
4.11. Pneumatic system . . . 101
4.12. Discussion . . . 104

5. Gripper structure **107**
5.1. Aluminium profile selection . . . 107
5.1.1. Strength analysis . . . 107
5.1.2. Rigidity analysis . . . 114
5.1.2.1. Results and discussion . . . 117
5.1.3. Structural reinforced solution . . . 119
5.1.3.1. Results and discussion . . . 126
5.1.4. Finite element analysis for the reinforced solution . . . 127
5.1.4.1. Beam numeric model . . . 127
5.1.4.2. 3D numeric model . . . 129
5.1.5. Final discussion . . . 131
5.2. Materials selection . . . 132
5.3. Aluminium profile subassembly . . . 133
5.4. Structural reinforcement subassembly . . . 135
5.5. Interfaces subassembly . . . 137

6. Conclusions **143**
6.1. Conclusion . . . 143
6.2. Future work . . . 144

Bibliography **147**

A. Industrial robot GP400 **151**
A.1. Robot technical specifications and technical drawing . . . 151

B. Suppliers catalogues **153**
B.1. SMC catalogue . . . 153
B.2. Bosch Rexroth catalogue . . . 153
B.3. RAMADA AÇOS catalogue . . . 153

C. Technical Drawings **155**

List of Figures

1.1. Logotype of ADIRA - Metal Forming Solutions, S.A. 2

2.1. Initial design of a press brake bending cell in ADIRA. 8
2.2. Layout for a press brake robotic cell. 9
2.3. Orientation table inside a robotic bending cell. 10
2.4. Regrip station. 10
2.5. Robotic bending solution (model RBR) by AMADA. 11
2.6. Automatic tool changer solution by AMADA. 11
2.7. Automatic gripper change station equipped in AMADA robotic bending solution. 12
2.8. Schematic representation of the punch, the plate, the die and press braking. 13
2.9. Press brake main components. 14
2.10. Example of different clamping systems used. 14
2.11. Manual clamping mechanism of a die using bolts. 15
2.12. Main axes of the back gauge and of the press brake highlighted. 16
2.13. Numerical control interface panel designed by ADIRA. 16
2.14. Schematic representation of the air bending. 17
2.15. Schematic representation of the bottoming bending. 18
2.16. Schematic representation of the coining bending. 19
2.17. Schematic representation of the three-point bending. 19
2.18. Air bending process spring back. 21
2.19. Effect of press brake deformation on a bended sheet metal. 22
2.20. Intermediate with adjustable wedges used in a hydraulic ADIRA press brake. 23
2.21. Schematic representation of a mechanical press brake machine. 24
2.22. A gripper being used by a blacksmith in the roman empire. 25
2.23. Mechanism for crane grippers designed by Leonardo Da Vinci (1452-1519). . 25
2.24. Broad classification of robot grippers. 29
2.25. Industrial robot equipped with a vacuum gripper. 30
2.26. Two basic type of vacuum cup solutions. 33
2.27. Inclined lift application - bellow cup. 33
2.28. Articulated joint flat vacuum cup. 34
2.29. Magnetic gripper connected to a robot's arm. 35
2.30. Mechanical control of the magnetic flow. 35
2.31. Electromagnetic gripper for picking cog wheels. 36
2.32. Parallel gripper with one mobile jaw and one fixed. 37
2.33. Standard gripper drives for parallel grippers. 37
2.34. Standard gripper drives for angular grippers. 39
2.35. Multi gripper (angular + vacuum) solution adopted by LVD. 41
2.36. Multi gripper manipulating a small sheet metal during a bending operation. 41
2.37. Multi gripper solution (parallel + vacuum). 42
2.38. Simple gripper solution by SafanDarley. 42
2.39. Adjustable gripper designed for a wide range of sizes. 43
2.40. Adjustable gripper built in aluminium profiles in a robotic bending cell. . . 44
2.41. Pneumatic magnetic gripper handling a part in a robotic bending cell. . . . 44

2.42. Cut section view - pneumatic control of the magnetic flow. 45
2.43. Vacuum gripper initial contact with a large sheet metal. 45
2.44. Vacuum gripper manipulating a large sheet metal. 46
2.45. Circular mechanical interface dimensions. 47
2.46. Design of a circular plate interface according to Table 2.45. 48
2.47. Technical drawing of a mechanical flange interface for both the gripper and the robot. 49
2.48. Zimmer solution for a manual locking mechanism (HWR2000). 50
2.49. Manual locking mechanism sequence (HWR2000). 50
2.50. SCHUNK quick change automatic grip solution. 51
2.51. Cut section view - SCHUNK locking mechanism. 52
2.52. Example of an automated coupling mechanism using an adapter plate for each side. 52

3.1. Press brake used by the customer in their current manual boat hull production line. 53
3.2. Example of one type of boat hull produced after the bending and welding operations. 54
3.3. Initial flatten boat hull. 55
3.4. 'V' shape location on the flatten sheet metal. 56
3.5. Draft of the four bending lines on the flatten boat hull. 56
3.6. U-bending schematic with special tools. 57
3.7. Flatten sheet metal after the four consequent bends (U-shape). 57
3.8. Flatten sheet metal after the final side bend. 58
3.9. Robotic bending cell initial layout. 59
3.10. Industrial robot from YASKAWA: GP400. 60
3.11. 3D CAD representation of the final gripper design solution. 61
3.12. Rendered image showing the connection between the robot and gripper. . . 62
3.13. Rendered image from the 3D CAD of the gripper. 63
3.14. 3D CAD representation of the aluminium profile subassembly. 64
3.15. 3D CAD representation of the structural reinforcement subassembly. . . . 65
3.16. 3D CAD representation of the vacuum cup subassembly. 65
3.17. 3D CAD representation of the interfaces subassembly. 66

4.1. 3D CAD of the final SMC vacuum cup solution selected. 70
4.2. Inclined manipulation scenario with an angle parameter, α. 71
4.3. Free body diagram of cup and workpiece. 73
4.4. Curve - F_{th} in function of α. 74
4.5. Schematic example of a six-axis robot. 75
4.6. Dynamic equilibrium of the forces diagram represented on the workpiece. . . 75
4.7. Curve - F_{th} in function of β. 76
4.8. Example of the selected vacuum cup from SMC catalogue. 79
4.9. Two options for mounting threads on top of the vacuum cup. 81
4.10. Mounting thread size table for the selected vacuum cup adapter with vertical vacuum entry. 82
4.11. Different examples of SMC buffers incorporated on vacuum cups. 82
4.12. Plate with thickness, h, divided by a midplane into 2 halves. 83
4.13. Available areas for the allocation of the cups on the workpiece for the first bending process. 84
4.14. Critical displacement zones due to the deflection of the workpiece. 85

4.15. Illustrative representation of the distance between the centre of the die to the end of the table. . . . 86
4.16. Illustration of the rows lines that pass through the cup centres. . . . 86
4.17. Vacuum cup distribution along both rows of the workpiece on SolidEdge. . . 88
4.18. Available areas for the allocation of the cups on the workpiece for the second bending process. . . . 88
4.19. Distances between the cup centre and the respective bending lines on SolidEdge. 89
4.20. Flatten boat hull shell geometry in Abaqus. . . . 90
4.21. Vacuum cup in Abaqus. . . . 90
4.22. Partition regions on the flatten boat hull geometry in Abaqus. . . . 91
4.23. Different mesh final results with and without the use of partitions in Abaqus. 92
4.24. Curve with the variation of the maximum vertical displacement values with the total number of elements. . . . 93
4.25. Curve with the variation of the maximum von Mises stress values with the total number of elements. . . . 94
4.26. First bending operation simulation results for the vertical displacement distribution. . . . 95
4.27. First bending operation simulation results for the von Mises stress distribution. 95
4.28. Second bending operation simulation results for the vertical displacement distribution. . . . 96
4.29. Second bending operation simulation results for the von Mises stress distribution. . . . 97
4.30. Detailed view showing the concentration zone of the first bending operation simulation results for the von Mises stress distribution. . . . 97
4.31. Two different vacuum cups subassembly. . . . 98
4.32. Cantilever beam bending analysis simplification of the bolted connection. . 99
4.33. Cross section of the C-shaped profile. . . . 100
4.34. 3D CAD representation of the vacuum ejector (ZL112A-K15LOU-DBL). . . 102
4.35. Pneumatic system between the air distribution network and the vacuum ejectors. . . . 102
4.36. Tube-tube pneumatic connection with a 'Y' union. . . . 103
4.37. Main block distributor at the centre of the gripper. . . . 103
4.38. Block distributors for each vacuum cup subassembly. . . . 104
4.39. Illustration of the bending sequence for the first bending process. . . . 105

5.1. Free body diagram of the profile. . . . 108
5.2. Example of a cross section of an aluminium profile. . . . 108
5.3. Bolted connection on the interface connected to the gripper profile. . . . 109
5.4. Vacuum cup subassembly position in the final gripper design solution. . . . 109
5.5. Bending moment representation in section i. . . . 112
5.6. Bending moment representation in section ii. . . . 112
5.7. Bending moment representation in section iii. . . . 113
5.8. Bending moment diagram. . . . 113
5.9. All profiles with displacements values bellow 40 mm. . . . 117
5.10. Rectangular profile during the bending operation. . . . 118
5.11. Bending operation displacement in function of weight per meter for each profile. 118
5.12. Last design iteration for the structural reinforcement. . . . 120
5.13. Illustration of the cross section of the reinforced solution. . . . 120
5.14. Different material composite cross section of the reinforced solution. . . . 121

5.15. Hand drawing of the geometric simplification of the reinforcement part cross section. . . . 122
5.16. Original cross section of the reinforced solution. . . . 123
5.17. Original cross section of the reinforced solution. . . . 124
5.18. Orthogonal coordinate system for the calculation of the second moments of area. . . . 125
5.19. Final assembly of the numeric beam model with the respective boundary conditions and load. . . . 128
5.20. Beam model variation of the bending operation displacement in function of the structural reinforcement length. . . . 128
5.21. Mesh refining region at the end of the aluminium profile. . . . 129
5.22. 3D numeric model assembly of the reinforced solution (L = 5260 mm). . . . 130
5.23. 3D model variation of the bending operation displacement in function of the structural reinforcement length. . . . 130
5.24. Structural reinforcement geometry. . . . 131
5.25. 3D CAD of the aluminium profile subassembly. . . . 133
5.26. Aluminium profile slot for fastening components to the structure. . . . 134
5.27. Aluminium profile 90x90 chosen from Bosch Rexroth catalogue. . . . 134
5.28. Profile connector for the end-face connection of the aluminium profile. . . . 135
5.29. Reinforcement part 3D CAD in SolidEdge. . . . 136
5.30. Plate part 3D CAD in SolidEdge. . . . 136
5.31. Welding of reinforcement part with the plates in SolidEdge. . . . 136
5.32. 3D CAD of the interfaces subassembly. . . . 137
5.33. 3D CAD of the gripper interface. . . . 138
5.34. 3D CAD of the U-shaped profile. . . . 140
5.35. 3D CAD of the gripper interface. . . . 141
5.36. Bolted connection between both robot interfaces. . . . 141

List of Tables

2.1. Hardness (Shore-A) for different materials. 32
2.2. Operating temperature values for different materials. 32

3.1. Weight and geometry dimensions of the flatten boat hull. 55
3.2. Mechanical properties of Al5052-H32. 55
3.3. Price quotation provided by the suppliers (*includes transportation). 67

4.1. Vacuum cup selection procedure considering the theoretical holding force, number of cups, and price. 70
4.2. Parameters considered for the static and dynamic force equilibrium. 71
4.3. Total number of vacuum cups and the suction force for each available diameter. 80
4.4. Price quotation for the ϕ100 mm and ϕ125 mm vacuum cup diameter options. 80
4.5. Length of each row. 87
4.6. Mesh refinement study results. 93
4.7. Variables used on the bending calculation of the C'-shaped profile. 100
4.8. Variables used on the bending calculation of the 'C'-shaped profile. 101
4.9. All SMC pneumatic fittings used for the system. 104

5.1. Variables for the interpretation of the free body diagram. 110
5.2. Mechanical properties of Al6060. 111
5.3. Twenty five profiles that fulfil the strength analysis requirement. 114
5.4. Price quotation for all six profiles. 119
5.5. Main dimensions of the structural reinforcement. 120
5.6. Variables for the reinforced solution analytical calculation. 123
5.7. Maximum displacements values for several reinforcement part lengths. . . . 129
5.8. Maximum displacements values for several reinforcement part lengths. . . . 131
5.9. Bending operation displacement for the analytical, beam, and 3D model. . . 131
5.10. Mechanical properties of S235jr. 132
5.11. Mechanical properties of Ck45. 132

Nomenclature

Abbreviations

2D	Two dimensional
3D	Three dimensional
BL	Bending Line
BSPT	British Standard Pipe Taper
CAD	Computer-aided design
CAM	Computer Aided Manufacturing
CE	'Conformite Europeenne'
DC	Direct Current
EPDM	Ethylene Propylene Diene Monomer Rubber
FEUP	Faculdade de Engenharia da Universidade do Porto
FKM	Fluoroelastomer
GDP	Gross Domestic Product
IFR	International Federation of Robots
MAG	Metal Active Gas
NBR	Nitrile Rubber
NPT	National Pipe Taper
NPTF	National Pipe Taper Fuel and Oil
OECD	The Organization for Economic Cooperation and Development
PL	Performance Level
PVC	Polyvinyl Chloride
Rc	British Standard Pipe Taper Internal
SWS	Quick-change System
SWK	Quick-change Master
SWS	Quick-change Adapter

1. Introduction

This dissertation, made within the scope of the course unit Dissertation of the Master's Degree in Mechanical Engineering during the second semester of 2023/2024 at the Faculty of Engineering of the University of Porto (FEUP), is the result of the project developed during this semester. This initial chapter concerns the clarification of the project motivation and main objectives. Besides that, the introduction of the company, the methodology used throughout the project and the structure of the report are also addressed.

1.1. Framework and motivation

Manufacturers of sheet metal parts are increasingly looking for automated solutions to increase the productivity of their production lines. The manipulation of products during the manufacturing process is often complex due to their size and geometry, and the analysis of the production process itself must always be taken into account. The implementation of robotic cells in industry enables the manufacturers to simplify, automate, and speed up the whole process and maximize the production line in order to achieve high cadences with good levels of quality.

Gripping devices, such as the ones located at the end of the robot's arm, are an essential part of the manipulation in the industry, offering a huge handling capability on any type of product regardless of it's dimensions, materials and geometries. With the implementation and continuous innovation of robotic cells, more attention has been addressed to this devices. In this research, the main emphasis will be on gripping devices used in industrial robots.

The proposed challenge involves a real case of process optimization in the manufacture of aluminium fishing boat hulls. The customer is looking to automate and simplify their manufacturing process of the hulls, converting the current manual production line into an automatic one by implementing a robotic bending cell. In robotic cell applications, the gripper is one of the critical components of the entire robotic cell. It is the main interface between the robot and the sheet metal, and since the sheet geometry is constantly changing with each bend operation, the gripper must be designed and customized to fit all the operations for a specific part. The gripper design must take into account the entire bending process to successfully realize all the predetermined bends as well as the geometry, weight, size, and material of the part.

The challenge of gripping a sheet plate for a boat hull comes mainly due to the part size, weight and geometry. The sheet plate weights 109 kg and has the following dimensions: 7416.8 x 1663.7 x 3.2 [mm] - (length x width x thickness). It is imperative to design a customize gripper that is able not only to withstand the weight of the plate but also to hold and manipulate the part through all of the bending operations, considering that the part has a length higher than 7 meters. Besides that, another crucial task is to guarantee that the deflection presented by the sheet plate while being manipulated is between acceptable

values. High deflection values will compromise the bending process.

1.2. Objectives

The main goal of this research is the development of a sheet metal manipulation system to be used in a robotic press brake bending cell to produce hulls for fishing boats.

To this end, the manufacturing technologies involved will be initially studied, evaluated and validated. The analysis and determination of the manufacturing sequence necessary to obtain the final part are crucial tasks for the gripper design, as well as selecting the industrial robot for the manipulation of the workpiece.

The greater focus will be on the development of the gripper for the robotic sheet metal manipulation. This includes the study of the grasping and manipulation method used, all the necessary analytical and numeric calculations through finite element analysis for the design and analyses of several components throughout the project.

The coupling interface will also be designed to perfectly connect the gripper and the robot. When choosing a robot for a specific task, there are a lot of different configurations regarding the gripper's fixation mechanism. Therefore, it is imperative to design a coupling device to ensure the correct attachment of the gripper to the robot.

The goal is to present all the final technical drawings and assembly drawings of the gripper.

Finally, an economic solution analysis will also done to understand the overall cost of the solution found and allow for possible improvements and optimizations of the project in the future.

1.3. Company background

ADIRA - Metal Forming Solutions, S.A. is a supplier of engineering solutions for the sheet metal processing industries. They develop innovative engineering solutions with intelligent functions, specializing in cutting, bending and forming sheet metal and adapting to the needs of each application. They also specialize in the production of hydraulic, electrical and hybrid press brakes, shearing machines and robotic bending cells. With more than 60 years of experience and customers in all four corners of the world, they respond efficiently to the most complex challenges. In this report, the company is refereed to as ADIRA [1].

Figure 1.1.: Logotype of ADIRA - Metal Forming Solutions, S.A [1].

Founded in 1956 by António Dias Ramos, ADIRA began producing furnaces, milling machines and planner machines. In the 1960s, the company evolved into the manufacture of machine tools for sheet metal forming, including the first mechanical guillotine, the first hydraulic press brake machine and the first fully hydraulic descending press brake machine manufactured in Portugal. The company invested in setting up offices, took part in international trade fairs and began exporting.

The 1970's were marked by the development and technological improvement of mechanical, hydraulic, and electric machines. It also marked the start of the partnership with the Faculty of Engineering of the University of Porto. England, Germany and Japan became destinations of the exports.

In the 1980's, the era of digital technology began with the development of the first 2D and 3D digital controls. United States of America, Australia and the Middle East became destinations of large-scale exports and the safety certification of machines were exported to France and Sweden. It was also marked by the introduction of automatic systems, such as front feeders and handling and storage solutions for the plates.

In the 90's, the investment in technological innovation lead to high-tech equipment, renovation of press brake layouts, new internal organization and the introduction of CAD and CAM technologies and Intranet. ADIRA became the first European manufacturer to obtain the ISO 9000 certification and the first in the world to have all of its entire range of products available with CE certification. Press Brakes with automatic deformation compensation systems were also introduced as well as hydraulic shearing machines with anti torsion systems. New market exports for the following regions: the Far East, Oceania, and Spain.

From 2000, the company started the implementation of robotic cells with laser cutting machines, the integration of automatic sheet metal storage systems and the expansion of robotic press brake bending cells. The company was sold to António Cardoso e Pinto, thus ending the involvement of the family Dias Ramos.

The 2010's was marked by the launch of new laser cutting machines: LE, LP and LF. The launch of GreenBender, a hybrid press brake machine, was a revolutionary solution recognised internationally.

Since 2017, ADIRA is owned by SC - SONAE Capital Industrials, SGPS, S.A., currently its sole shareholder. During its long years of production, ADIRA has focused on scientific research and technological development, encouraged by partners such as FEUP. The company always strives to provide specific solutions for each client, with high technological quality, excellent performance and reliability [1].

1.4. Methodology

The methodology adopted was as follows:

1. - Theoretical study and characterization of robotic bending cell and sheet metal bending as a manufacturing process;

2. - Literature review about end effector's design, actuation technologies, and industry solutions implemented already in robotic bending cells;
3. - Process of obtaining information and feedback from the client about all the data needed to characterize the problem;
4. - Study through various catalogues, articles, and other bibliographic documents on the calculation of vacuum cups;
5. - Choose a supplier for all pneumatic components, including the vacuum cups. Understanding the best type of vacuum cup and its accessories;
6. - Understand how the positioning of the suction cups along the workpiece affects its deflection;
7. - Finite element analysis to study the workpiece deflection for each bending operation;
8. - Selection of aluminium profiles for the main structure of the gripper and choosing a supplier for the profiles and respective accessories;
9. - Structural analytical calculation of the aluminium profile;
10. - Study about the implementation of a reinforcement part with the aluminium profile through analytical calculation and finite element analysis;
11. - Design of all components and subassemblies on a 3D CAD software: SolidEdge;
12. - Design and selection of the whole pneumatic system;
13. - Preparation of all technical and assembly drawings;
14. - Final economic solution analysis.

1.5. Thesis structure

The report is divided into six chapters: Introduction, Characterization of robotic bending cells and gripper's, Problem characterization and proposed solution, Vacuum system, Gripper structure, and Conclusions.

In the first chapter, it is explained the motivation and objectives adopted in the development of this report. It also has an introduction to the the company and discusses the methodology adopted and the structure of this report.

In the second chapter, a literature review was done concerning the main topics of this project: Robotic bending cells, bending as a manufacturing process, and the gripper's design.

The third chapter explains the proposed challenge and all the necessary information given by the customer for the automation of the aluminium boat hull production line. The flat-

ten boat hull geometry and mechanical properties, as well as all the bending manufacture operations were analysed. At the end, the final proposed solution was presented with the economic solution global cost.

In the fourth chapter, the focus was the calculation of the vacuum cups in order to guarantee a successful manipulation and avoid any dangerous scenarios. For this, a theoretical analytical model was used. The selection of the vacuum cup and the respective accessories was also covered. The allocation of the vacuum cups and the respective workpiece deflection study was studied individually for each bending operation.

The fifth chapter addresses the gripper structure design, which includes all structural calculations, finite element analysis, design of components, and manufacturing processes.

The final chapter concludes the ideas developed throughout the report. In addition, several issues for future work were addressed.

2. Characterization of robotic bending cells and gripper's

2.1. Introduction

Since the beginning of time, mankind has been pursuing solutions to alleviate the demands of their daily labour in order to save both time and human effort. This led to the innovation and evolution of machines, where the current goal is the automation of the global industry, allowing machines to do work that previously required human labour. As an example, robots fit this description perfectly since they are made by copying basic human interactions [2]. They are designed to do several complex actions and movements such as manipulating objects. Gripping devices, such as the ones located at the end of the robot's arm, are an essential part of the manipulation process, having evolved to help humans handle any type of product regardless of its dimensions, materials, and geometries. With the implementation and continuous innovation on robotic cells, more attention has been addressed to these devices. In this research, the main emphasis will be on gripping devices used in industrial robots.

Multiple topics are addressed in order to provide all the necessary technical information for a better understanding of the project. The comprehension of how a robotic press brake bending cell works is crucial to the global manufacturing process of the sheet metal and for the gripper design (manipulation method). Therefore, a global description of the sheet metal bending manufacturing process, the essential requirements and parameters to successfully realize the bending operation, the different types of press brake machines and its components are some of the topics addressed.

All of the theoretical concepts mentioned are imperative to fully understand how a press brake machine works, the existent solutions of robotic press brake bending cells and the constructive design solutions for the gripper.

2.2. Robotic press brake bending cell

A robotic cell is any station in the manufacturing industry, where a determined operation is being done by a robot instead of a person [3]. This leads to the automation of the whole process. Automated stations such as the one seen in Figure 2.1 are characterized by complete autonomy, being able to speed up, simplify, and maximise a production line in order to achieve high cadences with good levels of quality.

In the context of press brakes, a manual cell has a much lower performance efficiency than a robotic cell. Problems like an inexperienced workforce, unavailable material, unexpected



Figure 2.1.: Initial design of a press brake bending cell in ADIRA [4].

employee absences, and misplaced tooling do not exist in a robotic press brake cell [5].

There are three key factors where a robotic brake cell outperforms a manual one [6]:

1. Productivity;
2. Flexibility;
3. Profitability + Cost reduction.

In terms of production capacity, a robotic cell will have much higher productivity than a manual operation for several reasons. A robotic cell operates within a safe enclosed zone, which guarantees safety in the workplace, allowing the whole process to run at top speed, something that is not possible with manual operation [6]. Apart from that, manual operations will always involve inventory waste, lost time during transportation, issues with overproduction, and possible defects due to the operator. These problems that result in poor productivity can be eliminated with a robotic automation cell solution.

According to the International Federation of Robots (IFR), there is a study that found that investing in robots has contributed 10% of growth in the gross domestic product (GDP) per capita in countries from the Organization for Economic Cooperation and Development (OECD) from 1993 to 2016. A different study stated that the use of robots increased GDP by 10% in 17 European countries, between 1993 and 2007. Leaders on the global management consulting market such as the Boston Consulting Group also predicted that productivity will improve 30% over the next 10 years, due to the fact that robots are becoming more affordable, flexible and easier to program [7].

An automated cell brings a lot of advantages concerning the flexibility of the process. Firstly, there is the possibility of mounting the robot in a linear track, increasing it's working range and allowing the robot to operate with different machines within the area of the station. Besides that, there are several constructive solutions of different robots, with different sizes and payloads allowing the robot to be very versatile and adapt for specific applications, regardless of the sheet metal's size [6]. There are also many types of grippers

with different sizes and geometries that are able to adapt to distinct metal plates.

The implementation of a robotic bending process cell is an excellent way to decrease operational costs and increase profitability. These profits can be used to invest in increasing the productivity of the robotic cell and in process innovation.

2.2.1. Robotic bending cell layout

Figure 2.2 represents a standard layout example showing the main components of the cell.

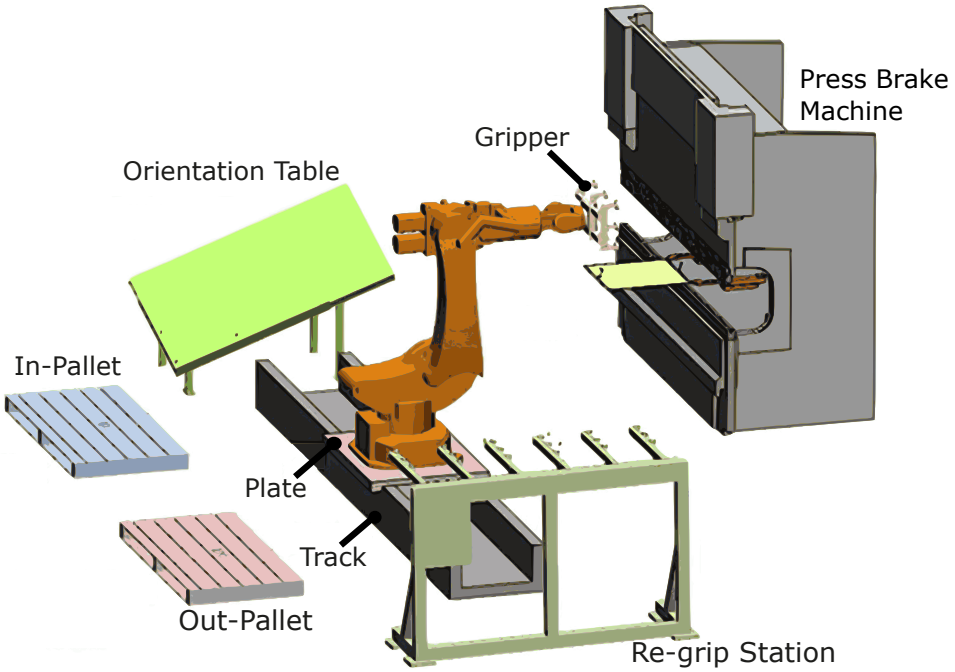


Figure 2.2.: Layout for a press brake robotic cell [8].

The main part of a robotic cell is the robot. The robotic arm is composed of several joints and links in different combinations [9]. The goal is for the arm to work similarly to a human arm. The robot is mounted on a plate which is connected to the track. The robot can move freely in the linear direction along the track. These mechanical linkages are usually driven by three types of actuators: electrical, hydraulic or pneumatic actuators [9]. A vital component of the robot is located at the end of the arm and is called end effector, also known as the gripper, depending on the type of device. It has the function of picking up and holding the sheet plate. This component will be analysed in depth in Section 2.4.

The layout seen in Figure 2.2 shows that the gripper will pick the plate at the in-pallet table. This table is designed for loading with a forklift. Then, the plate is moved to the orientation table or also called indexing table, as seen in Figure 2.3. This table is inclined so that the plate starts to slide down due to gravity until it stops at the two perpendicular edge stoppers. At the corner, there is a sensor that detects the plate and communicates this information to the robot. The sensor allows to define a reference position so the robot



Figure 2.3.: Orientation table inside a robotic bending cell [10].

knows the correct location to pick up the plate.

The robot picks up the plate and takes it to the press brake to realize the necessary bending operations. However, before this step, depending on the plate geometry, size and the desired bending operations, the robot may need to readjust the position of it's arm for the correct manipulation of the plate. To fix this issue, there is a regrip station, shown in Figure 2.4, usually built in aluminium profiles with magnets or vacuum cups in order to hold the plate while the robotic arm has time to readjust. Only then can the bending operation proceed.

The bended sheet metal is taken by the robot to the out-pallet table.

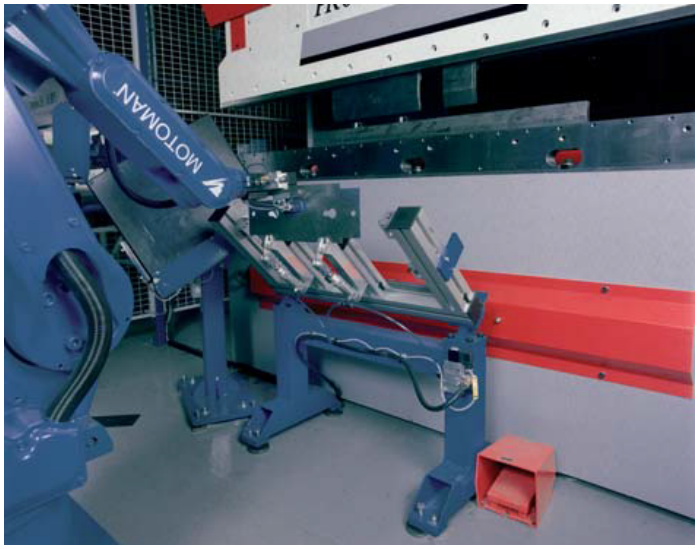


Figure 2.4.: Regrip station [6].

2.2.2. Robotic bending cell solutions in the industry

There are many companies specialized in press brake bending solutions all over the world. In this section is presented a robotic bending solution of AMADA.

AMADA provides an advanced robotic bending solutions with very high-end technology. One of these solutions can be seen in Figure 2.5.

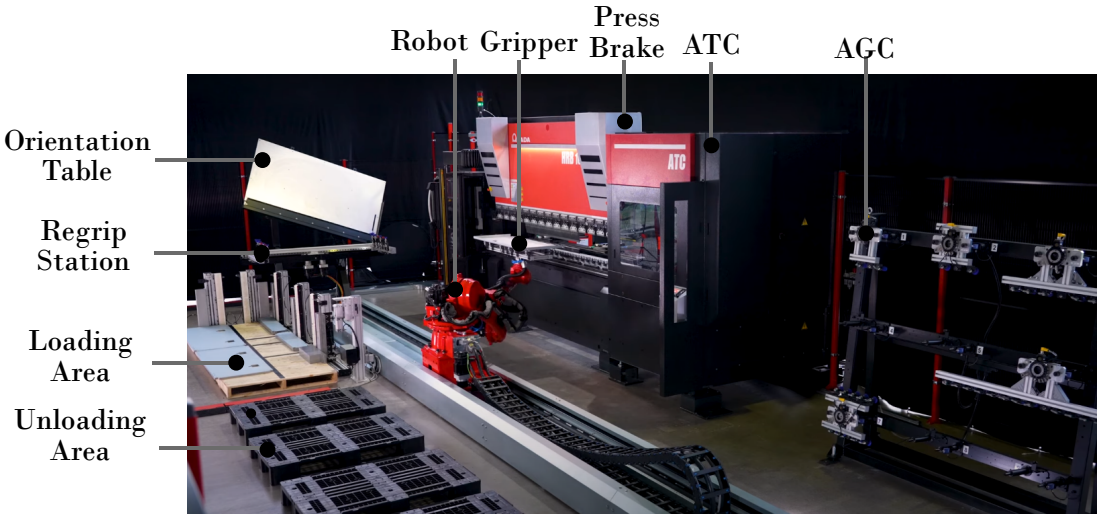


Figure 2.5.: Robotic bending solution (model RBR) by AMADA [11].

AMADA presents a innovative solution for the manipulation of different sizes and complex tool sets. The automatic tool changer (ATC) is a storage capable of holding several different tools in order to cover a wide range of bending requirements for specific operations, providing precision and flexibility. It is located right next to the press brake, as seen in Figure 2.6, and has the function to quickly change tool sets. As a result, it is possible to eliminate the costly delays that are associated with these operations. This solution allows users to triple or quadruple the number of setups carried out each day [11].



Figure 2.6.: Automatic tool changer solution by AMADA [11].

In order to ensure a wider range of applications and flexibility for different parts, the AMADA solution has been equipped an automatic gripper change station (AGC). It changes

the gripper automatically based on the operations pretended. This way, the robot is able to manipulate parts with different sizes, geometries and weight, increasing the flexibility of the robotic cell. Figure 2.7 presents the automatic gripper change station with different types of grippers. The robot puts down the gripper on it's correct position and then it fits into the selected new gripper flange, activating the clamping mechanism. This process is completely automated and does not require any human labour.

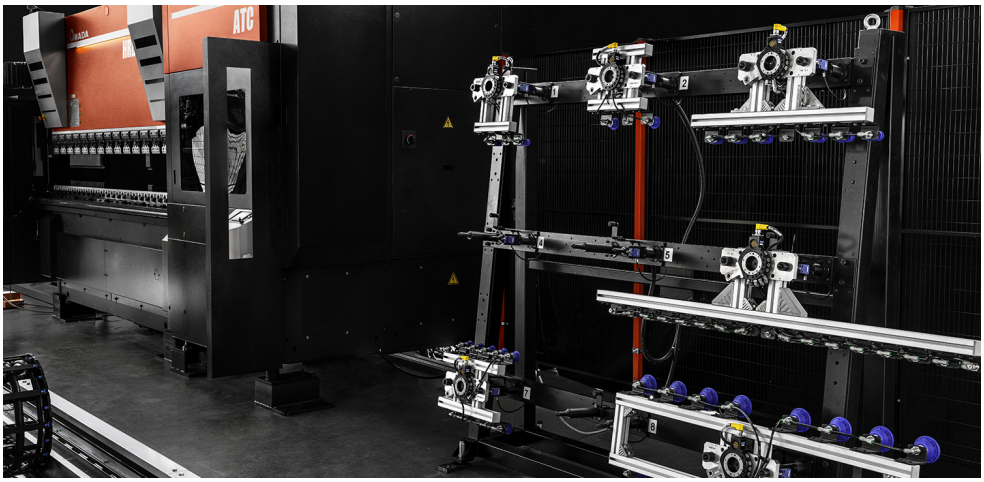


Figure 2.7.: Automatic gripper change station equipped in AMADA robotic bending solution [11].

2.3. Sheet metal bending manufacturing process

Press braking bending is one of the easiest operations carried out with sheet metal. It's primary function is to bend sheet metal, basically consisting in a cold plastic deformation [12]. The process is carried out by positioning the sheet metal between the movable punch (upper tool) and the stationary die (lower tool). Then, the punch goes down in the direction of the die, clamping the plate between both tools and pushes the sheet into it causing the plastic deformation intended, as seen in Figure 2.8. It may take several bends until the desired form has been achieved. For that, all of this bends need to be predetermined and the punch and die need to be designed and selected for specific lengths and shapes of the plate. Typically the machines are very long in order to be able to deform large pieces of sheet metals.

One huge advantage of this manufacturing process is the strengthening of the material that happens due to the dislocation movements which occur at the crystal structure of the material. This is called strain hardening (also called cold working) which takes place during the plastic deformation of the material, where the sheet metal is deformed into the final shape and this deformation creates dislocations which increase the strength.

The whole method requires a huge amount of force to bend the plate, measured in tonnage. Normally, the thicker the plate the higher the force tends to be. This bending force applied during the process is named F and causes the punch to penetrate into the die and the degree

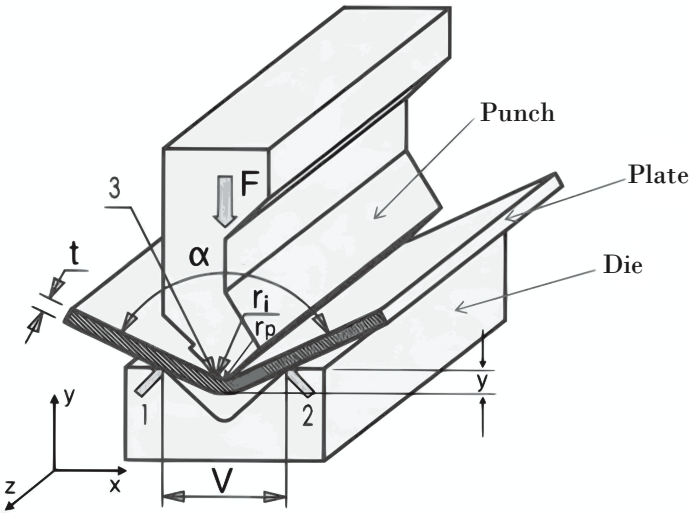


Figure 2.8.: Schematic representation of the punch, the plate, the die and press braking parameters [13].

of this penetration corresponds to the bending depth parameter - y. Both this parameters are illustrated in Figure 2.8.

The die vee (V), corresponds to the distance between both supports of the beam during the bending process and has a big influence on the required force in order to induce the necessary plastic deformation for the pretended bend. This parameter and the degree of the penetration caused by the punch also have an effect on the bending angle (α), represented in Figure 2.8.

The internal radius (r_i) has a crucial role on the success of the whole operation. It will either be influenced by the die vee, in the case of air bending or by the punch radius (r_p) in the case of bottoming bending [14].

2.3.1. Structure and components of a press brake

The press brake structure has several components, each serving distinct functions to achieve the desired outcomes of the bending process. To fully understand it's behaviour and operation, it is imperative to analyse the main parts of its structure. The main components of a press brake machine are represented in Figure 2.9.

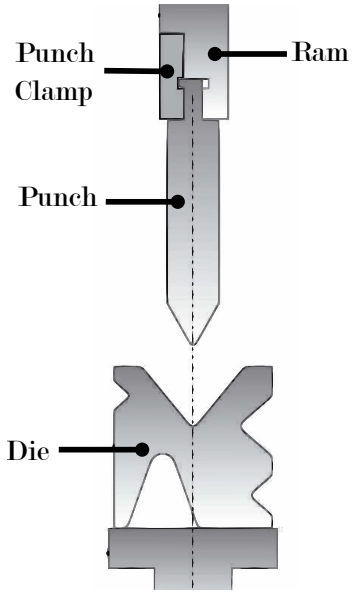
The frame is the main structure that supports the machine itself and the other parts together. In most bending machines it has a C shape and it is made from a very high strength material. The depth of the frame is referred to as throat depth, which represents the bending space available.

The ram or upper beam is the upper structure of the machine that has a linear vertical movement driven by a crank mechanism in a mechanical press brake or powered by one, two or more synchronized hydraulic cylinders. They usually are made from large, strong steel plates that hold the clamping mechanism which is connected to the punch tool.

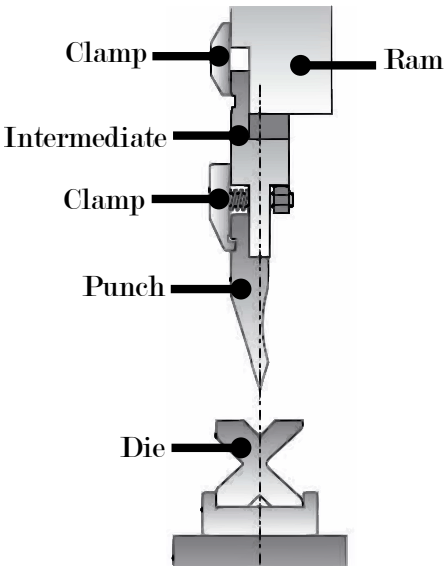


Figure 2.9.: Press brake main components [1].

As it is shown in Figure 2.10, the punch can be directly clamped into the ram or it can be clamped through by intermediates which is the most usual solution. In the first case, the punch is fixed by clamps on the front side of the ram. It can have a mechanical clamp using screws or a pneumatic or hydraulic clamping mechanism. In the second case, the punch is clamped by means of an intermediate which is hold by a mechanical clamp screwed or a pneumatic or hydraulic clamping mechanism. The intermediates are only removed if the operator needs extra space to realize the operation intended.



(a) Punch clamped directly into the ram.



(b) Punch clamped through intermediate.

Figure 2.10.: Example of different clamping systems used [12].

The bed or lower beam is the lower structure of the machine which is commonly stationary.

The tool holder for the die is installed in the table, which is located at the bed.

The die clamping mechanism is used to prevent the die from any kind of movement while the sheet metal is being bent. Once again, the mechanism can be manually clamped with screws and with a pneumatic or hydraulic mechanism. A manual clamping system is represented in Figure 2.11.

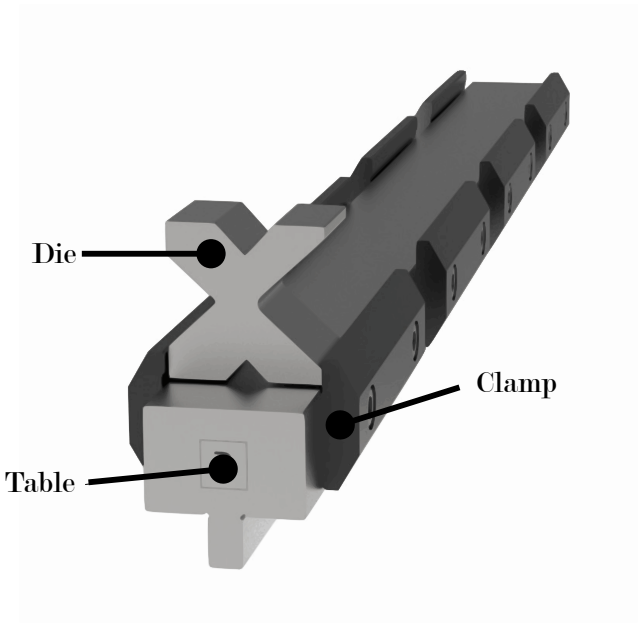


Figure 2.11.: Manual clamping mechanism of a die using bolts [15].

The back gauge has a crucial role during the bending process since is used to control and adjust the position and length of the steel plate, which is placed on the die of the bed, in order to ensure that it is in the correct position. Then, the plate is pushed until it reaches the stop finger. There are solutions with more than 1 finger stop with different heights and lengths.

As seen in Figure 2.12, the back gauge can have up to 6 total axis. The R axis indicates upward and downward movement, the Z axis refers to left and right movement and the X axis represents forward and backward movement. It is normally controlled with servo motors. The Y axis represents the axis of the press brake, each one for each individual cylinder.

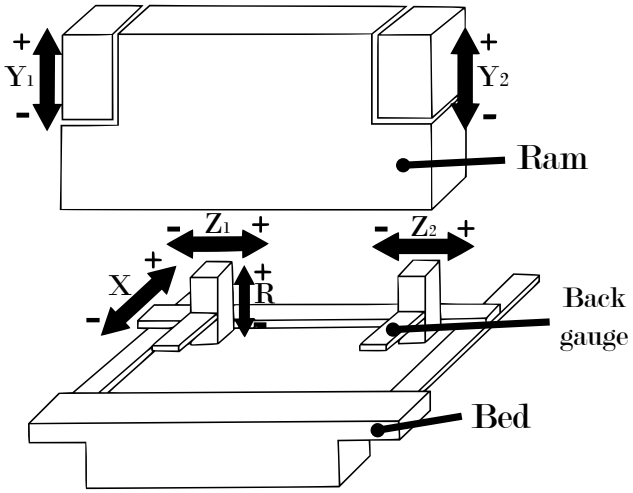


Figure 2.12.: Main axes of the back gauge and of the press brake highlighted [12].

The controller is responsible for controlling the press brake to execute specific programs and routines. It has the function to measure the positions of its mobile parts and activate the motors, hydraulic pistons, or other actuation sources that control the machine's movements. Figure 2.13 shows a computer numerical control (CNC) interface panel designed by ADIRA which continuously evaluates the parameters involved in the bending process.



Figure 2.13.: Numerical control interface panel designed by ADIRA [16].

2.3.2. Sheet metal bending techniques

There are different approaches used for the press brake bending process:

- Air bending;
- Bottoming bending;
- Coining bending;

- Three-Point Bending.

2.3.2.1. Sheet metal air bending

This approach is one of the most used type of bending in the industry. The sheet metal only gets in contact with the upper and lower tools in three points, the die shoulders (points 1 and 2) and at the punch tip (point 3). Therefore, the actual tooling angle is not that relevant. The bend angle is determined by how far the punch penetrates into the die. It is called 'air bending' because is used when air is between the sheet metal and the die vee [12]. This process can be seen in Figure 2.14.

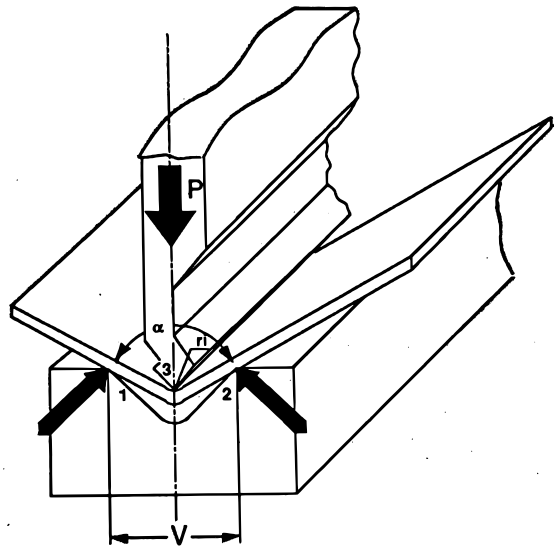


Figure 2.14.: Schematic representation of the air bending [14].

After the process, a phenomenon called spring back takes place, which will be analysed in depth in Section 2.3.3.

This method uses less bending force comparing with other bending types allowing the use of press braking bending machines with less tonnage capacity for a given application. There is also a lower wear on the tools used because the contact pressures are relatively low [14]. A big advantage is the possibility of using the same universal tool set in order to obtain a large angle range since it is possible to use a punch and die at 30° to obtain profiles with any angle from 30° to 180° [12]. On the other hand, the bending precision is lower than in other bending types and it is very affected by the quality of the machine and the tools used.

2.3.2.2. Sheet metal bottoming bending

During bottoming, the punch goes further than what happens during air bending and reaches the bottom of the die vee, pushing the sheet metal into the die vee. The internal radius is more precise, the sheet metal is yielded more and consequently the spring back phenomenon is lower than in the air bending. This method can be seen in Figure 2.15.

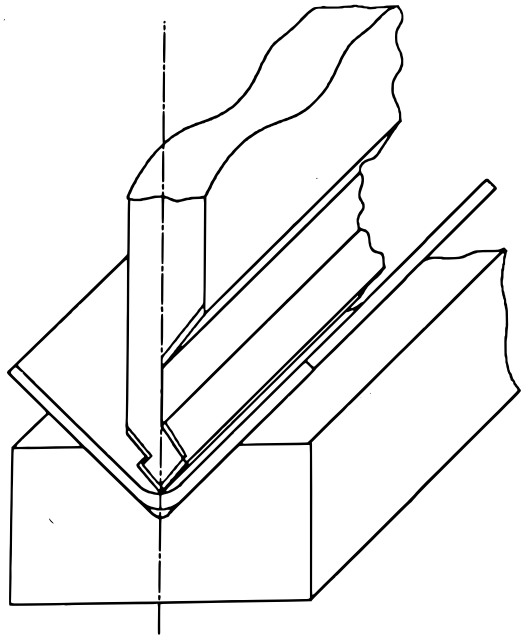


Figure 2.15.: Schematic representation of the bottoming bending [14].

This method is the most suitable one to obtain precise profiles and the punch and die must have the same angle to obtain good bending results. In case of big production series, it offers a good bending repetition since the bending angle is accurate and doesn't change much for identical sheet metals [12].

However, this method also presents some disadvantages. Since the punch goes into the very bottom of the die vee, it is impossible to obtain any angle correction by further penetration of the punch. It requires a dedicated tool set for a specific profile and it causes a higher wear on the tools used. This bending operation also requires a higher tonnage capacity than air bending, so it is more common in thinner sheet metals [12]. The necessity of applying higher forces to induce the plastic deformation of the profile, leads to the use of higher tonnage capacity press braking bending machines, which may be an obstacle, plus the the fact that a specific bending angle must have it's own dedicated tool set.

2.3.2.3. Sheet metal coining Bending

Contrary to the other two bending types, in coining the metal is not only bent, but also compressed by the impact of the punch into the die vee, as seen in Figure 2.16. In theory, with the required tonnage, the profile will bend to the exact angle of the tools, so it is imperative that both the punch and the die angle need to be exactly the same as the angle required by the profile, without having to worry about the spring back. For this, the die vee is smaller than for bottoming and air bending and it is five times the sheet metal thickness in order to prevent the punch tip from penetrating because of the smaller internal radius [12]. Since this type of bending requires extremely high tonnage, this tends to damage or compromise the integrity of the material. For this, press brake operators can only perform this method on lower thickness sheet metal (1-2 mm).

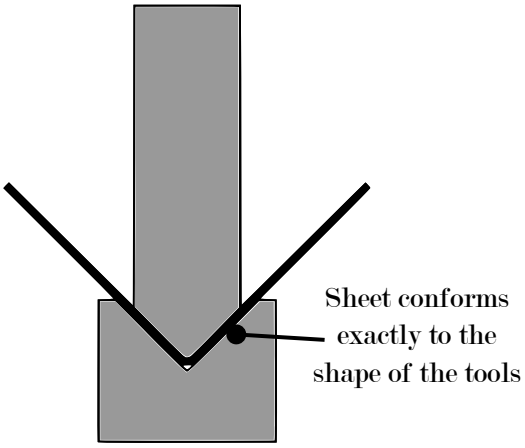


Figure 2.16.: Schematic representation of the coining bending.

The results obtained are very accurate and precise and since the punch tip penetrates the metal with very high tonnage, it eliminates the spring back phenomenon, as mentioned above. However, the tools wear quickly and for any angle and internal radius is necessary a specific set of punch and die.

2.3.2.4. Sheet Metal Three-Point Bending

This method is patented by the swiss firm *Hämmerle Zofingen*. The punch (S) is hydraulically controlled and penetrates the metal into the die, which is resting in both inner edges (point 2 and 3) [14]. This is seen in Figure 2.17.

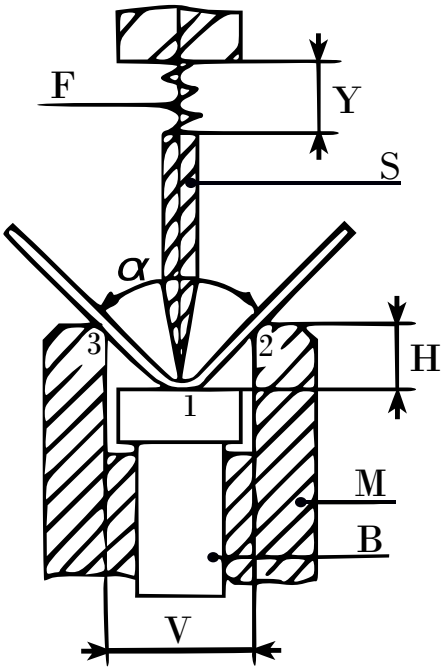


Figure 2.17.: Schematic representation of the three-point bending [14].

Where:

- F = Hydraulic Cushion;

- Y = Hyraulic Cushion travel;

- S = Punch;

- α = Bending angle;

- 1 = Bottom contact point at the die;

- 2 and 3 = Inner edges of the die;

- H = Depth of the die;

- V = Die vee;

- B = Adjustable bottom contact;

- M = Die.

To determine the bending angle, this technique involves using a special die that has a adjustable bottom tool that works as the third point of contact (point 1) [14]. In the recent years, this tool can be precisely adjusted in height via a servo motor. It's function is to determine the bending angle of the profile, with the bending angle increasing as the depth of the die bottom decreases.

The disadvantage of is this approach is the complexity of the machine and it's components, which results in being a very expensive method. It should only be used in special situations where it is necessary to achieve high precision in complex parts with several bendings [14].

2.3.3. Typical defects on the bending results

The desired final product after the bending process may not be exactly the same as the expected initially. The thickness variation, the resilience and strength of the material and the grain orientation are some of the parameters that will influence the final result. The spring back effect will also to be addressed since it is related to the yield strength of the material.

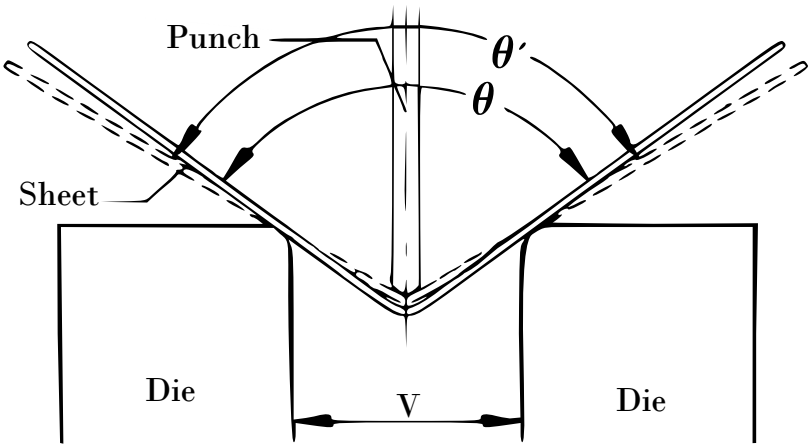


Figure 2.18.: Air bending process spring back [17].

2.3.3.1. Spring back

During the bending process the metal plate undergoes plastic deformation as the punch gets in contact with the plate. After obtaining the pretended bend, there is a tendency for the plate to return to its original position since the punch is no longer applying the downward force. This happens especially in air bending method. Taking into account this phenomena is of great important in order to obtain products with the desired tolerances. In most cases is an undesirable issue, therefore the estimation of the spring back values can prevent material loss, waste of time and workforce cost [17]. This effect can be seen in Figure 2.18 where θ represents the initial angle obtained after the bend and $\theta^{'}$ represents the final angle after the spring back phenomenon.

Spring back depends on the following points [12]:

- Yield strength of the material;
- Material Young's modulus;
- Bending type;
- Deformation Speed (directly proportional);
- Thickness of the sheet metal (directly proportional).

One usual way to prevent this is to over bend the plate in order to obtain the desired angle, taking into account the spring back. It is also possible to use coining bending with a very high tonnage without having to worry about the spring back.

Common values to compensate this effect are the following [14]:

- Aluminium: 0° to 12° (high grade aluminium alloy can go up to 33°);
- Mild Steel: 0.5° to 1.5°;
- Stainless Steel: 2° to 4°.

2.3.3.2. Press brake deformation

Traditional press brakes are actuated by two cylinders, one in each side, delivering high tonnage capacity in order to drive the ram. When a force is applied in the downward direction, a reaction force is also applied in the opposite direction, until the parts where the forces are applied start to yield. In a press brake, the forces applied by the cylinders will cause a very subtle bending of the ram in the upwards direction and the bed in the downwards direction, since they are exposed to a 3 point flexion.

As seen in Figure 2.19, this deformation will lead to the incorrect bend angle of the plate resulting in a curved profile, being more notable in longer parts. To compensate this deformation it is used the crowning system.

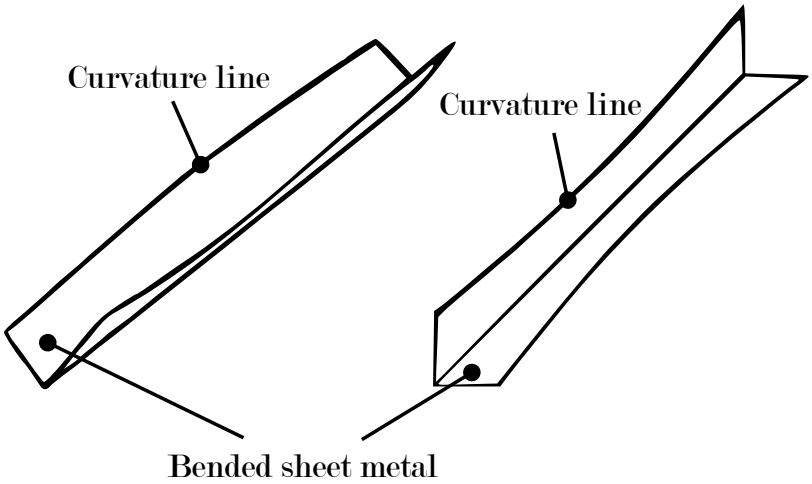


Figure 2.19.: Effect of press brake deformation on a bended sheet metal [12].

The crowning system essentially creates an opposite force during the bending of the part, in order to distribute equally the force applied by the press brake on the plate, avoiding the curved profile shape [12].

Intermediates are equipped with adjustable wedges to create an opposite curve during the bending and are a great example of a mechanical crowning system that can be located either in the ram or in the bed. Figure 2.20 shows an intermediate located in the ram with adjustable wedges. The usual solution seen in modern press brakes is an automatic crowning system. This system is integrated in the bed and also creates an opposite curve to compensate the deformation of the upper and lower beams. They are usually driven by a geared motor connected to the controller. The controller calculates the necessary crowning to induce based on the program that the operates are using [12].

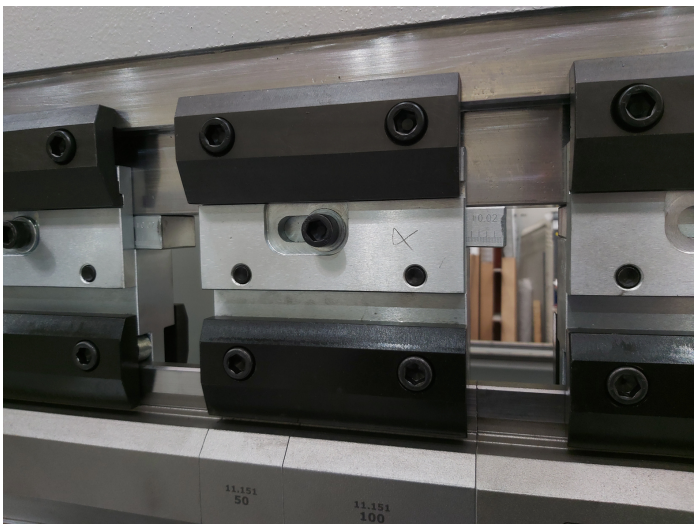


Figure 2.20.: Intermediate with adjustable wedges used in a hydraulic ADIRA press brake [16].

2.3.4. Bending machine classification

In all bending press machines, the tools are installed in the ram and the bed. The clamping mechanism is connected to the ram to secure the punch tooling. The type of actuation of the ram will define the classification of the bending press machine.

2.3.4.1. Mechanical actuation

In a mechanical bending machine, the power is transmitted to the ram through a mechanical transmission. The power is secured by the kinetic energy stored in the flywheel and by the started motor. This is seen in Figure 2.21. The machine operator controls the flywheel through a clutch and the movement is normally transmitted with a gear reducer and then is it transformed into the linear movement of the ram through a crank and connecting rod mechanism [14].

This type of machine is simple and straightforward, considering its lack of electronics and simple maintenance. The big disadvantage of this equipment is that the ram needs to complete a full cycle when engaged and can not be reversed. Besides this, the travel of the ram is short and it's non-adjustable. Today, this technology is less used in the industry.

2.3.4.2. Hydraulic actuation

This machines use one, two or more hydraulic cylinders to engage the ram. In contrast to mechanical press brakes, they are one of the most common solutions seen in the industry. Instead of relying on mechanical actuation, this type of machine applies pressure through hydraulic force to move the ram down. They offer the possibility of varying the speed and the force capacity of the hydraulic actuators, allowing to easily realise large forces at

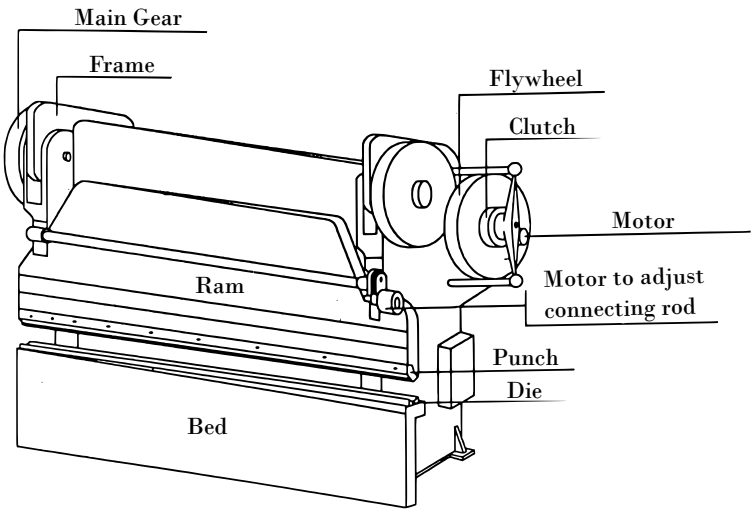


Figure 2.21.: Schematic representation of a mechanical press brake machine [14].

different speeds. The travel of the ram can also be adjusted. The operator has more precise control over the bends using the control panel to move the ram [14]. On the other hand, they cannot exceed the range of their rated tonnage.

2.3.4.3. Electric actuation

The concept of electric press brake machines is a recent bending technology that uses only an electric motor as a power source for controlling the ram movement. The traditional and most common hydraulic machines started to be replaced with electric alternatives that offer more precision, lower energy consumption and reduced maintenance costs. The eager for innovation and the eco-friendliness awareness opened the way for the electric approach which does not required any type of hydraulic fluid to operate. The disadvantage lies in the fact that the tonnage capacity is lower than the hydraulic one.

2.3.4.4. Hybrid actuation

The development of the hybrid press brake revolutionized the industry. This approach uses a servomechanism to guarantee a very high precision in the control of the hydraulic actuators. This includes an error feedback system that can detect any kind of anomaly such as leaks or pressure drops. This feedback signal is compared with the command signal. The resulting error signal is then amplified by the regulator and then used as an input control signal to the servo valve. The servo valve will control the hydraulic flow in the actuator in proportion to the drive current from the amplifier [18]. Finally, the actuator then forces the load to move, in order to correct the error.

This method usually use less hydraulic fluid, has a higher precision level to position correctly the ram to the required position and is also more efficient due to its lower energetic consumption [14].

2.4. End effector's design

Since Prehistoric Times, grasping tools have been developed and created to assist mankind in holding objects that are challenging due to their size, form or materials. Early tools were made of merely two rigid links that functioned as fingers on their own or with a pretty basic link design. There were multiple application areas that benefited from the use of these tools. In Figure 2.22, it is represented a tool similar to a gripper used in the early days of metallurgic manufacturing, which allowed blacksmiths to work safely with very high temperature materials. It is a very simple and effective design with the fingers curved to help handling big objects and to make it easier to grab them by the extremity points [19].



Figure 2.22.: A gripper being used by a blacksmith in the roman empire [19].

Figure 2.23 shows drawings made by Leonardo Da Vinci (1452-1519) for crane applications. These mechanical mechanisms were intended for heavy lift applications, using the same two finger gripper design.

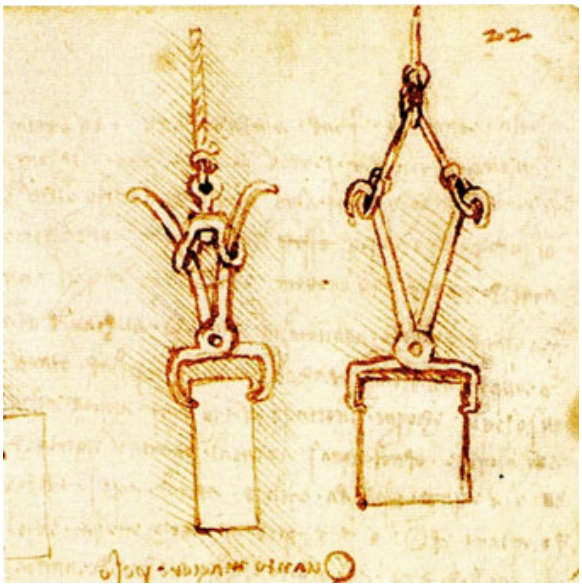


Figure 2.23.: Mechanism for crane grippers designed by Leonardo Da Vinci (1452-1519) [19].

Nowadays, the innovation and automation of the industry have led to the implementation of industrial robots, starting a new era of gripper applications. In order to meet the demands of this new era, further research on gripping techniques and methods was required.

When industrial robots interact with their surroundings, they need grippers to perform manipulation tasks. A gripper is a specially designed component used to pick, hold, place and pack objects. There are different gripper technologies for different applications, depending on the size, shape and weight of the object. In the context of robotic cells, they are used to reap the benefits of precision, performance and productivity. They are typically attached to the end of the robot arm through a coupling mechanism that allows the connection of both parts. The overall assembly of a robot system can be simplified with the right gripper design, decreasing the cost of implementing the system and increasing the overall reliability [20].

2.4.1. End effector safety design standard

The International Standard ISO/TR 20218-1, Robotics: Safety Design for Industrial Robot Systems, Part 1: End-effectors, provides guidance for the safety measures for the design and integration of end effectors used in robotic systems, such as in robotic cells.

2.4.1.1. Vocabulary about end effectors

In order to clarify the vocabulary used about end effectors, this document also presents some terms and definitions based on another international standard: ISO 14539:2000, Manipulating industrial robots, Object handling with grasp-type grippers, Vocabulary and presentation of characteristics.

An end effector is a 'device specifically designed for attachment to the mechanical interface to enable the robot to perform its task' [21]. According to the standard ISO 14539:2000, there are two types of end effectors [22]:

- Tool-type end effector;
- Gripper;
  - Grasp-type gripper;
  - Non-grasp-type gripper.

A tool-type end effector, instead of gripping the object, performs specific tasks. Some application examples are: arc welding torches, spot welding guns, laser cutting guns, and water jet cutting guns [22].

The gripper end effector has the function to seize, hold, grip, and place objects. In this category, there are two types of grippers. The grasp-type gripper grips an object with fingers [22]. Other sources refer to these grippers as impactive grippers because the prehension is obtained by impactive forces which impact against the surface of the object to be handled [23].

A non-grasp-type gripper grips objects without fingers. It can use vacuum, magnetic force, or other types of actuation [22]. Other sources refer to these grippers as astrictive grippers since the gripping force is produced by a field: vacuum suction, magnetism or electrostatic charge displacement [23].

2.4.1.2. Initial design considerations

The ISO/TR 20218-1 standard provides some important initial considerations to take into account before the design of an end effector [21]:

- Robot functions:
  - Automatic or manual robot;
  - Collaborative or non-collaborative robot;
- Space Available:
  - Dimensions of the end effector and workpiece;
  - Movement carried out by the end effector and workpiece;
  - End effector changing station (only if there is one);
- Time:
  - The life expectancy of the end effectors or it's constituent parts;
  - Exchange time of the end effector exchange system (only if there is a changing station);
- Others:
  - Workpiece shape and geometry;
  - Centre of gravity of workpiece;
  - Robot payload;
  - Grasping force;
  - Suction of vacuum cups;
  - Magnetic attraction properties;
  - Friction between grasping surface and the workpiece;
  - Speed and acceleration;
  - Relevant environmental data such as temperature.

2.4.1.3. Hazard identification and risk reduction measures

Hazard identification is used to evaluate all the risk assessments related to the intended use and the foreseeable misuse of the end effector. For this it is crucial an understanding of how end effectors interact with the other components of the robot system. For example, although the hazards are similar for collaborative and non-collaborative robotic applications, the exposure of the user to these hazards is very different. Some factors that should be considered for are the following [21]:

- Transportation;
- Assembly and installation;
- Setting up the system (teaching and testing the robot program);
- Cleaning or maintenance operations;
- Malfunction investigation or troubleshooting;
- Dismantling or disabling.

End effector designs can include design measures in order to reduce the associated risks. Reducing sharp edges, increasing edge radius or modifying edge profiles are great measures to reduce human contact that can result in injuries. In order to minimize the contact forces or pressures, the end effector mass should be as low as it is possible for the intended application. Impact energy can also be minimized by using deformable components, padding and cushioning materials [21].

Protective devices, for instance sensors, that are able to monitor the speed of the end effector, force-sensing and presence sensing technology can reduce the risk associated to the moving end effector especially during collaborative operations. Besides that, the implementation of an emergency stop function for both the robot and the end effector should be mounted in the same span of control [21].

When designing or selecting a gripper for an application, there are general features and functions that can be part of these risk reduction measures [21]:

- Manual release system to free entrapped fingers or other body parts when the power source is not available;
- Continuous gripping action even in the event of power source interruption to stop a workpiece from falling out;
- Ensure the minimum gripping force needed to achieve the prehension of the object instead of using the maximum lift force available.

When using vacuum grippers or magnetic grippers, the main safety concern lies on the suction loss or a change on the magnetic field due to an event of power source interruption. The following measures should be considered to reduce the risk [21]:

- Diverse vacuum or magnetic systems (each branch capable of holding the workpiece

in place);

- Selection of a device to generate vacuum or magnetic field with an appropriate Performance level (PL));
- Audio and visual signals to warn the operators that the object may fall out in the case of a power loss event.

2.4.1.4. Instructions for general use

A safety manual containing all the necessary information and instructions to ensure the correct use of the robotic system, in this case the end effector, should be provided by the integrator of the end effector solution. This should contain warnings about the various risks that the user will be subjected to. Information about movable parts or places where fingers could be crushed or trapped and how to escape from this situation, both with and without power; how to safely remove the workpiece manually if the system is stopped; or if a power loss can lead to the object falling out of the end effector are some of the multiple topics that must be mentioned [21].

2.4.2. Gripper types

There are many different types of grippers with different technologies and a wide variety of factors to take into account. The block diagram presented in Figure 2.24 gives an overview on a common classification of robotic gripper based on its technology.

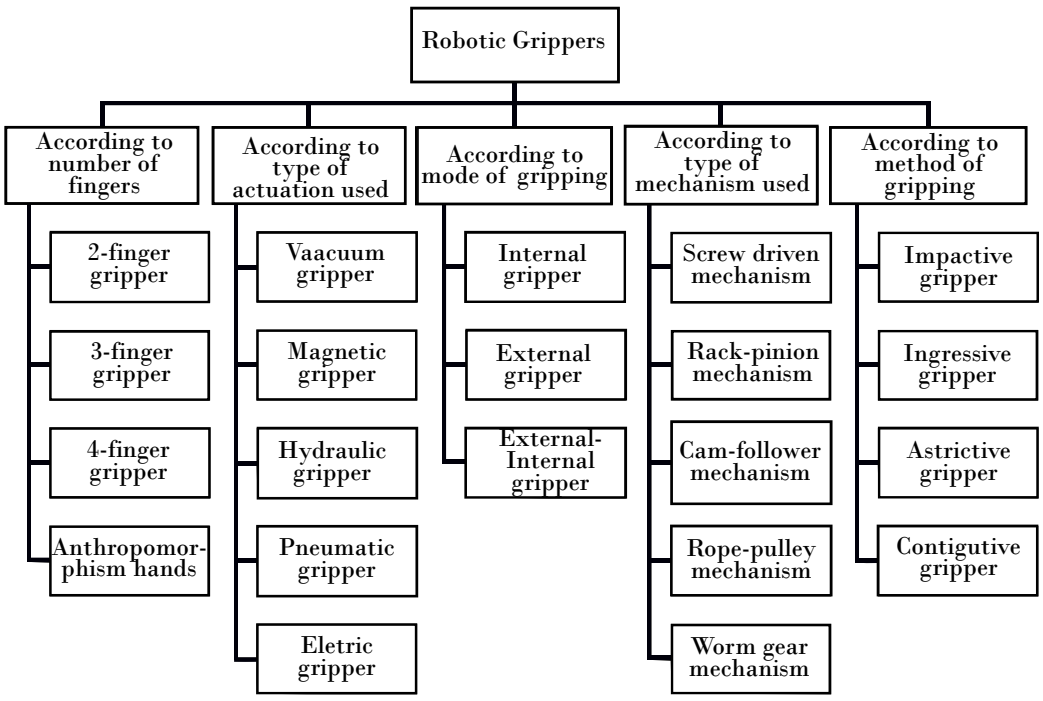


Figure 2.24.: Broad classification of robot grippers [23].

Regarding press brake robotic cells, the constructive solutions often seen in industry are

two point/finger grippers (parallel or angular), vacuum grippers and magnetic grippers. The parallel and angular gripper can be actuated by an electric, hydraulic or pneumatic source and are commonly used with a mechanical grasping mechanism such as jaw design (grasp-type gripper). These type of grippers are seen in the manipulation of small sheet plates with low weight. The three finger design is not a common design in robotic bending cells since it is used to pick up delicate parts with precision and strength, being a great solution to pick up both cylindrical or spherical objects [24].

If the workpiece handled is a heavy weight plate with several meters, vacuum or magnetic grippers solution are the best options (non-grasp-type gripper) [23].

2.4.2.1. Vacuum gripper

Vacuum grippers actuation stand out for being able to grip and move very large and heavy products, making them excellent choices for the manipulation of large metal plates and often used for gripping non-ferrous objects. Figure 2.25 shows a vacuum gripper used for the manipulation of small parts in a Trumpf robotic bending cell.

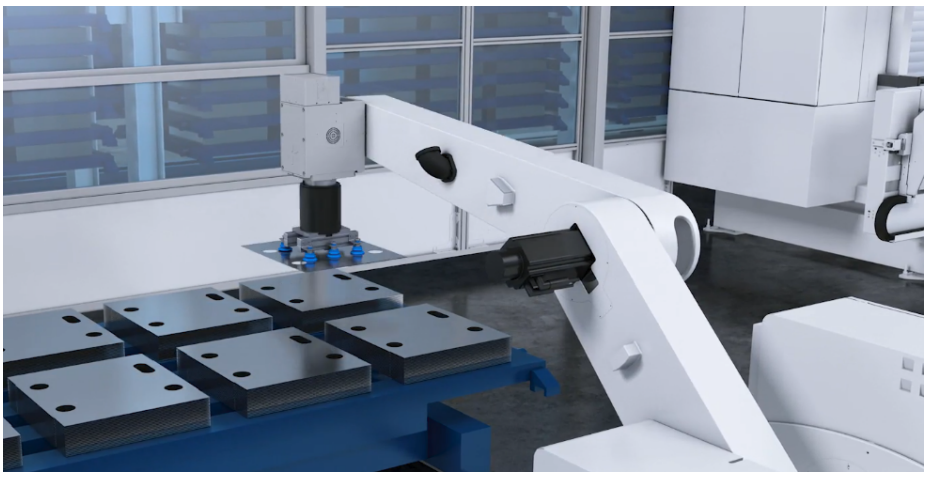


Figure 2.25.: Industrial robot equipped with a vacuum gripper [25].

They use vacuum cups as the gripping devices and are an essential part of the process of gripping a object. These vacuum cups use the difference between atmospheric pressure and a vacuum to hold, lift and move objects [24]. When the center of the vacuum cup is pressed against a non-porous and flat surface, the occupied volume of air between both of them is reduced because the air is forced out of the inside of the cup, causing a slight negative pressure within the cup. The cup keeps adhered to the surface of the object due to the pressure difference between the atmosphere on the outside of the cup and the low pressure cavity on the inside of the cup [26]. The maximum prehension force is defined by two factors: the surrounding air pressure and the surface area which can be accessed for gripping [23]. For releasing the object, air is pumped out into the vacuum cups. This vacuum pressure mentioned is usually created with the following devices [27]:

1. Vacuum pumps;
2. Ejectors (Venturi effect);
3. Suction bellows;
4. Pneumatic cylinders.

Vacuum pumps and vacuum ejectors are the devices often seen in robotic cells. Vacuum pump can generate a higher vacuum than the other devices and has little noise development. The initial expenses costs for accessories like air reservoir, the size and weight of the pump and the slow response time due to long pneumatic lines are some of its disadvantages. Vacuum ejectors are easier to mount and have a lower initial cost than the vacuum pump solution. They do not require any additional equipment and have a fast response. However, the high compressed air consumption leads to high operational costs and they require a noise damping system [23]. In both solutions, the device can either be integrated with the gripper or with the robot.

There are applications that require several vacuum cups with simultaneous vacuum distribution, leading to the ramification of the main pneumatic line. It is important to consider the diameter of these lines, since a small diameter leads to a higher air flow resistance and a large diameter leads to an increase in air evacuation time. As an example, the manipulation of a very large sheet metal will require several cups to hold its surface, therefore the ramification of the pneumatic lines and the different diameters are important factors to be considered [23].

A problem associated with vacuum grippers is the fall out of the sheet metal due to a power loss. This means that vacuum retention will not be ensured if the vacuum generator turns off leading to safety issues endangering the robotic cell and its components. The use of non-return valves can ensure additional vacuum retention safety if the vacuum system is compromised. However, even with this valves it is impossible to guarantee full air leak proof on the pneumatic lines. This solution can last from a few seconds to minutes, depending on the press fit of the valve inside the pneumatic line, until the object falls out of the gripper due to a loss in the gripping force of the vacuum cups over time.

Vacuum cups are available in a wide variety of materials, but most of the cups are made from four materials: nitrile rubber (NBR), Silicone, Polyurethane, and polyvinyl chloride (PVC). The material choice is based on the application intended. The hardness of the material and the temperature resistance are very important material characteristics for choosing a particular material [28].

The hardness of a material defines the ability of a vacuum cup to seal against the surface of the object. The Shore A Hardness Scale measures the hardness of flexible rubbers. A durometer is the instrument used to measure the hardness. The scale ranges from 5 (soft) to 100 (hard). This will show how flexible the cup is, allowing to determine for which applications is intended. A softer durometer means that in the presence of a object with contoured parts or sharp edges, the vacuum cup will grip more easily. Harder durometers are perfect for application with flat surfaces. The harder the material is, the longer its life is expected to be [28]. Table 2.1 presents the hardness values for different materials.

Table 2.1.: Hardness (Shore-A) for different materials [28].

Materials	Hardness/Shore-A
NBR	[40; 60]
Silicone	[40; 60]
Polyurethane	[30; 70]
PVC	[45; 55]

Table 2.2.: Operating temperature values for different materials [28].

Materials	Temperature/°C
NBR	[-40; 100]
Silicone	[-45; 200]
Polyurethane	[-25; 80]
PVC	[10; 65]

Regarding temperature resistance, most applications involving a gripper occur at room temperature. However, in pick-and-place situations such as in the frozen food packing industry or in the plastic injection mod industry it is important to choose a vacuum cup material that is adequate to the temperatures of the manipulated object [28].

Table 2.2 presents the operating temperature values for different vacuum cup materials.

NBR is the most used material for the cups and can be found in general applications having a very good oil and grease resistance. Since it has low cost and good wear resistance it is the standard material choice for most applications. NBR cups have normally 60 durometer (hardness) and are an excellent option for high temperature applications [28].

Silicone generally costs 30-50% more than NBR, although; it offers the huge advantage of having extreme temperature resistance, both cold and hot as seen in Table 2.2. Silicone cups are able to seal against rough surfaces such as cardboard sheet or corrugated plastic, since the are typically softer than NBR [28]. It presents the lower wear resistance of the four materials but has a good stability on handling oil and grease.

Polyurethane vacuum cups have very high wear resistance compared with silicone and NBR, being more suitable for high wear applications. They have less temperature resistance range, according to Table 2.2, and are more expensive [28]. It also has very good oil and grease resistance.

PVC cups present a low cost comparing to the other mentioned materials, but, since it is a plastic its mechanical properties are inferior. Rubber cups may wear quickly than PVC ones, but the PVC cups will most likely fracture at some point. They also have a limited hardness and temperature resistance range [28]. It has less oil and grease resistance comparing to rubber cups.

Concerning the existent vacuum cup solutions, there are two basic types: flats and bellows. There are other alternative solutions derived from these two designs such as ribbed suction

cups and double lip suction cups. A flat and bellow vaccum cup are presented in Figure 2.26.



(a) Flat suction cup with ribs.

(b) Bellow suction cup.

Figure 2.26.: Two basic type of vacuum cup solutions [29].

Flat vacuum cups provides very good excellent stability in high speed part manipulation, especially in a horizontal movement. Although they have a relative simple design, they deliver good results taking into account all the criteria. They are suitable for flat workpieces such as sheet metal parts, cartons, glass plates, and plywood plates [23].

A clear superiority of the bellows cup design is handling convex or even concave objects. While these cups are able to deform to the shape of the circular profile, flat cups are unable to do it. However, the prehension force obtained is lower comparing to the flats, which is a limiting factor for many heavy applications. They are suitable for delicate parts, uneven workpieces, flat surfaces with a large area and a high deflection.

The bellow cup is also a great option when the surface of the object being manipulated is not perpendicular to the surface of the lip of the vacuum cup, as seen in Figure 2.27.

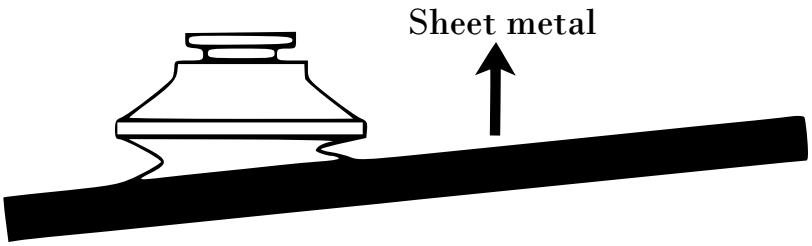


Figure 2.27.: Inclined lift application - bellow cup [29].

Flat cup may be an option if it is utilized an articulated ball joint with a lever compensator as seen in Figure 2.28, but it is a more expensive solution.

Even though the advantages of bellow cups seem to stand out, it is imperative to consider that flat cups are less expensive, more stable at high speeds, the volume inside a flat cup is less, being able to create a vacuum in shorter time and these cups tend to last longer, having less change of fracture or eventual stress points [30].



Figure 2.28.: Articulated joint flat vacuum cup [30].

2.4.2.2. Magnetic gripper

Magnetic grippers, as the one seen in Figure 2.29, can only be used for picking up ferrous materials. They are simple, require low maintenance and are very easy to control. Although they are limited to applications involving ferrous objects, they require minimal air consumption to actuate, which means that the associated air cost is very low, depending on the solution actuation. These grippers are able to grip an object very quickly and they can grip parts with holes on it, something that it is not possible when using vacuum grippers. However, if the part is moved too quickly, it can slip out of the gripper, the presence of oil at the surface can reduce the strength of the magnets and machining chips can stay attached to the gripper when unloading the part [31].

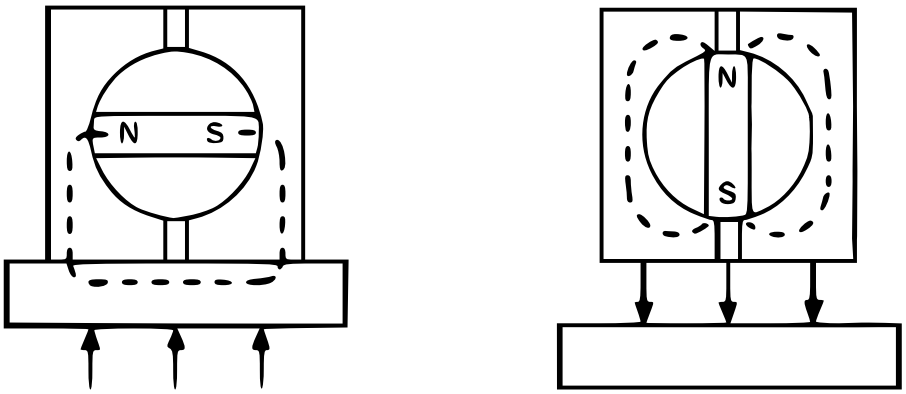
In relation to robotic bending cells, this is a great for applications requiring the bending of steel plates, but can not be used with aluminium plates since aluminium is a non-ferrous metal. For this situation, a vacuum gripper is definitely the right option.

Concerning magnetic gripper solutions, there are 2 basic types: Permanent magnet gripper and electromagnet gripper. Other alternative derived from these two types are also available such as permanent electromagnet and pneumatic magnetic grippers.

Permanent magnet grippers are actuated by a permanent magnet (magnetized material), meaning that they are in continuous actuation, not needing any external power source to operate. It is necessary a mechanism for releasing the object, so that the magnet flux path is diverted away from the gripping surface, but in order to prevent long term deterioration it is maintained through the magnet. This kind of gripper can have retention pressures as high as 100 to 200 $\mathrm{kN\,m^{-2}}$ [23]. Besides that, since there is no electric current flowing it means that even if a power loss occurs the gripper remains actuated. The magnetic flow during the part prehension and the part release is presented in Figure 2.30.



Figure 2.29.: Magnetic gripper connected to a robot's arm [31].



(a) Part prehension. (b) Part release.

Figure 2.30.: Mechanical control of the magnetic flow [23].

Although gripper magnets are able to sustain their magnetic force for very long periods of time, the deterioration of the magnetic field strength may happen due to the presence of high temperatures. Ceramic magnets can operate up to approximately 100 °C, AlNiCo magnets can are usable up with temperatures up to 45 °C and other rare materials (Samarium- Cobalt, Neodymium-Boron, etc.) have a great ratio between magnetic field strength to weight ratio and can function up to 200 °C. Most applications require magnets to be sintered and to have protective coating against corrosion. A problem with magnetic material is that they can remain magnetized even after the disappearance of the magnetic field. To fix this, a thin polymer coating on the magnetic surface can be applied [23].

Electromagnetic grippers use electric current to generate a magnetic field through a wire wound into a coil. If electric current is flowing through the wire the magnetic field becomes active, otherwise the magnetic field disappears. These kind of grippers can pick up and drop objects much faster than the permanent magnets one, which is a great advantage when time is a crucial factor. They are also used when the application requires lifting heavy loads [32]. Figure 2.31 represents a very simple electromagnetic gripper.

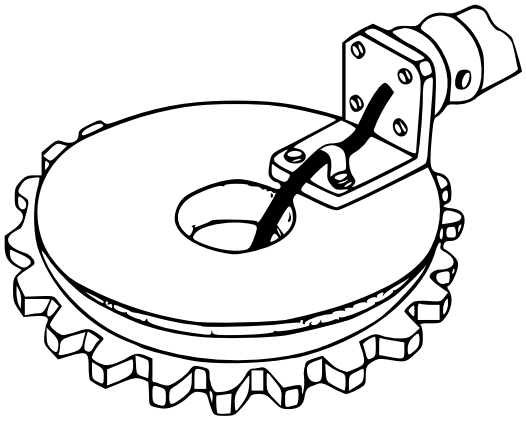


Figure 2.31.: Electromagnetic gripper for picking cog wheels [23].

The gripping force depends on the following factors [23]:

- Dimensions of the contact area between the object;
- The contact area that is effectively used for the gripping force;
- Roughness of the surfaces in contact;
- Material properties and the magnetic field strength of the electromagnet.

These grippers have simple constructive solutions with no moving parts, have an uncomplicated energy supply, have no power losses due to friction and they have huge applications in terms of object size and geometry.

On the other hand, they are limited to ferrous materials, have longer release times due to magnetic remanence, leave dust or other particles adhering to the magnets, and if a power failure occurs, this will lead directly to the release of the object, damaging it or injuring someone. The current draw is also considerably high which is not efficient. The separation of thin sheets can be difficult due to magnetic permeability and if the gripper is driven the direct current (DC) the product may become magnetized, adding extra work and costs to demagnetize the part [23].

2.4.2.3. Parallel and angular gripper

The parallel gripper grasp objects by applying force either from the inside or the outside of the part. It normally has an actuator and a mechanical mechanism to move the jaws. In the inside gripping movement the jaws are opened and in the outside gripping movement the jaws are closed. It is one of the most seen designs and very useful in industrial applications. Its main components are the actuator, the gripping jaw, which is in contact with the object, and the mechanical mechanism between the actuator and the fingers. The actuator is the power source and can either be pneumatic, electric or hydraulic. An example of a simple design parallel gripper is shown in Figure 2.32 which only requires the movement of only one jaw. It is driven by a linear pneumatic cylinder that drives the mobile jaw. The return

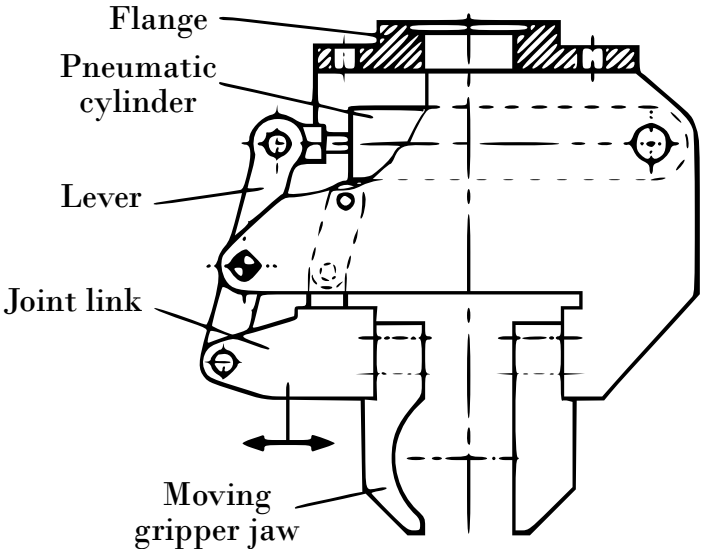


Figure 2.32.: Parallel gripper with one mobile jaw and one fixed [23].

is obtained with a return spring within the cylinder and the implementation of sensors for end of stroke detection is necessary [23].

A great variety of driver actuations for parallel jaw grippers are available, as seen in Figure 2.33. Gear mechanisms are often used to achieve the desired motion characteristics. Most grippers applications will require the synchronization of the jaw movement. However, if necessary it is possible to implement a independent jaw motion as well [23].

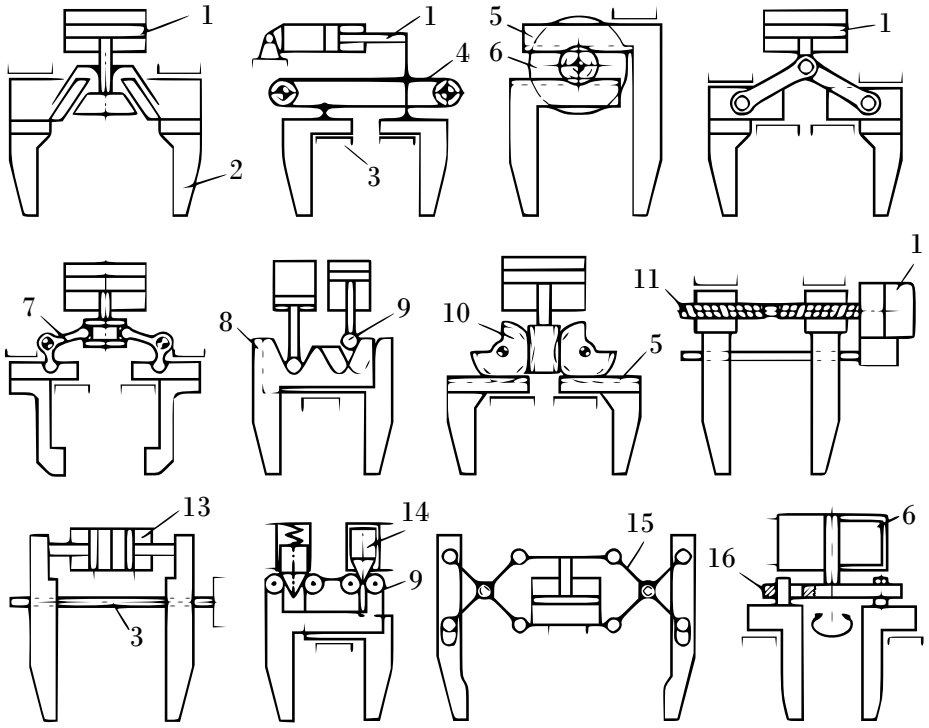


Figure 2.33.: Standard gripper drives for parallel grippers [23].

The components present on the different driver actuation's for parallel jaw grippers are defined below:

1. Pneumatic cylinder;
2. Gripper finger;
3. Straight guide;
4. Toothed belt;
5. Toothed rack;
6. Rotary pneumatic cylinder;
7. Angle lever;
8. Cam slide;
9. Roller;
10. Gear segment;
11. Lead screw;
12. Gear motor;
13. Two cylinder;
14. Pneumatic piston;
15. Scissor gear;
16. Cam disk.

While in a parallel gripper the fingers will approach each other remaining parallel, an angular gripper the fingers close towards each other by rotating around an axis. These grippers hold objects by moving their jaw along a curved path. They can accommodate a wide range of applications since they can open their jaws up to 90 °. Figure 2.34 presents a wide diversity of designs with different actuations [23].

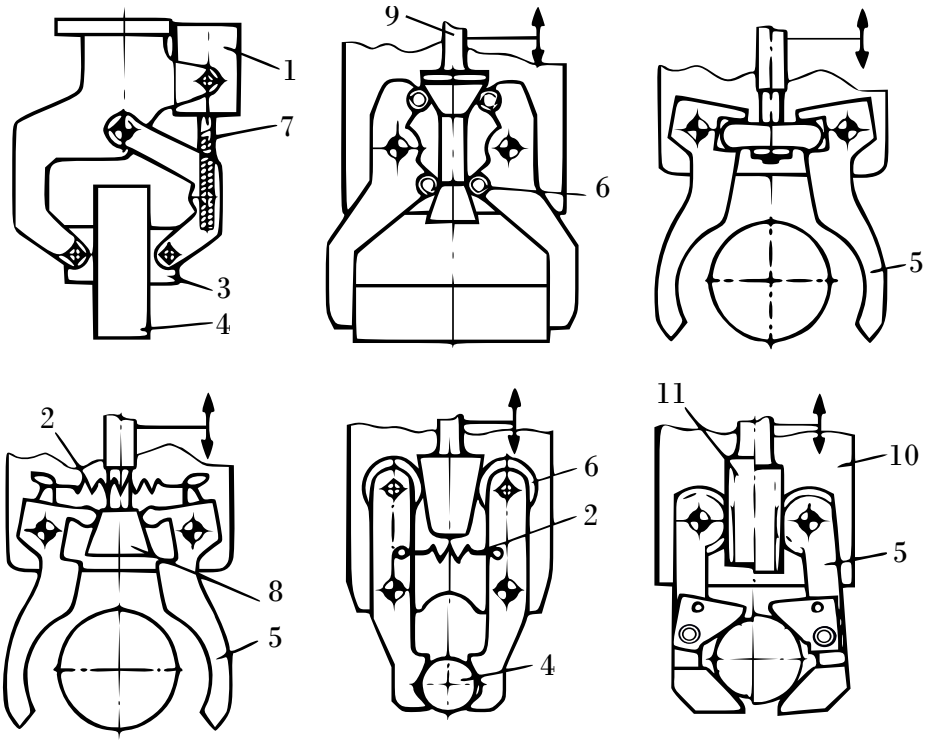


Figure 2.34.: Standard gripper drives for angular grippers [23].

The components present on the different driver actuation's for angular jaw grippers are defined below:

1. Electric motor;
2. Return spring;
3. Gripper jaw;
4. Object;
5. Gripper finger;
6. Roller;
7. Lead screw;
8. Cone;
9. Pneumatic cylinder;
10. Base plate;
11. Toothed rack.

As mentioned before, pneumatic, electric and hydraulic are the most common types of actuation used in jaws/fingers design mechanism.

Pneumatic grippers uses compressed air to operate its gripping mechanism. The actuation is done with pneumatic cylinders located in the gripper housing or by externally cylinders and both double-acting cylinders as single-acting with spring return are available [23]. There are valves to let the compressed air flow, leading to the piston movement in the two directions. The force exerted on by the jaws depends on the air pressure available [2]. They can be used in the biotech and pharmaceutical industry, injection and plastic molding, automatic robotic cells, etc [24].

Hydraulic grippers are designed for heavy load applications having a great performance on handling heavy parts. The piston moves due to the pressurized fluid, triggering the fingers, opening and closing as necessary. Although these grippers have an excellent gripping power, they have several disadvantages such as the necessity of having oil pump, a reservoir and high maintenance [24].

Electric grippers are designed to easily control the speed and the grip force of the jaws. Being able to control these factors is an enormous advantage when handling fragile objects. Besides that, they usually are more affordable than pneumatic solutions.

They also can be equipped with a servomechanism and are appropriate for application that require high speed and light gripping force. They come with microprocessor to control the force and speed. The gripper receives an input command from the robot control unit. This command is sent to the gripper control module which is responsible for driving the gripper motors. Finally, the servo-electric motor reacts to this signal [24].

2.4.3. Grippers solutions used in robotic bending cells available in industry

Various different gripper solutions for handling sheet metal in a robotic bending cell are presented below. These grippers are used in robotic bending cells that are available on the market and designed by known manufacturing companies in the metal forming industry. For a simpler analysis, the solutions presented will be divided into the following categories: small parts manipulation, medium part s manipulation and large parts manipulation. However, it is imperative to take into account the thickness and weight of the part. Even for a small plate, if it has a high thickness it may require a bigger gripper with more lifting power.

2.4.3.1. Small parts manipulation

Regarding solutions for small sheet plate manipulation, it is very common to see what is called multi grippers. These grippers use two or more prehension techniques to hold the part. They are flexible and versatile since they can adapt to multiple applications.

LVD presents a multi gripper solution that can hold objects by closing one finger around a curved path (angular gripper) and can also hold using vacuum cups (vacuum gripper). As seen in Figure 2.35 and 2.36, the gripper uses a pneumatic cylinder to move around a curved path making it a very versatile solution that effortlessly handles different part sizes

and geometries. It can bend complex parts without ever regripping and can easily move between in the cell. The gripper handles parts from 35 x 100 [mm] to 400 x 600 [mm], up to 4 kg [33].

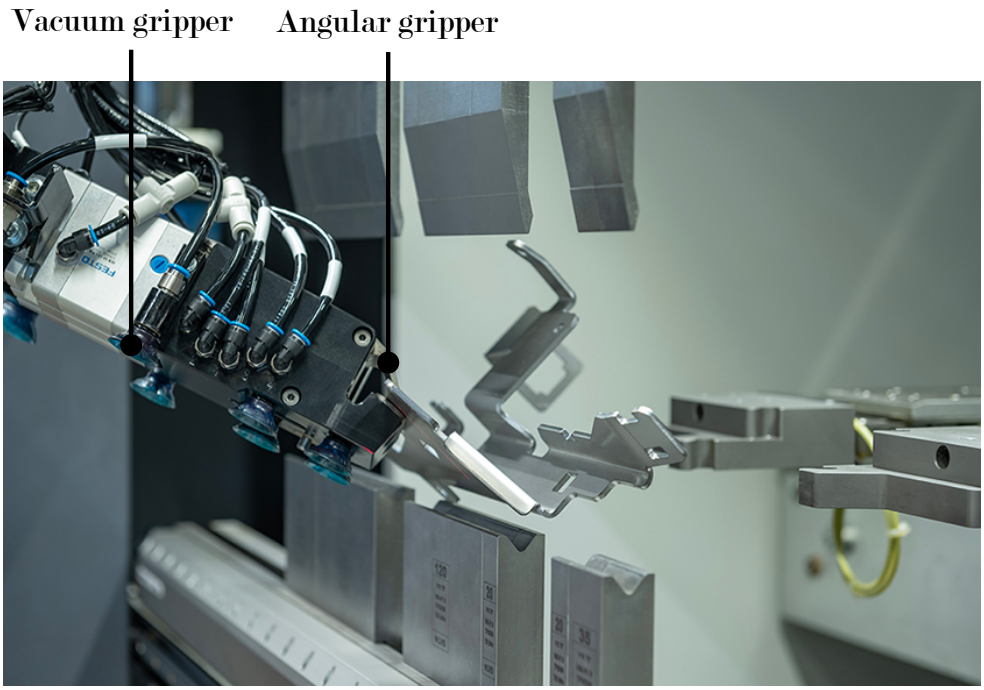


Figure 2.35.: Multi gripper (angular + vacuum) solution adopted by LVD [33].

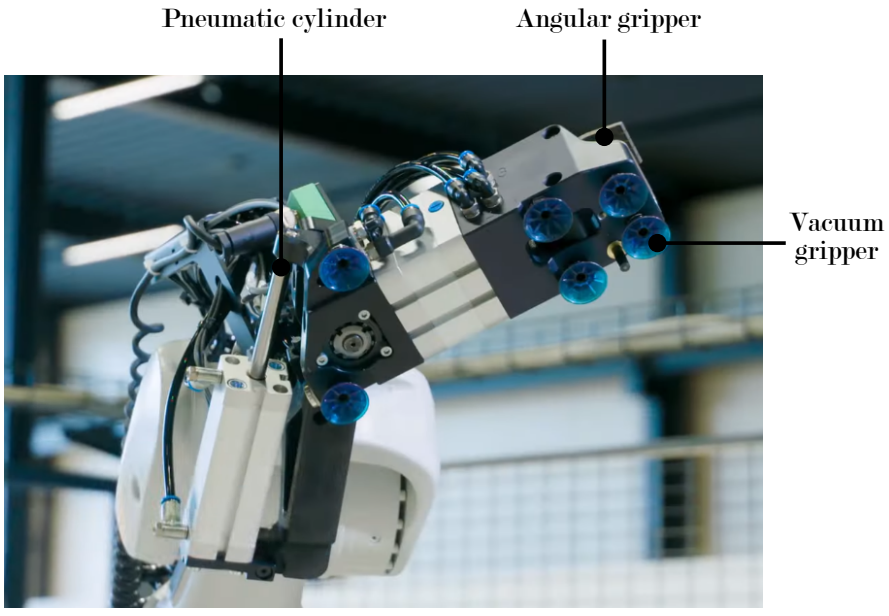


Figure 2.36.: Multi gripper manipulating a small sheet metal during a bending operation [33].

Figure 2.37 shows Bystronic multi gripper solution that combines a parallel gripper with a vacuum gripper (1 vacuum cup). It has a simpler design and it is smaller than the one from LVD, which is ideal for handling even smaller parts.

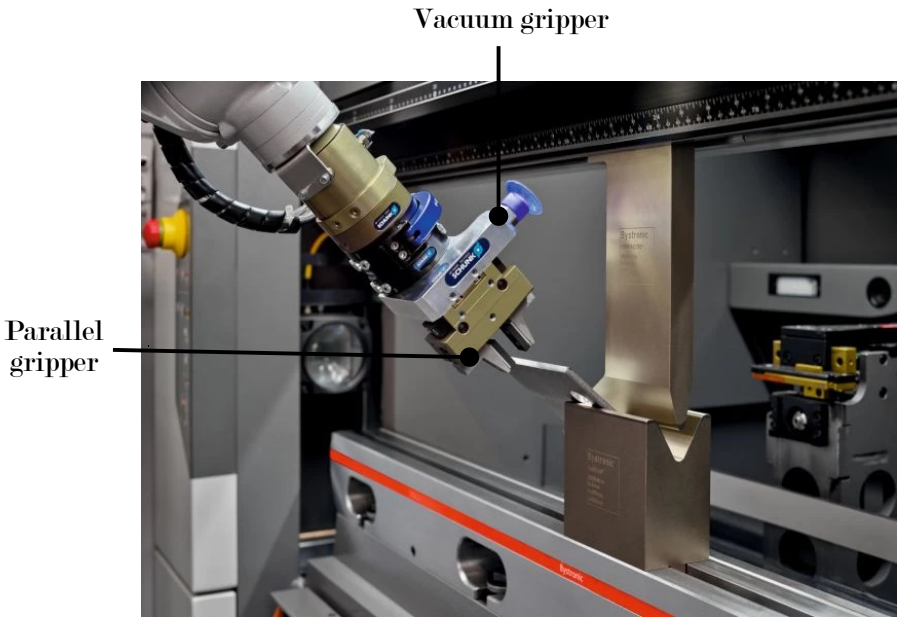


Figure 2.37.: Multi gripper solution (parallel + vacuum) [34].

Figure 2.38 shows SafanDarley simple solution. The main structure of the gripper is a bent plate with a basic design. It is a cheaper constructive solution, but it is not as versatile as the previous options.

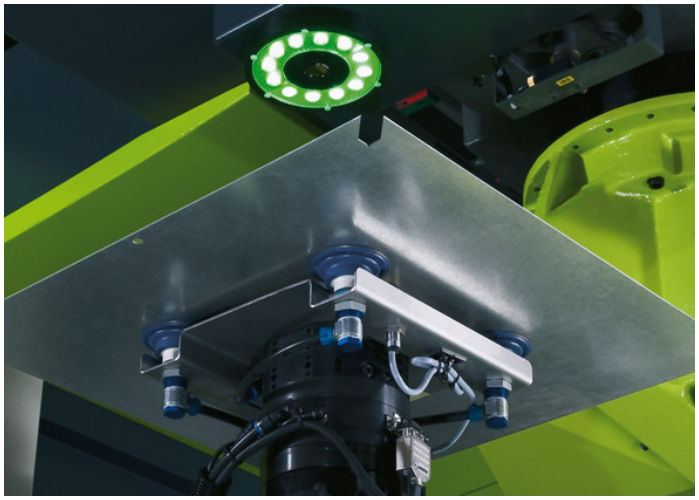


Figure 2.38.: Simple gripper solution by SafanDarley [35].

2.4.3.2. Medium parts manipulation

Figure 2.39 presents an adjustable gripper designed by Trumpf that allows the user to create the gripper configuration that best suits the application. It is possible to manually adjust the distance from each vacuum cup to the profile at the centre of the gripper, allowing it to handle a wide range of sheet metal sizes (small-medium).



Figure 2.39.: Adjustable gripper designed for a wide range of sizes [25].

The solution presented by Dafan is a more bulky vacuum gripper that can handle larger sheet plates than the previous solution. It has two rows of vacuum cups, each one inserted into an aluminium profile. These profiles are excellent accommodation structures for a larger gripper since they have low weight and allow the manual adjustment of the vacuum cups position along the profile length, as seen in Figure 2.40.

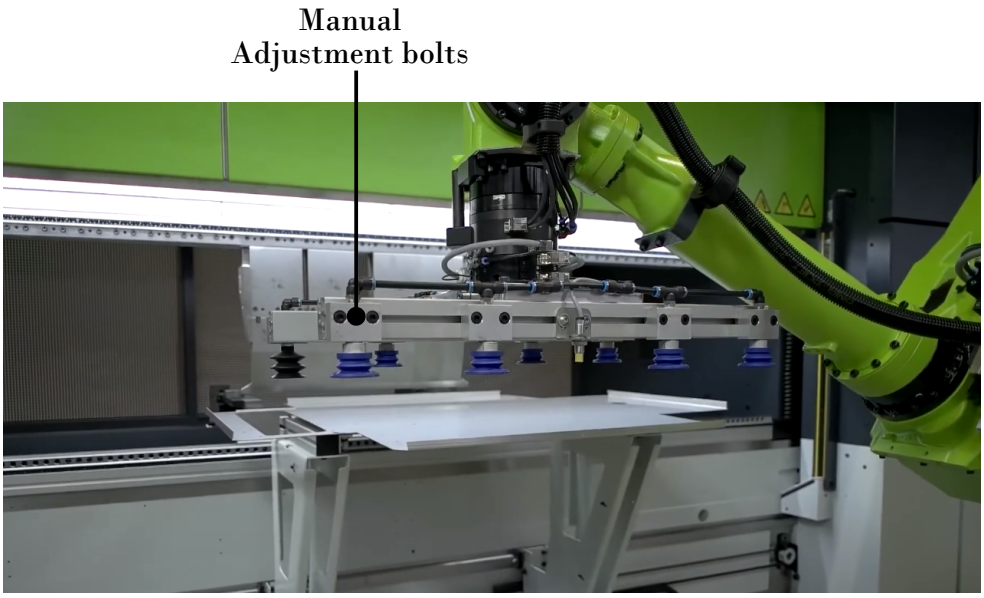


Figure 2.40.: Adjustable gripper built in aluminium profiles in a robotic bending cell [36].

A magnetic gripper solution that is often seen in the industry of sheet metal manipulation is the pneumatic magnetic gripper. It handles the part with great speed and precision and has a great lifting power. The one seen in Figure 2.41 can lift up to 100 kg and it belongs to Goudsmit Magnetics [37]. One of their speciality in various magnetic grippers for the sheet metal manipulation industry.

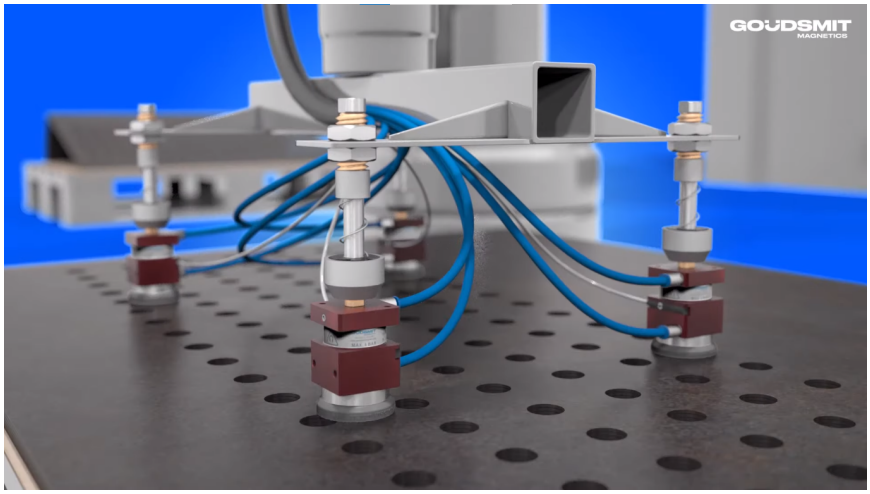
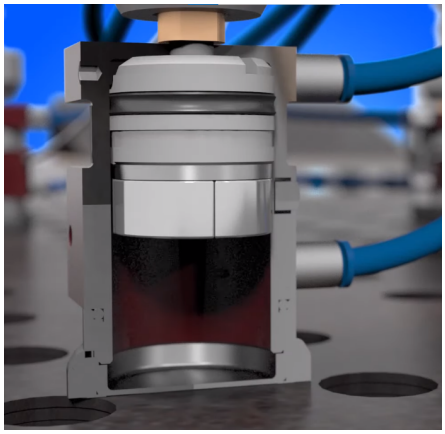
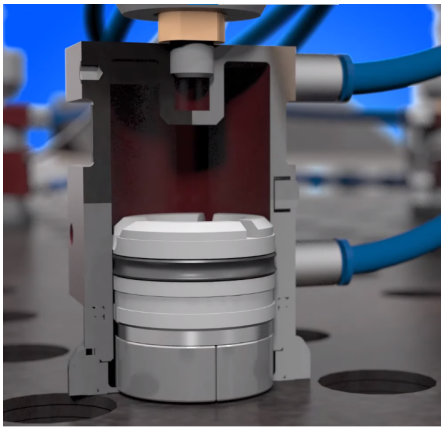


Figure 2.41.: Pneumatic magnetic gripper handling a part in a robotic bending cell [37].

Figure 2.42 represents how the magnetic field is activated or deactivated due to the pneumatic control of the compressed air. In an event of a power loss they can still hold the plate since it does not depend on electric current.



(a) Permanent magnet up - Sheet release.



(b) Permanent magnet down - Sheet prehension.

Figure 2.42.: Cut section view - pneumatic control of the magnetic flow [37].

2.4.3.3. Large parts manipulation

The larger the sheet metal is, the less common it is to see a solution available on the market. If the plate is several meters long, the solution needs to be customized for the costumer. These special solutions are not usually available since they have a very specific purpose, which makes them very expensive.

Salvagnini did a solution for a large and heavy sheet metal. The vacuum cups are accommodated in two staked aluminium profiles, as seen in Figure 2.43 and 2.44. Besides that, there is a structure made of these profiles in the centre of the gripper as well. They have the function to grant stability and resistance to the whole gripper. This is a main concern in larger grippers.

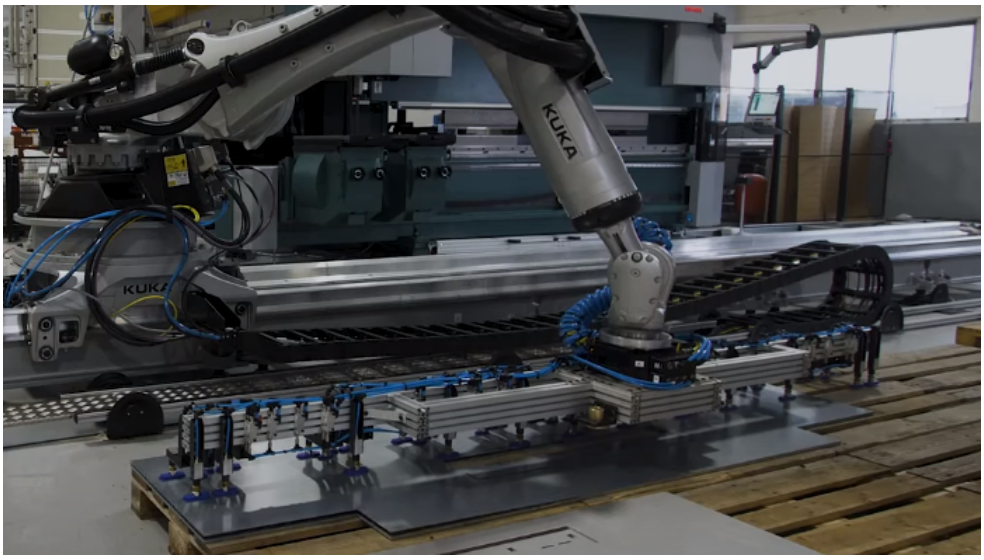


Figure 2.43.: Vacuum gripper initial contact with a large sheet metal [38].

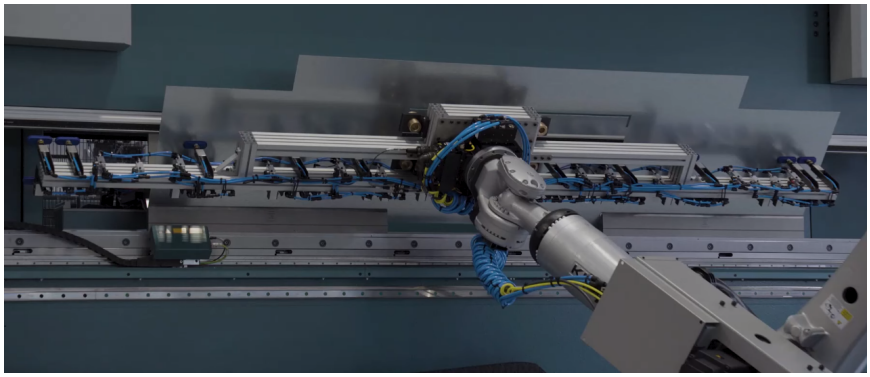


Figure 2.44.: Vacuum gripper manipulating a large sheet metal. [38].

2.4.4. Coupling interface between gripper and robot

There are different configurations regarding the gripper's fixation mechanism in order to ensure the correct attachment between the robot and the gripper. The main function of the interface is to ensure the exchangeability and to the keep the accurate orientation of the gripper. A bad connection between both can lead to catastrophic events inside the bending cell. There are several solutions available in the industry for the integration of both components. The coupling mechanism can consist in a mechanical or an automatic solution.

2.4.4.1. ISO standard for mechanical interfaces - plates

Regarding the design of the mechanical interface, there is an international standard that covers the subject. ISO 9409-1:2004 facilitates the design of plates as mechanical interfaces for the manipulation of industrial robots. It focus on the dimensioning of the plate, covering the main dimensions, designation and marking for a circular plate as a flange interface. So, it provides useful information to dimension both bolt patterns for each side of the flange: gripper side and robot side. It does not cover load-carrying ranges of the interface. It needs to be designed considering the weight of the application and the robot payload capacity [39].

Mechanical interfaces whose dimensions are in accordance with this standard are designated as follows [39]:

$$\text{ISO 9409-1 - } d_1 \text{ - N - } d_4$$

Where:

- d_1 - Pitch circle diameter;

- N - Number of threaded holes;

- d_4 - Thread of hole.

The standard recommends that the dimensions of the interface be specified according to Table 2.45 - series 1. In special situations where the dimensions specified in series 1 are not sufficient for the intended application, the series 2 may be used in it's place.

Position	Pitch circle diameter, d_1		d_2	d_3	d_4	d_5	d_6	t_1	t_2	t_3	t_4	t_5	t_6	Number of holes
	Series 1	Series 2	h8	H7		H7		min.	min.	min.			min.	N
1	25		34	16	M4	4	See 4.4	6	4	4	See NOTE	0,2	0,5	4
2		31,5	40	20	M5	5			5					
3	40		50	25	M6	6			6	6			1	
4		50	63	31,5										
5	63		80	40										
6		80	100	50	M8	8			8			0,4		6
7	100		125	63										
8		125	160	80	M10	10		8	10	8				
9	160		200	100										
10		160	200	100	M12	12			12					11
11		200	250	125										6
12		200	250	125	M16						22			12
13	250	250	315	160	M12						See NOTE			6
NOTE The minimum depth of the threaded holes, t_4, is dependent on the material of the end effector coupling devices														

Figure 2.45.: Circular mechanical interface dimensions [39].

Figure 2.46 shows an example of a technical drawing for one of the sides of the mechanical interface, following all the recommendations of Table 2.45 - position 10.

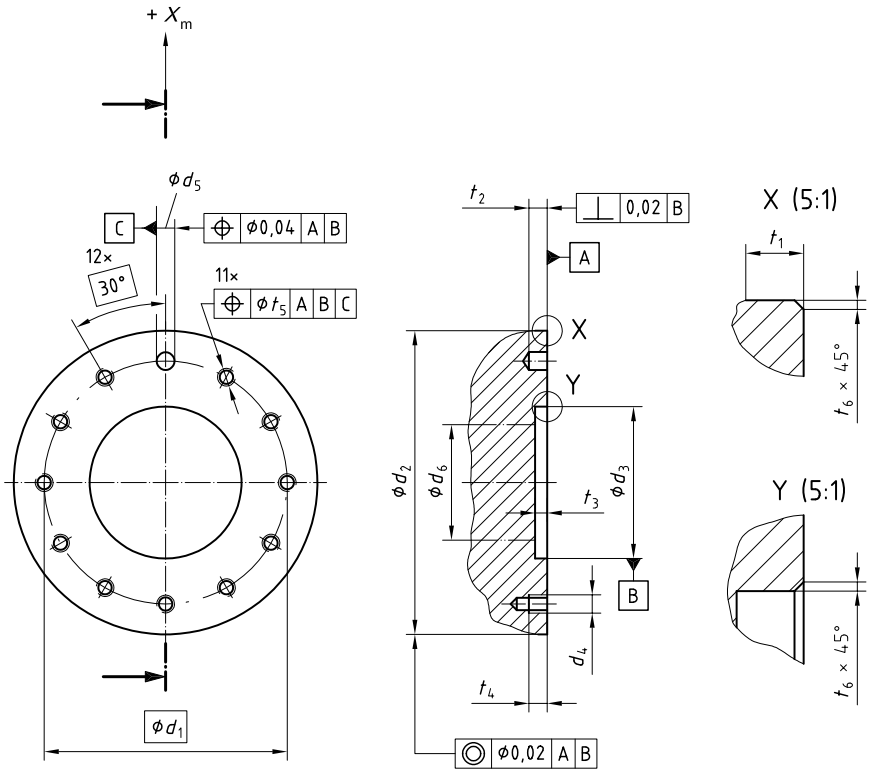


Figure 2.46.: Design of a circular plate interface according to Table 2.45 [39].

The values of d_2 (flange diameter), d_3 (centring diameter) and d_5 (pin diameter) presented on the Table 2.45 are dependent on the application. The pin diameter is intended to have a pin fitted there if necessary.

If the application requires routing service lines for whatever reason, the corresponding diameter is d_6 and shall have a value equal or less than d_3.

The correct designation of this circular plate is: ISO 9409-1 - 160 - 11 - M12.

Some robot and gripper manufacturers do not follow this standard and they create their own bolt patterns for the interface. This can be a problem since, depending on the robot manufacturer chosen, the connection may require a different bolt pattern. If the manufacturer is following the standard, the dimensioning of the two bolt patterns for the gripper side and the robot side can be easily implemented on the flange interface.

2.4.4.2. Manual coupling solution

A manual coupling interface is implemented by means of fastening elements such as bolts or other manual mechanism requiring human intervention. This is an excellent choice for a robotic bending cell that is able to bend and manipulate all the parts intended without having to change the gripper. If the gripper needs to be switched by another gripper fre-

quently to adapt for the manipulation of another part, it requires human labour and time losses, which decrease cell productivity. However, it is imperative to take into account that a manual solution can be a lot cheaper than an automatic one.

A technical drawing of a mechanical interface made by Robotiq that follows the recommendations of the standard is represented in Figure 2.47 [40]. There are two bolt patterns, one for the robot side (interior pattern) and the other for the gripper side (external pattern) to ensure the correct attachment for both sides. The standard designation for the pattern on the robot side is: ISO 9409-1-31.5-4-M5. Although this is a viable, simple, and economic solution for an interface, in order to change the gripper, it is necessary to loosen the bolts from the gripper side and then tighten them again with the new gripper, which costs a lot of time.

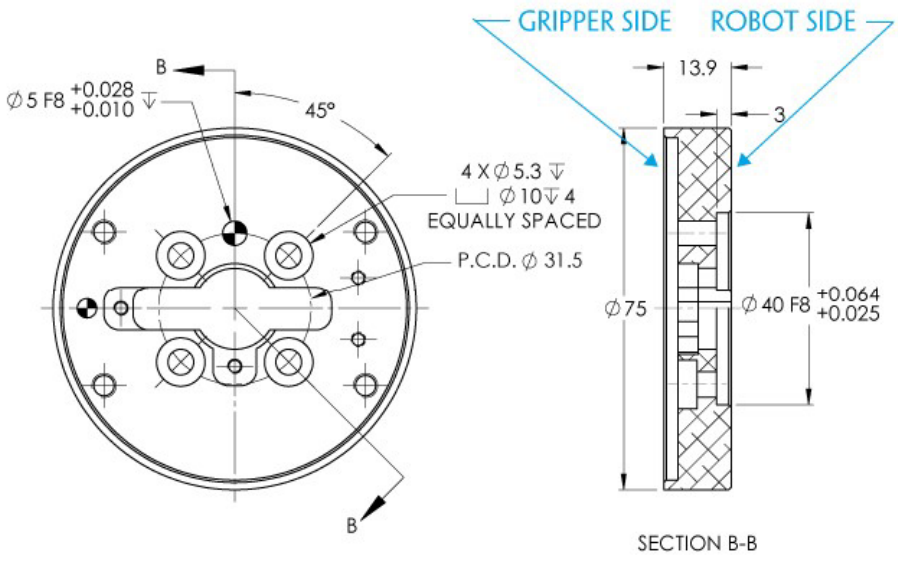


Figure 2.47.: Technical drawing of a mechanical flange interface for both the gripper and the robot [40].

Zimmer group is a manufacture specialist in the fields of automation and machine tooling technology. They have an interface solution - HWR2000 - which is designed exclusively for a manual operation. It offers an easier manual locking mechanism which minimise loss times by allowing a complete gripper change in seconds. It consists of two interfaces, as seen in Figure 2.48, one coupled onto the robot side and the other on the gripper side through bolt patterns that follow the previously analysed standard. It also has an integrated air transfer system for housing pneumatic hoses.



Figure 2.48.: Zimmer solution for a manual locking mechanism (HWR2000) [41].

The attachment and locking of both interfaces is made with an allen wrench by moving the eccentric shaft in one direction or the other. Figure 2.49 shows the locking mechanism sequence. There is an intermediate step (2) where the two interfaces will securely attach through two pins, not allowing the grippers and the workpiece to fall unintentionally. However, the locking position is only achieved in the final step (3) by turning the eccentric shaft into the locking position [41].

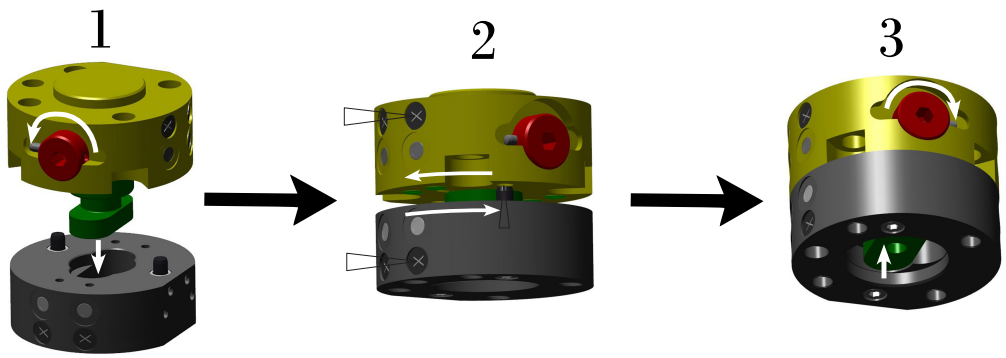


Figure 2.49.: Manual locking mechanism sequence (HWR2000) [41].

2.4.4.3. Automatic coupling solution

Automatic coupling systems are innovative solutions that are a must in robotic bending cells with automatic gripper change. The robot is programmed to automatically place the current gripper on the gripper change station in the proper position, activate the clamping mechanism, and fit it into the gripper flange whenever the operator wishes to switch grippers. The most common solution is pneumatic actuation. This automatic solution may incorporate a mechanical interface as an adapter plate if the attachment on the robot side or the gripper side is still not compatible.

This is an excellent solution for flexible and versatile robotic bending cells. Being able

to automatically change the gripper without manual intervention is a great advantage that leads to a higher cell productivity and a wider range of applications. This will increase the application efficiency, cycle time and process reliability.

SCHUNK is a manufacture specialist on tool clamping technologies. Their quick-change system (SWS) automatic grip solution is mounted onto the robot and the gripper, and pneumatically couples onto your tool ensuring that the connection is secure [42]. This solution already incorporates the standard ISO 9409-1 mounting pattern for easy attachment to the majority of robots available on the market without the requirement for an additional adapter plate. However, in some situations the use of an adapter plate as a mechanical interface may be necessary. The SCHUNK solution, seen in Figure 2.50, is divided into two interfaces. The quick-change master (SWK) whici is coupled through a bolt pattern on the robot side and the quick-change adapter (SWA) on the gripper side. In a robotic bending cell with an automated gripper change station, the SWK is always coupled onto the robot and the SWA onto the gripper. For each gripper in that station, they must have the SWA interface already coupled in order to attach to the robot when a gripper change is being carried on automatically.

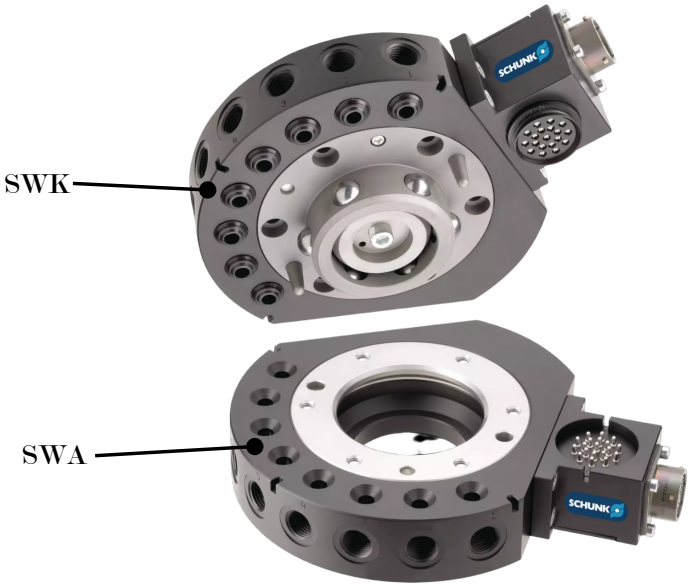
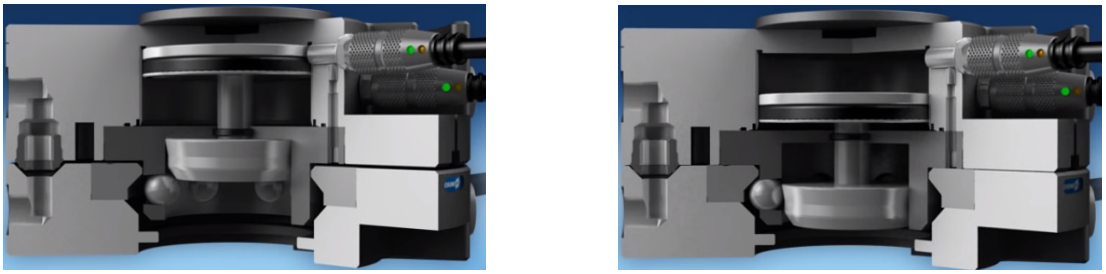


Figure 2.50.: SCHUNK quick change automatic grip solution [42]

The locking mechanism consists in a pneumatically driven locking piston that pushes the spheres seen in Figure 2.51 into a conical cavity.

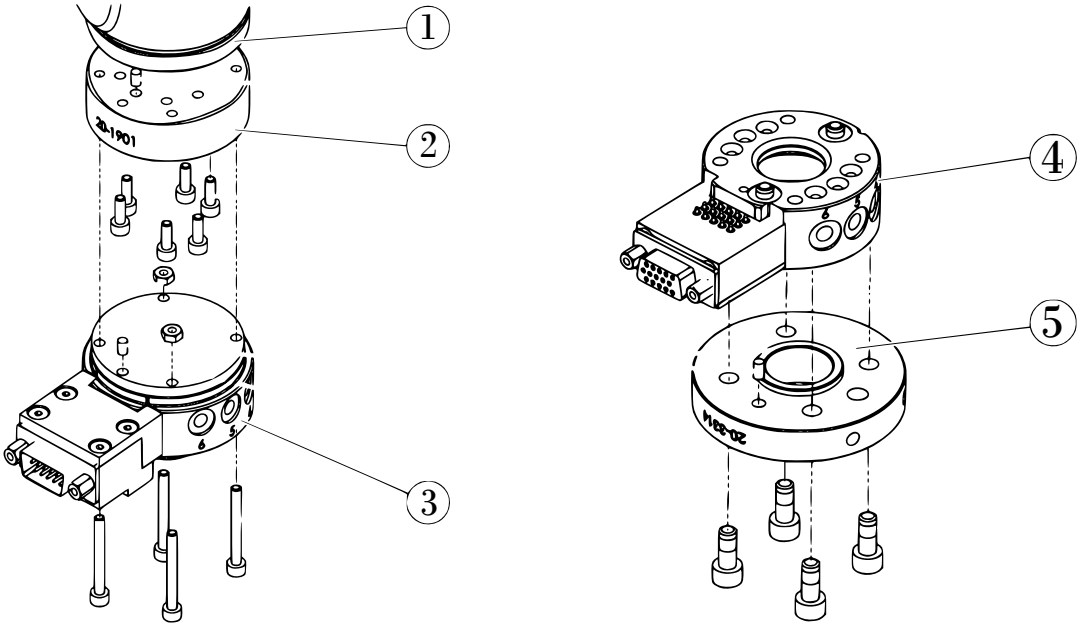


(a) Top dead centre piston position (locking mechanism not engaged).

(b) Bottom dead centre piston position (locking mechanism engaged).

Figure 2.51.: Cut section view - SCHUNK locking mechanism [42].

As an example, Figure 2.52 represents the SCHUNK automatic solution with 2 adapters plates, one the robot side and one for the gripper side, to ensure the correct attachment between all the interfaces.



(a) Robot side.

(b) Gripper side.

Figure 2.52.: Example of an automated coupling mechanism using an adapter plate for each side [42].

1. Robot;
2. Adapter plate (mechanical interface) - robot side;
3. SWS;
4. SWA;
5. Adapter plate (mechanical interface) - gripper side.

3. Problem characterization and proposed solution

3.1. Introduction

The proposed challenge involves a real case of process optimization in the manufacture of aluminium fishing boat hulls. The customer has a manual production line to manufacture boat hulls using old equipment and wants to renew and automate the whole process. The main manufacture process used by the customer to transform the initial flatten sheet metal into a boat hull is the sheet metal bending. The flatten part goes through multiple bends in order to achieve the final shape of a boat hull. In the end, welding is used in the necessary locations in order to close the hull. Figure 3.1 shows a press brake that is being used by the operators to manually bend the parts and it also shows different sheet metals that will be bent into different boat hulls.



Figure 3.1.: Press brake used by the customer in their current manual boat hull production line.

The customer produces multiple boat hulls with different shapes, dimensions, weight and geometries. As an example, Figure 3.2 shows a boat hull after both the bending and welding process.



Figure 3.2.: Example of one type of boat hull produced after the bending and welding operations.

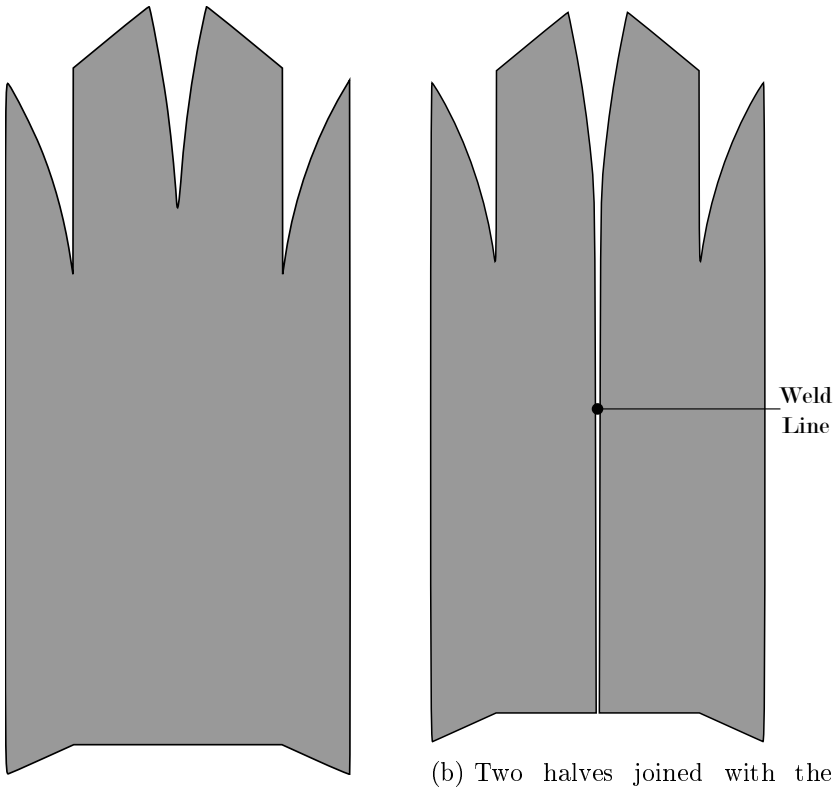
The customer was looking to automate and simplify their manufacturing process of the hulls, converting the current manual production line into an automatic one by implementing a robotic bending cell. Therefore, it is imperative to design a gripper that needs to be able to manipulate the part through all bending operations, taking into account the part's geometry, material, dimensions and weight. Besides that, one of the requests was to develop the gripper, implementing a modular design that would allow for the adjustment of each cup position if needed for other applications.

3.2. Flatten boat hull

For this study, the client requested that the gripper be designed to handle the largest and heaviest boat hull produced by them, as it would be the most challenging one. The flatten sheet metal before it undergoes any manufacture process is presented in Figure 3.3. Since this specific boat hull is larger than the common ones, the flatten sheet metal is divided into two symmetric parts. Each part will go through the necessary bending operations and then they will be welded together in the middle.

The challenge of gripping this sheet metal comes mainly due to the part size, weight and geometry, as seen in Table 3.1. A crucial task upon the design of the gripper is to guarantee that the deflection of the sheet metal itself while being manipulated through the bending operations is between acceptable values. This is very challenging due to the considerable small thickness of the workpiece. High deflection values can compromise the whole bending process. Besides that, the 'V'-shape of this part may cause a stress concentration at the end of the 'V' and each side of the 'V' will have more tendency to present higher deflection values, if the workpiece is only grasp on the left or the right side of the 'V'. The 'V' shape geometry is presented in Figure 3.4.

As said previously, the material of the boat hull is the aluminium alloy 5052-H32. It has good weldability, workability and very good corrosion resistance in marine atmospheres, which is a very important characteristic for a boat hull. Table 3.2 presents the mechanical



(a) Top view.

(b) Two halves joined with the welding line.

Figure 3.3.: Initial flatten boat hull.

Table 3.1.: Weight and geometry dimensions of the flatten boat hull.

Length/mm	Width/mm	Thickness/mm	Weight/kg
7416.8	1663.7	3.2	109.18

properties of this aluminium alloy.

Table 3.2.: Mechanical properties of Al5052-H32.

Properties	Values
Young's modulus, E/GPa	70
Poisson's ratio, ν	0.33
Density, ρ/kg m^{-3}	2680
Yield Strength, σ_y/MPa	193
Tensile Strength, σ_r/MPa	228

The grasping method used for the gripper will be achieved using vacuum cups since aluminium is a non-ferrous metal and do not allow the use of a magnetic gripper. In this case, a vacuum gripper is the obvious choice because they are able to grip and move very large and heavy workpieces, making them excellent choices for the manipulation of large, non-ferrous workpieces [23].



Figure 3.4.: 'V' shape location on the flatten sheet metal.

3.3. Bending manufacture operations

All the bending operations realized on the flatten sheet metal were provided by the customer. The technical drawing containing all the relevant information cannot be presented here due to the confidentiality issues. Figure 3.5 shows a draft containing all the main dimensions, and the four bending lines (BL).

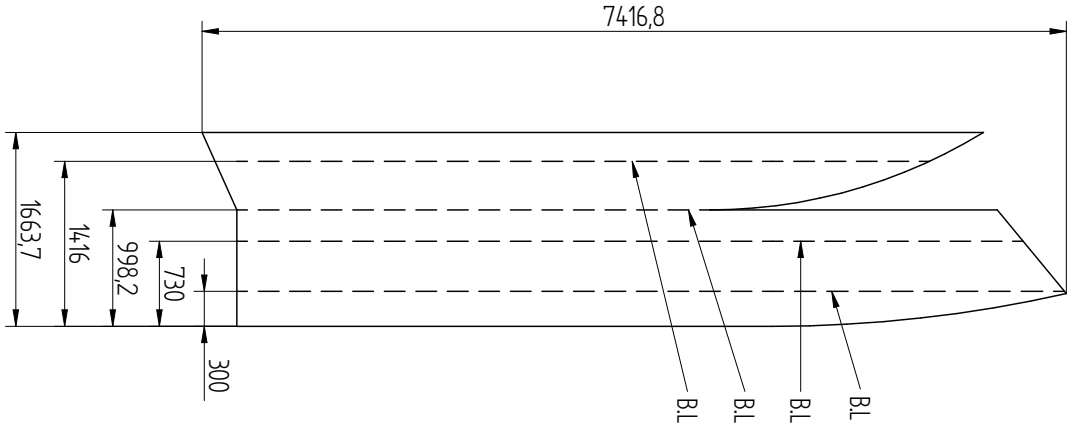


Figure 3.5.: Draft of the four bending lines on the flatten boat hull.

Firstly, the part undergoes three bending operations. These bending operations are achieved using special tools, such as a radius punch, in order to obtain a U-shape in the cross section geometry. Figure 3.6 shows an example of this process using special tools. A radial punch is large enough to penetrate the sheet metal to form the U-shape bend.

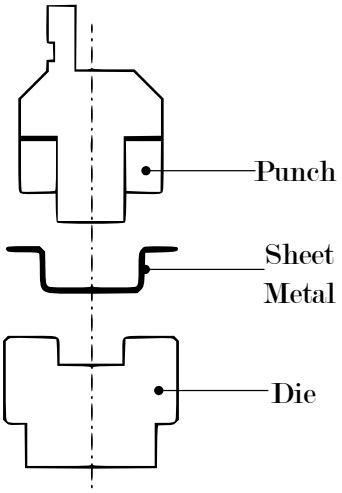


Figure 3.6.: U-Bending schematic with special tools [43].

The purpose of these three bending operations is to increase the strength of the material due to cold working. When the part is subjected to this bending process, the aluminium's crystalline structure will change permanently, causing an increase in strength [14]. Besides that, changing the thickness geometry with this U-shape will also mean less deflection of the flatten part since the second moments of area on both cross-section axes will increase, leading to a higher flexural rigidity (stiffness of a material when subjected to bending). Figure 3.7 shows the part after this first process.

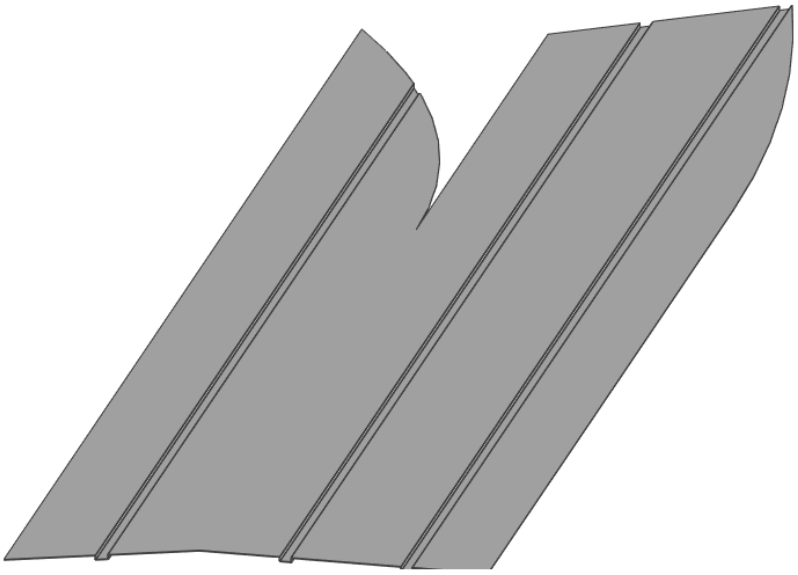


Figure 3.7.: Flatten sheet metal after the four consequent bends (U-shape).

Finally, the sheet metal will undergo one more bending process. This one is a standard bending operation using a standard tool set in order to bend the part with the specific bending angle of 30°. This operation is responsible for shaping the side of the boat hull, as seen in Figure 3.8. This final bending process is the most challenging one, since the gripper can only grasp the workpiece on the left side of the bending line or on the right side, which

means a large deflection of the workpiece. The goal is to use the same gripper as a handling system for both bending processes.

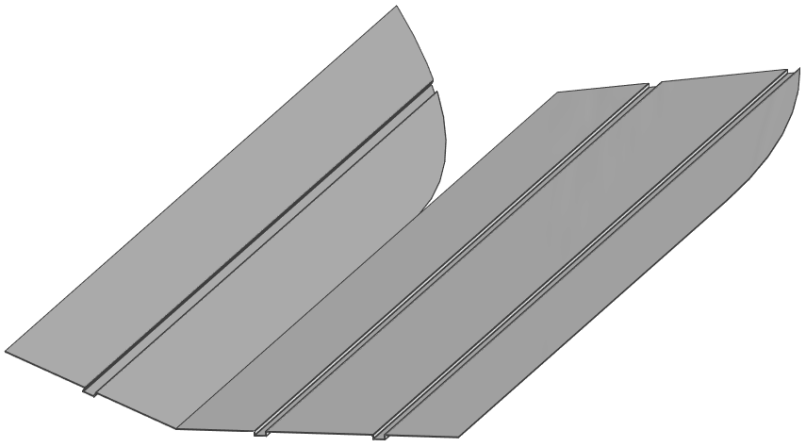


Figure 3.8.: Flatten sheet metal after the final side bend.

The gripper needs to be designed taking into account these two bending steps that will take place inside a robotic bending cell. Afterwards, the two symmetrical parts are going to be welded in the middle, and several other operations will take place in order to shape the bent sheet metal into a boat hull. The following manufacturing processes aren't relevant to the gripper design.

3.4. Robotic bending cell implementation

The engineering team at ADIRA did an initial cell layout, as seen in Figure 3.9. Two eight meter press brakes with different characteristics were selected (1, 2), each one responsible for each bending operation previously seen. The robot (3) is placed in the middle of the two machines and has a track in order to move from one side of the cell to the other. A reference table (4) and both pallet stations were also introduced in the layout (5).

As already said, this is only the first design iteration for the robotic bending cell layout. The whole design and location of the components can change entirely. The need for a regrip station will be assessed during the course of the project. It will also be assessed whether it is possible to carry out all operations using only one gripper, which would be the ideal solution. As mentioned earlier, the second part of the bending process may not be possible to do using a gripper as the manipulation system. This would change the design for the robotic bending cell layout and the need to find a new automated solution for that process. Therefore, this concern will also be addressed in the following chapters and a study will be done analysing the possibility of carry out that operation with a vacuum gripper.

3.5. Initial robot selection

Before starting the project, the robot needed to be selected. When it comes to robotic bending cells, the robot is challenged by precise angular or linear motions and consider-

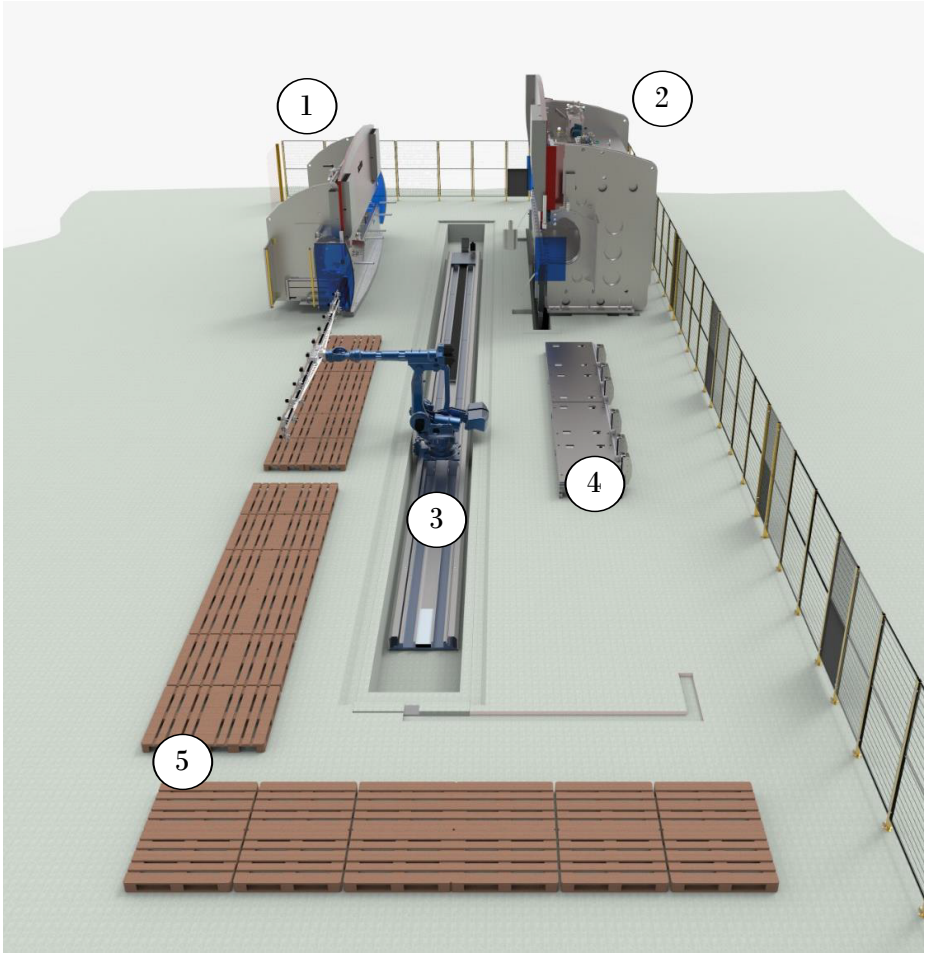


Figure 3.9.: Robotic bending cell initial layout.

able reaction forces and moments. For these applications, a robust robot is a must that can handle high repetitive accurate motions, reasonable axis speeds, and present very good path performance, whether it is circular or linear movements [44].

The manufacture of industrial robots chosen was YASKAWA, since ADIRA is already used to work with their robot solutions. They are one of the largest manufactures of industrial robots and offer a wide range of solutions for different handling robot applications. For robotic bending cell applications, they recommend the use of their GP series [44].

The two major differences between each model of the GP series is the payload and the covered area. The maximum covered area defines the area of the workspace the robot can reach, which can be important depending on the specific task that the robot will perform. The payload is usually the first technical specification used to define and choose a robot. It corresponds to the mass that the robot wrist can support, whether it is the workpiece mass or the gripper mass. It is expressed in kilogram.

For this application, the payload is a crucial specification for the design of the gripper. The robot payload must withstand both the gripper and the workpiece mass. The workpiece mass is 109.18 kg. Regarding the gripper mass, it is only possible to estimate a value based on similar solutions or projects available on the market, such as the ones discussed in Section

2.4.3. The gripper mass was estimated to be around 250 kg. The robot payload must be higher than the sum of both masses, as seen in equation (3.1).

$$\text{Payload} \geq 109.18 + 250 \Leftrightarrow \text{Payload} \geq 359.18\,\text{kg} \tag{3.1}$$

In YASKAWA GP series, the robot with the closer and higher payload than 359.18 kg is the GP400 represented in Figure 3.10.

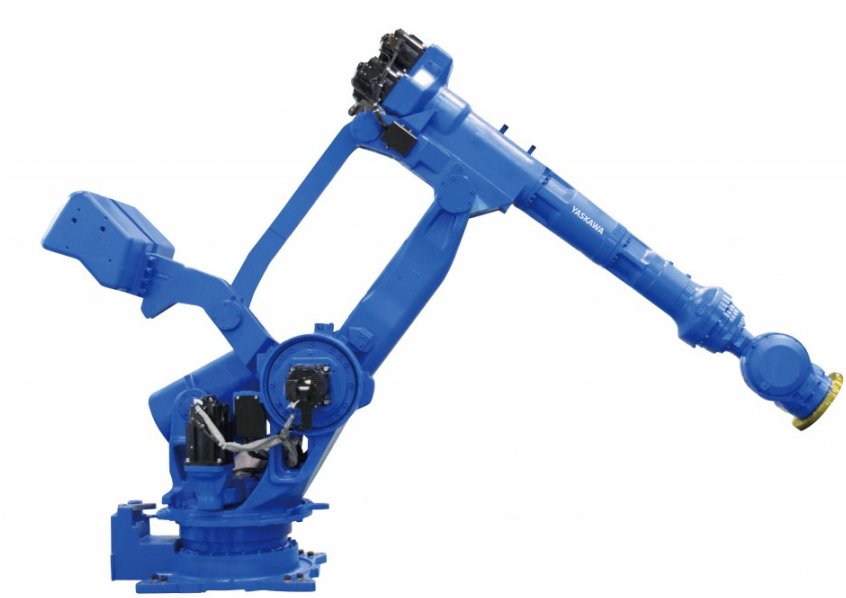
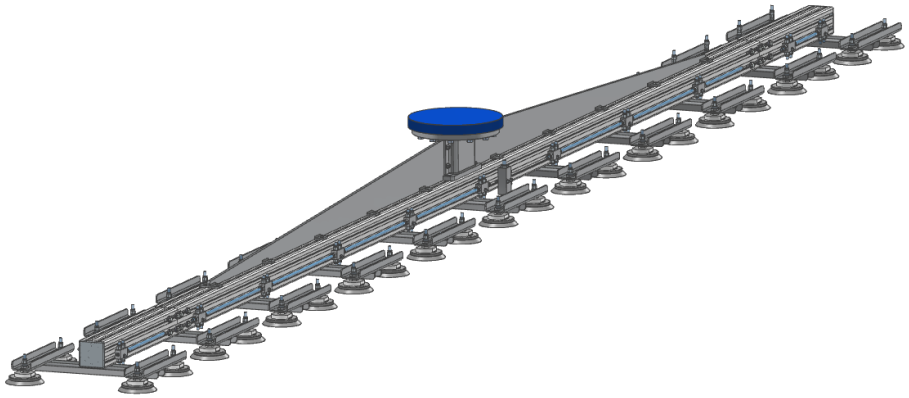


Figure 3.10.: Industrial robot from YASKAWA: GP400 [44].

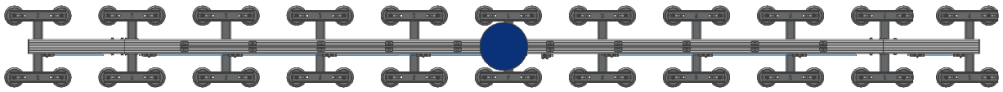
The GP400 handling robot provides a payload of 400 kg and a maximum reach of 2942 mm. Appendix A shows all the technical specifications of the robot and the technical drawing of the robot. The technical draw is very useful to design the interface for the gripper and the robot.

3.6. Proposed gripper design solution

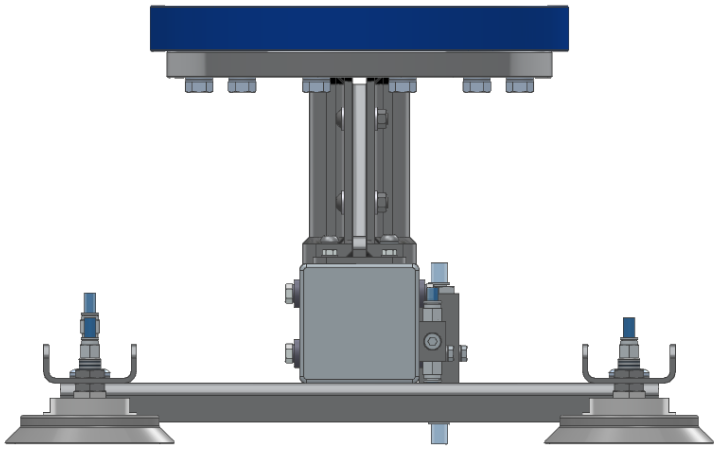
Figure 3.11 shows the 3D CAD of the final gripper design solution on the SolidEdge software. The pneumatic tubes were cut in order to allow the full visualization of the gripper.



(a) First isometric view.



(b) Top view.



(c) Left view.

Figure 3.11.: 3D CAD representation of the final gripper design solution.

Some of the most important characteristics that were achieved with this gripper design are the following:

1. High reliability combined with easy maintenance service;
2. Structural reliability with respect to the stability of the workpiece position and path

orientation;

3. Reduce as much as possible to satisfactory values the deflection of the gripper during the workpiece manipulation;
4. Optimum adjustment of the gripper considering the operations that will be performed;
5. Large adjustment range of the vacuum cups due to the adopted modular design of the gripper that will be able to grasp parts with different shapes and sizes;
6. Robustness of the whole structure;
7. Good wear resistance of all parts designed;
8. Easy transportation, assembly, and installation;
9. A very robust vacuum system with more than one branch of vacuum generation capable of holding the workpiece in place;
10. Design of all parts with reduced sharp edges and increased edge radius in order to reduce human contact injuries;
11. Safe coupling connection between the gripper interface and the robot interface;
12. Simple gripper design with a low global mass.

Figure 3.12 and Figure 3.13 shows rendered images of the gripper and its connection to the robot, for a better high quality visualization of the proposed solution.

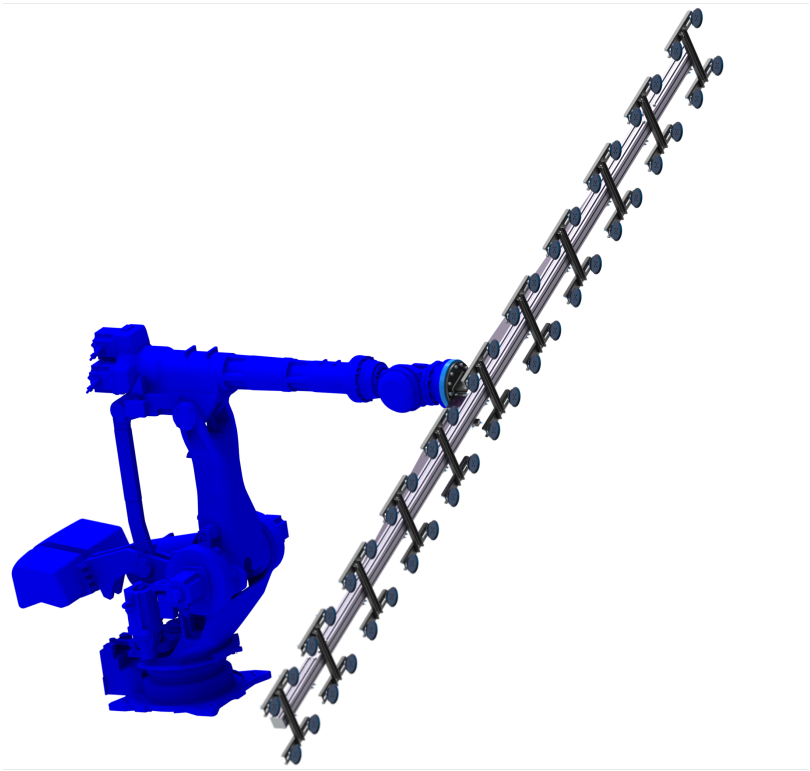


Figure 3.12.: Rendered image showing the connection between the robot and gripper.

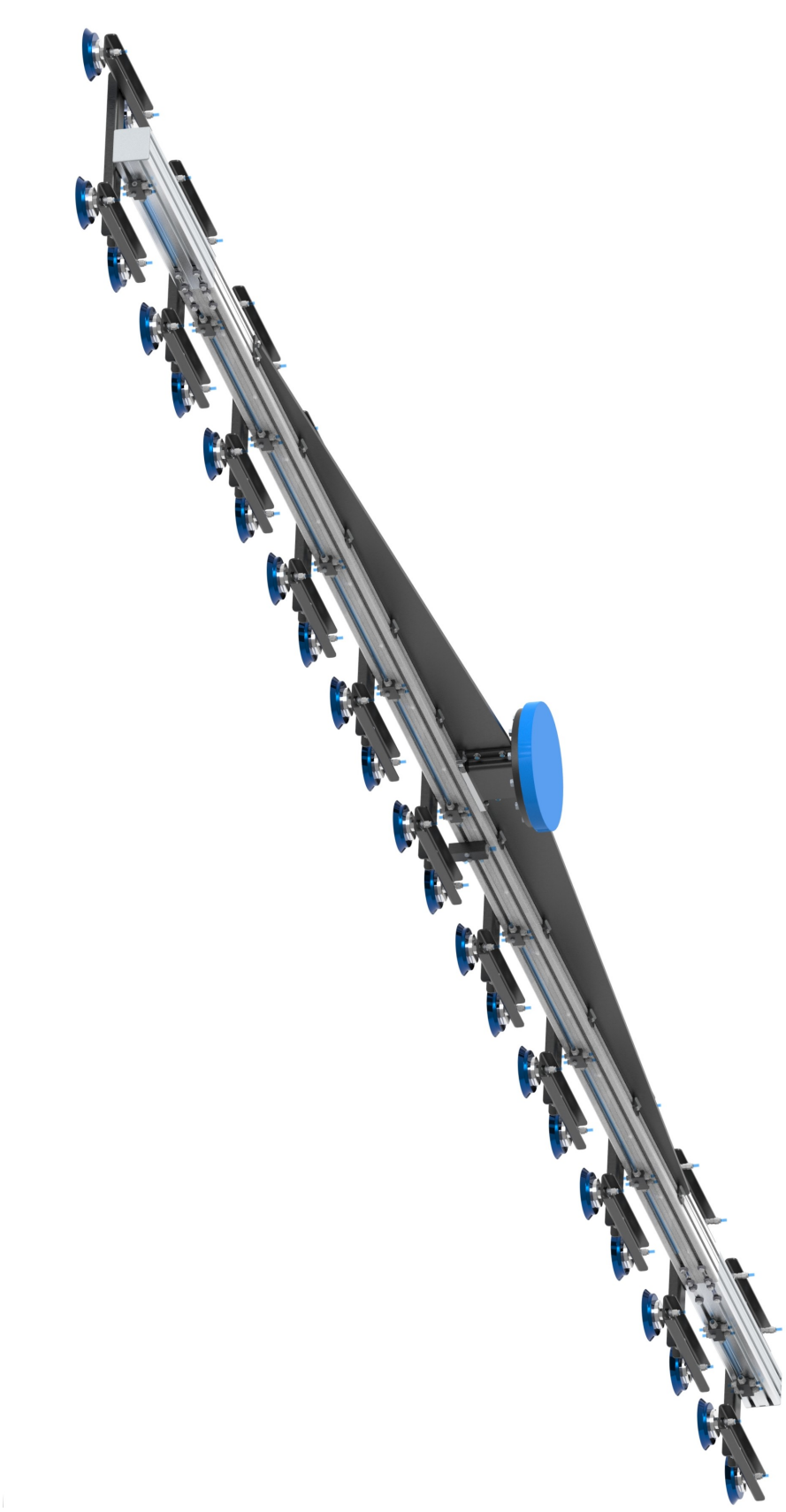


Figure 3.13.: Rendered image from the 3D CAD of the gripper.

3.6.1. Gripper subassemblies

There are four subassemblies in which the gripper can be divided:

1. Aluminium profile subassembly;
2. Structural reinforcement subassembly;
3. Vacuum cups subassembly;
    - Vacuum Cup - 310 mm;
    - Vacuum Cup - 280 mm;
4. Interfaces subassembly.

Figure 3.14 shows the aluminium profile subassembly which consists of aluminium profiles, which represent the main structure of the gripper where all the other parts are connected.

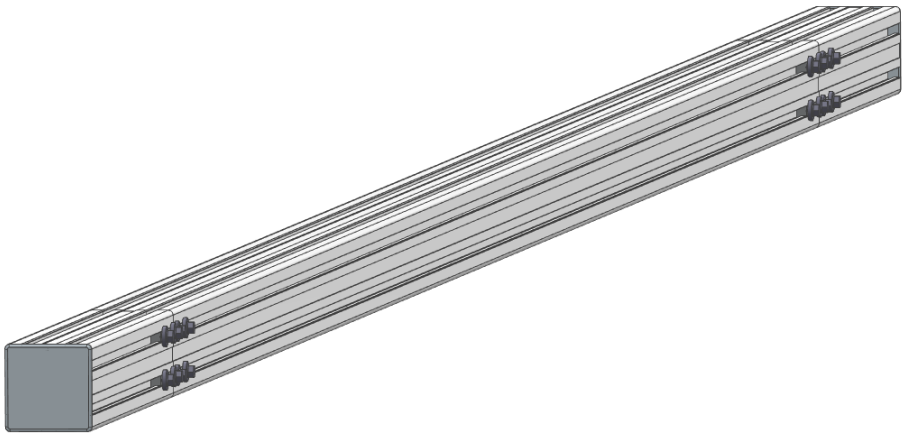


Figure 3.14.: 3D CAD representation of the aluminium profile subassembly.

The subassembly presented in Figure 3.15 consists on the structural reinforcement triangular part used to provide additional strengthening to the aluminium profiles. It is fastened into the aluminium profile.

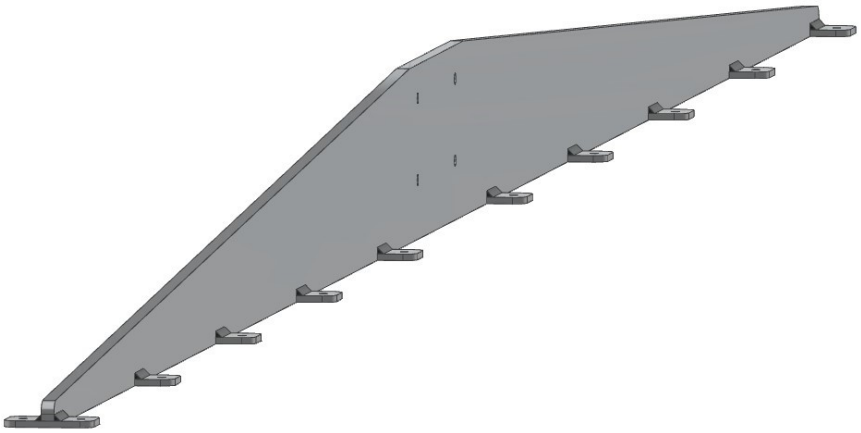
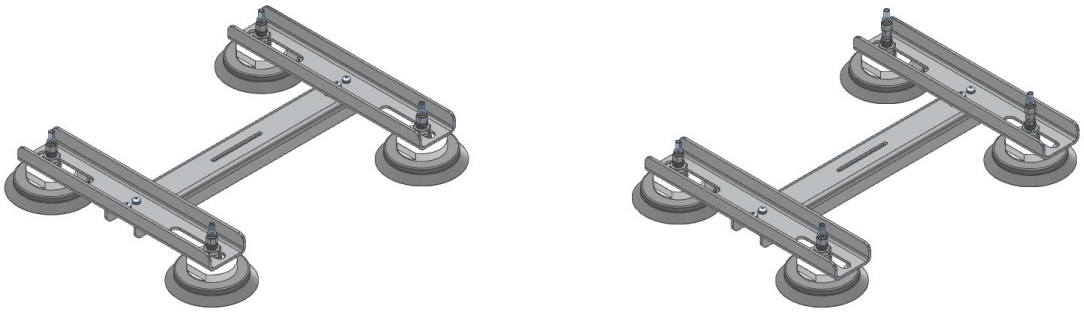


Figure 3.15.: 3D CAD representation of the structural reinforcement subassembly.

Figure 3.16 shows the vacuum cup subassembly, which consists on two 'C' shape profiles connected by another 'C' shape profile, that hold a group of vacuum cups. There are a total of eleven vacuum cup subassemblies. Vacuum ejectors were used to create the vacuum pressure inside the vacuum cups by draining the air through the pneumatic system.



(a) 310 mm subassembly. (b) 280 mm subassembly.

Figure 3.16.: 3D CAD representation of the vacuum cup subassembly.

The interfaces subassembly, as seen in Figure 3.17, consists on the male interface that will attach to the female interface of the robot, the gripper interfaces which will connect to the aluminium profile, and the two 'U'-shaped profiles which will secure the connection to the structural reinforcement. All parts are welded.

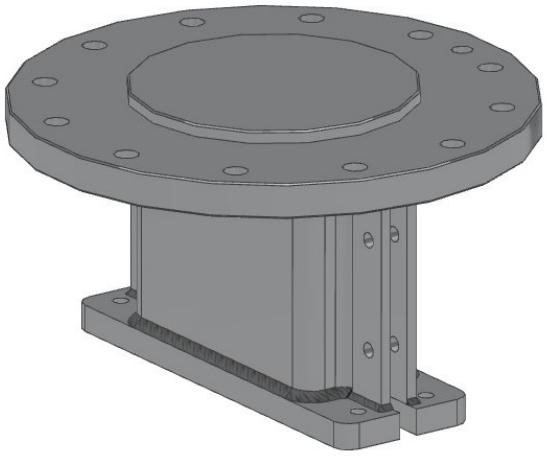


Figure 3.17.: 3D CAD representation of the interfaces subassembly.

3.6.2. Economic analysis

This section delves into the analysis of the overall economic cost associated with the proposed gripper solution design, considering all components and engineering services required. By examining the cost structure, the goal is to present a clear understanding of the investment require. It is important to provide the economic impact of the gripper solution in order to enable future decision-making and strategic planning. This analysis is also crucial for future improvements with the goal of reducing the overall cost.

All steel parts designed expected for the male robot interface were manufactured from the structural steel S235jr, provided by Amorins & Silva, Lda. They supplied all the steel plats and all the laser cutting and bending manufacture operations, as well as the zinc plating of the parts.

Ramada Aços is responsible for providing a cylindrical profile made from Ck45 which was used for the manufacturing of the robot male interface, as seen in Figure 3.17 (Interfaces subassembly).

Equinotec - Soluções de Engenharia, Lda. was is in charge of supplying the aluminium profiles and all the respective accessories.

SMC was responsible for delivering all pneumatic components for the vacuum system and for the whole pneumatic assembly on the gripper.

Fabory supplied all the mechanical connectors (bolts, washers, nuts, and pins).

There is no quotation for the machining and welding manufacture processes because they were done by ADIRA.

Table 3.3 presents all the price quotations provided by the suppliers that were involved in this project.

Table 3.3.: Price quotation provided by the suppliers (*includes transportation).

List of Suppliers	Price/€
Ramada	54.20
Equinotec	1033.82
SMC	2897.35
Amorins & Silva	211.6
Fabory	12.64
Total	4209.41*

The total investment required for this solution is 4203.61 €.

4. Vacuum system

4.1. Introduction

When designing a gripper for the manipulation of a very large sheet metal, the precision, reliability and safe manipulation of the part are mandatory features. The calculation and selection of the vacuum cups and respective allocation on the flatten part is of extreme importance.

In fact, the vacuum cups are responsible for holding the part throughout the bending operations. Comprehending the distribution of forces exerted on the sheet metal by the vacuum cups is imperative to guarantee a successful manipulation and avoid any dangerous scenario where the part may fall from the vacuum cups. Factors such as surface area, suction force, number of vacuum cups, robot acceleration, friction between the cup and the part's surface, and safety factors are extremely important to take into account.

The allocation of the vacuum cups on the flatten part is also a crucial task, especially when grasping a large surface area. The vacuum cups need to be properly allocated to maintain the balance throughout the sheet metal. In this case, since the flatten aluminium part has a very large surface area with a complex geometry due to the 'V' shape, studying the position of the cups and the deflection of the part is a must. For different vacuum cup position, the deflection of the workpiece will change. It is imperative to analyse these boundary conditions in order to ensure a safe manipulation of the part throughout the two bending processes.

Finally, the vacuum cup subassembly structure design will be discussed as well as the whole pneumatic system to allow the flow of compressed air between all vacuum cups and the vacuum ejectors.

4.2. Vacuum cup selection procedure and result

The selection of the vacuum cups is made based on a multi-criterion process. The solution must accomplish simultaneously: support the maximum load (attainable with small or large cups); assure that the deflection of the flatten boat hull does not interfere with the bending process; have a minimum cost.

Considering the maximum theoretical holding force necessary to manipulate the workpiece and the respective price quotation for each vacuum cup, two options were selected from the SMC catalogue as seen below.

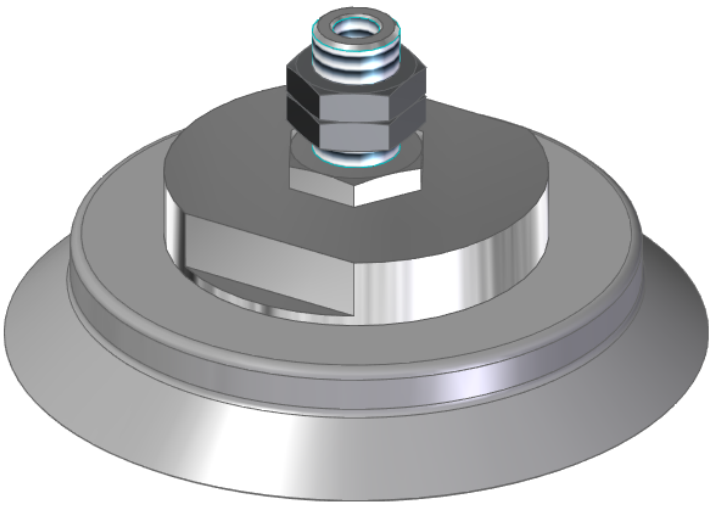


Figure 4.1.: 3D CAD of the final SMC vacuum cup solution selected [45].

Table 4.1.: Vacuum cup selection procedure considering the theoretical holding force, number of cups, and price.

Vacuum Cup Option	SMC Technical Reference	Diameter/mm	Number	Price/€
1	ZPT100HN-A16	100	63	1440.18
2	ZPT125HN-A16	125	40	900.00

The option 2 was chosen because it is the most economic choice. The 3D CAD is shown in Figure 4.1.

After this, the workpiece deflection and the respective vacuum cup allocation were studied through a finite element analysis. At the end, it was concluded that the results obtained from the forty ϕ125 mm cups were very satisfactory making it a valid choice for the manipulation of the workpiece. Adding this to the fact that it is cheaper, the ϕ125 mm was the final choice.

4.3. Total theoretical holding force

The total theoretical holding force is the magnitude of the total force necessary to hold the workpiece without falling, either in a static or dynamic situation. In a practical application, factors such as the deformation of the workpiece, the surface finish, the type and shape of the vacuum cup and the available space for allocating the cups play a crucial role to ensure a safe manipulation.

The static free body diagram of the vacuum cup and workpiece, considering different

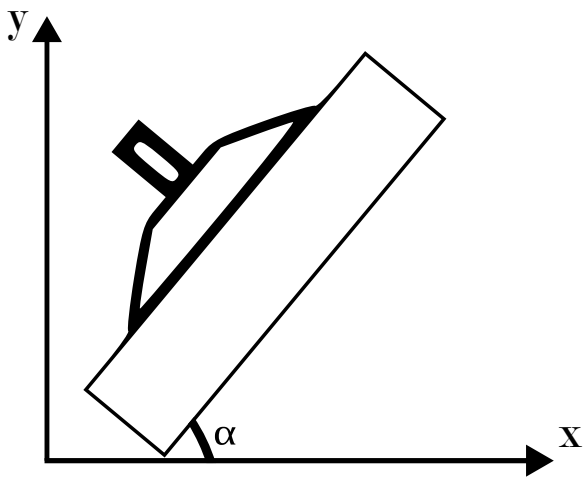


Figure 4.2.: Inclined manipulation scenario with an angle parameter, α.

manipulation scenarios, will be analysed in order to calculate the necessary total theoretical holding force. The two manipulation scenario are the following: horizontal workpiece manipulation and vertical workpiece manipulation.

Although all bending operations are done while the part is in a horizontal position, it is imperative to consider the part's motion from the initial pick-up position until the bending operation. Therefore, both scenarios take place in a practical application. The best course of action is to consider a generic inclined scenario with an angle parameter (α) corresponding to the angle between the workpiece and the horizontal x-axis, as represented schematically in Figure 4.2.

4.3.1. Parameters

Before analysing the static and dynamic force equilibrium, it is necessary to establish all the parameters taken into account and their range of variation. They are presented in Table 4.2.

Table 4.2.: Parameters considered for the static and dynamic force equilibrium.

Parameters	Description	Values
m/kg	Workpiece mass	$109.18\,\mathrm{kg}$
α, $\beta/^\circ$	Angle	$0 \leq \alpha, \beta \leq 90^\circ$
μ	Coefficient of friction	0.5
$a/\mathrm{m\,s^{-2}}$	Robot acceleration	$0.5\,\mathrm{m\,s^{-2}}$

The mass of the flatten boat hull is $109.18\,\mathrm{kg}$.

The angle parameter is 0° for horizontal manipulation situation and 90° for vertical manipulation situation, but in real life the workpiece is going to be manipulated in the following range $[0; 90]^\circ$. So, while calculating the theoretical holding force, the influence of different angles will be studied in order to determine the worst-case scenario of manipulation.

The friction coefficient plays no role in a horizontal situation. Only when shear forces

exist ($\alpha > 0°$) does friction become important to consider. The standard values of friction between the workpiece and the vacuum cups used are the following [23]:

- Oil surface: 0.1
- Wet surface: 0.2-0.3
- Wood, metal, glass, stone: 0.5
- Rough surface: 0.6

For this application, it was considered a coefficient of friction of 0.5. The only manufacture process that the flatten boat hull underwent was laser cut to achieve the intended geometry which does not require oil. So, it is not to expect remains of oil on the part surface.

Robot acceleration parameter was used in the dynamic free body diagram. The manufacture does not provide a maximum value of acceleration for each of the robot axis. The acceleration value will be defined by the robot programmer using a software containing the dynamic model of the robot. However, the robot acceleration that should be used and inputted by the robot programmer on the robot software must be a very small acceleration. For this workpiece, with the main dimensions and complex geometry, which will lead to structural mechanical complications, the robot programmer must limit the maximum robot acceleration to very small values: $0 < a < 0.5\,\mathrm{m\,s^{-2}}$. For the theoretical analytical model, it was chosen the acceleration value of $0.5\,\mathrm{m\,s^{-2}}$.

4.3.2. Static free body diagram analysis

The static free body diagram is represented in Figure 4.3.

Where:

- F_{th}/N - Theoretical holding force;

- P/N - Gravity force due to workpiece mass;

- N/N - Normal reaction;

- $\mu N/\mathrm{N}$ - Friction force.

The gravity force is calculated with equation (4.1).

$$P = m \cdot g \tag{4.1}$$

Where:

- m/kg - corresponds to the workpiece mass;

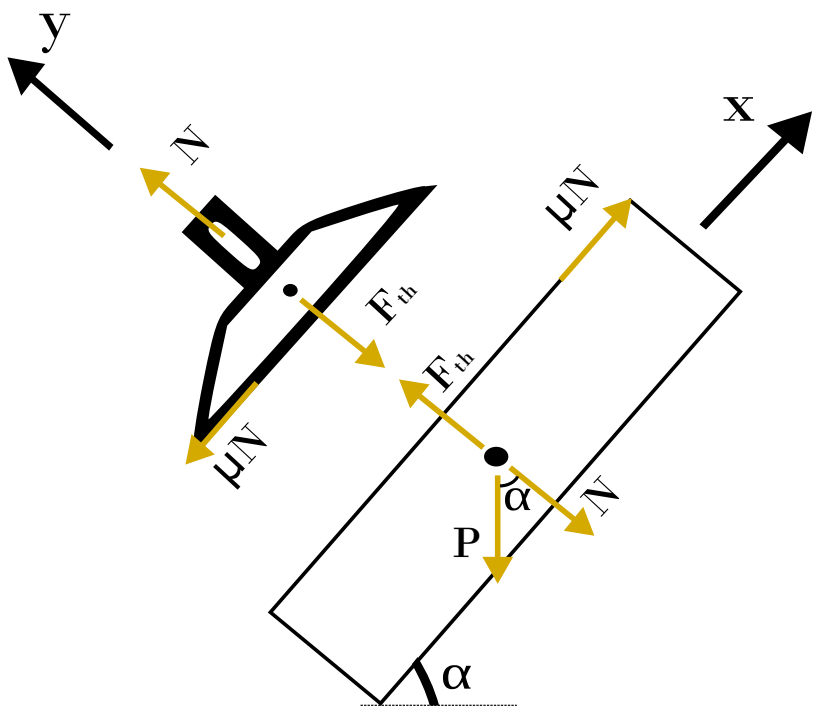


Figure 4.3.: Free body diagram of cup and workpiece.

- $g/\mathrm{m\,s^{-2}}$ - corresponds to the gravity constant on earth (approximately equal to $9.81\,\mathrm{m\,s^{-2}}$).

The theoretical holding force is determined through the equilibrium of forces as represented in equation (4.2).

$$\begin{cases} \sum F_y = 0 \\ \sum F_x = 0 \end{cases} \Leftrightarrow \begin{cases} F_{th} = (N + P_y) \\ \mu N = P_x \end{cases} \Leftrightarrow \begin{cases} F_{th} = N + mg\cos\alpha \\ N = \frac{mg\sin\alpha}{\mu} \end{cases} \Leftrightarrow \begin{cases} F_{th} = mg\left(\frac{\sin\alpha}{\mu} + \cos\alpha\right) \\ N = \frac{mg\sin\alpha}{\mu} \end{cases} \tag{4.2}$$

The curve presented in Figure 4.4 shows the values of the theoretical holding force (F_{th}) as function of the angle (α).

The analysis of the curve presented in Figure 4.4, shows that there is a significant difference between the necessary holding force for a horizontal manipulation ($\alpha = 0°$) and for a vertical manipulation ($\alpha = 90°$). This reflects impact of the friction between the workpiece and the cup. A lower coefficient of friction will lead to a higher holding force.

The highest theoretical holding force is obtained through the maximum of the curve presented in Figure 4.4 by setting the derivative of F_{th} in function of α equal to zero, as represented in equation 4.3.

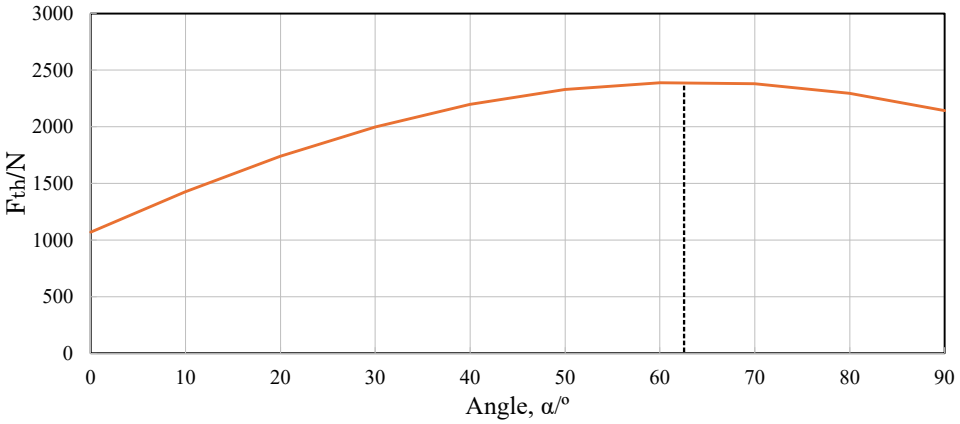


Figure 4.4.: Curve - F_{th} in function of α.

$$\begin{aligned} \frac{dF_{th}}{d\alpha} = 0 \Leftrightarrow mg\left(\frac{1}{\mu}\cos\alpha - \sin\alpha\right) = 0 \Leftrightarrow \frac{1}{\mu}\cos\alpha - \sin\alpha = 0 \\ \Leftrightarrow \cos\alpha = \mu\sin\alpha \Leftrightarrow \tan\alpha = \frac{1}{\mu} \\ \Leftrightarrow \alpha = \arctan\left(\frac{1}{\mu}\right) \end{aligned} \tag{4.3}$$

So, the worst case scenario theoretical holding force is 2394.97 N and the respective angle is 63.43°. This value of the theoretical holding force was not calculated considering a safety factor parameter. The safety factor will only be considered on the dynamic force equilibrium because it takes into account that all the theoretical parameters that define the problem including the workpiece acceleration. The static force equilibrium was an initial step towards the dynamic force equilibrium, and the force values calculated in this section will not be used for the selection of the vacuum cups.

4.3.3. Dynamic free body diagram analysis

The big difference in the dynamic force balance is the consideration of the robot acceleration during the manipulation movement. The robot selected is a six-axis robot which gives it the ability to move like a human arm. Each joint has at least one servo motor that moves to support that part of the robot. Figure 4.5 shows a schematic example of a common six-axis robot design with all the joints movement.

The robot is able to move more than one joint at a time achieving different speed and acceleration values. Since this is a theoretical force calculation, the complex dynamic model of the robot was not taken into account and the different values of maximum linear or angular acceleration corresponding to each joint are unknown.

The worst situation for the acceleration direction is represented in the dynamic free body diagram in Figure 4.6. The acceleration vector can be decomposed into the x and y direction. In the x direction, the acceleration component (a_x) is opposed to the friction force. In the y direction, the acceleration component (a_y) is opposed to the theoretical holding force. Both

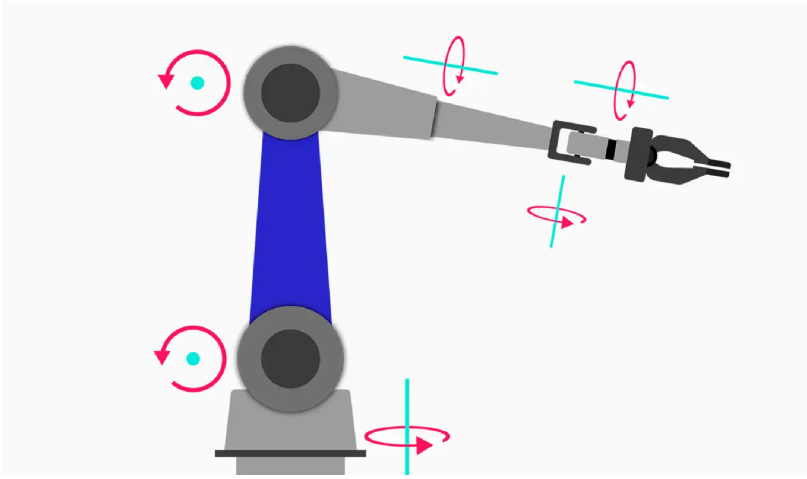


Figure 4.5.: Schematic example of a 6-axis robot [46].

this conditions will lead to the higher value of the theoretical holding force. The value of β that will ensure the higher necessary holding force will be 63.43°, the same as the α angle parameter.

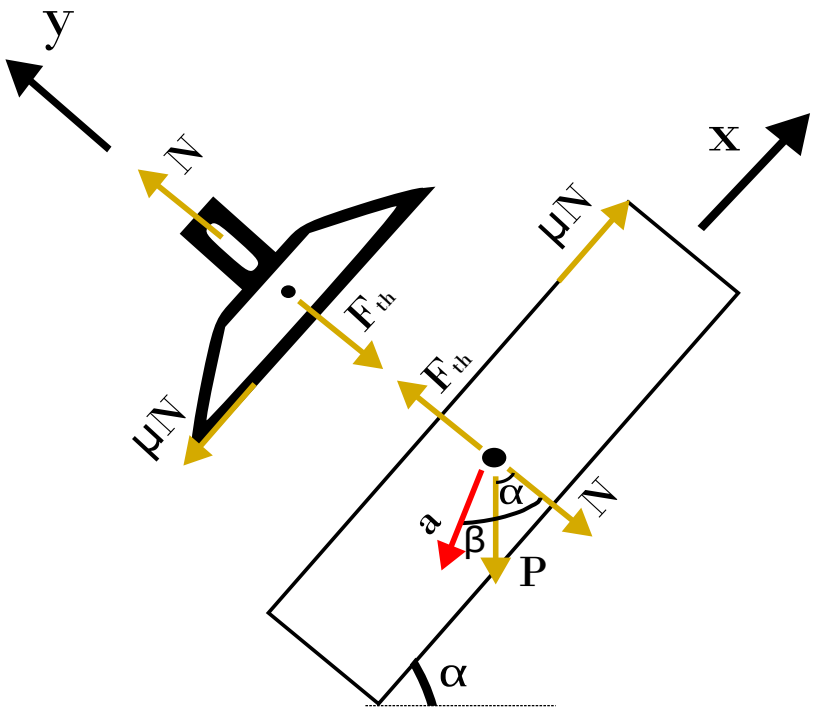


Figure 4.6.: Dynamic equilibrium of the forces diagram represented on the workpiece.

The theoretical holding force is determined through the equilibrium of forces as represented in equation (4.4).

$$\begin{cases} \sum F_y = ma_y \\ \sum F_x = ma_x \end{cases} \Leftrightarrow \begin{cases} F_{th} - N - P_y = ma_y \\ \mu N - P_x = ma_x \end{cases} \Leftrightarrow \begin{cases} F_{th} = N + P_y + ma_y \\ N = (mg\sin\alpha + ma_x)\,\frac{1}{\mu} \end{cases}$$
$$\Leftrightarrow \begin{cases} F_{th} = \left[\frac{m}{\mu}\,(g\sin\alpha + a\sin\beta) + m\,(g\cos\alpha + a\cos\beta)\right] \\ N = \frac{m}{\mu}(g\sin\alpha + a\sin\beta) \end{cases} \tag{4.4}$$

The curve presented in Figure 4.7 shows the values of the theoretical holding force (F_{th}) in function of the angle (β).

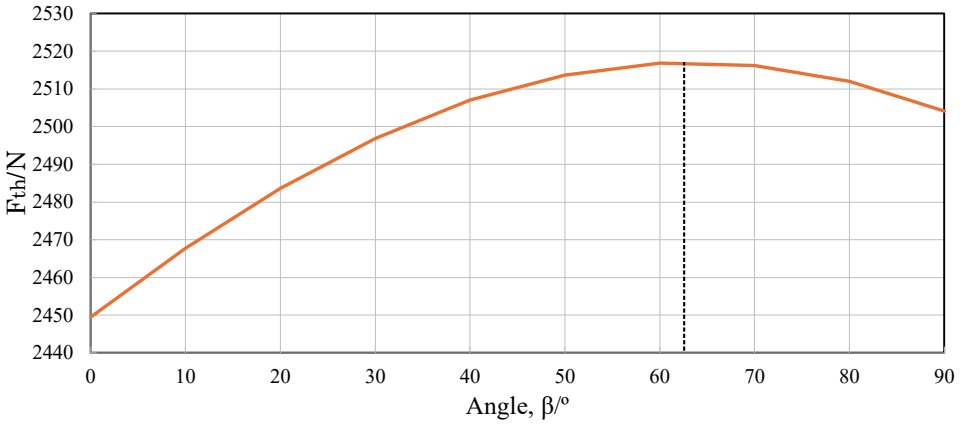


Figure 4.7.: Curve - F_{th} in function of β.

As seen in the graph above, the value of β for the critical situation is the same as the value of α ($\beta = \alpha = 63.43°$), meaning that the direction of the acceleration is the same as the direction of the gravity force.

The theoretical holding forcing value for the worst case scenario of a dynamic event is 2517.04 N.

4.3.4. Safety factor

Since there are several factors that aren't considered for the calculation of the theoretical force, it is imperative to consider a safety factor value. According to Schmalz, a world-leading supplier of vacuum technology, the German accident prevention regulation (UUV) recommends a safety factor of 2.5 or higher when manipulating workpieces [47]. If the application was merely a pick-up-and-place horizontal manipulation situation, a lower safety factor would be a suitable choice. However, in this application, it was considered the worst-case scenario inclined situation where shear forces exist and will lead to the higher holding force. Besides that, taking into account the main dimensions and mass of the part, it's rigidity which will behave and deform like a thin plate, the complex geometry, and the necessary safety standards demanded by a robotic bending cell to ensure the safety of all the operators, whether they are doing a maintenance operation or are outside the cell, a higher safety factor must be considered. It is also not possible to spread the vacuum cups throughout the entire surface of the workpiece due to the restrictions of the bending lines location during the bending process. This leads to a critical deflection problem of the

workpiece which will be analysed in this Chapter. The real dynamic behaviour of the robot is also very important to take into account in this safety factor. As seen before, the robot is able to accelerate and move the workpiece with different joints and with linear and/or angular motions. This dynamic behaviour of the robot was not described in the theoretical calculation.

After considering all this factors, a safety factor of 5 was chosen in order to provide an extreme safety environment inside the robotic bending cell. Therefore, the theoretical holding force is determined by equation (4.5):

$$\begin{aligned} F_{th} = \left[\frac{m}{\mu}\left(g\sin\alpha + a\sin\beta\right) + m\left(g\cos\alpha + a\cos\beta\right)\right] \cdot S.F \\ \Leftrightarrow F_{th} = 2517.04 \cdot 5 \\ \Leftrightarrow F_{th} = 12\,585.20\,\mathrm{N} \end{aligned} \tag{4.5}$$

Finally, the value of the holding force taking into account the safety factor is 12 585.20 N.

4.4. Vacuum cup suction force

After determining the total force needed to hold the workpiece, the number of vacuum cups needed must be determined. Equation (4.6) calculates the suction force for one vacuum cup [23].

$$F_v = \Delta P \cdot A = (P_{abs} - P_{atm}) \cdot A \tag{4.6}$$

Where:

- F_v/N - Single vacuum cup suction force;

- ΔP/MPa - Pressure difference ($P_{abs} < P_{atm}$) ;

- A/mm^2 - Effective interface area between cup and workpiece surface;

- P_{abs}/MPa - Applied vacuum pressure inside the cup volume;

- P_{atm}/MPa - Atmospheric pressure on the outside of the cup (depends on the geographical height).

This pressure difference can also be called negative gauge pressure which refers to the difference in pressure between any vacuum and atmospheric pressure. In practice is impossible to apply 100% vacuum pressure inside the cup volume. In fact, the negative vacuum pressure (ΔP) usually ranges from 10% to 90% vacuum; however, negative pressures above

60% are very expensive to obtain. A standard value recommended by suppliers for vacuum applications is $-0.6\,\text{bar}$ ($-0.06\,\text{MPa}$) provided by one or more vacuum ejectors.

This is the simplest method to calculate the suction force. However, since this is also a theoretical calculation it is imperative to consider safety parameters. First, the deformation coefficient that takes into account the deformation that the cup is subjected when under pressure that may occur in the lipped part of the suction head. This can lead to a reduction in the effective surface area since it directly affects the diameter. This value is usually between [0.6; 0.9]. An average value that is used in most applications is 0.80, which was the value considered for this calculation [23].

Since the majority of the vacuum cups available are circular, the area is calculated using the area of a circle, which is presented in equation (4.7) [23].

$$A = \frac{\pi \cdot (D \cdot n)^2}{4} \tag{4.7}$$

Where:

- D/mm - Inside vacuum cup diameter;

- n - deformation coefficient.

Another important parameter to consider is the efficiency of the system (η), which is related to leakage losses and surface contaminants [23]. The flow of air through the leakages in the sealing zone on contact between the suction cup lip and the surface of the workpiece reduces the effective suction force, the speed, and the overall lifting force of the gripper. The presence of surface contaminants can aggravate this situation, leading to critical retention force losses. Besides that, it is important to ensure additional vacuum retention safety if one of the vacuum ejectors is compromised. Considering the high vacuum and security demand for this application, a lower efficiency value was chosen: 0.67 $\left(\approx \frac{2}{3}\right)$.

Finally, the equation (4.8) presents all the parameters considered for the calculation of the vacuum cup suction force.

$$F_v = \Delta P \cdot \frac{\pi \cdot (D \cdot n)^2}{4} \cdot \eta \tag{4.8}$$

The number of vacuum cups (z) is obtained with following equation (4.9):

$$z = \frac{F_{th}}{F_v} \tag{4.9}$$

The only parameter unknown in order to determine the final number of cups is the diameter of the vacuum cup. All the diameters available by the supplier were considered and the number of vacuum cups necessary to each diameter were determined.

4.5. Vacuum cup selection

There are several types of vacuum cups with different shapes, materials, accessories, intended for different applications and surfaces. The supplier chosen was SMC, one of the leading manufactures in the pneumatic industry and the current supplier of ADIRA. They have a section in their catalogue with high rigidity reinforced vacuum cups intended for transferring heavy or large workpieces. This section of the catalogue is presented in Appendix B.1 [45]. Section 2.4.2.1 reviewed the main characteristics and design options when selecting vacuum cups for a vacuum gripper which will be taken into account for the selection of the following cup.

Theses cups are available as flat type with ribs or as bellow types. The advantages of flat type pad really stand out for this application since the workpiece is a flat sheet metal without convex or even concave surfaces and the surface is parallel to the surface of the lip of the vacuum cup. Flat cups will provide excellent stability, have a higher prehension force and are the ideal choice for handling thin flat smooth surfaces such as sheet metals. The ribs make the cup stiffer and tend to increase the suction force.

The pad materials available are the following: NBR, silicone, uhrethane rubber, fluoroelastomer (FKM), and ethylene propylene diene monomer rubber (EPDM). The material chosen was the NBR. It is the most common material used in this industry, especially in sheet metal handling due to it's oil and grease resistance, good wear resistance and low cost. It is a standard choice for applications that do not require any high temperature demands. Since this is a common choice, suppliers usually have it in stock most of the time, which means that orders will be shipped quickly.

The pad diameters available are the following: $\phi 40\,\text{mm}$, $\phi 50\,\text{mm}$, $\phi 63\,\text{mm}$, $\phi 80\,\text{mm}$, $\phi 100\,\text{mm}$, and $\phi 125\,\text{mm}$. An example of this vacuum cup type is represented in Figure 4.8.



Figure 4.8.: Example of the selected vacuum cup from SMC catalogue [45].

4.5.1. Number of vacuum cups

As seen before, the number of vacuum cups needed to manipulate the flatten boat hull will depend on the inside volume diameter of the vacuum cup, as seen in equation (4.8) and (4.9). Using both equations, it was determined for each diameter available, the suction force and the total number of cups corresponding to each diameter. This can be seen in Table 4.3.

Table 4.3.: Total number of vacuum cups and the suction force for each available diameter.

D/mm	F_v/N	z
40	-32.33	3890
50	-50.52	250
63	-80.20	157
80	-129.32	98
100	-202.07	63
125	-315.73	40

As expected, a larger diameter results in a higher suction force being applied by each vacuum cup, requiring fewer cups overall. The initial diameter choices were ϕ100 mm and ϕ125 mm, since more than nighty eight vacuum cups looks like an exaggerated amount for the application. Nevertheless, in the following sections the allocation of the cups will be analysed and the number of cups and the corresponding diameter will be chosen. For now, the options ϕ100 mm and ϕ125 mm are the ones considered for this application.

Table 4.4 shows the price quotation that was requested to SMC regarding the costs of both vacuum cups, since the price difference between both could be important to consider.

Table 4.4.: Price quotation for the ϕ100 mm and ϕ125 mm vacuum cup diameter options.

D/mm	z	Price/€
100	63	1440.18
125	40	900.00

Sixty three ϕ100 mm vacuum cups cost 1440.18€ and forty ϕ125 mm vacuum cups costs 900.00€. Going with the ϕ100 mm option would cost 60.02 % more than going with the ϕ125 mm option. This is a significant difference that must be considered when choosing one of these options. When studying the allocation of the cups and respective deformation of the flatten boat hull, if forty cups is sufficient, it will be the final choice since it is cheaper.

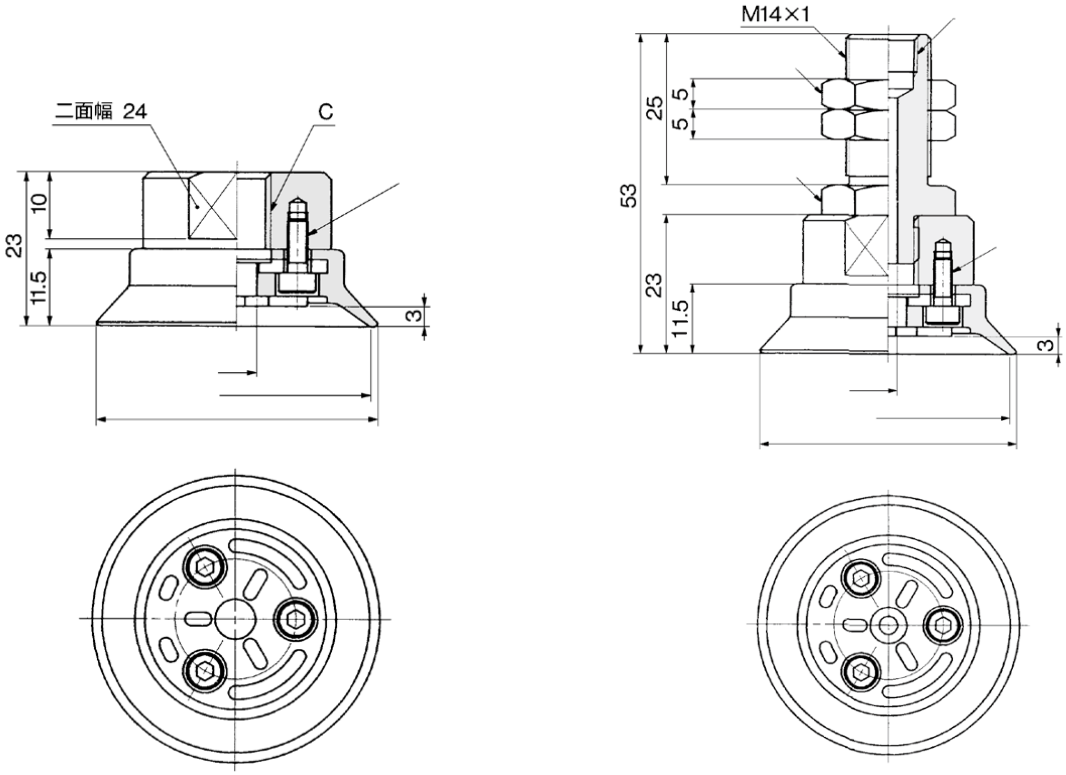
4.5.2. Accessories: adapter and buffer

SMC provides 2 accessories for the vacuum cup: the adapter, and the buffer (also called level compensator).

The adapter is a little aluminium interface located at the top of the cup that allows the user to mount the pneumatic line into the mounting thread sizes available in order to allow

the air flow to the vacuum entry location on the adapter. SMC provides two locations for the vacuum entry: lateral or vertical. The choice is only dependent on the application and how the pneumatic lines will be arranged.

SMC also provides two options for mounting threads with different sizes: male or female thread. The only difference is that the male thread already comes with a mounting pneumatic thread size appropriated for the connection of a pneumatic fitting to attach the pneumatic tube. Two technical drawings of the vacuum cup with the female and with the male thread are seen in Figure 4.9



(a) Female mounting thread.

(b) Male mounting thread.

Figure 4.9.: Two options for mounting threads on top of the vacuum cup [45].

The male thread is the best practical option because it allows the direct attachment of a pneumatic fitting to connect the pneumatic line. The lateral or vertical vacuum entry will depend entirely on the gripper constructive solution adopted. For this application, both solutions could be incorporated in the gripper design. The vertical vacuum entry was chosen for the pneumatic tube assembly.

Figure 4.10 presents a table containing all the mounting thread size options available for this cup with a vertical vacuum entry. For a male thread and considering the ϕ100 mm and ϕ125 mm cups, there are only three options for the thread size: British Standard Pipe Taper Internal (Rc), National pipe taper (NPT) or National pipe taper- fuel and oil (NPTF). The NPT and NPTF are almost identical thread types that follow the American National Standard Pipe thread. Rc follows the British Standard Pipe Taper (BSPT). ADIRA uses the British Standard for the pneumatic threads, so that was the one selected: Rc1/8 (Symbol A16).

Mounting thread size (Vacuum inlet)

			Symbol	Thread size	Pad diameter		
					ø40, ø50	ø63, ø80	ø100, ø125
Mounting	Male thread	M14 x 1	A14	Rc1/8	●	—	—
			A14N	NPT1/8	●	—	—
			A14T	NPTF1/8	●	—	—
		M16 x 1.5	A16	Rc1/8	—	●	●
			A16N	NPT1/8	—	●	●
			A16T	NPTF1/8	—	●	●
	Female thread		B8	M8 x 1.25	●	●	—
			B10	M10 x 1.5	●	●	—
			B12	M12 x 1.75	—	●	●
			B16	M16 x 1.5	—	●	●

Figure 4.10.: Mounting thread size table for the selected vacuum cup adapter with vertical vacuum entry [45].

Buffers are usually seen in applications with large and thin workpieces that require multiple cups such as the flatten boat hull. These workpieces have the tendency to deform while being manipulated. This leads to differences in the vacuum cup heights that can compromise the manipulation task. Buffers are used to compensate these differences due to the deflection of the part caused by its self weight. Besides that, they also provide shock and vibration absorption. Figure 4.11 shows different examples of SMC buffers incorporated on vacuum cups.

The big disadvantage occurs in applications that require the manipulation of the workpiece in different directions using linear and/or rotational motions. The simple motion of turning the part upside down will cause the buffers to compensate for new differences in cup height, changing the geometry of the workpiece. In this robotic bending cell, if the flattening boat hull geometry keeps changing due to this phenomenon, the robot will keep losing the reference position for picking up the part every time the cups are detached in order to move to a different position. Even a slight geometry change can affect the bending results and compromise the bending operations. Even though the robot could be programmed to take all these variations into account, it is generally a good practice to avoid the use of buffers in these applications. Therefore, the use of buffers was not considered. Buffers are an excellent option in simple horizontal pick-and-place applications since this phenomenon does not happen.



Figure 4.11.: Different examples of SMC buffers incorporated on vacuum cups [45].

4.6. How to study the deflection of the workpiece

The position of the cups and the deflection of the workpiece needs to be analysed for two different scenarios. The first scenario is the bending process which corresponds to the three U-shape bending operations. The second scenario is the second bending process which corresponds to the bend that will shape the side of the boat hull. Each process may require a different vacuum cup allocation in order to minimize the deflection of the part. However, the aim is to use the same vacuum cup allocation for both processes if possible.

The first thing to consider before understanding the best way to analyse this problem is to define the flatten boat hull as a plate. A plate is a three dimensional solid body which is limited by two surfaces. The distance between them is called thickness and is much smaller than the other dimensions. It is typical to use a plane parallel to the surfaces to divide a plate's thickness, h, into equal halves. This plane is referred to as the plate midplane. The direction of the plate thickness measurement is perpendicular to the midplane. This can be seen in Figure 4.12. In relation to its other dimensions, a plate's thickness has a significant impact on its flexural qualities [48].

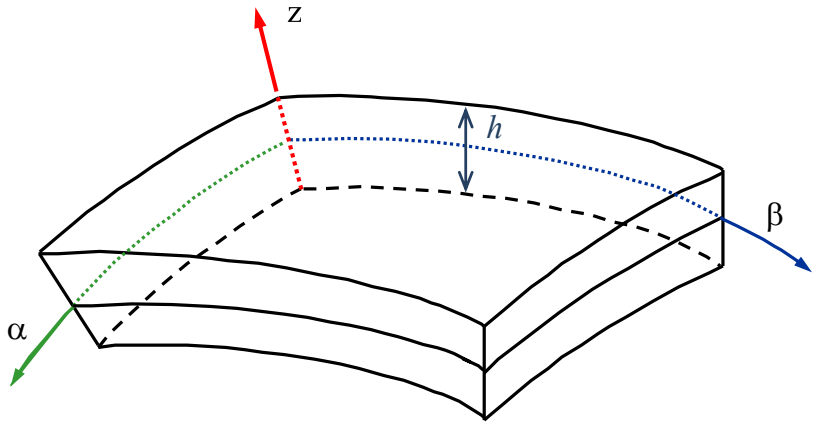


Figure 4.12.: Plate with thickness, h, divided by a midplane into 2 halves [48].

Plates can be divided into three categories: thin plates with small deflections, thin plates with large deflections, and thick plates. A standard criterion often applied to define a thin plate is the following: the ratio of the thickness, t, to the smaller span length (a) should be less than 1/20 [48]. This is represented in the following equation (4.10).

$$\frac{t}{a} < \frac{1}{20} \Leftrightarrow \frac{3.2}{1663.7} < \frac{1}{20} \Leftrightarrow 0.0019 < 0.0500 \tag{4.10}$$

So, the flatten boat hull can be considered a thin plate.

For the analytical analysis of thin rectangular plates there are several methods used such as the classical plate theory which uses the Kirchhoff hypothesis, Navier's and Lévy's solutions, and even energy methods solutions like the Ritz method. All these solutions present governing solutions for the deflection of thin plates, but they are three different methods, each of which takes different things into account and being more suitable depending

on the application.

The flatten boat hull doesn't have a rectangular geometry, instead it has a very complex geometry to analyse the deflection and to obtain the stress and displacement fields through analytical methods such as the ones just mentioned. Therefore, a finite element analysis will be used to structurally analyse the workpiece.

4.7. First bending process analysis

The first step is to study the best location region on the flatten boat hull to position the forty vacuum cups. For this operation, there are four possible areas on the workpiece to allocate the vacuum cups that are shown in Figure 4.13. The dashed lines represent the bending lines for this operation.

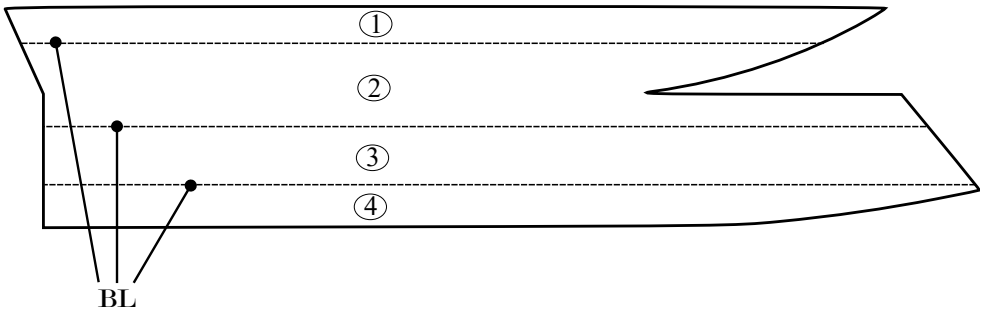


Figure 4.13.: Available areas for the allocation of the cups on the workpiece for the first bending process.

The row or rows of cups can only be placed along area 1, 2, 3 and 4. Considering once again the very large surface area of the workpiece, it's weight, and thin thickness, it is imperative to grasp it both on the left and right side of the 'V'. If the vacuum cups are placed only in one side of the 'V' the opposite side will definitely present very high values of displacement in that region. Besides that, by only placing the cups on one side of the 'V', at the end of the 'V' there may be a critical stress concentration zone that may lead to a structural failure.

Therefore, the first allocation that should be tried is to place the vacuum cups in area 2 to hold the workpiece on the two sides of the 'V' shape. Two rows of vacuum cups, one on the left side of the 'V' and the other on the right side of the 'V' is the best way to approach the problem. Another advantage of placing the cups in this position is that it may be possible to do the three bends in a row without the need of a regrip station. The robot can manipulate the workpiece to do the bends in one side, and then rotate it 180° in the air, and then bend the other side, without ever needing a regrip station.

The number of cups per row and the distance of the cups to the bending line must be defined.

The distance of each row of cups to the respective bending line should be as low as

possible, and it will have a high influence on the deflection of the workpiece. The critical displacement zones are represented in Figure 4.14. The circles represent the vacuum cups. The number is merely illustrative.

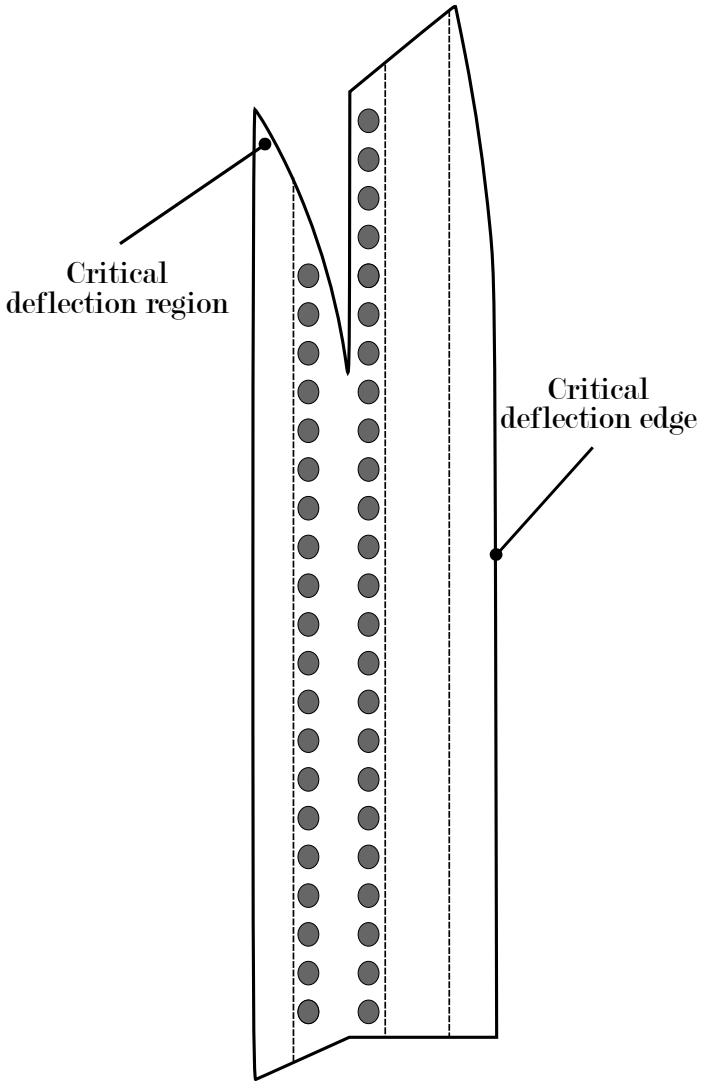


Figure 4.14.: Critical displacement zones due to the deflection of the workpiece.

The vacuum cups are restricting the active degrees of freedom on that $\phi 125\,\text{mm}$ contact surface. Therefore, taking into account the distributed load (self-weight) throughout the surface of the workpiece, the bending moment caused by this load, which is responsible for causing the deflection of the plate, will be as high as the distance from the cup to the edges. Then, the higher the distance from the row of cups to the bending line is, the higher the displacement values will be at the edges of the workpiece.

By placing both rows of cups the closest possible to the respective bending line, the bending moment is going to be lower, which leads to a lower displacement values at the critical zones of the workpiece. However, the cup cannot be placed exactly next to the bending line. The distance between the centre of the die and the end of the table, where the die is clamped, represented in 4.15, must be taken into account. The distance between the centre of the vacuum cup and the bending line needs to be higher than the sum of the

distance, d, with the radius of the cup.

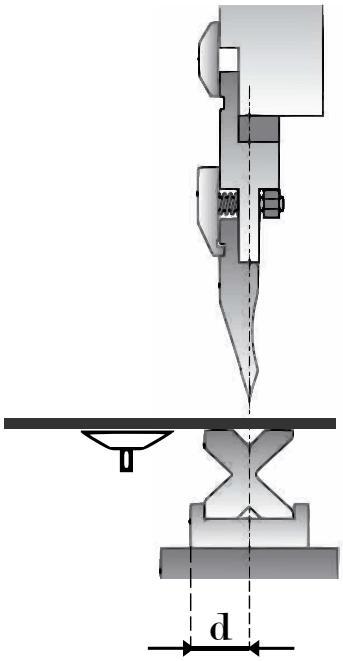


Figure 4.15.: Illustrative representation of the distance between the centre of the die to the end of the table [12].

This distance, d, for the specific table used in the selected press brake for this operation, is 52.5 mm and is clamped though a hydraulic mechanism. Therefore, the distance between the centre of the vacuum cup and the bending line needs to be higher than 115 mm. The distance chosen was 140 mm based on a conservative approach.

Using the functionalities of the SolidEdge software, with this distance considered, the distance between both rows, measuring from the centre of each cup, is 406 mm. This can be seen in Figure 4.16.

The number of cups per row must be determined. The approach used was to measure the length of each row that goes through the cups centre. The distances measured are presented in Table 4.5.

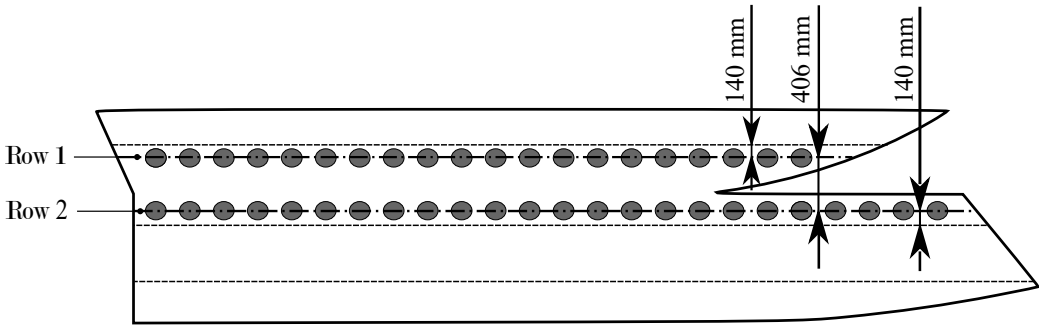


Figure 4.16.: Illustration of the rows lines that pass through the cup centres.

Table 4.5.: Length of each row.

Row number	Length/mm
1	5734.97
2	6630.80

The sum of both distances is 12 365.77 mm. Then, the ratio between each row distance and the total length was determined in order to get a rough idea in percentage about the number of cups in each row. This is seen in equation 4.11 and 4.12.

$$\frac{5734.97}{12365.77} \cdot 100 = 46\,\% \tag{4.11}$$

$$\frac{6630.80}{12365.77} \cdot 100 = 54\,\% \tag{4.12}$$

Considering the total number of cups equal to forty, the number of cups that will be placed on row 1, z_1, is determined in equation 4.13.

$$z_1 = 40 \cdot 0.46 \Leftrightarrow z_1 = 18.4 \Leftrightarrow z_1 \approx 18 \tag{4.13}$$

The number of cups that will be placed on row 2, z_2, is determined in equation 4.14.

$$z_2 = 40 \cdot 0.54 \Leftrightarrow z_2 = 21.6 \Leftrightarrow z_2 \approx 22 \tag{4.14}$$

This method was used to obtain an approximate number of the cups in both rows. If necessary, those numbers can be slightly changed.

Finally, the only thing left is the distance between the cup centres in each row. If the cups on both rows were aligned, it would allow them to be organized into groups of two or more, which would not only simplify the gripper design but also allow for a more modular solution. Besides that, if the cups are in groups of two or more, the pneumatic system will also be easier to implement and to assembly all pneumatic tubes throughout the gripper structure. During the gripper assembly in real life, having the cups organized in groups and aligned in the width direction will make it much easier and accurate to assembly all the vacuum cups in the desired position. This vacuum cup allocation can be seen in Figure 4.17.

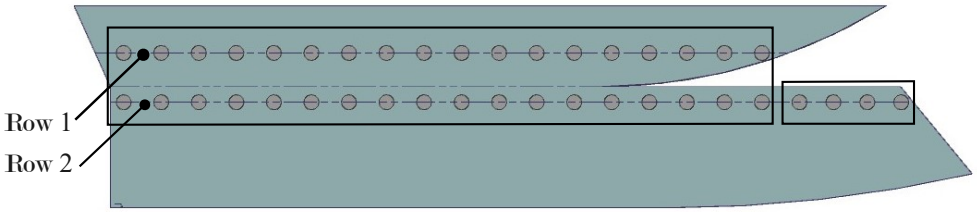


Figure 4.17.: Vacuum cup distribution along both rows of the workpiece on SolidEdge.

The last 4 cups on the right side of the 'V' shape have a 280 mm distance from cup centres, while the rest of the cups to the left have a 310 mm distance from cup centres. This allowed the implementation of the cup layout and still manage to keep the last cup at the left of the 'V' very close to the edge to minimize the displacement in that critical displacement region.

4.8. Second bending process analysis

The first step to analyse this second bending process is also to study the best location region on the flatten boat hull to position the forty vacuum cups. For this operation, there are five possible areas on the workpiece to allocate the vacuum cups that are shown in Figure 4.18. The BL represents the bending line for this operation and the other dashed lines represent the bending operations already done.

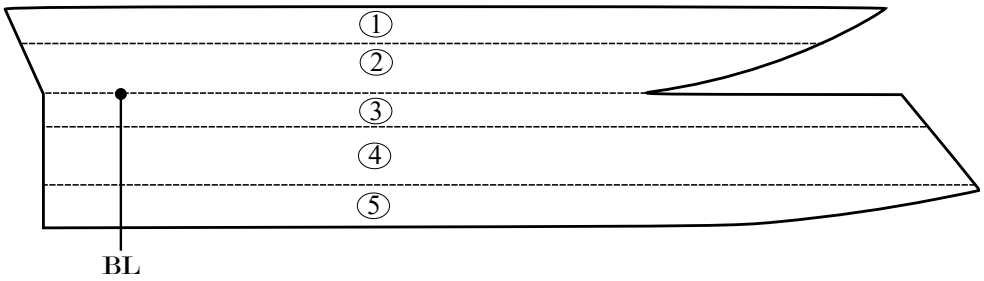


Figure 4.18.: Available areas for the allocation of the cups on the workpiece for the second bending process.

For this process, the goal is towards the bending line that divides the 'V' shape. Although there are five available areas seen in Figure 4.18, this bending operation is only viable if the vacuum cups are all on the left side of the 'V' or all on the right side of the 'V'. Otherwise, the operation is impossible since one of the sides must go inside the press brake for the bending operation. This makes the whole process very challenging since the free side of the workpiece will be subjected to a very high deflection.

The obvious choice for placing the cups is on the right side of the 'V' because the left side has a small surface area and a small distance from the desired bending line to the left edge. This means a lower bending moment and consequently a lower deflection in comparison with the opposite scenario.

The areas 3 and 4 are the obvious choices for placing the cups. It is crucial that one row

of cups is the closest possible to the bending line in order to reduce the distance between that row of cups to the left edge to lower the bending moment.

The goal is to use the same gripper used on the first bending process so the vacuum cups rows configuration will be exactly the same. One of the rows will be placed on surface area 3 and the other row on area 4. The distance between both rows (measuring between the cups centre) is 406 mm. Figure 4.19 represents the same methodology used for the first bending process to check if it is possible to place both rows in those areas without any collision with the bending lines.

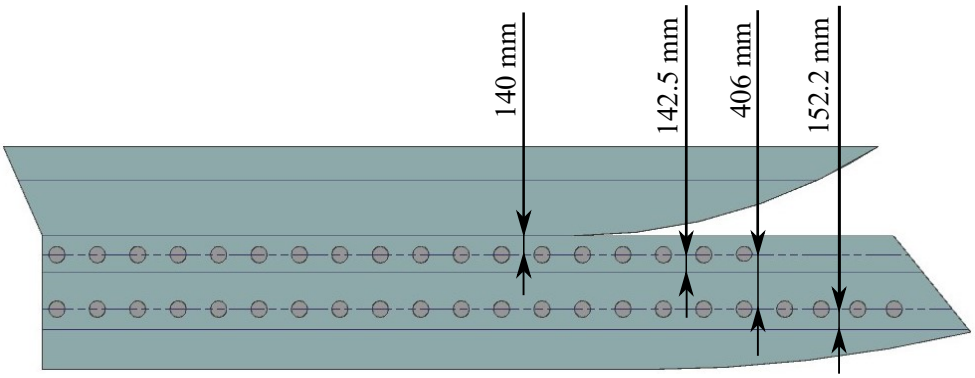


Figure 4.19.: Distances between the cup centre and the respective bending lines on SolidEdge.

The minimum safe distance between the cup centre and the bending line is 140 mm. According to the row layout seen in Figure 4.19, the same gripper can be used.

4.9. Finite element analysis of the workpiece manipulation

This section is reserved to the creation of numerical models using the finite element analysis software Abaqus. This model allows the study of the behaviour of the flatten boat hull under different boundary conditions, which will correspond to the different allocations of the vacuum cups.

4.9.1. Constituent parts

This numeric model has two parts: the flatten boat bull and the vacuum cup.

The 3D CAD of the flatten boat hull was imported from the software SolidEdge into Abaqus as a 3D deformable part. The planar shell feature was added by sketching the feature on the selected face of the part because the workpiece needs to be analysed as a shell part, as seen earlier. Plates are a limit case of shells since they are bounded by two flat surfaces and shells by surfaces with non zero curvature. The shell part in Abaqus is represented in Figure 4.20.



Figure 4.20.: Flatten boat hull shell geometry in Abaqus.

A simplification of the vacuum cup was created in Abaqus using it's modulation capacity though a revolution feature. The only important feature that the cup must have is a circular face with a diameter of 125 mm that will be in contact with the flatten boat hull. During contact that will be established between the cup surface and the workpiece surface, the deformation of the cup will be negligible. The cup part was created as a 2D discrete rigid part which is a part that is so much stiffer than the rest of the numeric model that it's deformation is not considered during the finite element analysis [49]. Figure 4.21 shows the geometry of the vacuum cup in Abaqus.



(a) Front view of the cup after the revolution feature.

(b) Vacuum cup circular surface with ϕ125 mm.

Figure 4.21.: Vacuum cup in Abaqus.

4.9.2. Material

The material of the workpiece is the aluminium alloy Al5052 and it was defined as linear isotropic with an elastic behaviour. For this, the density, Poisson's ratio and Young's modulus must be defined. The properties can be seen in Table 3.2 and the values with the system of units used in Abaqus are presented bellow:

- Young's modulus: 70 000 MPa
- Poisson's ratio: 0.33
- Density: $2.68 \times 10^{-9}\,\mathrm{t\,mm^{-3}}$

The yield strength and tensile strength are not relevant in a linear elastic analysis since the material will never reach plasticity. Nonetheless, it's values are important when analysing the stress field obtained in the finite element analysis simulation.

After the material was defined, a shell section with a corresponding thickness of 3.2 mm was assigned to the flatten boat hull part.

The vacuum cup is a rigid part so it was not assigned any material.

4.9.3. Constraints and boundary conditions

A tie constraint was used to simulate the grasping of the vacuum cup to the workpiece due to the vacuum provided by the ejector. The goal was to tie the nodes of the $\phi 125\,\text{mm}$ circular surface of the cup to the nodes of the surface of the flatten boat hull during the simulation. A rigid body constraint was also created to constrain the motion of all the cups in the assembly to the motion of a single reference point.

In order to restrict and prevent all the linear and rotational motion as well as all other active degrees of freedom of the vacuum cups, it was used the reference point created for the rigid body constraint and it was assigned the boundary condition encastre.

4.9.4. Load

The only load that needs to be considered in the assembly is the self-weight of the workpiece. Therefore, it was defined a gravity load applied to the whole model, even though the vacuum cups are not subjected to this load due to their rigid behaviour. The initial acceleration value necessary to move the robot will be neglected in this numerical analysis.

The generation of a new step was necessary in order to define the load selected and being able to properly run the simulation. Since this system has no contact condition or plasticity and the material model is linear elastic, the creation of a general static step was sufficient in order to obtain the results intended.

4.9.5. Mesh creation and refinement study

The geometry of the flatten boat hull is complex, with curved edges. The partition toolset in Abaqus allows the user to divide a complex part into simple regions with structured or swept meshing techniques. This allows the user to gain more control over mesh generation, is an efficient way to reduce the simulation computation time, and may improve the accuracy of the results. Figure 4.22 shows the partitions regions on the workpiece. The green region was obtained with a structured meshing technique and the yellow regions were obtained with a swept meshing technique.

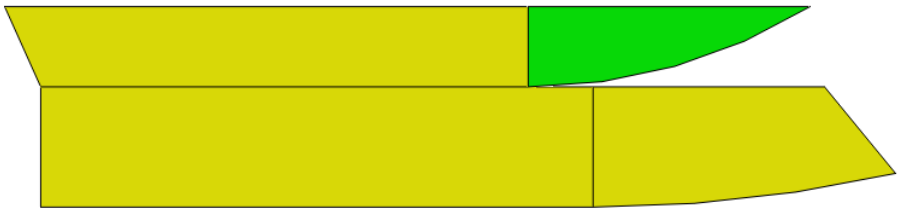
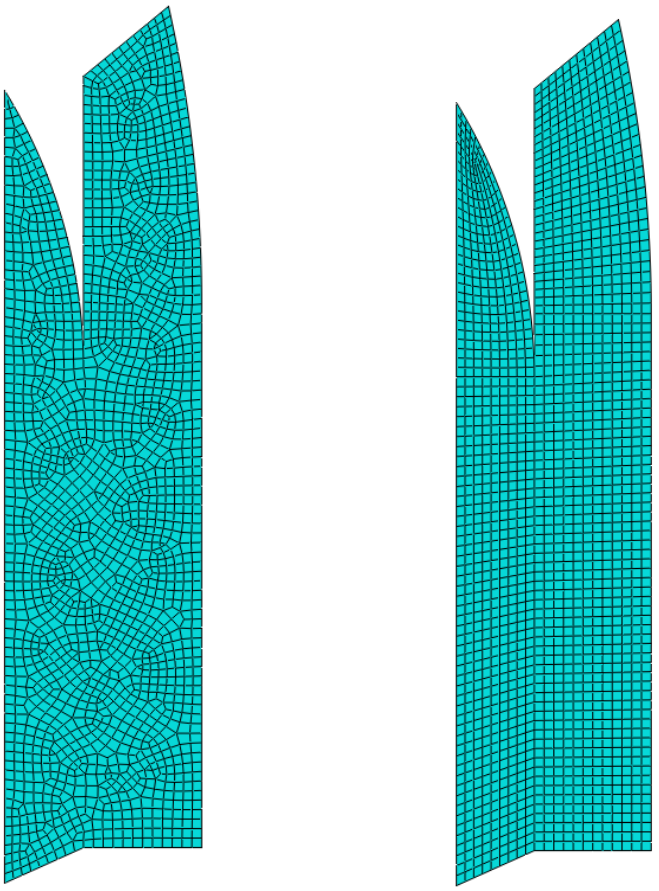


Figure 4.22.: Partition regions on the flatten boat hull geometry in Abaqus.

Figure 4.23 shows the difference in the final mesh of the workpiece with and without the use of partitions. The approximated global element size chosen was 80 mm in order to allow the accurate visualization comparison of both images.



(a) Flatten boat hull mesh without partition meshing techniques.

(b) Flatten boat hull mesh with partition meshing techniques.

Figure 4.23.: Different mesh final results with and without the use of partitions in Abaqus.

Although the first bending process numeric model was the one chosen for the mesh refinement study, this approach was used in both models.

Mesh refinement is a technique used in finite element analysis to enhance the accuracy of the simulations by refining the mesh. This approach optimizes computational resources and improves simulation efficiency. The starting point is typically a coarse mesh, which is a grid with relatively large elements covering the entire computational domain. Refining the mesh improves the accuracy of results by using a fine mesh. However, there is a compromise. On the one hand, a very large element size may result in inaccurate results. On the other hand, an over refined mesh can lead into an unnecessarily higher computational time and an accumulation of numeric errors that might compromise the results. Therefore, the goal is to find the element size that allows the best compromise between the simulation accuracy results and it's computational time and memory cost.

It is also important to note that some regions may require a different refinement than others, depending on the numeric model.

Table 4.6 presents the maximum values of displacement and stress for the first bending process numeric model simulations. For each simulation, the approximated global element size used on the meshing of the flatten boat hull part was decreased from the previous one in order to study it's impact on the simulation results. The computation time was also registered for each simulation. The stress field was obtained through von Mises criterion.

Table 4.6.: Mesh refinement study results.

Element Size/mm	Number of elements	Max. von Mises Stress/MPa	Max. Displacement/mm	Computational Time/s
15	49061	30.21	26.07	44
12.5	70652	32.06	26.21	55
11.5	83843	33.41	26.29	52
10	112475	34.72	26.4	59
8	174704	36.95	26.44	94
7.5	198914	37.6	26.43	118
5	447721	38.7	26.44	409

Figure 4.24 and 4.25 present the variation of the maximum vertical displacement and maximum equivalent stress, respectively with the total number of elements on the flatten boat hull mesh.

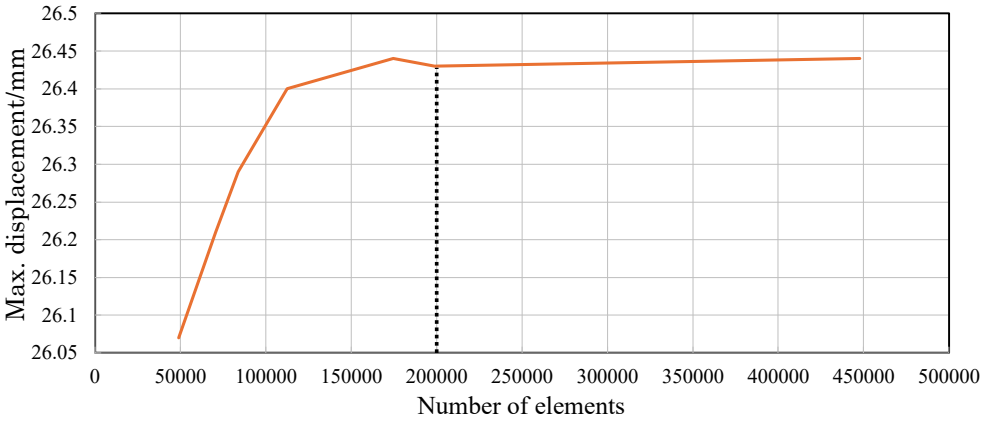


Figure 4.24.: Curve with the variation of the maximum vertical displacement values with the total number of elements.

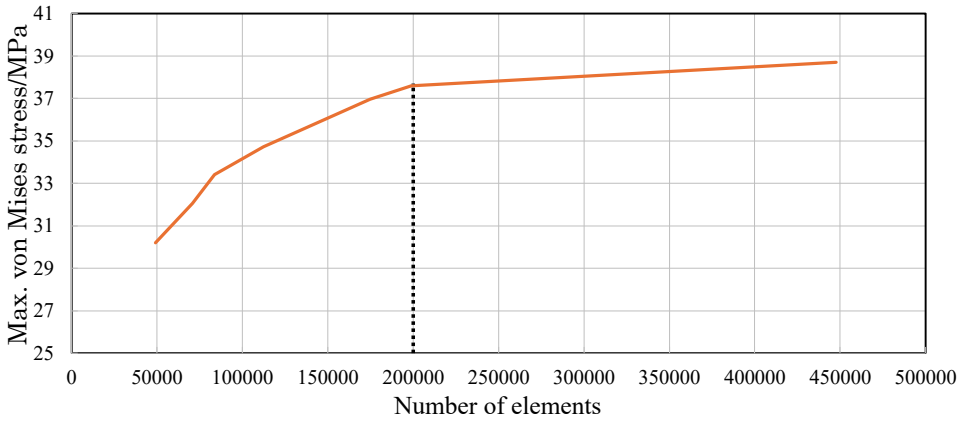


Figure 4.25.: Curve with the variation of the maximum von Mises stress values with the total number of elements.

As seen in Figures 4.24 and 4.25, the values of the vertical displacement and von Mises stress start to stabilize around 200000 elements. Therefore, the increase on the number of elements causes the von Mises stress and displacement values to converge to more accurate results at the cost of computational time. The final mesh of the flatten boat hull part should have an approximated element global size of 8 mm because it represents a great compromise between the accuracy of the results and the respective computational cost.

For both bending process numeric models, the element size chosen for the flatten boat hull was 8 mm, based on this mesh convergence study. The total number of nodes was 176036 and the total number of elements was 174704.

4.9.6. First bending process simulation

Figure 4.26 shows the simulation results for the vertical displacement distribution throughout the flatten boat hull.

Figure 4.26 and 4.27 have an associated deformation scale of 28.06 so that the bending effect is noticeable on the deflection of the workpiece. Otherwise, as the displacement values are very small, without a deformation scale factor it wouldn't be noticeable.

The maximum vertical displacement value is 26.44 mm and happens at the expected critical zone, on the left side of the 'V'. The opposed expected critical edge located on the right side of the 'V' has a displacement value of 25.23 mm. Both values are completely acceptable and will not compromise the manipulation or bending process of the workpiece. The robot needs to be programmed in order to raise the workpiece before entering the press brake to compensate for the maximum displacement obtained: 26.44 mm. As soon as the flatten boat hull reaches the die, the robot may start to lower it until it touches the die. The only thing left is to push it forward until it reaches the finger stop of the back gauge, and then the bending operation can be successfully done.

Concluding, the vacuum cups allocation is validated when it comes to the vertical displacement field.

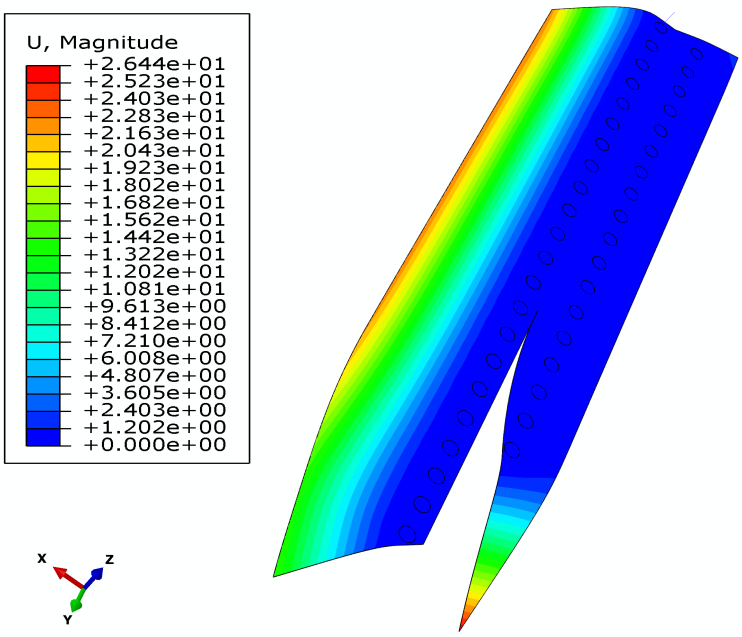


Figure 4.26.: First bending operation simulation results for the vertical displacement distribution.

Figure 4.27 shows the simulation results for the von Mises stress distribution throughout the flatten boat hull.

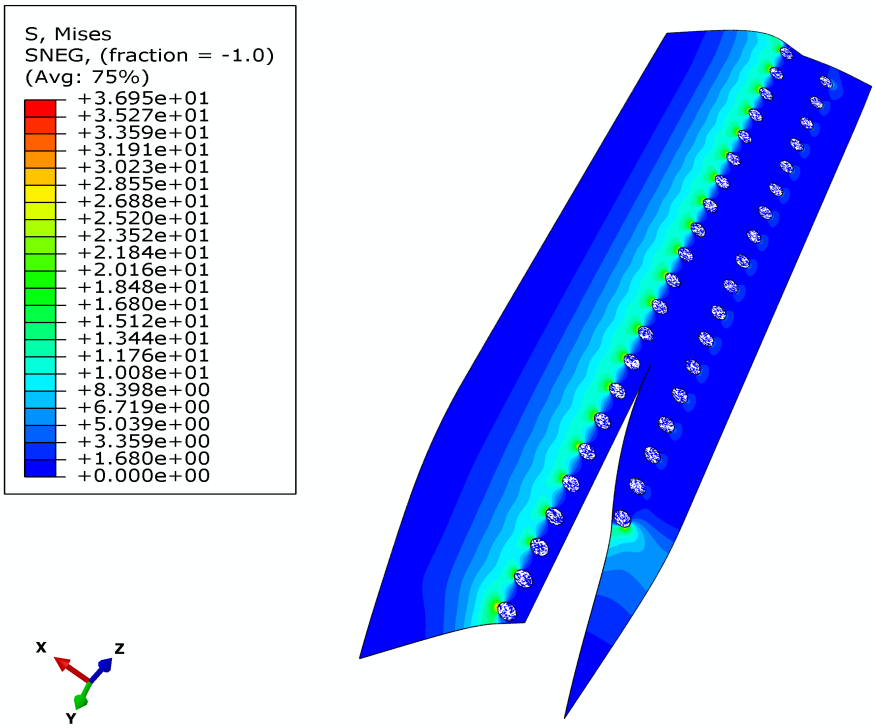


Figure 4.27.: First bending operation simulation results for the von Mises stress distribution.

By analysing the von Mises stress distribution represented in Figure 4.27 it is possible to conclude that the zones closer to the vacuum cups have higher stress values. This happens because the cups are restricting the degrees of freedom in that circular surface area. So, if the bending moment diagram were made, it would be noticed that the bending moment caused by the workpiece self-weight has a maximum value in the nearby cup's surface area. This can be seen in the cups located at the right side of the 'V' since the distance from the cups to that edge is higher, meaning a higher bending moment causing higher stresses.

It is also important to refer that the yield strength of the aluminium was never reached, which is extremely important since the workpiece must not present any deformation in the plastic regime. The maximum stress value obtained was 36.95 MPa. Taking into account the properties of this aluminium alloy seen in Table 3.2, the safety factor, $S.F$, can be determined with equation (4.15).

$$S.F = \frac{\sigma_y}{\sigma_{\text{eq}}} \Leftrightarrow S.F = \frac{193}{36.95} \Leftrightarrow S.F = 5.22 \tag{4.15}$$

4.9.7. Second bending process simulation

Figure 4.28 shows the simulation results for the vertical displacement throughout the flatten boat hull due to the workpiece deflection.

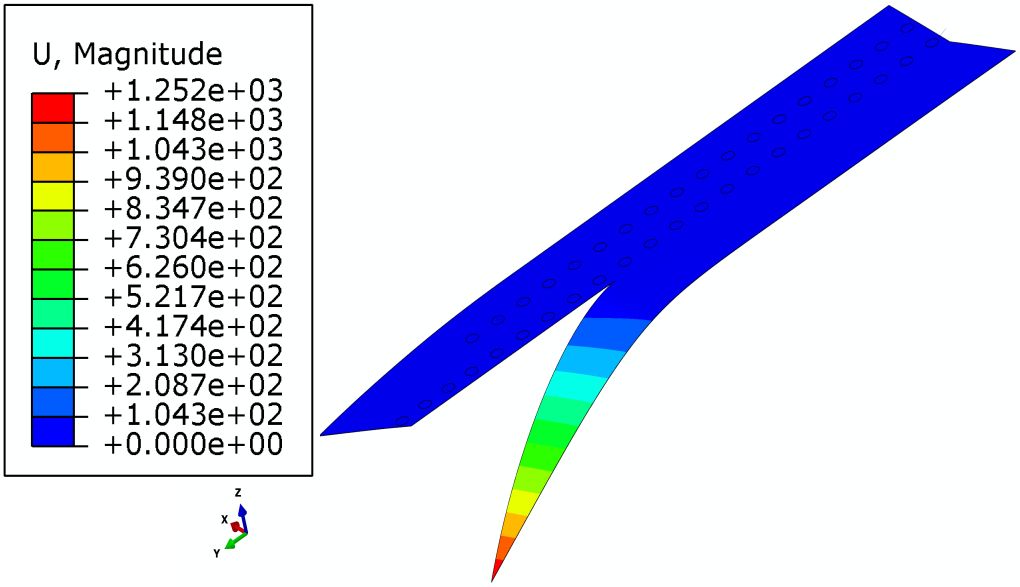


Figure 4.28.: Second bending operation simulation results for the vertical displacement distribution.

The first conclusion to take from this numeric simulation is that by only placing cups in one side of the 'V', the other side will be subjected to very high displacement values due to the 'V' shape geometry. The maximum displacement value obtained was 1252 mm which obviously compromises the bending operation. This value seems to be too big for what was expected, and it will be analysed in the stress field distribution results.

In this situation, even if the right side of the 'V' was completely covered by cups, the

results would still be catastrophic. The problem is that in this operation it is not possible to place cups in both sides of the 'V' which causes this massive problem that makes impossible the manipulation of the flatten boat hull.

Figure 4.29 shows the simulation results for the von Mises stress distribution throughout the flatten boat hull.

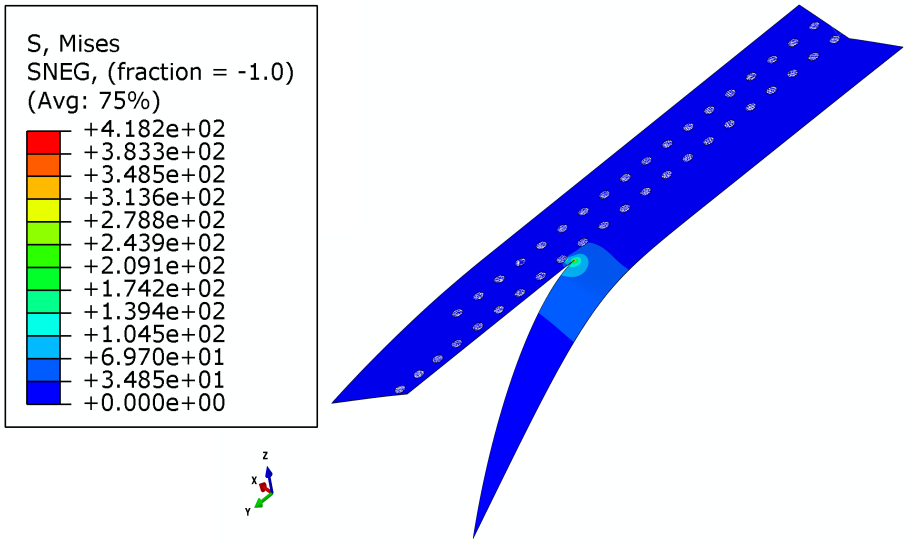


Figure 4.29.: Second bending operation simulation results for the von Mises stress distribution.

There is a massive stress concentration zone at the end of the 'V' due to the fact that it was not possible to place cups in both sides of the 'V'. This stress concentration is seen in Figure 4.30.

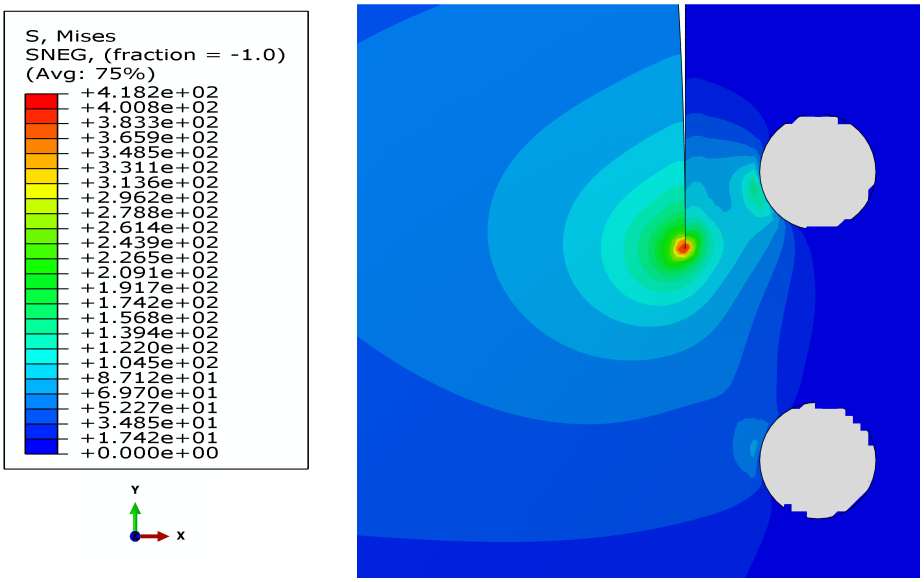


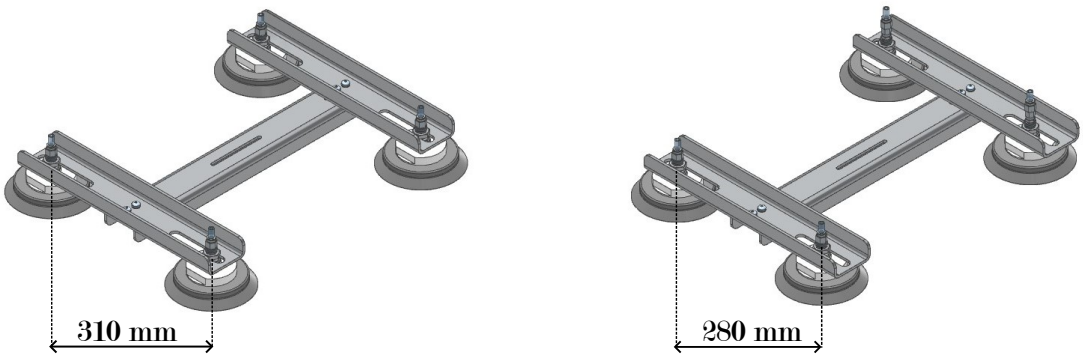
Figure 4.30.: Detailed view showing the concentration zone of the first bending operation simulation results for the von Mises stress distribution.

The maximum stress value is 418.2 MPa at the stress concentration zone. All stress values inside the green region are higher than 200 MPa. Theses value far exceeds the yield stress of the material (193 MPa) and some even the tensile stress (228 MPa). In the numeric model, the material was defined as linearly isotropic with an elastic behaviour. Therefore, the simulation would never show the material beginning to enter the plastic deformation regime. However, since the maximum stress value is much higher than the yield stress, the workpiece will start to deform permanently at the stress concentration zone until it reaches the point of rupture and starts to break. This happens because the maximum stress value is also higher than the tensile strength. This explains why the maximum displacement value obtained was 1252 mm. Since the material regime in the numeric model is linear elastic, even though the stresses obtained are higher than the yield strength, the simulation did not consider it, therefore the displacement values got much higher.

The only solution for this situation is to place cups on both sides of the 'V', which is not possible for the bending operation. It is impossible to manipulate the flatten boat hull with a gripper such as the one used for the first operation. This study was very important to understand that another solution needs to be found for the automation of the second bending operation. Nonetheless, the development and design of the gripper for the first bending operation will be carried out.

4.10. Vacuum cup subassembly

The vacuum cup subassembly, as seen in Figure 4.31, consists on two C-shape profiles (Profile 2) connected by another C-shape profile (Profile 1), that hold a group of vacuum cups. The technical drawings and the assembly drawing that shows how the components fit together and relevant technical information is available in Appendix C.



(a) 310 mm subassembly. (b) 280 mm subassembly.

Figure 4.31.: Two different vacuum cups subassembly.

As seen previously, there are two different vacuum cup position arrangements. One has a distance of 310 mm between the centre of the cups and the other has a distance of 280 mm. This arrangement allowed to group four vacuum cups together.

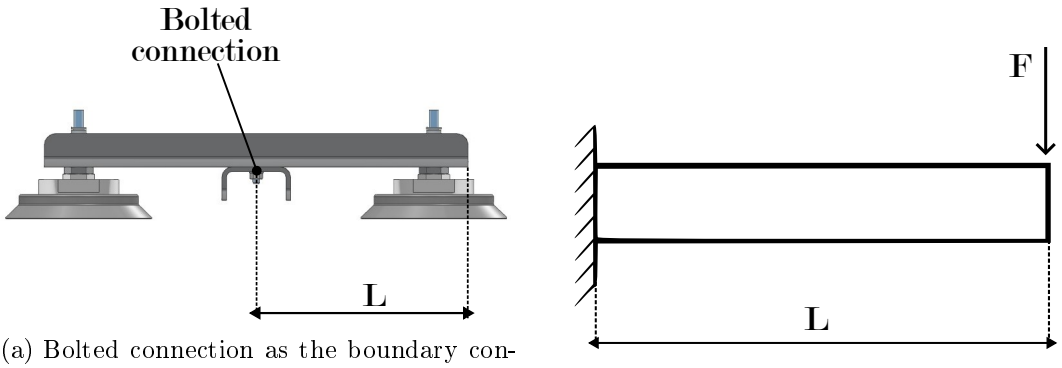
The 280 mm subassembly should only have two vacuum cups in each one, considering the vacuum cup allocation previously determined. However, four cups were placed in each subassembly just in case they were needed for other applications. Therefore, a pneumatic accessory called vacuum saving valve was incorporated on those two spare vacuum cups. It is used in applications where some of the vacuum cups are not holding the workpiece, so it ensures that the reduction of vacuum pressure is restricted and the workpiece may remain held by the rest of the pads [23].

The C-shape profile 1 and 2 geometries will be obtained with laser cutting as well as the through holes for the bolted connections since the low thickness of the steel plate allows the laser to cut with precision the oval shaped holes and the rest of the holes. The flanges will be bent using the bending manufacturing process.

All the oval shaped holes provide a large adjustment range not only for the vacuum cups, but also of the C-shaped profile in relation with the main aluminium profile. This ensures a modular design of the gripper that will be able to adapt to different geometries if necessary.

The reason for the C-shaped profile is to contribute to the bending strength of both profiles. During the bending operation, the gripper is positioned horizontally and each vacuum cup is subjected to the total theoretical holding force divided by the forty vacuum cups. This geometry minimizes the deflection of the profiles and helps keeping the workpiece as flat and level as possible in order to not compromise the bending manufacturing process. A simple bending solicitation calculation was done to validate the structural behaviour of the profiles.

C-shaped profile 2 will be analysed as a cantilever beam to simplify the problem, as seen in Figure 4.32. The bolted connection was represented as a fixed boundary condition to allow the symmetric representation of the problem as a cantilever beam.



(a) Bolted connection as the boundary condition.

(b) Cantilever beam simplification.

Figure 4.32.: Cantilever beam bending analysis simplification of the bolted connection.

The load applied to the end of the part is equal to the theoretical holding force divided by the forty cups, as seen in equation (4.16). This is a more conservative approach since this force was calculated with a very high safety factor for the calculation of the vacuum cups.

$$F = \frac{F_{th}}{40} \Leftrightarrow F = 314.63\,\mathrm{N} \tag{4.16}$$

The cross section and respective centroid of the part is represented in Figure 4.33. Table 4.7 presents the second moments of area, Young's modulus of the material, the load, and the length values.

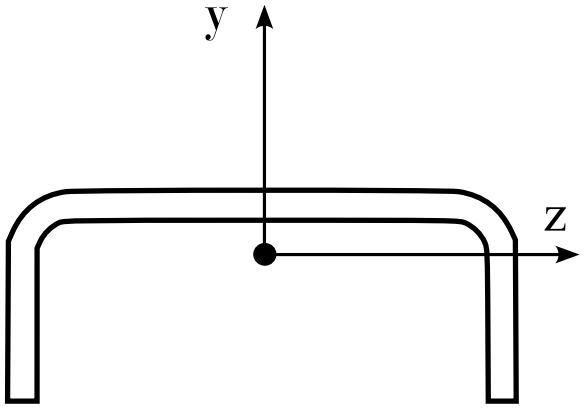


Figure 4.33.: Cross section of the C-shaped profile.

Table 4.7.: Variables used on the bending calculation of the C'-shaped profile.

Parameters	Values
F/N	314.63
L/mm	185
E/MPa	210000
I_z/mm^4	33986.99
I_y/mm^4	304056.46

The maximum bending moment, M, was calculated with equation (4.17).

$$M = F \cdot L \Leftrightarrow M = 58\,206.55\,\mathrm{N\,mm} \tag{4.17}$$

The maximum bending stress was calculated with equation (4.18). The distance from the neutral axis to the furthest point at the cross sections is equal to 18.57 mm.

$$\sigma_{\max} = \frac{M \cdot y_{max}}{I_z} \Leftrightarrow \sigma_{\max} = 3.55\,\mathrm{MPa} \tag{4.18}$$

Where:

- σ_{max}/MPa - Maximum stress at the critical point;

- $y_{\max}$/mm - Distance from the neutral axis to the furthest point at the cross section;

- I_z/mm^4 - Second moment of area relative to z-axis.

The maximum bending stress obtained is insignificant compared to the yield strength of structural steel. The structural strength of the profile is validated.

The maximum deflection was calculated with equation (4.19) used for cantilever beams [50].

$$\delta_z = \frac{F \cdot L^3}{3EI_z} \Leftrightarrow \delta_z = 0.095\,\text{mm} \tag{4.19}$$

The maximum bending operation displacement value obtained was 0.095 mm, which is negligible for the rigidity integrity of the profile.

This analysis was also done for the C-shaped profile 1 which connects the other two profiles. The load applied is double the previous one because each side of the profile is subjected to the load of two vacuum cups. Table 4.8 presents the second moments of area, Young's modulus of the material, the load, and the length values.

Table 4.8.: Variables used on the bending calculation of the 'C'-shaped profile.

Parameters	Values
F/N	629.27
L/mm	225
E/MPa	210000
I_z/mm^4	32119.30
I_y/mm^4	208384.78

The distance from the neutral axis to the furthest point at the cross sections is equal to 17.95 mm. The maximum bending stress and the maximum bending operation displacement were calculated in equation (4.20) and (4.21).

$$\sigma_{\text{max}} = \frac{M \cdot y_{max}}{I_z} \Leftrightarrow \sigma_{\text{max}} = 12.20\,\text{MPa} \tag{4.20}$$

$$\delta_z = \frac{F \cdot L^3}{3EI_z} \Leftrightarrow \delta_z = 0.36\,\text{mm} \tag{4.21}$$

Both results do not compromise the structural integrity of the profile.

4.11. Pneumatic system

The whole pneumatic system will be explained from the vacuum cup to the ejectors. All pneumatic components were selected from SMC with their help for this specific application,

and the respective technical information is available on the assembly drawings parts list in Appendix C.

The first step was to select the vacuum ejectors. SMC recommended four multi-stage vacuum ejectors (ZL112A-K15LOU-DBL), represented in Figure 4.34, with a maximum suction flow rate of $100\,\mathrm{L\,min^{-1}}$ on each and an achievable vacuum pressure of $-84\,\mathrm{kPa}$. The type of material to manipulate determines the vacuum tightness, and consequently the air consumption. For a safe implementation of the solution, experimental tests must be carried out, having in mind that if the four vacuum ejectors are not enough, the pneumatic system was designed to allow the insertion of more ejectors ir order to ensure that the system functions properly. The ejectors will be placed on the back of the robot.

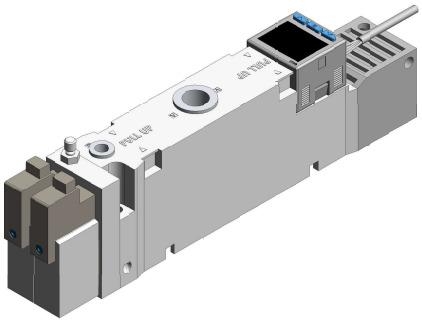
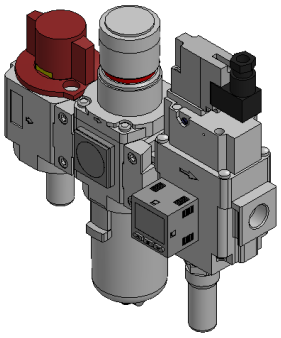


Figure 4.34.: 3D CAD representation of the vacuum ejector (ZL112A-K15LOU-DBL) [51].

This ejector has a $\phi 6\,\mathrm{mm}$ supply port where it will be connected to the the factory's compressed air distribution network. Before the connection to the air distribution network, a SMC air treatment unit (AC30-RBA001), represented in Figure 4.35, was also selected with an air filtration system. A double branch male elbow (KQ2ZD06-03AS), represented was also selected to allow four pneumatic tubes to exit from the air treatment system to the four ejectors.



(a) 3D CAD of the SMC air treatment [51].



(b) 3D CAD of the elbow connection [52].

Figure 4.35.: Pneumatic system between the air distribution network and the vacuum ejectors.

The vacuum port of each ejector has a ϕ12 mm. A tube-tube connection with a 'Y' union (KQ2U12-00A), as seen in Figure 4.36, was used to transform the four exit pneumatic tubes into two pneumatic tubes.



Figure 4.36.: Tube-tube pneumatic connection with a 'Y' union [53].

A ramification of the main pneumatic line is essential for applications that require several vacuum cups with simultaneous vacuum distribution. The smaller the diameter is, the higher the air flow resistance. However, a larger diameter is associated with a increase in air evacuation time [23]. For this application, it was considered a ramification of ϕ12-ϕ10-ϕ8 mm.

The two pneumatic tubes coming from the vacuum ejector will connect directly to a distributor block that will divide and branch the pneumatic system. The two pneumatic tubes of ϕ12 mm will be transformed into two pneumatic tubes of ϕ10 mm as seen in Figure 4.37. One tube will be directed to the right side of the gripper and the other to the left side. These tubes are connected to block distributors on each vacuum cup subassembly.

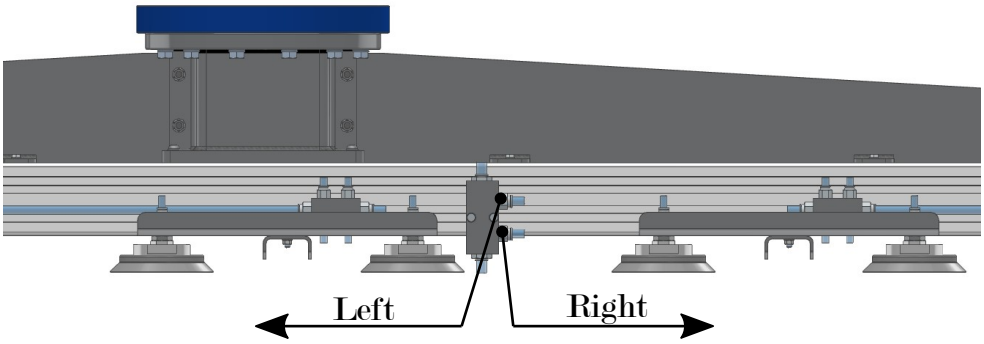


Figure 4.37.: Main block distributor at the centre of the gripper.

All vacuum cup subassemblies have a block distributor, shown in Figure 4.38, that will branch off the ϕ10 mm air supply tube into four ϕ8 mm, each one that will connect to the vacuum cup of that subassembly. For the last distributor at both right and left side, a pneumatic cap had to be inserted to block the the passage of air.

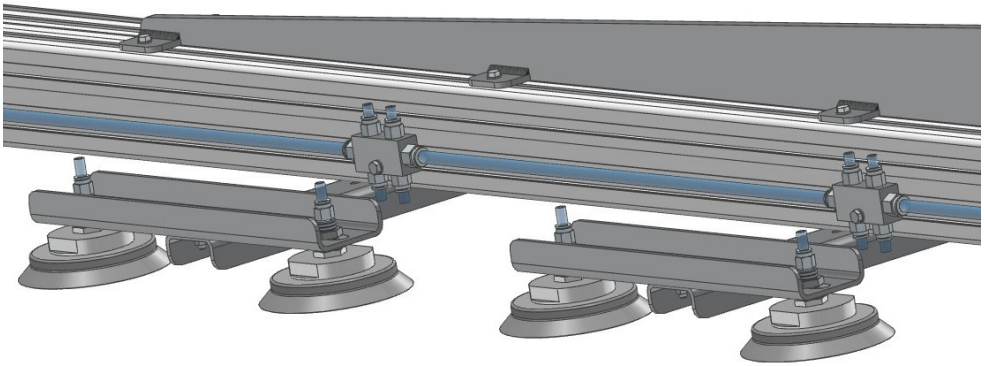


Figure 4.38.: Block distributors for each vacuum cup subassembly.

For all the pneumatic connections between the tubes and the distributors or the cups, pneumatic fittings were used. It is a pneumatic coupling used to connect pneumatic tubes for the compressed air to pass through. The pneumatic fitting must be selected taking into account the diameter of the applicable tube and the connection thread. Table 4.9 presents all the fittings used for this system.

Table 4.9.: All SMC pneumatic fittings used for the system.

SMC pneumatic fitting	Diameter/mm	Connection thread
KQ2H12-03AS	ϕ12	Rc3/8
KQ2H10-04AS	ϕ10	Rc1/2
KQ2H10-02AS	ϕ10	Rc1/4
KQ2H08-01AS	ϕ8	Rc3/8

4.12. Discussion

The vacuum cup selection, respective characteristics and accessories, total number of cups, and their position on the flatten boat hull were studied and established for both bending processes.

For the first bending operation, the workpiece manipulation was validated with the vacuum cups position established throughout the flatten boat hull. A possible bending sequence for this process is represented in Figure 4.39.

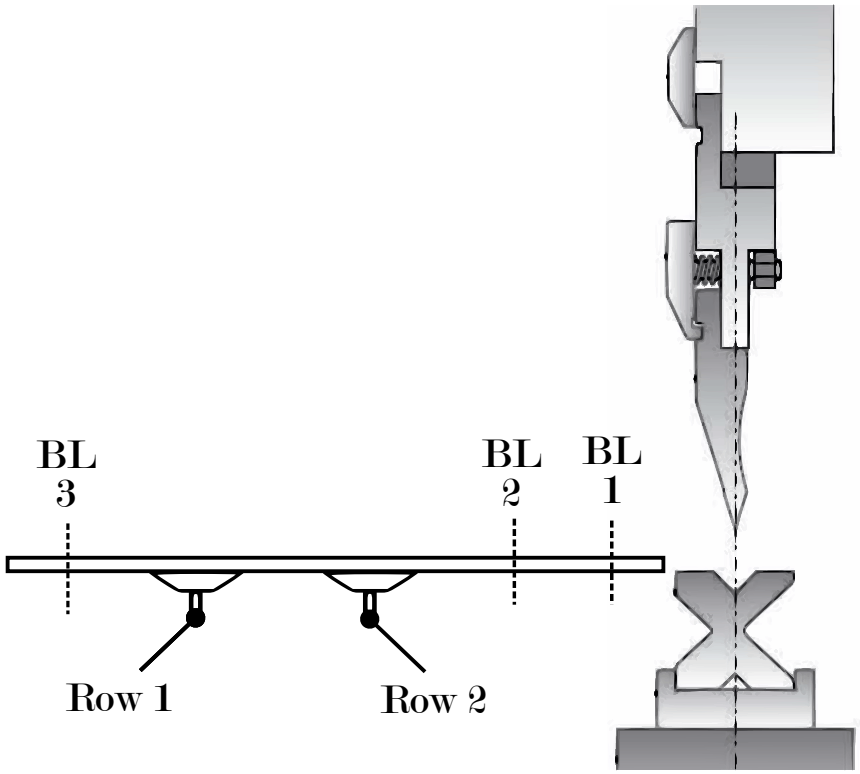


Figure 4.39.: Illustration of the bending sequence for the first bending process [12].

The gripper would be grasping the workpiece with the vacuum cups from bellow to allow more unrestricted motions. The bending sequence would be the following: BL 1, BL2, and BL 3. After the first two bends, the robot would need to do a rotative motion of 180° in air to rotate the workpiece in order to do the final bending BL 3, without the need for a regrip station. As seen in the previous discussion on the finite element analysis, the robot would also need to be programmed in order to raise the workpiece before placing it on the press brake die to compensate for the maximum displacement obtained: 26.44 mm. In real life, the displacement field throughout the workpiece may vary slightly comparing to the numeric results. Therefore, it is imperative to do experimental tests with the robot, in order to ensure a safe manipulation and to allow the robot programmer to test it several times until the final desired result is achieved and the bending operation can be completed with success.

For the second bending operation, the conclusion from the finite element analysis was that it was impossible to manipulate the workpiece with the same gripper and vacuum cups position as the first bending operation. The problem lies on not being able to place the cups on both sides of the 'V', leading to a critical stress concentration zone that structurally compromises the manipulation. However, the finite element analysis was performed with the flatten boat hull without the previous three bending operations, which would increase the strength of the material due to cold working. Besides that, the U-shape bendings would also cause an increase on the second moments of area on the workpiece cross section, which would lead to a lower deflection.

Instead of doing a finite element analysis considering the workpiece as a shell with a constant cross section thickness, a 3D finite element analysis could be implemented taking

into account the 3D geometry of the cross section with the 'U'-shape bendings. However, creating an accurate mesh for a very thin plate with a complex cross-section is difficult and time-consuming. The mesh must be fine enough to capture the thinness and the geometric intricacies, leading to a large number of elements. Standard 3D elements might not be well-suited for very thin structures, where specialized shell or plate elements would be more appropriate. Using inappropriate elements can lead to inaccuracies in stress and deformation predictions. Due to the complex 3D geometry, the appearance of distorted elements is a common issue that can lead to numerical inaccuracies. Maintaining good element quality in a complex geometry is challenging. This will be discussed for future works.

Finally, the vacuum cup subassembly of the gripper was presented and structurally analysed. The pneumatic system that allows the vacuum system to operate was also covered.

The structural design and development of the gripper for the first bending operation will be analysed in the following Chapter 5.

5. Gripper structure

In this chapter, the gripper design was addressed from scratch. The main structure, the connection between the gripper profile and all other subassemblies, the design of components, manufacturing processes and materials used, and the structural calculations were covered. The final goal was to present all the technical drawings for the gripper assembly.

5.1. Aluminium profile selection

In the gripper design, there were an enormous number of iterations and changes. Initially, all the structural analysis and calculations were done considering the payload of 400 kg, since it was impossible to know the final mass of the gripper. The mass kept changing throughout the design process, which led to several iterative processes; the structural calculations were redone several times; and even the design of the part's geometries kept changing. Due to the complexity of this process and the massive quantity of iterations done, it is impossible to address all the changes performed throughout the gripper's development.

In this section, the structural analysis of the profile was first analysed without the structural reinforcement. Afterwards, the structural part was also analysed in order to reinforce the profile according to bending and to avoid the use of a very expensive profile.

5.1.1. Strength analysis

The first step was to study the strength resistance of all profiles subjected to bending. Euler-Bernoulli beam theory was used for the analytical structural analysis of the profile. This theory is the simplest classical theory for beam bending. It assumes that the cross section of the beam is always perpendicular to the neutral axis, even after the beam deformation. It also assumes that the dimensions of the cross section are small compared to the beam's length, and it does not take into account the shear deformation, although it can be used to determine shear stresses [50].

There are also other theories such as the Timoshenko beam theory which is an extended version of the Euler-Bernoulli beam theory that considers the effects of shear deformation and states that the cross section after the deformation does not have to be perpendicular to the neutral axis [50].

The Euler-Bernoulli theory was chosen because the profile behaves as a very long beam (high length to thickness ratio).

The first step to study the mechanical structural behaviour of the beam is to understand the bending stress state involved. The profile will be subjected to the weight of the gripper,

including all the parts, and the weight of the workpiece. For analytical purposes, this can be simplified into a distributed load applied on the profile surface. Therefore, the profile will only be subjected to a bending stress state. The free body diagram of the profile and its cross section axis are represented in Figure 5.1 and 5.2.

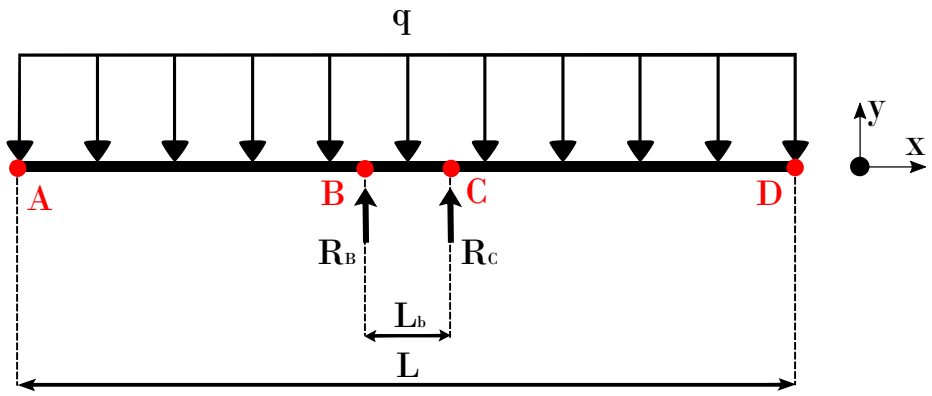


Figure 5.1.: Free body diagram of the profile.

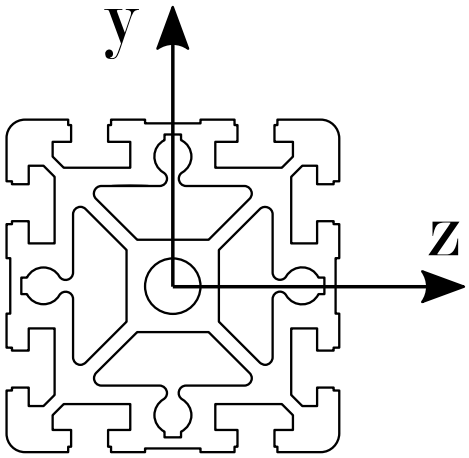


Figure 5.2.: Example of a cross section of an aluminium profile.

Where:

- $q/\mathrm{N\,mm^{-1}}$ - Distributed load applied on the profile;

- R_B/N - Reaction on the pinned support at point B;

- R_C/N - Reaction on the pinned support at point C;

- L_b/mm - Distance between the bolts located at the gripper interface;

- L/mm - Total length of the profile.

The pinned supports located at point B and C represent a simplification of the bolted

connection of the interface into the profile. This can be seen in Figure 5.3.

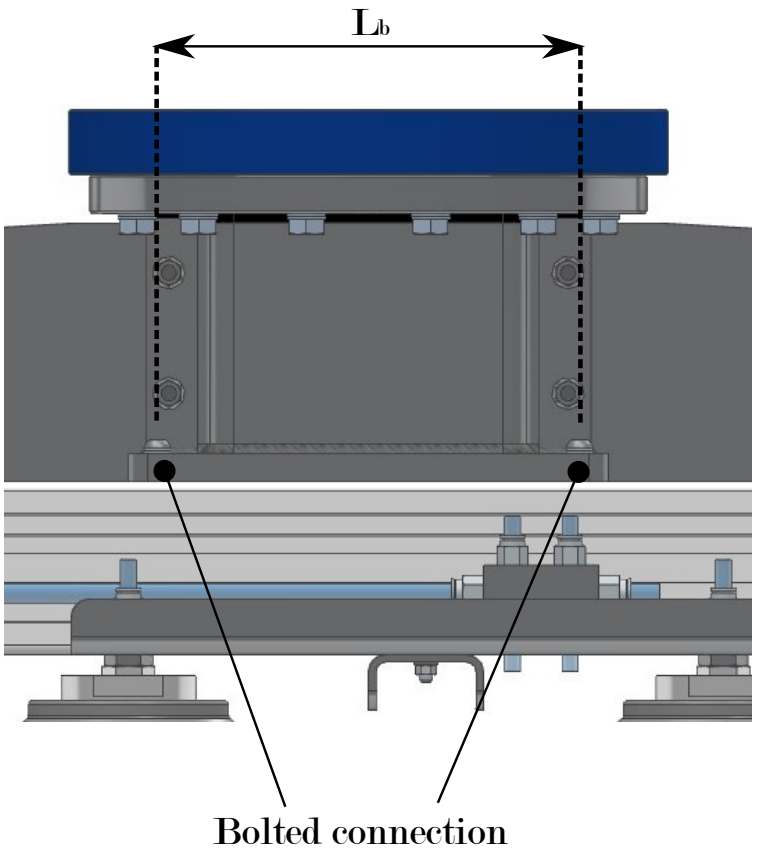


Figure 5.3.: Bolted connection on the interface connected to the gripper profile.

The length, L, of the aluminium profile must also be determined. For that, the distance between cup centres on the highest length row was measured on SolidEdge software. The distance measured was equal to 6420 mm. However, the aluminium profile doesn't need to be that long because the vacuum cup subassembly allows several modular adjustments. The cups can be positioned outside of the profile, as seen in Figure 5.4.

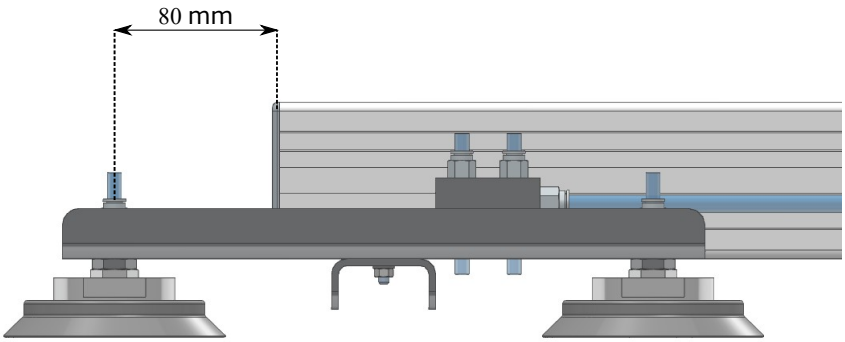


Figure 5.4.: Vacuum cup subassembly position in the final gripper design solution.

So, 80 mm were removed from each each of the profile. The final profile length is determ-

ined in equation (5.1).

$$L = 6420 - 2 \cdot 80 \Leftrightarrow L = 6260\,\text{mm} \tag{5.1}$$

The distributed load, q, corresponds to the distributed load caused by the self weight of the global mass of the gripper and the workpiece. Initially, this value was considered to be equal to the payload of the robot: 400 kg. The distributed load is given by equation (5.2).

$$q = \frac{m \cdot g}{L} \Leftrightarrow q = \frac{400 \cdot 10^{-3} \cdot 9.81 \cdot 10^{3}}{6260} \Leftrightarrow q = 626.84 \times 10^{-3}\,\text{N mm}^{-1} \tag{5.2}$$

Where:

- m_{total}/t - Sum of the global mass of the gripper and workpiece;

- $g/\text{mm s}^{-2}$ - Gravity constant on earth;

The dimensions and distributed load were presented in Table 5.1.

Table 5.1.: Variables for the interpretation of the free body diagram.

Variables	Values
$q/\text{N mm}^{-1}$	$626.84 \cdot 10^{-3}$
L/mm	6260
L_b/mm	220

The resistance of a beam subjected to bending is determined by comparing the maximum stress at the critical point, σ_{max}, with the yield stress, σ_y , of the material used. In the case of bending, the maximum stress occurs at the furthest point from the neutral axis. For this situation, the following equation (5.3) is used to determine the maximum stress.

$$\sigma_{max} < \sigma_y \Leftrightarrow \frac{M \cdot y_{max}}{I_z} < \sigma_y \tag{5.3}$$

Where:

- σ_{max}/MPa - Maximum stress at the critical point;

- $M/\text{N mm}$ - Maximum bending moment;

- y_{max}/mm - Distance from the neutral axis to furthest point at the cross section;

- I_z/mm^4 - Second moment of area relative to z-axis.

For the selection of normalized profiles, the manufacture usually provides the moment of resistance, W, which corresponds to the resistance of the beam to bending, relative to an axis. It is defined as the maximum moment that can be withstand by the cross section of the profile without causing yielding. This is important in the selection of profiles since it ensures that the profile chosen will not fail under the applied loads. The moment of resistance is calculated through equation (5.4).

$$W = \frac{I}{y_{max}} \tag{5.4}$$

Where:

- W/mm^3 - Moment of resistance.

With equation (5.3) and (5.4), the criterion for selection of the profile is presented in equation (5.5).

$$\frac{M}{W} < \sigma_y \Leftrightarrow W > \frac{M}{\sigma_y} \tag{5.5}$$

The moments of resistance for all available profiles in Bosch Rexroth catalogue can be consulted in Appendix B.2. The mechanical properties of the aluminium alloy Al6060 used on the profiles are presented in Table 5.2 [54].

Table 5.2.: Mechanical properties of Al6060.

Properties	Values
Young's modulus, E/GPa	70
Poisson's ratio, ν	0.34
Density, $\rho/\text{kg m}^{-3}$	2700
Yield Strength, σ_y/MPa	195
Tensile Strength, σ_r/MPa	245

The only thing left is the determination of the maximum bending moment through the bending moment diagram considering the free body diagram already presented.

The reactions on both supports were calculated using the static equilibrium of forces and moments, shown in equation (5.6).

$$\begin{cases} \sum M_B = 0 \\ \sum F_y = 0 \end{cases} \Leftrightarrow \begin{cases} -qL \cdot \frac{L_b}{2} + R_c \cdot L_b = 0 \\ R_B + R_C - qL = 0 \end{cases} \Leftrightarrow \begin{cases} R_c = \frac{qL}{2} \\ R_B = \frac{qL}{2} \end{cases} \tag{5.6}$$

Next, the profile will be divided into three sections in order to obtain the bending moment equation for each section.

Figure 5.5 represents section i: $0 \leq x \leq x_B = \frac{L}{2} - \frac{L_b}{2}$.

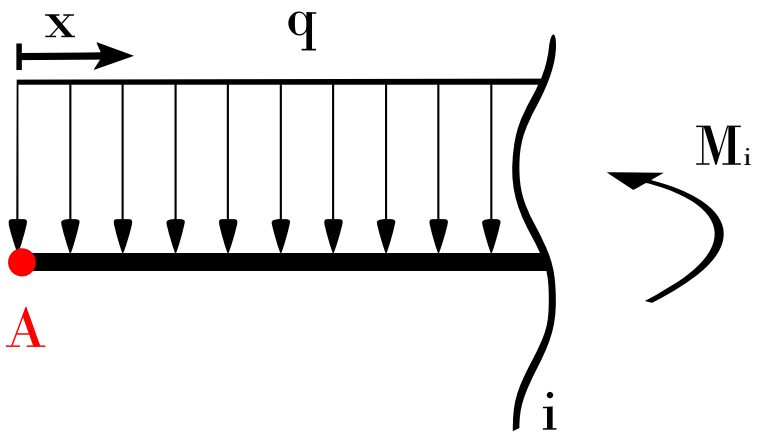


Figure 5.5.: Bending moment representation in section i.

The bending moment for this section is calculated in equation (5.7).

$$\sum M_i = 0 \Leftrightarrow M_i + qx \cdot \frac{x}{2} = 0 \Leftrightarrow M_i = -\frac{qx^2}{2} \tag{5.7}$$

Figure 5.6 represents section ii: $x_B \leq x \leq x_C = \frac{L}{2} + \frac{L_b}{2}$.

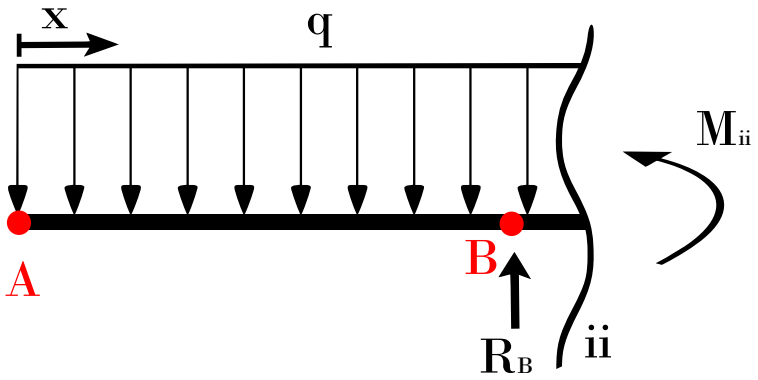


Figure 5.6.: Bending moment representation in section ii.

The bending moment for this section is calculated in equation (5.8).

$$\begin{aligned} \sum M_{ii} = 0 &\Leftrightarrow M_{ii} + qx \cdot \frac{x}{2} - \frac{qL}{2} \cdot (x - x_B) \\ &\Leftrightarrow M_{ii} = -\frac{qx^2}{2} + \frac{qL}{2}\left(x - \frac{L}{2} + \frac{L_b}{2}\right) \end{aligned} \tag{5.8}$$

Figure 5.7 represents section iii: $x_C \leq x \leq L$.

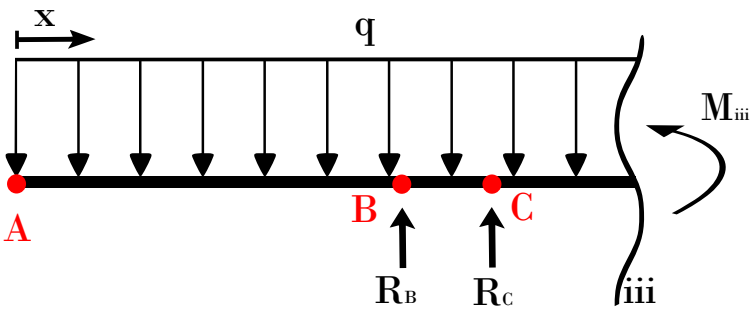


Figure 5.7.: Bending moment representation in section iii.

The bending moment for this section is calculated in equation (5.9).

$$\begin{aligned} \sum M_{iii} = 0 \Leftrightarrow M_{iii} - \frac{qL}{2}(x - x_B) - \frac{qL}{2}(x - x_C) + qx \cdot \frac{x}{2} = 0 \\ \Leftrightarrow M_{iii} - \frac{qL}{2}\left(x - \frac{L}{2} + \frac{L_b}{2}\right) - \frac{qL}{2}\left(x - \frac{L}{2} - \frac{L_b}{2}\right) - \frac{qx^2}{2} = 0 \\ \Leftrightarrow M_{iii} = qxL - \frac{qL^2}{2} - \frac{qx^2}{2} \end{aligned} \tag{5.9}$$

Finally, the bending moment diagram is determined as seen in Figure 5.8.

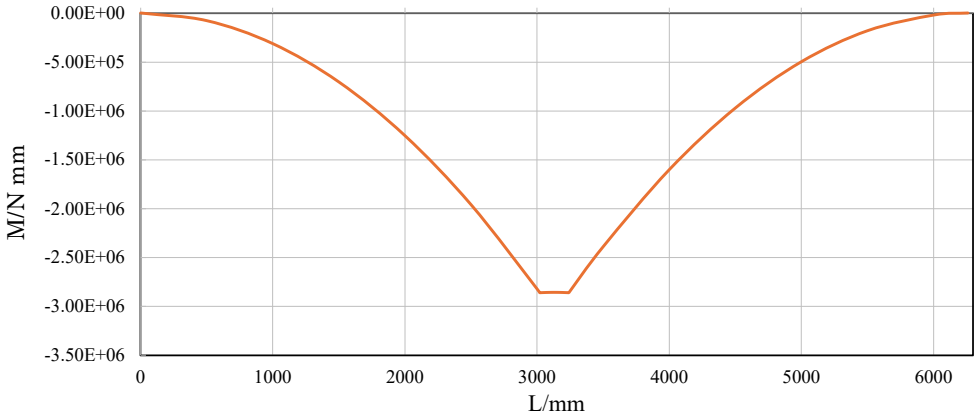


Figure 5.8.: Bending moment diagram.

The maximum bending moment happens at section B and C. It is given by equation (5.10).

$$M = -\frac{q}{8}(L - L_b)^2 \Leftrightarrow M = -2858.50 \times 10^3 \,\mathrm{N\,mm} \tag{5.10}$$

The moment of resistance is determined with equation (5.5).

$$W > \frac{M}{\sigma_y} \Leftrightarrow W > \frac{2858.50 \cdot 10^3}{195} \Leftrightarrow W > 14.66 \times 10^3 \,\mathrm{mm}^3$$

It also included a safety factor of 1.5 for the moment of resistance, as seen in the following equation (5.11).

$$W > 14.66 \cdot 10^3 \cdot 1.5 \Leftrightarrow W > 21.99 \times 10^3\,\mathrm{mm}^3 \tag{5.11}$$

The Bosch Rexroth catalogue, presented in Appendix B.2, provides the moment of resistance for both axis of the cross section (W_z and W_y), depending in the position of the profile when subjected to the bending moment. In this application, the profile will be conditioned by the manipulation motions of the robot. This means that the moment of resistance must be higher than $21.99 \times 10^3\,\mathrm{mm}^3$ for both axis. After consulting the catalogue, twenty five profiles fulfil this requirement, as seen in Table 5.3.

Table 5.3.: Twenty five profiles that fulfil the strength analysis requirement.

Number	Bosch Rexroth Profiles
1	40x80L 2NVS
2	40x80L 3NVS
3	40x160L
4	80x80L
5	80x80L 4N
6	80x80L 4NVS
7	80x80L 6N
8	80x120L
9	80x160L
10	45x180
11	45x270
12	90x90SL
13	90x90L
14	90x90L 4N
15	90x90L 4NVS
16	90x90
17	90x180L
18	90x180
19	90x360
20	50x100L
21	50x150L
22	100x100L
23	100x200L
24	60x60
25	60x90

5.1.2. Rigidity analysis

The deflection of the profile caused by the bending solicitation must be analysed. It is expected high transverse displacement values at both ends of the profile because the profile

has a very high length.

By applying the Elastic Integration method, the differential equation of the elastic curve is obtained. This is represented in equation (5.12).

$$\frac{d^2y}{dx^2} = \frac{M}{EI_z} \tag{5.12}$$

Where:

- E/MPa - Young's modulus;

- M/N mm - Maximum bending moment;

- I_z/mm^4 - Second moment of area relative to z-axis.

With this equation, doing a double integration of the differential equation, the slope in each section $\left(\theta = \frac{dy}{dx}\right)$, and the deflection of the beam (y = δ(x)) are obtained. These equations need to be determined for each section. Although, since the profile is symmetrical, section i and iii will both have the same governing equations for the slope and deflection. The equations are only going to be calculated for section i and ii.

For section i, the first integration equation (5.13) (slope equation) is the following:

$$\begin{aligned} \frac{d^2y}{dx^2} = \frac{-\frac{q}{2}x^2}{EI} \Leftrightarrow EI\frac{dy}{dx} &= -\frac{q}{6}x^3 + C_1 \\ \Leftrightarrow EI \cdot \theta_i(x) &= -\frac{q}{6}x^3 + C_1 \end{aligned} \tag{5.13}$$

For section i, the second integration equation (5.14) (deflection equation) is the following:

$$\begin{aligned} EI\frac{dy}{dx} = -\frac{q}{6}^3 + C_1 \Leftrightarrow EI \cdot y &= -\frac{q}{24}x^4 + C_1x + C_2 \\ \Leftrightarrow EI \cdot \delta_i(x) &= -\frac{q}{24}x^4 + C_1x + C_2 \end{aligned} \tag{5.14}$$

For section ii, the first integration equation (5.15) (slope equation) is the following:

$$\begin{aligned} \frac{d^2y}{dx^2} &= \frac{-\frac{q}{2}x^2 + \frac{qL}{2}\left(x - \frac{L}{2} + \frac{L_b}{2}\right)}{EI} \\ \Leftrightarrow EI \cdot \theta_{ii}(x) &= -\frac{q}{6}x^3 + \frac{qL}{2}\left(\frac{x^2}{2} - \frac{L}{2}x + \frac{L_b}{2}x\right) + C_3 \end{aligned} \tag{5.15}$$

For section ii, the second integration equation (5.16) (deflection equation) is the following:

$$\begin{aligned} EI\frac{dy}{dx} &= -\frac{qx^3}{6} + \frac{qL}{2}\left(\frac{x^2}{2} - \frac{L}{2}x + \frac{L_b}{2}x\right) + C_3 \\ \Leftrightarrow EI \cdot \delta_{ii}(x) &= -\frac{q}{24}x^4 + \frac{qL}{2}\left(\frac{x^3}{6} - \frac{L}{4}x^2 + \frac{L_b}{4}x^2\right) + C_3x + C_4 \end{aligned} \tag{5.16}$$

Where:

- C_1, C_2, C_3, C_4 - Integration constants.

These integration constants are determined from the profile free body diagram boundary conditions.

The first boundary condition considered is represented in equation (5.17). Considering the pinned support reactions in the free body diagram seen in Figure 5.1 and the uniform load along its entire length, it is possible to conclude that the slope is zero at the midpoint of the profile.

$$\theta_{ii}\left(\frac{L}{2}\right) = 0 \tag{5.17}$$

The second boundary condition considered is represented in equation (5.18). The slope in section i and the slope in section ii must be equal to each other at their common point B.

$$\theta_i(x_B) = \theta_{ii}(x_B) \tag{5.18}$$

The third and fourth boundary conditions considered are represented in equation (5.19) and (5.20), respectively. The displacement in both sections i and ii at their common point B, where is located the pinned support, must be equal to 0.

$$\delta_i(x_B) = 0 \tag{5.19}$$

$$\delta_{ii}(x_B) = 0 \tag{5.20}$$

The system of equations for the calculation of the integration constants is presented in equation (5.21).

$$\begin{cases} -\frac{q}{6}\left(\frac{L}{2}\right)^3 + \frac{qL}{2}\left(\frac{\left(\frac{L}{2}\right)^2}{2} - \frac{L}{2}\frac{L}{2} + \frac{L_b}{2}\frac{L}{2}\right) + C_3 = 0 \\ -\frac{q}{6}{x_B}^3 + C_1 = -\frac{q}{6}{x_B}^3 + \frac{qL}{2}\left(\frac{{x_B}^2}{2} - \frac{L}{2}x_B + \frac{L_b}{2}x_B\right) + C_3 \\ -\frac{q}{24}{x_B}^4 + C_1 x_B + C_2 = 0 \\ -\frac{q}{24}{x_B}^4 + \frac{qL}{2}\left(\frac{{x_B}^3}{6} - \frac{L}{4}{x_B}^2 + \frac{L_b}{4}{x_B}^2\right) + C_3 x_B + C_4 = 0 \end{cases} \tag{5.21}$$

Using Microsoft Excel mathematical functionalities, this system of four equations could be solved in order to obtain all 4 integration constants. With all the parameters known and the second moments of area for both axis of all profiles available in the Bosch Rexroth catalogue in Appendix B.2, the displacement values can be determined for the twenty five profiles that fulfilled the strength analysis requirement.

5.1.2.1. Results and discussion

Initially it was established a maximum transversal displacement (occurring at both ends of the profile) of 40 mm. This value was defined taking into account the 400 kg payload. It is expected in the last iteration to obtain a lower global mass of the gripper and workpiece, leading to lower maximum displacement values. If the robot rotates the gripper, the second moments of area of the profile cross section subjected to bending will change since the axis of the cross section will also rotate.

So, this maximum transversal displacement values is a must for both situation: δ_z and δ_y. Figure 5.9 presents a graph containing all profiles of the twenty five with both displacement values bellow 40 mm.

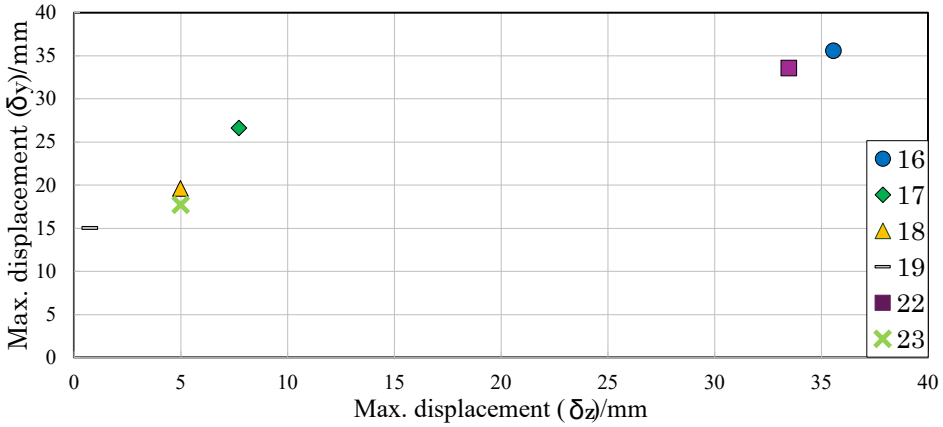


Figure 5.9.: All profiles with displacements values bellow 40 mm.

The last 6 profile candidates were the following:

16. 90x90
17. 90x180L
18. 90x180
19. 90x360

22. 100x100L 23. 100x200L

There is also another critical thing to consider. The 40 mm maximum displacement was chosen taking into account the manipulation and different motions that gripper are subjected due to the robot. However, during the bending operation it is crucial to minimize even more the maximum displacement of the profile in that horizontal bending position because it could compromise the bending operation results. So, it was also established a maximum bending operation displacement of 8 mm for the gripper profile. This is equal to the lowest displacement between δ_z and δ_y. For a quadrangular symmetrical profile, the values of δ_z and δ_y will be the same. However, for a rectangular profile, such as the one in Figure 5.10, the z-axis of the cross section must be parallel to the workpiece surface plane during the bending operation so that the maximum bending operation displacement is the lowest possible. In other words, the profile has to be rotated 90° for the horizontal bending position.

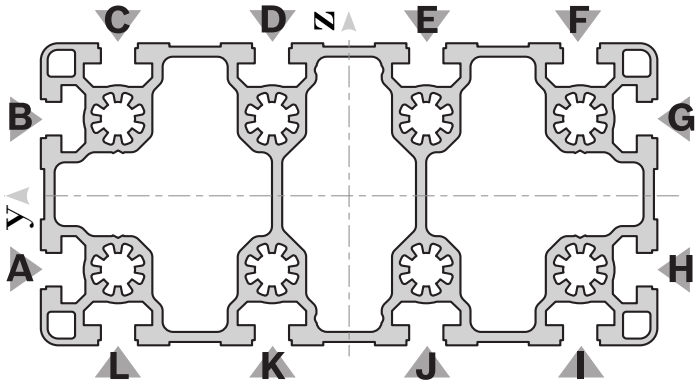


Figure 5.10.: Rectangular profile during the bending operation [54].

Figure 5.11 shows the six profiles maximum bending operation displacement and their weight per length.

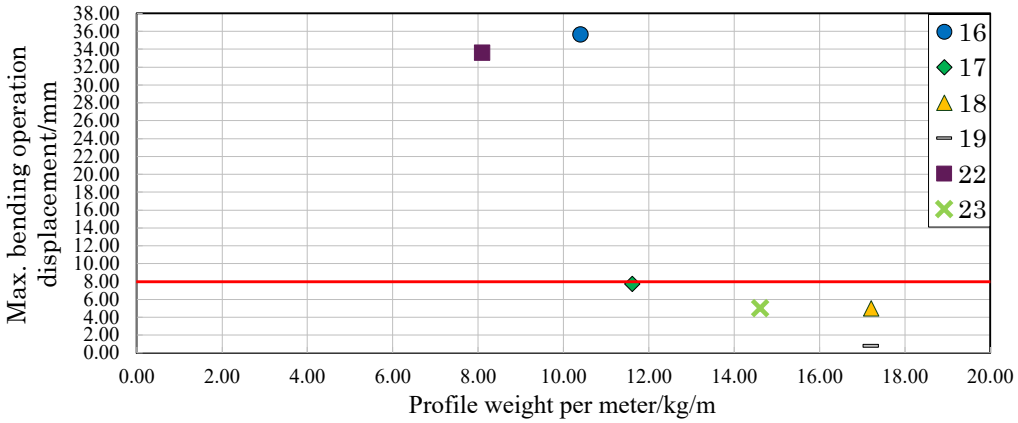


Figure 5.11.: Bending operation displacement in function of weight per meter for each profile.

The distributed load considered was the 400 kg robot payload. However, it is essential

to ensure the lowest weight possible for the profile because at the end all structural calculations were redone considering the final assembly weight of the gripper. All the profiles that fulfil the 8 mm are rectangular profiles. Due to its geometry, they have much higher second moments of inertia subjected to bending during the bending operation compared to the quadrangular profiles. The two profiles that do not meet the requirement are indeed quadrangular profiles.

The obvious choice would be profile 17 (90x180L) since it fulfils the requirement and has the lowest weight per length of all the profiles that are acceptable. However, it is imperative to take into account the price for each profile presented in Table 5.4.

Table 5.4.: Price quotation for all six profiles.

Number	Bosch Rexroth Profiles	Price/€
16	90x90	757.71
17	90x180L	1013.68
18	90x180	1564.50
19	90x360	2829.52
22	100x100L	724.78
23	100x200L	1468.72

It was noticed that all four profiles with displacements bellow 8 mm are far more expensive than the two profiles that do not meet the requirement. Therefore, aiming to make the global gripper design solution a lot cheaper, a structural part was designed to reinforce the profile to bending. Both the 90x90 (16) and 100x100L (22) profiles have a similar price. At the end, the profile 16 was chosen because it occupied lesser volume than the profile 22, even though it was slightly more expensive and heavier.

5.1.3. Structural reinforced solution

This section presents the analytical calculation of the deflection using a reinforced solution: aluminium profile + steel structure reinforcement. All the results, respective discussion and comparison will also be presented.

The geometry of the structural part has a massive impact on the profile deflection and on the stresses caused by the bending moment. The cross section of the structural part has a critical role because, by increasing the height and thickness, it will lead to an increase in the second moments of area, which will reduce the deflection of the whole structure. The length and other dimensions will also have a great impact on the deflection. It is imperative to understand that by increasing these dimensions, the weight of the part would also increase which contributes to the increase of the gripper deflection. Therefore, the inclusion or not of a reinforcement part and its design and geometry also changed several times during the project. Figure 5.12 shows the final iteration design for the structural reinforcement.

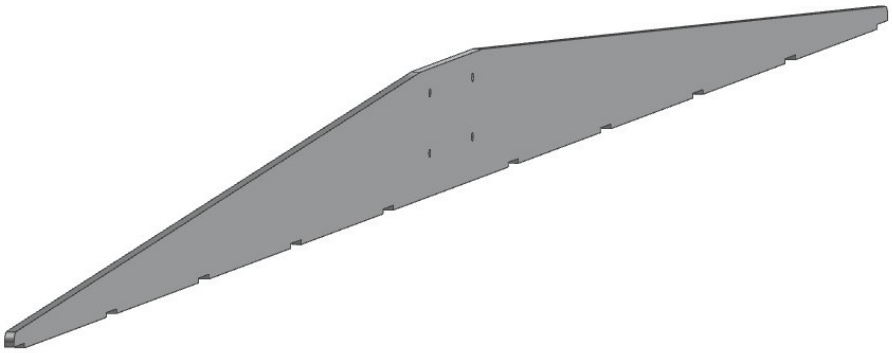


Figure 5.12.: Last design iteration for the structural reinforcement.

The main dimensions of the reinforcement are presented in Table 5.5.

Table 5.5.: Main dimensions of the structural reinforcement.

Dimensions	Values
Length	4260 mm
Height	135 mm
Thickness	10 mm

The cross section of the reinforced solution is presented in Figure 5.13.

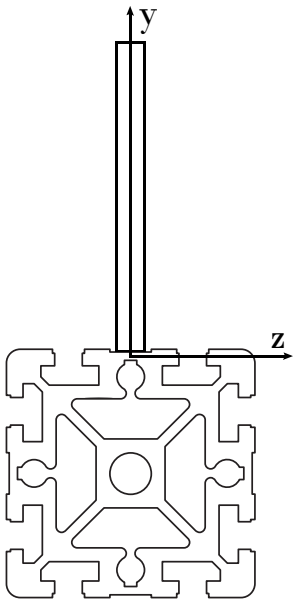


Figure 5.13.: Illustration of the cross section of the reinforced solution.

The Transformed Section Method was used to analyse the deflection of both beams considering that the profile is made of aluminium and the structure reinforcement is made of steel (S235jr) [55].

The first step is to transform the both cross sections into an equivalent section made only from one material. This original cross section is seen in Figure 5.14. For calculations purposes, the structural reinforcement is the beam 1 and the 90x90 profile is the beam 2.

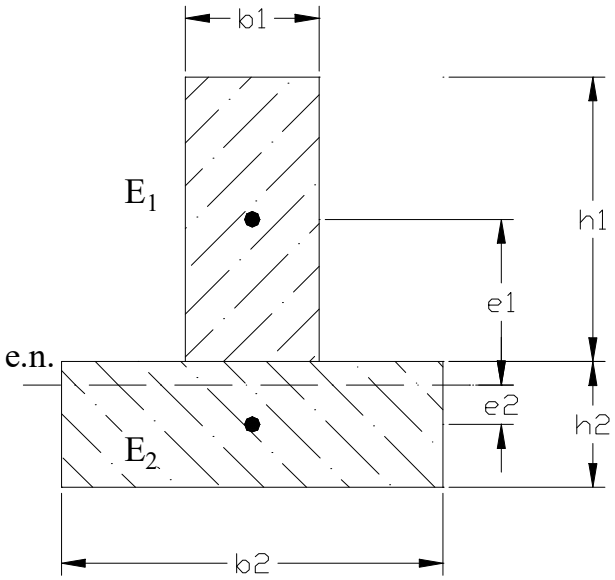


Figure 5.14.: Different material cross section of the reinforced solution [55].

Where:

- E_1, E_2/MPa - Young's modulus;

- b_1, b_2/mm - Width of the beams;

- h_1, h_2/mm - Height of the beams;

- e_1, e_2/mm - Distance from each centroid to the neutral axis.

The structural reinforcement cross section is constantly changing along its length, due to the triangular geometry. An analytical simplification was done, considering a constant rectangular cross section that is the same as the cross section at the centre of mass of the structural reinforcement (triangular prism solid simplification). This is shown in Figure 5.15.

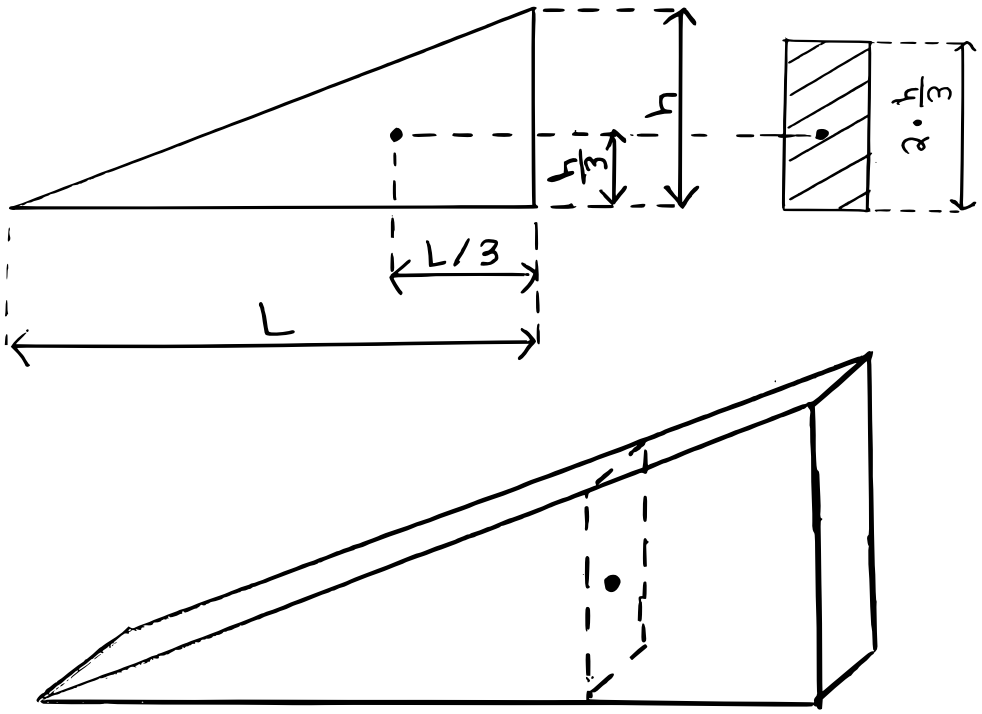


Figure 5.15.: Hand drawing of the geometric simplification of the reinforcement part cross section.

The vertical distance to the centroid is $\frac{h}{3}$. Therefore, the height of the cross section will be the double, as seen in equation (5.22). The width of the cross section remains the same.

$$h_1 = 2 \cdot \frac{h}{3} \Leftrightarrow h_1 = 2 \cdot \frac{135}{3} \Leftrightarrow h_1 = 90\,\text{mm} \tag{5.22}$$

The section was transformed into an equivalent section by changing the beam 1 material from steel to aluminium. The equivalent cross section is seen in Figure 5.16.

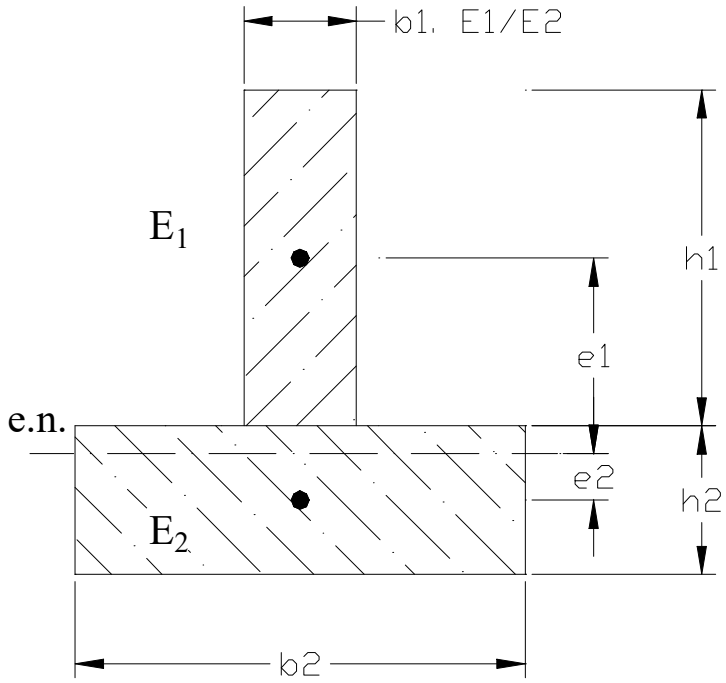


Figure 5.16.: Original cross section of the reinforced solution [55].

As seen, the width from beam 1 was changed by multiplying by the coefficient: $\frac{E_1}{E_2}$.

All the variables were defined in Table 5.6.

Table 5.6.: Variables for the reinforced solution analytical calculation.

Parameters	Values
E_1/MPa	210000
E_2/MPa	70000
b1/mm	10
h1/mm	90
b2/mm	90
h2/mm	90

The following step is to determine the principle second moments of area at the centroid of the reinforced beam. First, the centroid needs to be determined with the following equations (5.23) and (5.24).

$$\bar{z} = \frac{z_1 A_1 + z_2 A_2}{A_1 + A_2} \Leftrightarrow \bar{z} = 45\,\text{mm} \tag{5.23}$$

$$\bar{y} = \frac{y_1 A_1 + y_2 A_2}{A_1 + A_2} \Leftrightarrow \bar{y} = 81.72\,\text{mm} \tag{5.24}$$

- A_1, A_2/mm^2 - Area of the section;

- z_1, z_2, y_1, y_2/mm - Distances from the origin of the origin of the coordinate system represented in Figure 5.17 to the respective beam centroid.

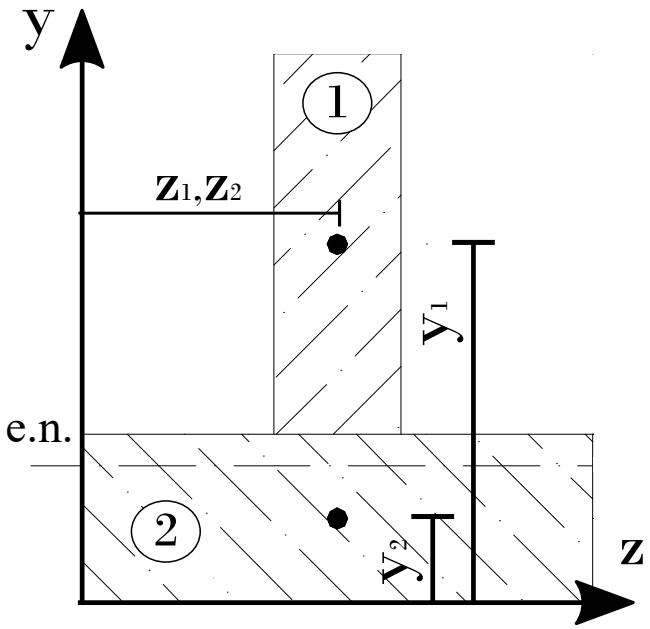


Figure 5.17.: Original cross section of the reinforced solution [55].

After this, the parameters e_1 and e_2 are easily determined using equations (5.25) and (5.26), respectively.

$$e_1 = h_2 + \frac{h_1}{2} - \bar{y} \Leftrightarrow e_1 = 53.28\,\text{mm} \tag{5.25}$$

$$e_2 = h_2 - \bar{y} \Leftrightarrow e_2 = 36.72\,\text{mm} \tag{5.26}$$

Figure 5.18 was used for the calculation of the second moments of area of the reinforced beam.

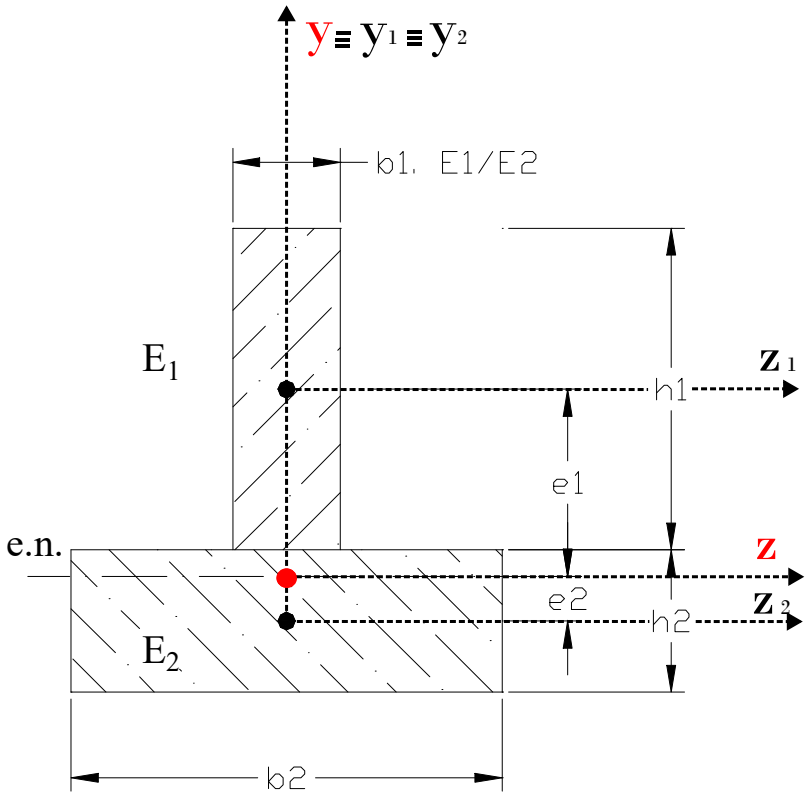


Figure 5.18.: Orthogonal coordinate system for the calculation of the second moments of area [55].

The second moments of areas at the centroid of beam 2 (Iz_2, Iy_2) are available on the Bosch Rexroth catalogue (Appendix B.2) and are equal to 2 998 000 mm^4.

The second moments of area at the centroid of beam 1 (Iz_1, Iy_1) were calculated using the equation (5.27) and (5.28) for rectangular cross sections.

$$Iz_1 = \frac{b_1 \frac{E_1}{E_2} \cdot h_1^3}{12} \Leftrightarrow Iz_1 = 1\,787\,785.71\,\text{mm}^4 \tag{5.27}$$

$$Iy_1 = \frac{h_1 \cdot \left(b_1 \frac{E_1}{E_2}\right)^3}{12} \Leftrightarrow Iy_1 = 191\,147.58\,\text{mm}^4 \tag{5.28}$$

Then, the principal second moments of area of the centroid of the reinforced beam can be determined. Firstly, the second moments of area relative to the z-axis for both beams were determined using the Steiner's theorem, as seen in equation (5.29) and (5.30).

$$Iz_1' = Iz_1 + A_1 \cdot (e_1)^2 \Leftrightarrow Iz_1' = 9\,307\,277.86\,\text{mm}^4 \tag{5.29}$$

$$Iz_2^{'} = Iz_2 + A_2 \cdot (e_2)^2 \Leftrightarrow Iz_2^{'} = 191\,147.58\,\text{mm}^4 \tag{5.30}$$

Then, the second moment of area relative to z-axis at the reinforced beam centroid is calculated with equation (5.31).

$$Iz = Iz_1^{'} + Iz_2^{'} \Leftrightarrow Iz = 17\,486\,922.98\,\text{mm}^4 \tag{5.31}$$

The second moments of area relative to the y-axis at the centroid of the reinforced solution are calculated with equation (5.32).

$$Iy = Iy_1 + Iy_2 \Leftrightarrow Iy = 3\,189\,147.58\,\text{mm}^4 \tag{5.32}$$

Finally, both deflections (δ_z and δ_y) can be determined using the principal second moments of area just calculated, considering the exactly same deflection analysis used for the profile in Section 5.1.2, which was already described in a Microsoft Excel spreadsheet. All other parameters remained the same.

5.1.3.1. Results and discussion

The maximum analytical displacements values obtained for the reinforced solution were the following:

$$\begin{cases} \delta_z \text{ (bending operation displacement)} = 6.10\,\text{mm} < 8\,\text{mm} \\ \delta_y = 33.45\,\text{mm} < 40\,\text{mm} \end{cases}$$

The reinforced solution is validated because the displacement values are bellow the maximum displacements values previously established.

At the end of the constructive solution design for the gripper, the global final mass of the gripper, m_{total}, was determined. Considering all the parts in the assembly including the reinforced solution, the value was 183.68 kg. The total mass that the gripper needs to support is calculated in equation (5.33).

$$\begin{aligned} m_{total} = m_{gripper} + m_{workpiece} \Leftrightarrow m_{total} &= 183.68 + 109.18 \\ \Leftrightarrow m_{total} &= 292.86\,\text{kg} \end{aligned} \tag{5.33}$$

Taking into account a more conservative approach and the fact that the robot acceleration was considered negligible during the structural calculations due to being very small, this value was rounded up to 300 kg.

Finally, the maximum analytical displacements values were recalculated for the reinforced solution:

$$\begin{cases} \delta_z \text{ (bending operation displacement)} = 4.57\,\text{mm} < 8\,\text{mm} \\ \delta_y = 25.08\,\text{mm} < 40\,\text{mm} \end{cases}$$

The final bending operation displacement obtained using the reinforced solution is 5.83 times lower than the one using only the same aluminium profile without the structural reinforcement. This shows how effective the reinforced solution implemented is.

5.1.4. Finite element analysis for the reinforced solution

There are two reasons why a finite element analysis was also done to further study the deflection of the reinforced solution.

On the one hand, it is important to validate the analytical results using finite element analysis and to study the influence of the length of the structural reinforcement on the final deflection results. The aim is to reduce the length of the beam several times in order to see its influence on the final deflection results, while the length of the aluminium profile remains unchanged. On the other hand, it is also important to take into account that in order to solve this problem analytically, a simplification of the cross section of the reinforcement part was done. So, a finite element analysis using the reinforcement part geometry was also done to study its impact on the final deflection results.

5.1.4.1. Beam numeric model

The best way to study the impact of the structural reinforcement beam length and to validate the analytical results is to use the beam modelling functionalities in Abaqus, which approximates the three-dimensional beam into a one-dimensional part. For that, a length has to be given and the respective cross section dimensions and material properties.

For the aluminium profile, it was used a generalized cross section profile and the respective area and second moments of area were given. For the structural reinforcement, a rectangular cross section was defined.

After the sections and the materials have been assigned, the mesh was created using a standard beam element: B21.

In the model assembly, the goal was to represent the free body diagram previously presented in Figure 5.1. In order to represent the connection between the profile and the aluminium part, both beam surfaces were tied into each other with a tie constraint. A boundary condition was created to simulate the pinned support and a symmetric boundary conditions was created in the middle of the beam to simplify the numeric model. Finally, a distributed load was created representing the 300 kg. The assembly can be seen in Figure 5.19.

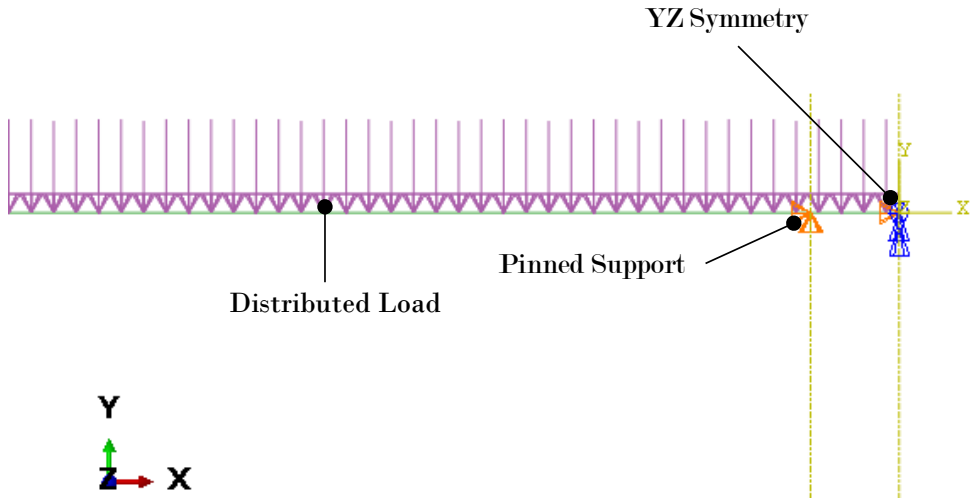


Figure 5.19.: Final assembly of the numeric beam model with the respective boundary conditions and load.

A mesh refining study was also implemented on all the following numeric models. The simulation final data were the following:

- Total number of nodes: 2652;
- Total number of elements: 2650 linear line elements of type B21.

Table 5.7 and Figure 5.20 presents the maximum displacements values for all the simulated lengths.

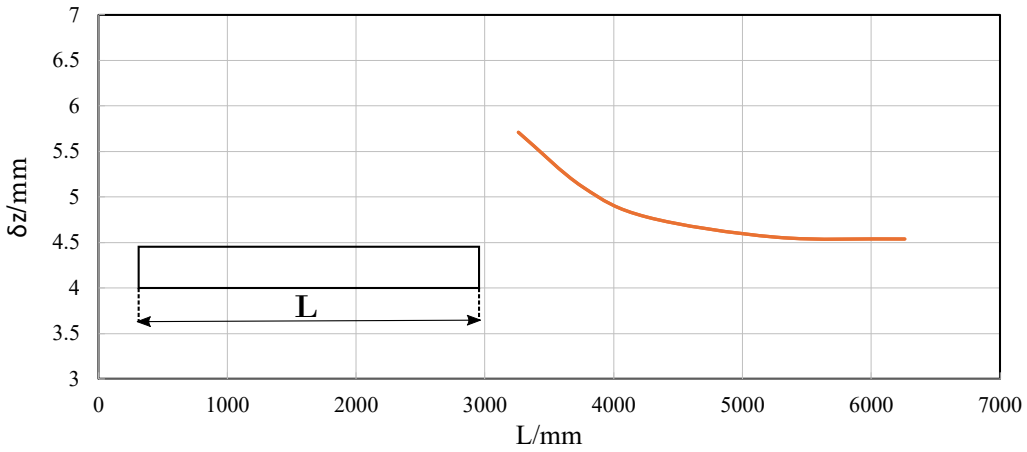


Figure 5.20.: Beam model variation of the bending operation displacement in function of the structural reinforcement length.

Table 5.7.: Maximum displacements values for several reinforcement part lengths.

L/mm	δ/mm
6260	4.54
5260	4.56
4260	4.78
3760	5.11
3260	5.71

5.1.4.2. 3D numeric model

For the final numeric study, the aim was to analyse the deflection of the reinforced beam using the triangular geometry of the reinforcement part without the simplification of the constant rectangular cross section.

The aluminium profile 2D geometry was imported to Abaqus and then extruded into a 3D deformable solid. The structural reinforcement part was modelled in Abaqus with the correct dimensions. The materials were defined for both parts.

Both parts were meshed with partitions. The element used was the C3D8R, a general linear brick element. The aluminium profile mesh was extremely refined at both ends of the profile in order to obtain very precise results on the maximum displacement mesh regions, as seen in Figure 5.21.

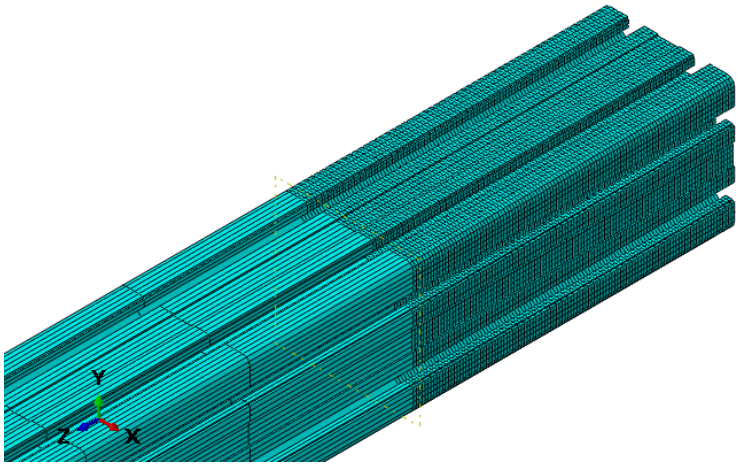


Figure 5.21.: Mesh refining region at the end of the aluminium profile.

For connecting the beams in assembly, a tie constraint was used to tie both surfaces. A symmetry boundary condition was created for the plane y-x. Another boundary condition for the pinned support was also established. The distributed load was created and applied throughout the upper surface of the aluminium profile. The assembly of the reinforced solution can be seen in Figure 5.22.

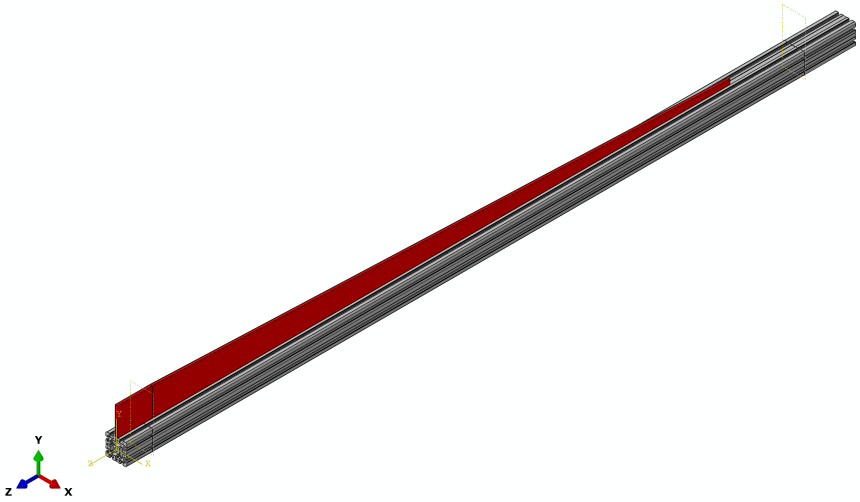


Figure 5.22.: 3D numeric model assembly of the reinforced solution (L = 5260 mm).

The numeric simulation results for this model are presented in Table 5.8 and Figure 5.23. The simulation data is presented bellow:

- Total number of nodes: 212280;
- Total number of elements: 148131 linear hexahedral elements of type C3D8R.

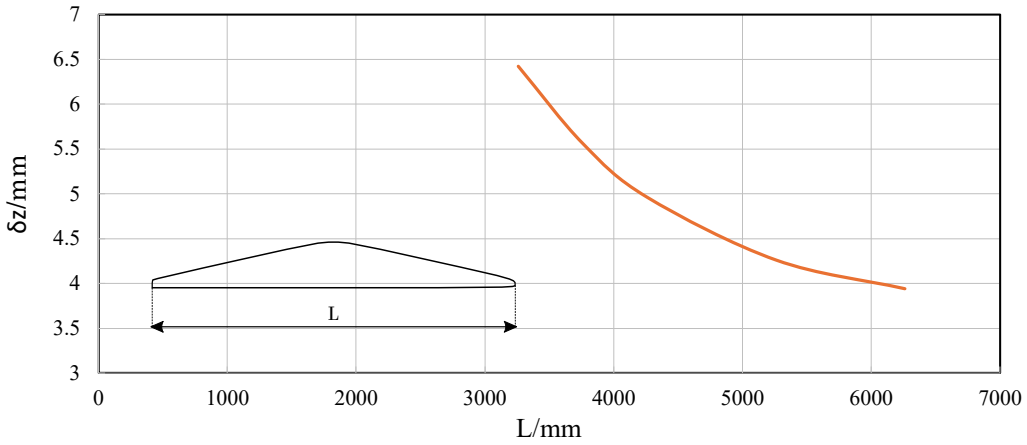


Figure 5.23.: 3D model variation of the bending operation displacement in function of the structural reinforcement length.

Table 5.8.: Maximum displacements values for several reinforcement part lengths.

L/mm	δ/mm
6260	3.94
5260	4.26
4260	4.96
3760	5.56
3260	6.42

5.1.5. Final discussion

Table 5.9 presents all displacement results from each model in function of the structural reinforcement lengths

Table 5.9.: Bending operation displacement for the analytical, beam, and 3D model.

L/mm	Analytic model δ/mm	Beam model δ/mm	3D model δ/mm
6260	4.57	4.54	3.94
5260	-	4.56	4.26
4260	-	4.78	4.96
3760	-	5.11	5.56
3260	-	5.71	6.42

For a length equal to 6260 mm, the analytical model displacement and the beam model displacement are identical. However, the displacement obtained on the 3D model is slightly lower. This reflects the influence of the structural reinforcement geometry that is only considered in the 3D model.

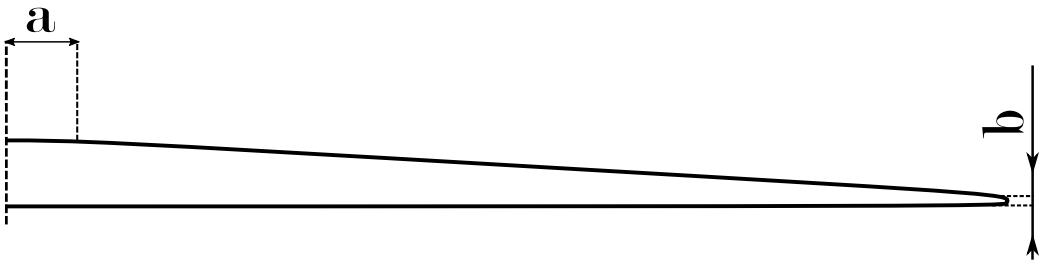


Figure 5.24.: Structural reinforcement geometry.

Besides the height, width, and thickness of the triangle, the values of a and b, have a great influence on the deflection of the reinforced solution. If these values are increased, the deflection will be lower. This influence is seen on the 3D model. However, in both the analytical calculation and beam model simulation, it was considered a constant rectangular cross section that did not take this effect into account. This is the reason the displacement value is a little bit lower in this numeric model, for a length of 6260 mm.

The length was decreased 1000 mm twice, and then it was decreased 500 mm twice once the impact of the length started to become more notorious. The maximum displacement values start to increase significantly for lengths bellow 4260 mm, for both numeric models. However, the decrease of the length has a higher influence on the 3D numeric model, especially bellow 4260 mm. The deflection presented by the beam model is less influenced by the length reduction because of the constant rectangular cross section.

The final length chosen was the 4260 mm since it would allow a decrease of 2000 mm from the initial length which meant a weight reduction on the global mass. Initially, the goal was to obtain a maximum bending operation displacement lower than 8 mm. A more conservative approach was adopted since the maximum displacement for both models is lower than 5 mm. This is an excellent result and structurally validates the deflection of the reinforced solution during the bending operations.

5.2. Materials selection

All steel parts designed expected for the male robot interface were manufactured from the structural steel S235jr. This steel is commonly used in general structural applications, it has good weldability, machinability and presents good results after laser cutting. The average mechanical properties for this material are presented in Table 5.10.

Table 5.10.: Mechanical properties of S235jr [56].

Properties	Values
Young's modulus, E/GPa	210
Poisson's ratio, ν	0.3
Density, ρ/kg m^{-3}	7850
Yield Strength, σ_y/MPa	235
Tensile Strength, σ_r/MPa	360

The robot male interface was manufactured from a cylindrical profile made from Ck45 structural steel. This steel offers higher strength than S235jr and is suitable for more demanding mechanical applications. Although it is not great for laser cutting, it presents good machinability. The average mechanical properties for this material are presented in Table 5.11.

Table 5.11.: Mechanical properties of Ck45 [57].

Properties	Values
Young's modulus, E/GPa	210
Poisson's ratio, ν	0.3
Density, ρ/kg m^{-3}	7850
Yield Strength, σ_y/MPa	305
Tensile Strength, σ_r/MPa	580

All the designed parts and the respective manufacturing processes are discussed in the following sections.

5.3. Aluminium profile subassembly

The Aluminium profile subassembly consists of aluminium profiles, which represent the main structure of the gripper where all the other parts are connected. This is seen in Figure 5.25. All the components in this subassembly were selected from Bosch Rexroth catalogue.

The assembly drawing that shows how the components fit together and relevant technical information is available in Appendix C.

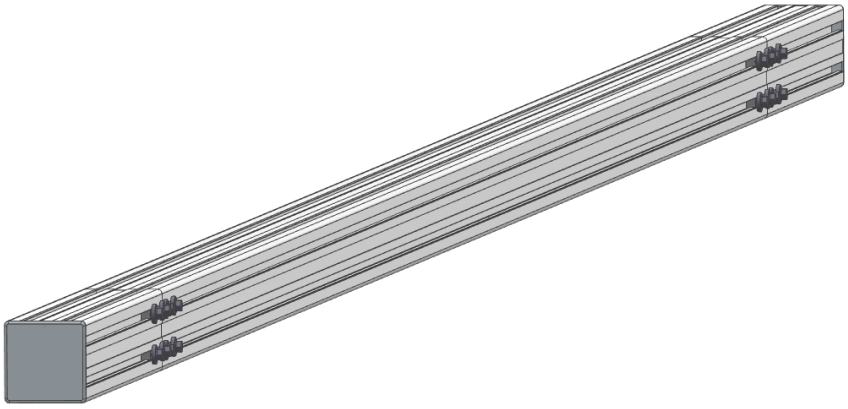


Figure 5.25.: 3D CAD of the aluminium profile subassembly.

An aluminium profile was chosen due to several reasons. Firstly, aluminium is significantly lighter than other metals such as steel, which reduces the weight of the profile. Despite being a lighter material, aluminium provides substantial strength and durability, presenting a high strength to weight ratio. For this application this is very important since the global mass of the gripper should be as low as possible, while still ensuring the structural robustness of the gripper. Finally, one of the most important reasons is the multifunctionality of these profiles. They are modular solutions, having slots for fastening a diverse range of components to the structure, as it can bee seen in Figure 5.26. This is really advantageous for the design of the gripper since it is possible to easily connect any part or other subassembly to the aluminium profile without having to do any kind of machining work.

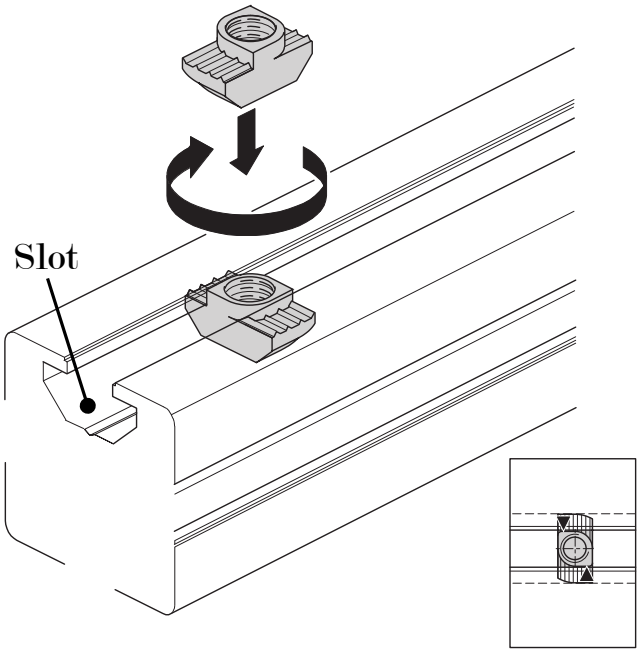


Figure 5.26.: Aluminium profile slot for fastening components to the structure [54].

The aluminium profile all and the accessories were provided by Equinotec - Soluções de Engenharia, Lda. They are the representatives in Portugal of Bosch Rexroth. Figure 5.27 final choice for the profile was a 90x90 with a 10 mm slot. The maximum length available is 6070 mm. The desired profile length for the gripper is 6260 mm. This value will be explained in the following section. So, three profiles were selected: one profile with 5000 mm, and two profiles with 630 mm.

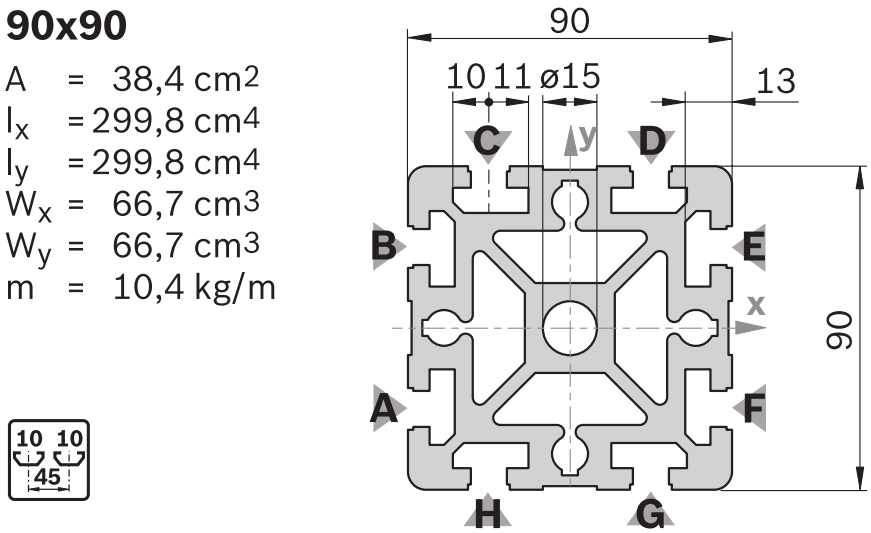


Figure 5.27.: Aluminium profile 90x90 chosen from Bosch Rexroth catalogue [54].

The connection of the profiles was achieved using a profile connector, as seen in Figure 5.28.. It consists in a single profile connector composed with four nuts. The connection kit is also available in the catalogue and includes four bolts, four disc spring washers and

four thick flat washers. This can be consulted in the catalogue in Appendix B.2. For the connection of two profiles 90x90, it was used two profiles connectors in each side, one for each slot.

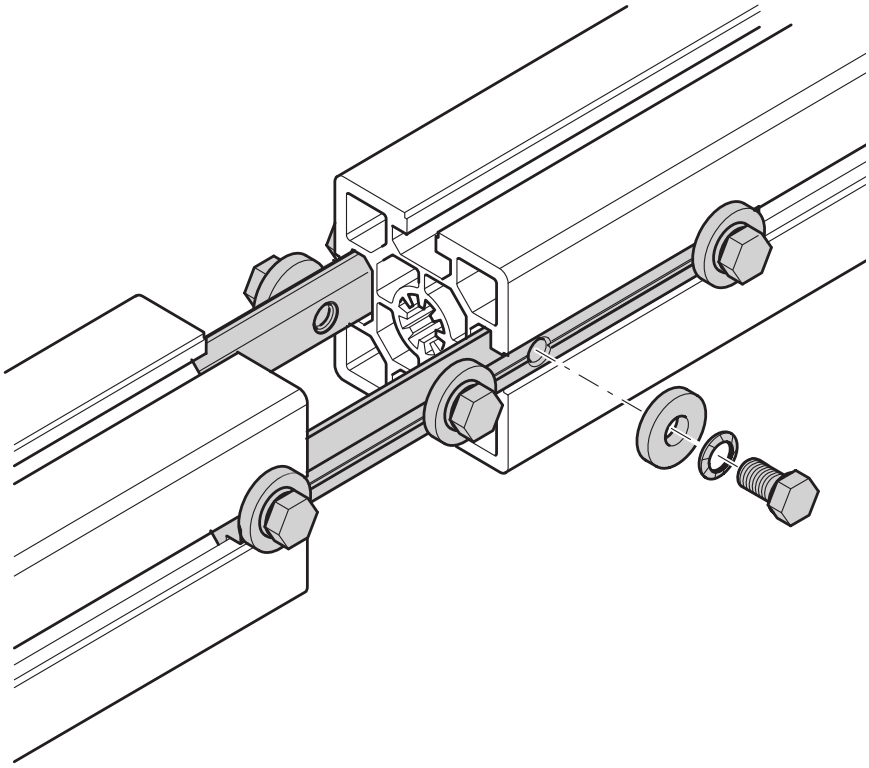


Figure 5.28.: Profile connector for the end-face connection of the aluminium profile [54].

Finally, at both ends of the profile it was inserted a cap cover to avoid human contact injuries during the assembly of the gripper due to the sharp edges of the profiles.

5.4. Structural reinforcement subassembly

This subassembly consists on the structural reinforcement part and all the small plates that are welded to it. This small plates will be fastened into the aluminium profile using the T-nuts (Appendix B.2). Both parts were manufactured with the structural steel S235jr.

The technical drawings and the assembly drawing that shows how the components fit together and relevant technical information is available in Appendix C.

Figure 5.29 shows the reinforcement part in SolidEdge. The outside geometry of the part will be obtained with the laser cutting manufacturing process, as well as the four through holes for the connection to the interface subassembly through bolts.

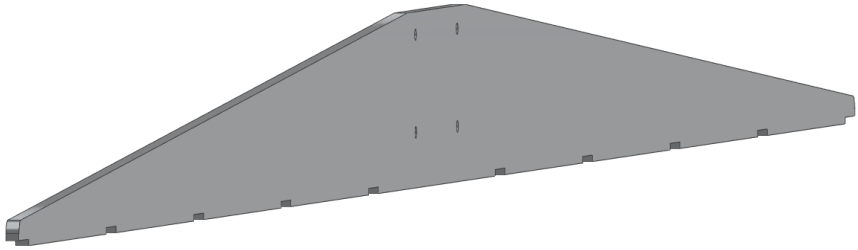


Figure 5.29.: Reinforcement part 3D CAD in SolidEdge.

The plate geometry and holes for the connection to the profile will also be obtained with laser cutting. Figure 5.30 shows the part in SolidEdge.

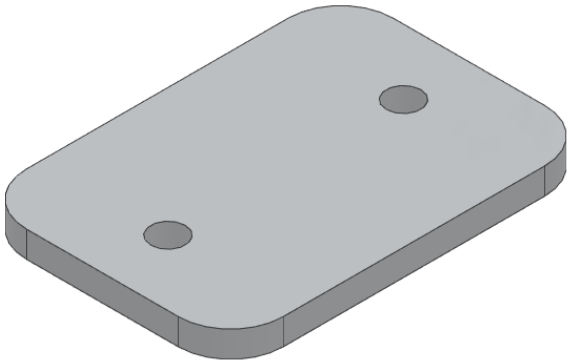


Figure 5.30.: Plate part 3D CAD in SolidEdge.

After that, the plates will be welded to the reinforcement part with MAG welding technique, as seen in Figure 5.31.

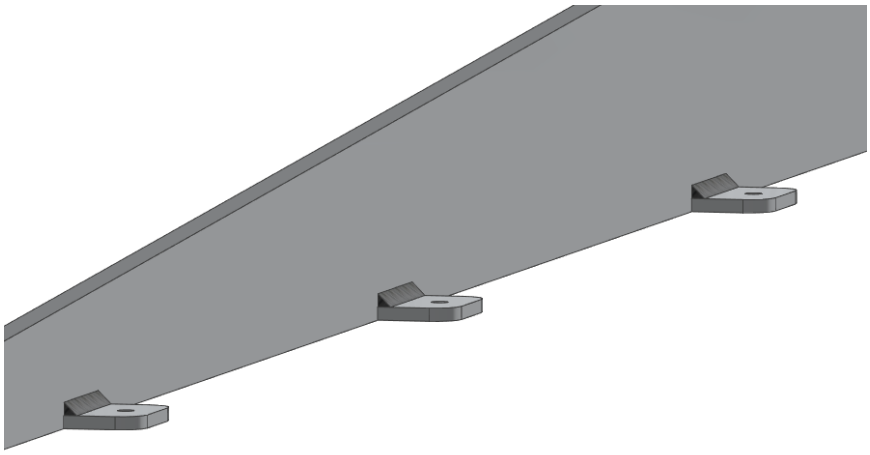


Figure 5.31.: Welding of reinforcement part with the plates in SolidEdge.

All the necessary drawing tolerances for the through holes were respected.

5.5. Interfaces subassembly

The interfaces subassembly, as seen in Figure 5.32, consists on the male interface for the robot, the gripper interfaces, and the two U-shaped profiles which will secure the connection to the structural reinforcement. The gripper interfaces and the U-shaped profiles material is the structural steel S235jr. The robot male interface material is the structural steel Ck45.

The technical drawings and the assembly drawing that shows how the components fit together and relevant technical information is available in Appendix C.

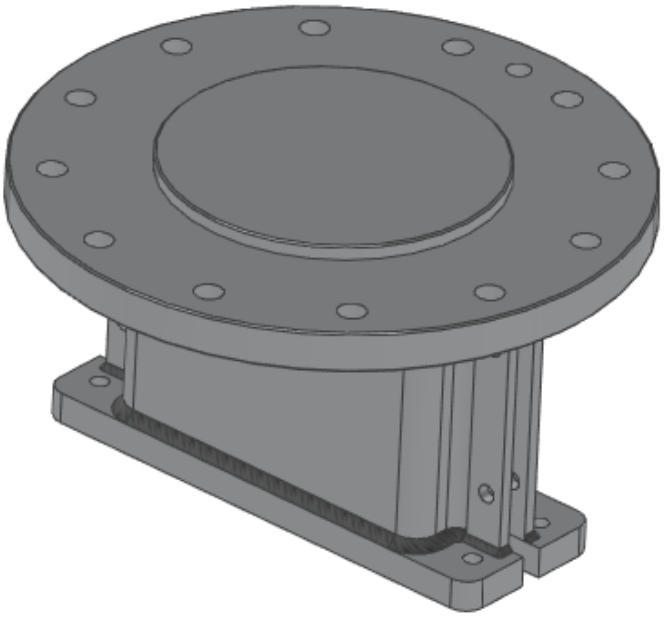


Figure 5.32.: 3D CAD of the interfaces subassembly.

The components will be discussed in the following order:

1. Gripper interface;
2. U-shaped profiles;
3. Male robot interface.

The gripper interface consists in two equal separated parts that are directly connected with the gripper profile with bolts. It is divided into two parts because the structural reinforcement will be placed right in the middle of them throughout the profile length. The interface is shown in Figure 5.33.

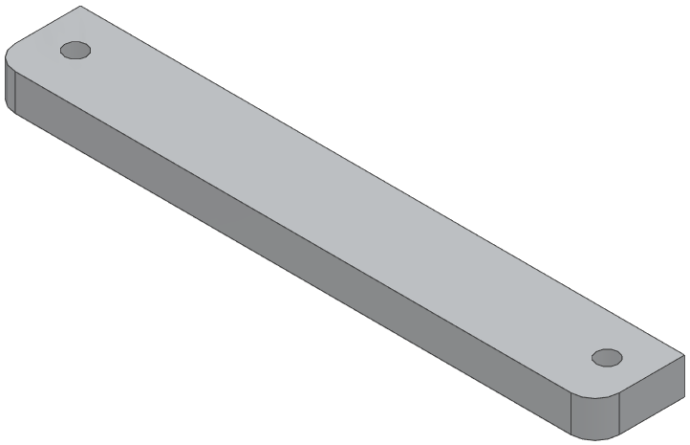


Figure 5.33.: 3D CAD of the gripper interface.

This component will be achieved using laser cutting. The round geometry at the corners was designed to avoid any contact human injury during the assembly of the gripper. The holes will not be obtained with laser cutting because the thickness of the interface is 15 mm and the through holes diameter are 9 mm (H13) for M8 bolts that will be fastened into a T-nut on the profile. Therefore, the laser cutting is not precise enough to ensure the adequate precision from one side to the other of the interface. After the laser cutting process, the holes were machined.

A simple load analysis of the bolts was done in order to ensure the safe attachment between the profile and the interface. Firstly, the stress caused by the maximum axial force that is subjected to the bolts needs to be calculated, as seen in equation (5.35). For this, it was considered the final load caused by the 300 kg. The cross section area of a bolt can de determined using the equation (5.34) [58]. The selected bolts have a 8.8 grade, a major diameter of 8 mm (M8), and a coarse thread pitch of 1.25 mm.

$$\begin{aligned} A_t = (0.7854)(d_c - 0.9382p)^2 \Leftrightarrow A_t = (0.7854)(8 - 0.9382 \cdot 1.25)^2 \\ \Leftrightarrow A_t = 36.61\,\text{mm}^2 \end{aligned} \tag{5.34}$$

Where:

- A_t/mm^2 - Cross section area of a bolt;

- d_c/mm - Crest diameter (major diameter) of the bolt;

- p/mm - Pitch of the bolt.

$$\sigma_{max} = \frac{F \cdot \frac{1}{n}}{A_t} \Leftrightarrow \sigma = \frac{300 \cdot 9.81 \cdot \frac{1}{4}}{36.61} \Leftrightarrow \sigma = 20.10\,\text{MPa} \tag{5.35}$$

Where:

- σ_{max}/MPa - Tensile stress on the bolt;

- n - Number of bolts.

The proof load, σ_{proof}, is defined as the maximum tensile stress that the bolt can be subjected to without resulting in plastic deformation. The proof load is usually between 85 % and 95 % of the yield strength [58]. For a class grade bolt of 8.8 the proof stress is equal to 580 MPa. Therefore, the safety factor for the tensile stress analysis of the bolt is calculated in equation (5.36).

$$S.F = \frac{\sigma_{\text{proof}}}{\sigma_{\text{eq}}} \Leftrightarrow S.F = \frac{580}{20.10} \Leftrightarrow S.F = 28.86 \tag{5.36}$$

Bolts should not be designed to work against shear stresses since they have little shear strength. If the bolt is tightened with the correct preload, the friction between the interface surface and the aluminium surface will ensure that the bolt is not subjected to pure shear stresses. However, it is imperative to do a load analysis as well. According to von Mises criterion, which is commonly used for ductile materials, the relation between the tensile yield stress and the shear yield stress is seen in equation (5.37).

$$\tau_{\text{proof}} = \frac{\sigma_{\text{proof}}}{\sqrt{3}} \Leftrightarrow \tau_{\text{proof}} = \frac{580}{\sqrt{3}} \Leftrightarrow \tau_{\text{proof}} = 334.86\,\text{MPa} \tag{5.37}$$

This relation will be applied to the proof load. The the safety factor for the shear stress analysis of the bolt is calculated in equation (5.38).

$$S.F = \frac{\tau_{proof}}{\sigma_{max}} \Leftrightarrow S.F = \frac{334.86}{20.10} \Leftrightarrow S.F = 12.50 \tag{5.38}$$

The safety factors for both the tensile and shear stress analysis were very high, ensuring a safety connection between the interface and the profile. Although the safety factors may seem very high, there are several factors that these calculations do not considered. There is a high stress concentration factor in the transitions of the thread, which is even worse if the bolt is subjected to shear stresses. Besides that, the constant motions as well as the vibrations from the robot can compromise the connection. Considering these factors, nord-lock washers were used to ensure a more secure connection. Besides that, M8 bolts are more used in the industry than small major diameter bolts, and there is usually more stock available at the factory floor.

The U-shaped profiles consists in two equal separated parts that are welded (MAG welding technique) into the gripper interface and the male robot interface. It is divided into two parts because the structural reinforcement will be placed in the middle of them and connected into it with four bolts. The 3D CAD of the part is seen in Figure 5.34.

The flatten part will be manufactured through laser cutting process in order to obtain the rectangular geometry. After that, the four necessary bends will be done using the bending manufacturing process. Finally, the through holes will be machined at the end, to ensure

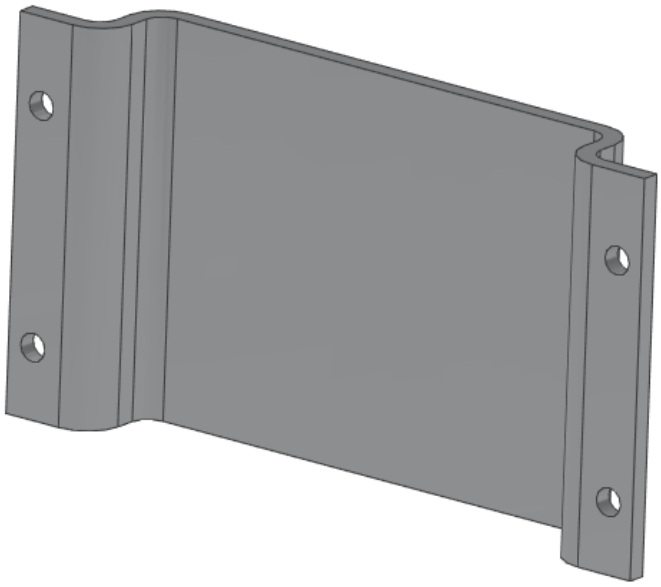


Figure 5.34.: 3D CAD of the U-shaped profile.

that they are drilled at the right location for the bolted connection with the structural reinforcement part.

The male robot interface is one of the most demanding parts of the assembly. It has an extremely important role in ensuring a safe attachment to the robot. Initially, the solid Ck45 steel cylinder will be welded into the U-shaped profiles. Post-weld machining is imperative for this part since the tolerances on a finished welding are tighter than realistically can be achieved from a component that was pre-machined and then welded together. The male robot interface has high demand for dimensional and geometrical tolerances and must be machined after the welding process.

The connection between the male robot interface and the female interface must respect the already established dimensions and tolerances of the female interface. The 2D drawing of the robot is presented in Appendix A. The drawing presents all the dimensional tolerances that need to be respected in order to ensure a precise connection. All the necessary information about the bolts used and pin are also there.

Figure 5.36 shows the bolted connection between the male interface that was designed and the female robot interface (blue part).

Nord-lock washers were also used for this application to prevent loosening or loss of tension of the bolted connection due to the robot vibration.

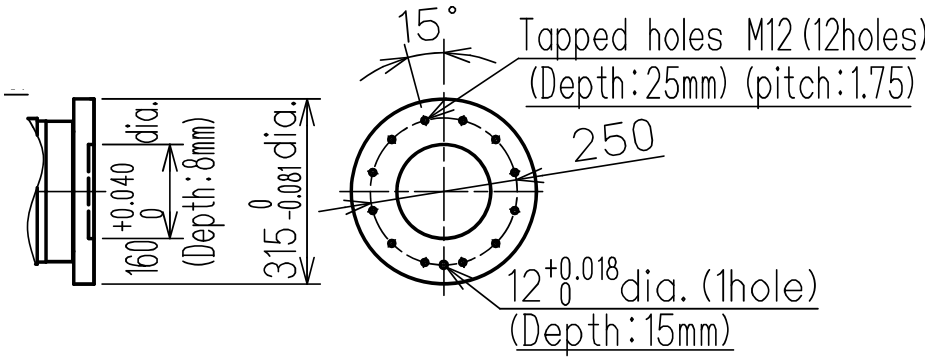


Figure 5.35.: 3D CAD of the gripper interface [44].

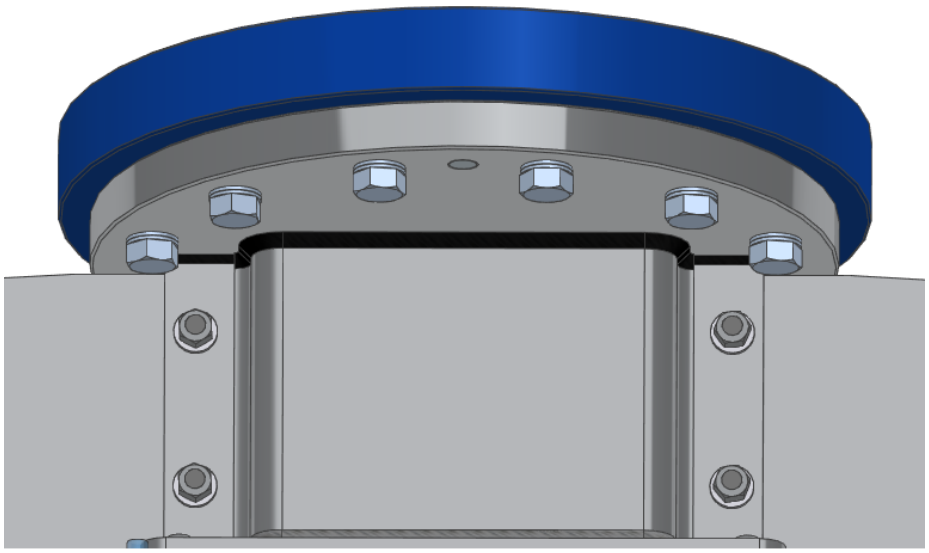


Figure 5.36.: Bolted connection between both robot interfaces [44].

6. Conclusions

6.1. Conclusion

The aim of this dissertation was the development of a gripper to be integrated in a robotic press brake bending cell to produce aluminium boat hulls. The customer was looking for an automated solution to increase the productivity of their production line in order to achieve high cadences and good levels of quality. The main manufacture process used to transform the initial flatten sheet metal into a boat hull is the sheet metal bending manufacture process. This main bending process is divided into two different bending operations. Considering these two operations, the initial goal was to design a gripper capable of handling the flatten boat hull through these operations. For that, two main studies were addressed: Vacuum cup selection and calculations, and the respective allocation on the flatten boat hull.

As the boat hull was made from an aluminium alloy, a vacuum type actuation was used to grasp the workpiece. The vacuum cups are the closest element to the workpiece and are in direct contact during all the manipulation, holding the part throughout the bending operations. The goal was to comprehend the distribution of forces exerted on the sheet metal by the vacuum cups in order to ensure a safe manipulation and avoid any dangerous scenarios where the part may fall out. A theoretical analytical calculation model was implemented which took into account several factors such as surface area, suction force, number of vacuum cups, vacuum pressure, robot acceleration, friction between surfaces, safety factors, and others. The worst case manipulation scenario was determined and all the calculations were based on that scenario. At the end, it was concluded that forty SMC ϕ125 mm thin flat vacuum cups with ribs were the ideal choice for this application. All the accessories and technical characteristics of the vacuum cup were also analysed.

The next step was to determine the proper allocation of all the cups throughout the flatten boat hull. For this application, the workpiece very large surface area, complex geometry, and low thickness lead to the crucial study of the part's deflection with different vacuum cup position arrangements. Each bending operation may or not require a different vacuum cup allocation in order to minimize the deflection of the part. Using finite element analysis, the second bending operation manipulation was not possible to achieve using a similar gripper design as the one for the first bending operation due to the restrictions on the position of the vacuum cups due to the bending line, which would lead to a critical structural failure because of a stress concentration zone. For those reasons, the development of the gripper was directed only for the first bending operation.

The design of the gripper was very challenging. Its structural resistance to bending solicitations was analysed. The critical issue was the deflection of the gripper since it was composed of an aluminium profile with a length higher than six meters. In the end, it was chosen a reinforced solution consisting of an aluminium profile paired with a custom de-

signed structural reinforcement, which achieved the desired results and allowed to minimize the global cost of the solution. Finally, all the technical drawings were done.

Regarding the methodology adopted in this project, it was undoubtedly an excellent opportunity to get in touch with various professors and engineers from different areas, where I was able to discuss and learn about various topics relevant to the work in question. In fact, several areas were explored, such as: the bending manufacture process, robotic bending cells, design of grippers, applied mechanics, machine design, structural calculations, finite element analysis, data management, and the design of a pneumatic system.

On the other hand, the access to a business environment was a fundamental experience that all students should have throughout their academic career. In fact, during these 5 months I have acquired many new skills, since I was being accompanied by professionals who had already experience in machine design in different areas, whose knowledge was undoubtedly very important for my master's thesis project and for my growth as a mechanical engineer.

6.2. Future work

There are some interesting proposals for further development of this project.

Performing experimental tests would be useful to further study the behaviour of the gripper which would would allow for future improvements and for possible issues to be analysed and fixed. Firstly, the workpiece manipulation with the forty vacuum cups must be analysed with experimental tests to ensure that there is no danger during handling. Whether the four vacuum ejectors have enough suction flow to guarantee the adequate vacuum pressure between the vacuum cups and the workpiece surface must also be addressed during the tests. Other experimental tests should be carried out to study the accuracy and precision of the bending operations on the workpiece.

Once the solution has been validated, it would be interesting to analyse possible enhancements and improvements on the gripper design that may help reduce the price, while maintaining its structural integrity and performance. For example, a detailed study on the structural behaviour of the reinforced solution where different type of geometries are studied through finite element analysis to understand the impact of each one in the deflection values of the gripper.

A fatigue analysis of the gripper could also be implemented, focusing on the interface subassembly where welded joints may prove to be critical. The key consideration is the impact of the robot's accelerations and decelerations. This involves evaluating stress concentrations and potential crack initiation points in the welded joints, aiming to improve durability and performance under repetitive motion cycles.

An instruction manual for the gripper should also be done for safety assembly procedures and warnings.

Finally, a solution for the workpiece manipulation during the second bending operation must be found. A more complex finite element analysis could be implemented to study the deflection of the flatten boat hull considering the three U-shape bends on the geometry. The results and conclusions may be different. Nonetheless, it is always possible to adapt the current gripper design with a new solution that allows the manipulation of the workpiece through the second bending operation.

Bibliography

[1] A. M. F. Solutions, "Adira - empresa." https://adira.pt/empresa/, 2024. Accessed: 2024-02-20.

[2] M. S. Azim, *Designing a universal gripping solution for handling part variations in a robot application*. Tampere University, 2019.

[3] S. Bouchard and L.-P. Gagnon, *Lean Robotics: A Guide to Making Robots Work in Your Factory*. Quebec City, Canada: Robotiq Inc., 2018.

[4] A. M. F. Solutions, "Adira - célula robotizada." https://adira.pt/celula-robotizada/, 2024. Accessed: 2024-02-28.

[5] P. Vandromme, "The robotic press brake gets flexible for metal fabrication operations." https://www.thefabricator.com/thefabricator/article/bending/the-robotic-press-brake-gets-flexible-for-metal-fabrication-operations, 2023. Accessed: 2024-02-15.

[6] Y. N. AB, "Increased productivity with robotised press-brake operation." https://www.roboplan.pt/upload/press-brake_56e2a3a8e5d1e.pdf, 2012. Accessed: 2024-02-15.

[7] I. F. of Robotics, "The impact of robots on productivity, employment and jobs," 4 2017.

[8] Metalix, "Setting up the robotic bending cell." https://www.metalix.net/products/mrobot/setting-up-the-robotic-bending-cell/, 2024. Accessed: 2024-02-15.

[9] V. M. F. Santos, *Robótica Industrial*. Departamento de Engenharia Mecânica, Universidade de Aveiro, 2004.

[10] T. T. University, "Robot bending workplace and its components." https://www.tthk.ee/inlearcs/robot-bending/robot-bending-workplace-and-its-components/, 2024. Accessed: 2024-02-20.

[11] AMADA, "Amada - células automatizadas de quinagem." https://www.amada.eu/pt-pt/produtos/maquinas-e-automacao/quinadoras/celulas-automatizadas-de-quinagem/rbr/, 2024. Accessed: 2024-02-28.

[12] M. Sala, *Bending Handbook*. Rolleri Professional Bending, 2015.

[13] J. A. B. Pacheco, *DOBRAGEM DE CHAPA E ENCURVAMENTO DE TUBOS METÁLICOS*. FEUP - Universidade do Porto, Faculdade de Engenharia, Porto, Portugal, 2022.

[14] J. A. B. Pacheco, *Utilização de Quinadoras e Guilhotinas*. Associação Portuguesa das Tecnologias de Conformação Plástica, 1992.

[15] Rolleri, "Rolleri - die adapters." https://www.rolleritools.com/products/

bending-solutions/tool-holders/die-adapters/ad17-7866.html, 2024. Accessed: 2024-02-22.

[16] G. A. R. Almeida, *Estudo de Novo Conceito de Interface de Cilindros-Estrutura em Quinadoras Hidráulicas*. Faculdade de Engenharia da Universidade do Porto, 2022.

[17] M. Özdemir, "Optimization of spring back in air v bending processing using taguchi and rsm method," *Mechanika*, vol. 26, pp. 73–81, 2 2020.

[18] K.-E. Rydberg, *Hydraulic Servo Systems : Dynamic Properties and Control*. Linköping University, Fluid and Mechatronic Systems, 2016.

[19] M. Ceccarelli, *Grasping in Robotics*. London: Springer, 2013.

[20] J. Hernandez, M. S. H. Sunny, J. Sanjuan, I. Rulik, M. I. I. Zarif, S. I. Ahamed, H. U. Ahmed, and M. H. Rahman, "Current designs of robotic arm grippers: A comprehensive systematic review," 2 2023.

[21] ISO Central Secretary, "Robotics – Safety design for industrial robot systems – Part 1: End-effectors," Standard ISO/TR 20218-1:2018, International Organization for Standardization, Geneva, CH, 2018.

[22] ISO Central Secretary, "Manipulating industrial robots – Object handling with grasp-type grippers – Vocabulary and presentation of characteristics," Standard ISO 14539:2000, International Organization for Standardization, Geneva, CH, 2000.

[23] G. Monkman, S. Hesse, R. Steinmann, and H. Schunk, *Robot Grippers*. Wiley, 2007.

[24] M. Chitroda and D. B. K. Patle, "A review on technologies in robotic gripper," May 2023.

[25] TRUMPF, "Trumpf - trubend cell 5000." https://www.trumpf.com/en_GB/products/machines-systems/bending-machines/trubend-cell-5000/, 2024. Accessed: 2024-02-22.

[26] B. Kumar, "Design constraints of vacuum gripper of robots - as a pick and place operating tool," *International Journal of Science & Technology*, 10 2016.

[27] B. Kumar, "Vacuum cup grippers for material handling in industry," *International Journal of Innovative Science, Engineering & Technology,*, vol. 4, pp. 187–194, 06 2017.

[28] D. Pascoe, "Vacuum cup materials." https://fluidpowerjournal.com/vacuum-cup-materials/, 2018. Accessed: 2024-02-15.

[29] D. Pascoe, "Basic vacuum cup selection." https://fluidpowerjournal.com/basic-vacuum-cup-selection/, 2018. Accessed: 2024-02-15.

[30] D. Pascoe, "The vacuum cup – explained," *Fluid Power Journal*, 11 2008.

[31] ROBOTIQ, "How to choose the right end effector for your application." https://ingenieria.uncuyo.edu.ar/catedras/how-to-choose-the-right-end-effector-f.pdf, 2013. Accessed: 2024-02-20.

[32] K. Mohammed, "Design of a gripper tool for robotic picking and placing," 2010.

[33] L. Group, "Lvd group - dyna-cell robotised press brake." https://www.lvdgroup.com/en/press-brakes/robotised-press-brakes/dyna-cell, 2024. Accessed: 2024-03-5.

[34] Bystronic, "Bystronic - automated press brake mobile bending cell." https://www.bystronic.com/usa/en-us/ba/automated-press-brake-mobile-bending-cell, 2024. Accessed: 2024-03-5.

[35] SafanDarley, "Safandarley - r-brake 130t." https://safandarley.com/uk/r-brake-130t, 2024. Accessed: 2024-03-5.

[36] SafanDarley, "R-brake - bending box with special tools." https://www.youtube.com/watch?v=yiGOpgaqf_c, 2020. Accessed: 2024-03-5.

[37] G. M. D. by magnetism, "Goudsmit magnetic gripper animation - for robotic sheet handling." https://www.youtube.com/watch?v=hcXJ98mXHZE, 2019. Accessed: 2024-03-6.

[38] Salvagnini, "Salvagnini press brake: robotic bending of heavy sheet metal." https://www.youtube.com/watch?v=cqcfQVzi6BI, 2022. Accessed: 2024-03-5.

[39] ISO Central Secretary, "Manipulating industrial robots – Mechanical interfaces – Part 1: Plates," Standard ISO 9409-1:2004, International Organization for Standardization, Geneva, CH, 2004.

[40] Robotiq, "Hand-e instruction manual." https://assets.robotiq.com/website-assets/support_documents/document/online/Hand-E_Instruction_Manual_Web_20190306.zip/Hand-E_Instruction_Manual_Web/Content/6.%20Specifications.htm, 2019. Accessed: 2024-04-1.

[41] Zimmer Group, "Zimmer Group - HWR2000 Manual Tool Changer." https://www.zimmer-group.com/en-us/technologies-components/components/handling-technology/tool-changer/manual/series-hwr2000, Accessed: 2024-04-2.

[42] SCHUNK, "Schunk sws change system." https://schunk.com/de/en/automation-technology/change-systems/sws/c/PGR_1135, 2024. Accessed: 2024-03-7.

[43] Tecnostamp, "Gold line: Special tools for all press brake on request." https://www.tecnostamp.eu/our-line/gold-line/, 2024. Accessed: 2024-04-29.

[44] Y. E. GmbH, "Motoman gp400." https://www.yaskawa.eu.com/products/robots/handling-mounting/productdetail/product/gp400_695, 2024. Accessed: 2024-05-30.

[45] SMC, "Made to order zp/zp2 series." https://ca01.smcworld.com/catalog/VacuumPad-en/mpv/VPad-p298-312_314-343-ZP2-OM_en/data/VPad-p298-312_314-343-ZP2-OM_en.pdf, 2024. Accessed: 2024-03-14.

[46] A. Greear, "What is a 6-axis robot?." https://www.realpars.com/blog/

6-axis-robot, 2024. Accessed: 2024-05-14.

[47] Schmalz, "Design of the suction cup." https://www.schmalz.com/en/vacuum-knowledge/the-vacuum-system-and-its-components/vacuum-suction-cups/design-of-the-suction-cup/, 2024. Accessed: 2024-05-14.

[48] A. C. Ugural, *Plates and Shells: Theory and Analysis*. CRC Series in Applied and Computational Mechanics, Boca Raton, FL: CRC Press, Taylor & Francis Group, fourth ed., 2018. Original edition published under the title: Stresses in plates and shells.

[49] I. ABAQUS, "Abaqus/cae user's manual: Rigid parts." https://classes.engineering.wustl.edu/2009/spring/mase5513/abaqus/docs/v6.6/books/usi/default.htm?startat=pt03ch11s07s01.html, 2006. Accessed: 2024-05-22.

[50] J. S. Gomes, *Capítulo V - Tensões de Flexão em Vigas*. Faculdade de Engenharia da Universidade do Porto, 2008.

[51] SMC, "Zl112a, multi-stage ejector." https://www.smc.eu/pt-pt/search?searchTerm=ZL112A-K15LOU-DBL, 2024. Accessed: 2024-05-30.

[52] SMC, "Double branch universal male elbow - kq2zd." https://www.smc.eu/pt-pt/search?searchTerm=KQ2ZD06-03AS, 2024. Accessed: 2024-05-30.

[53] SMC, "Union "y" - kq2u*-00." https://www.smc.eu/pt-pt/search?searchTerm=KQ2U12-00A, 2024. Accessed: 2024-05-30.

[54] B. Rexroth, "Basic mechanic elements 14.0." https://www.boschrexroth.com/en/gb/media-details/e4b73828-3e16-46cf-b003-112c6d172303, 2020. Accessed: 2024-04-30.

[55] R. N. Jorge, *Mecânica das Estruturas - Flexão*. FEUP - Universidade do Porto, Faculdade de Engenharia, Porto, Portugal, 2022.

[56] R. AÇOS, "C1 - aços de construção ao carbono." https://www.ramada.pt/pt/produtos/acos/aa-os-de-construa-ao-ao-carbono/c1_.html, 2017. Accessed: 2024-05-30.

[57] R. AÇOS, "F10 - aços de construção ao carbono." https://www.ramada.pt/pt/produtos/acos/aa-os-de-construa-ao-ao-carbono/f10-.html, 2022. Accessed: 2024-05-30.

[58] S. Schmid, B. Hamrock, and B. Jacobson, *Fundamentals of Machine Elements*. CRC Press, 2013.

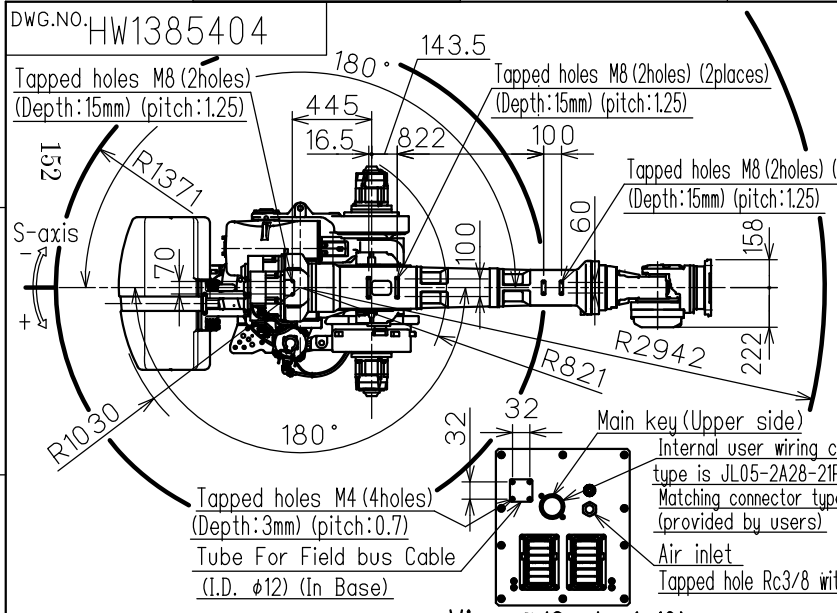
A. Industrial robot GP400

A.1. Robot technical specifications and technical drawing

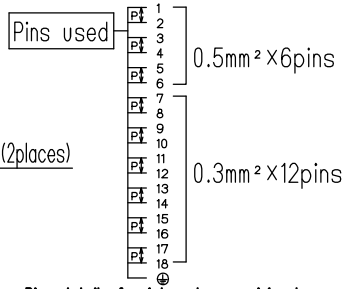
All the technical information about the robot is available in the following online catalogue: https://www.yaskawa.eu.com/Global%20Assets/Downloads/Brochures_Catalogues/Robotics/MOTOMAN_Robots/GP-Series/Flyer_Robot_GP400_E_11.2020.pdf.

The technical drawing of the robot (GP400) is presented bellow.

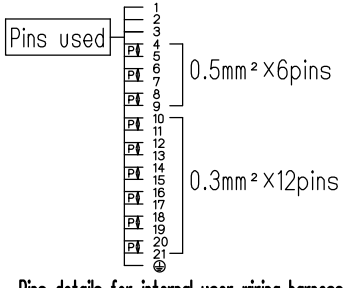
DWG.NO. HW1385404



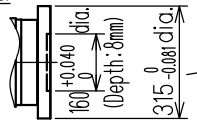
View C (Scale 1:10)

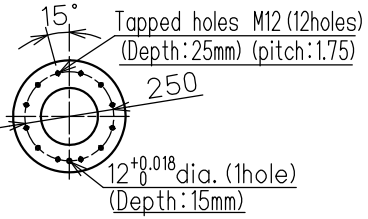


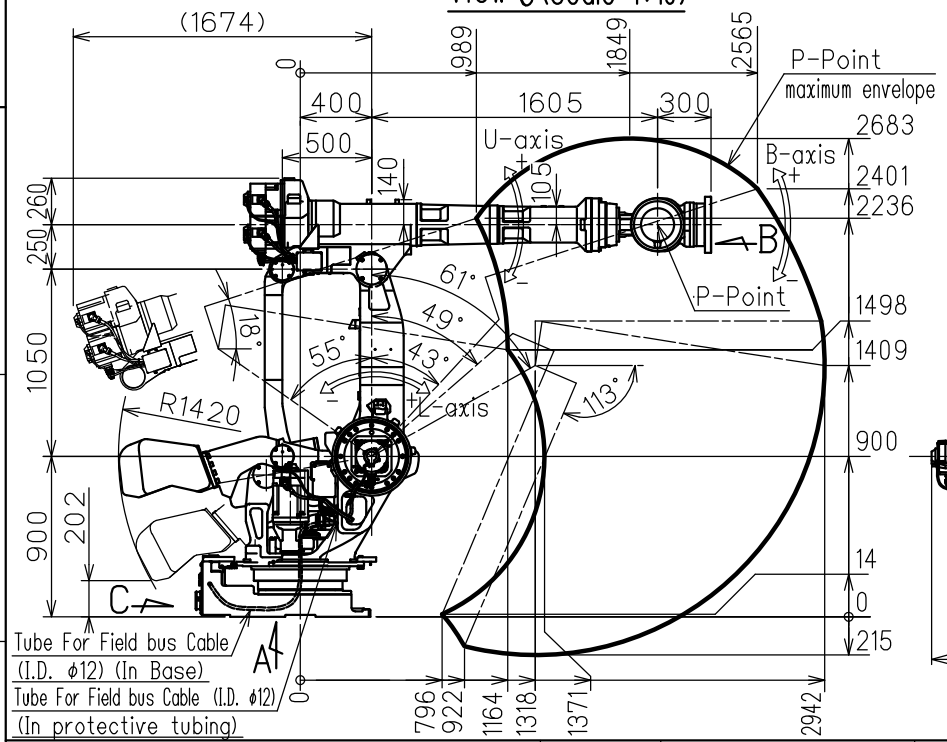
Pins details for internal user wiring harness (Casing side)



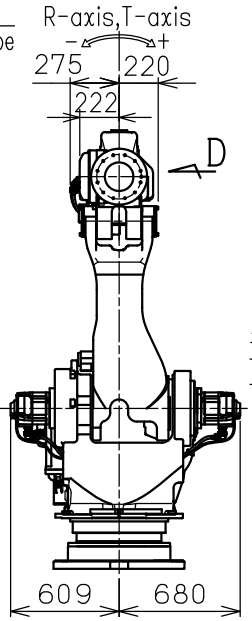
Pins details for internal user wiring harness (Base side)

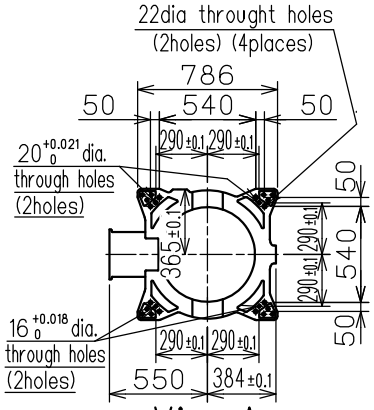






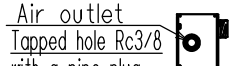
ViewB Detail of wrist frange (Scale 1:15)



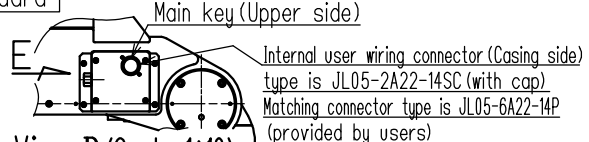


ViewA

Type	Note
YR-1-06VX400-A00	Standard



View E (Scale 1:10)



View D (Scale 1:10)

Item		Model: MOTOMAN-GP400
Configuration		Vertically articulated
Degree of Freedom		6
Payload	Wrist	400kg
	On U-arm	50kg
Repeatability (※1)		0.1 mm
Range of Motion	S-Axis (Turning)	-180° - +180°
	L-Axis (Lower Arm)	-55° - +61°
	U-Axis (Upper Arm)	-113° - +18°
	R-Axis (Roll)	-360° - +360°
	B-Axis (Pitch/Yaw)	-115° - +115°
	T-Axis (Twist)	-360° - +360°
Max Speed	S-Axis	1.78rad/s (102°/s)
	L-Axis	1.69rad/s (97°/s)
	U-Axis	1.69rad/s (97°/s)
	R-Axis	1.40rad/s (80°/s)
	B-Axis	1.40rad/s (80°/s)
	T-Axis	3.00rad/s (172°/s)
Allowable Moment	R-Axis	2989N·m (305kgf·m)
	B-Axis	2989N·m (305kgf·m)
	T-Axis	1343N·m (137kgf·m)
Allowable Inertia (GD²/4)	R-Axis	500kg·m²
	B-Axis	500kg·m²
	T-Axis	315kg·m²
Approx.Robot mass		2840 kg
Protected structure		Body: IP30 Wrist: IP67
Mounting method		Floor-mounted
Ambient Conditions	Temperature	0 to +45℃
	Humidity	20 to 80%RH (Non-condensing)
	Vibration	4.9m/s² (0.5G) or less
	Altitude	1000m or less
	Others	·Free from explosive or corrosive gas and liquid. ·Free from dust,soot,oil,or water. ·Free from electrical noise. ·Free from strong magnetic fields.
Power Requirements		7.0KVA
Controller		YRC1000

※1 Repeatabilitiy is conformed to ISO 9283.
※2 The manipulator is in the home position.

Units: mm

Note:
1.All rights reserved.
2.Please note that the data is subject to be deleted without advance notice.
3.No warranty is given in relation to the data including the specification.
4.We are not responsible for any damages or loss caused by the use of the data.

FOR STUDY PURPOSE ONLY

SCALE 1 :30

YASKAWA 株式会社 安川電機

Reference Drawing

TITLE MOTOMAN-GP400 DIMENSION DIAGRAM

DRWN DATE Oct.03.'17

DWG.NO. HW1385404 ②

SIZE A3

B. Suppliers catalogues

B.1. SMC catalogue

All the technical information about the vacuum cups and the respective accessories is available in the following online catalogue: https://ca01.smcworld.com/catalog/VacuumPad-en/mpv/VPad-p298-312_314-343-ZP2-OM_en/data/VPad-p298-312_314-343-ZP2-OM_en.pdf

B.2. Bosch Rexroth catalogue

All the technical information about the aluminium profiles and the respective accessories is available in the following online catalogue: https://www.boschrexroth.com/media/e4b73828-3e16-46cf-b003-112c6d172303

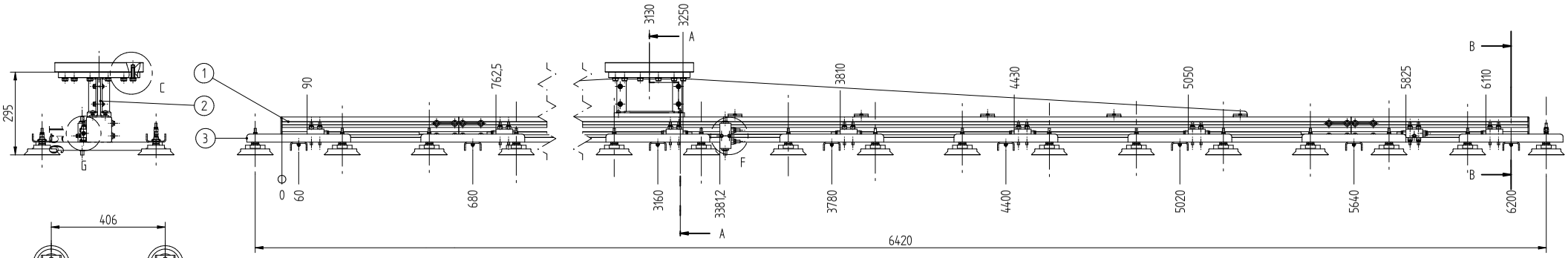
B.3. RAMADA AÇOS catalogue

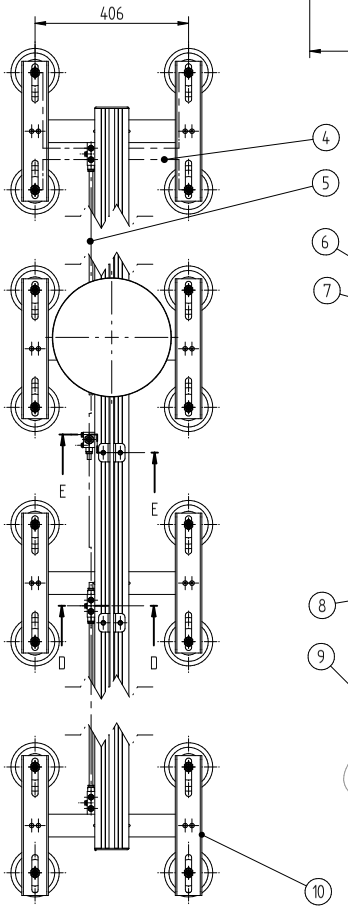
All the technical information about S235jr and Ck45 structural steels is available in the following online catalogue: https://www.ramada.pt/ficheiros_upload/ramada_catalogo_10_2018181206105824.pdf

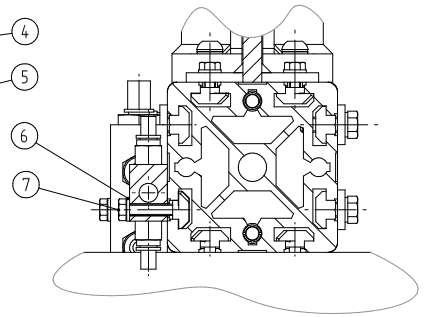
C. Technical Drawings

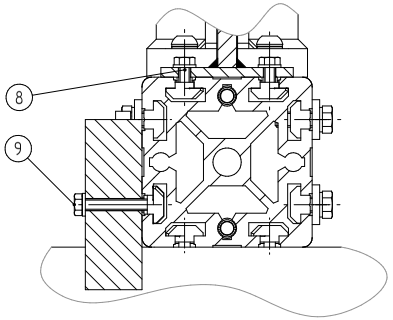
The thirteen technical drawings are organized in the following way:

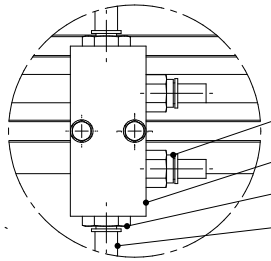
1. Gripper assembly drawing (contains parts list);
2. Aluminium profiles assembly drawing (contains parts list);
3. Welding drawing of the structural reinforcement (contains parts list);
    - Technical drawing of the structural reinforcement;
    - Technical drawing of the steel plate;
4. Vacuum cup assembly drawings (contains parts list);
    - Technical drawings of both C-shape profiles;
5. Welding drawing of the interfaces (contains parts list);
    - Machining drawing of the interfaces after welding;
    - Technical drawing of the gripper interface;
    - Technical drawing of the U-shape profiles.

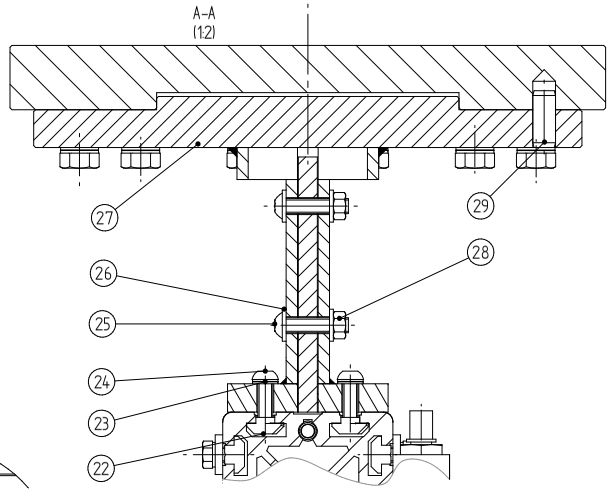


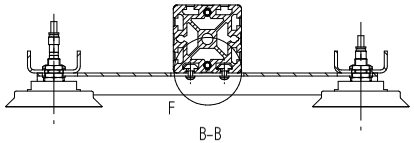


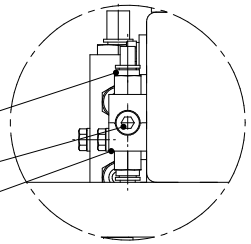


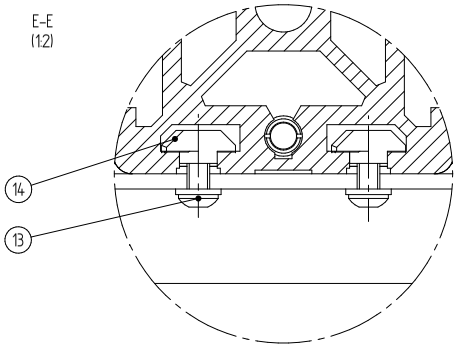


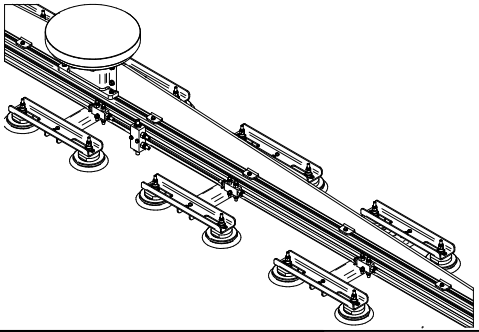












Quantity	Title	Item Number	Comments
1	Perfis Alumínio subassembly	1	
1	Reforço estrutural subassembly	2	
9	Subassembly Ventosas 310	3	
1	Polyurethane tube 8, 20m	4*	SMC TU0805BU-20S
1	Polyurethane tube 10, 20m	5*	SMC TU1065BU-20
56	Plain washer	6*	ISO 7091 – 6 – 100 HV
11	Hexagonal bolt	7*	DIN 933 – M6x30 – 8.8
20	Hexagonal bolt	8*	DIN 933 – M6x16 – 8.8
2	Hexagonal bolt	9*	DIN 933 – M6x40 – 8.8
2	Ventosas subassembly 280	10	
12	Nord-lock washer	11	DIN 25201-4-12
12	Hexagonal bolt	12	DIN 933 – M12x40 – 8.8
22	Hexagon socket button head screw	13*	ISO 7380-1 – M6x16 – 10.9
55	T-nut M6	14*	Bosch Rexroth 3 842 530 285
11	Pneumatic Distributor C21818	15	SMC C2 18 18 14
2	Pneumatic cap	16	SMC KME-TPM-C-14
44	Razor 8 1/8	17	SMC KQ2H08-01AS
1	Polyurethane tube 12, 20m	18*	SMC TU1208BU-20
2	Razor 10 1/2	19	SMC KQ2H10-04AS
1	Pneumatic distributor C23212	20	SMC C2 38 12
22	Razor 10 1/4	21	SMC KQ2H10-02AS
4	T-nut M8	22*	Bosch Rexroth 3 842 530 287
4	Nord-lock washer	23*	DIN 25201 – 4 – 8
4	Hexagon socket button head screw	24*	ISO 7380-1 – M8x25 – 10.9
4	Hexagon socket button head screw	25*	ISO 7380-1 – M8x35 – 10.9
8	Plain washer	26*	ISO 7091 – 8 – 100 HV
1	Interfaces subassembly	27*	
4	Hexagonal nut	28*	DIN 934 – M8 – 8
1	Cylindrical dowel pin	29*	ISO 2338 – 12 m6 x 30 – St

Toleranciamento ISO 8015 | ISO 2768-mK-E			ESCALA: 1:5
SEE PARTS LIST	MASSA Mass: 183,7 kg		
MATERIAL MATERIAL	TRAT. TERM. / DUREZA HEAT TREATMENT / HARDNESS	COR COLOUR	ACABAMENTO SURFACE FINISH

	DATA DATE	RUBRICA SIGN.	DES. Nº DWG NR
PROJECTOU DESIGNED BY	18/04/2024	Gonçalo Martins	Assembly – Gripper
DESENHOU DRAWN BY	19/04/2024	Gonçalo Martins	
APROVOU APPROVED BY	18/04/2024	Gonçalo Martins	

adira

Gripper Assembly
Assembly Gripper

Nº ARTIGO ITEM NR

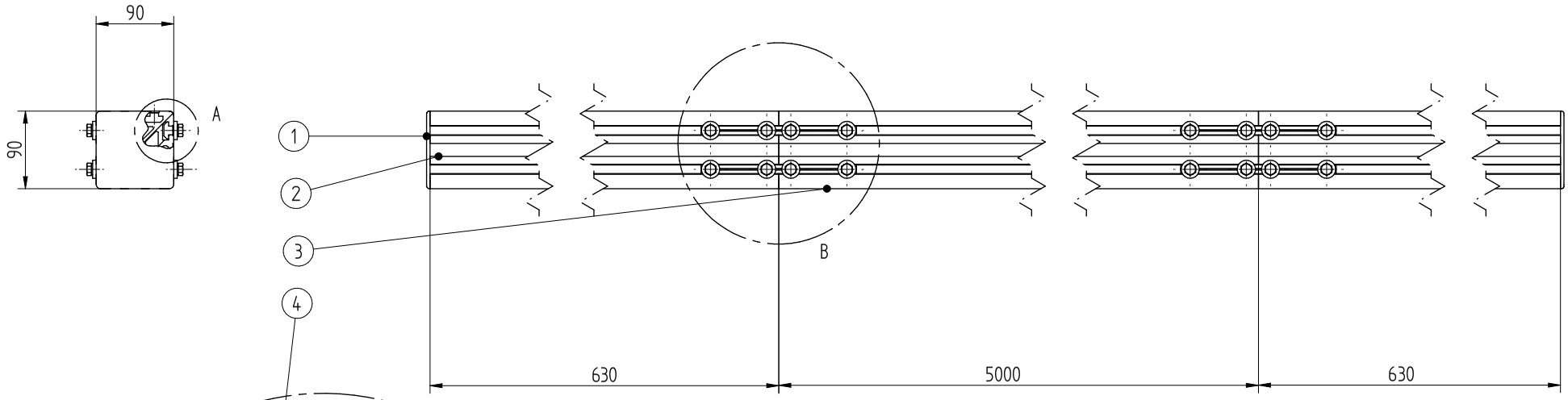
VERSÃO REVISION: A

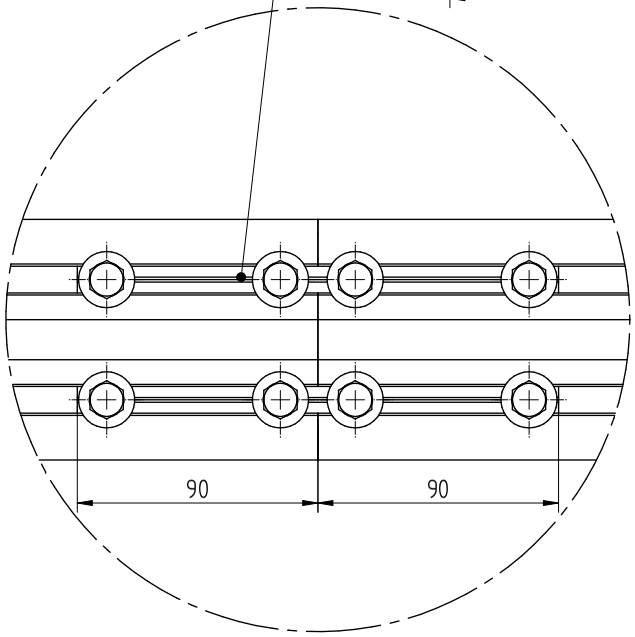
SIMILAR A SIMILAR TO

FOLHAS SHEET: 1/1

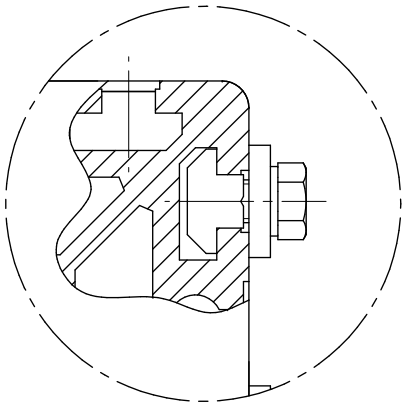
Este documento contem informação propriedade da ADIRA Metal Forming Solutions S.A que não pode ser reproduzida, divulgada a entidades terceiras ou fabricada por qualquer meio sem a autorização escrita da ADIRA Metal Forming Solutions S.A. This document contains proprietary information of ADIRA Metal Forming Solutions S.A. But cannot not be reproduced, disclosed to others or used for manufacturing purposes without written permission from ADIRA Metal Forming Solutions S.A.

ADIRA / CAD - 2003
Solid Edge

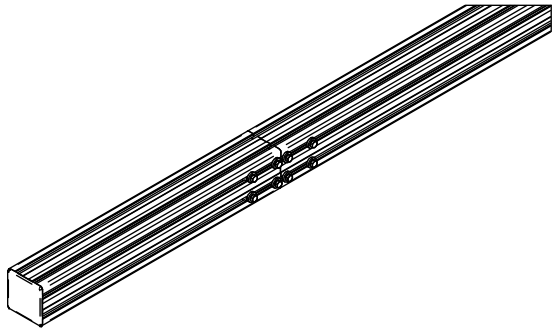




B
(1:2)



A
(1:1)



Quantity	Title	Item Number	Comments
2	Profile cap cover	1	Bosch Rexroth 3 842 548 760
2	Profile 90x90 630	2	Bosch Rexroth 3 842 990 500
1	Profile 90x90 5000	3	Bosch Rexroth 3 842 990 500
8	Profile connector	4	Bosch Rexroth 3 842 528 746 (includes bolts+washers)

Toleranciamento ISO 8015 | ISO 2768-mK-E

ESCALA: 1:5

MASSA *Mass* 67,2 kg

MATERIAL *MATERIAL*

TRAT. TERM. / DUREZA *HEAT TREATMENT / HARDNESS*

COR *COLOUR*

ACABAMENTO *SURFACE FINISH*

	DATA *DATE*	RÚBRICA *SIGN*
PROJECTOU *DESIGNED BY*	16/04/2024	Gonçalo Martins
DESENHOU *DRAWN BY*	03/06/2024	Gonçalo Martins
APROVOU *APPROVED BY*	16/04/2024	Gonçalo Martins

DES. Nº *DWG NR*

SubAssembly - Profiles Connected

Perfis Alumínio subassembly
Subassembly aluminium profiles

Nº ARTIGO *ITEM NR.*

VERSÃO *REVISION* A

SIMILAR A *SIMILAR TO*

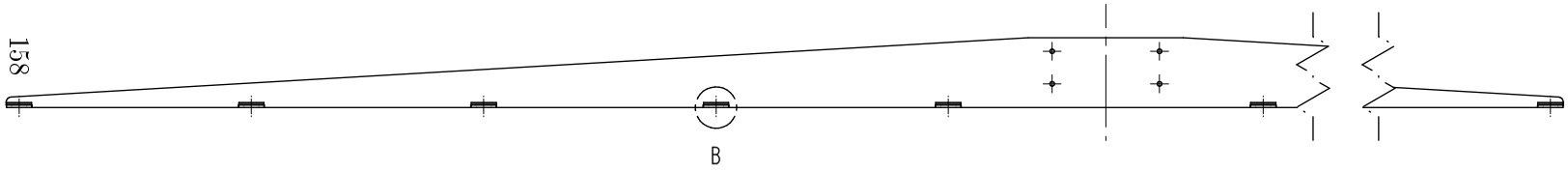
FOLHAS *SHEET* 1/1

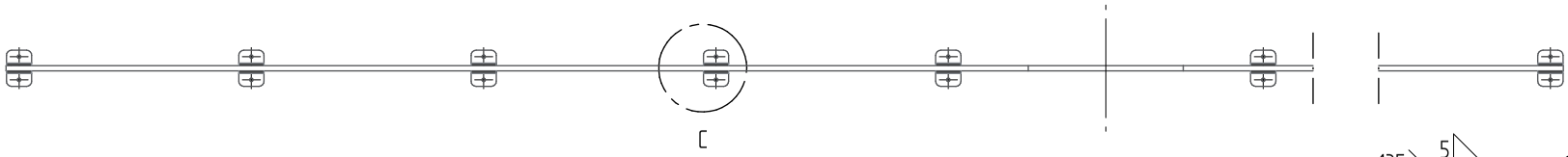
Este documento contem informação propriedade da ADIRA Metal Forming Solutions SA que não pode ser reproduzida, divulgada ou utilizada para fins de fabricação sem a autorização escrita da ADIRA Metal Forming Solutions SA. *This document contains proprietary information of ADIRA Metal Forming Solutions SA that cannot be reproduced, disclosed to others or used for manufacturing purposes without written permission from ADIRA Metal Forming Solutions SA.*

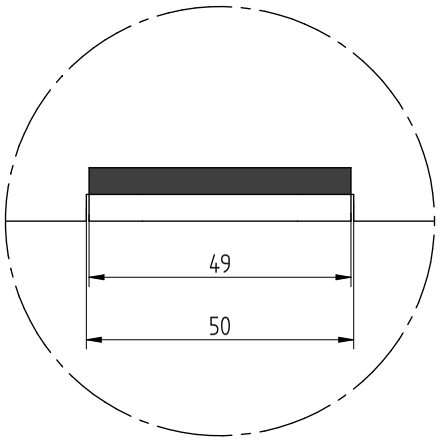
157

ISO - E

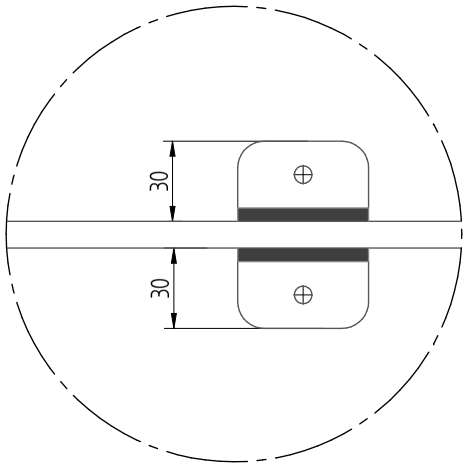
ADIRA / CAD - 2003
Solid Edge



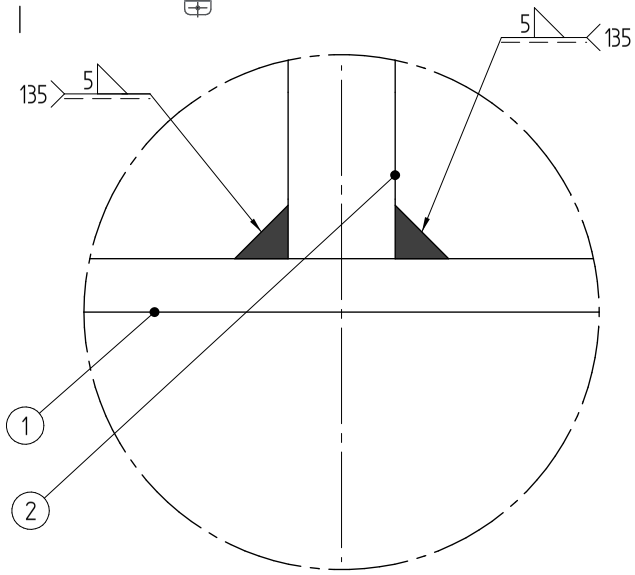




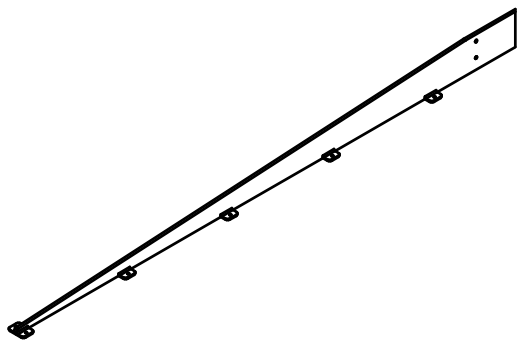
B
(1:1)



C
(1:2)



A
(2:1)



Quantity	Title	Item Number	Comments
10	Reforça_chapa	1	
1	Reforça_Estrutural	2	

Toleranciamento ISO 8015 I ISO 2768-mK-E			ESCALA: 1:10
	MASSA *Mass* 28,3 kg Zinc finish 5µm		
MATERIAL *MATERIAL*	TRAT. TERM. / DUREZA *HEAT TREATMENT / HARDNESS*	COR *COLOUR*	ACABAMENTO *SURFACE FINISH*

	DATA *DATE*	RÚBRICA *SIGN*
PROJECTOU *DESIGNED BY*	31/05/2024	Gonçalo Martins
DESENHOU *DRAWN BY*	04/06/2024	Gonçalo Martins
APROVOU *APPROVED BY*	31/05/2024	Gonçalo Martins

DES. Nº *DWG NR*: Reforço estrutural soldadura/welding

adira

Reforço estrutural subassembly
Subassembly structural reinforcement

Nº ARTIGO *ITEM NR.*

VERSÃO *REVISION*: A

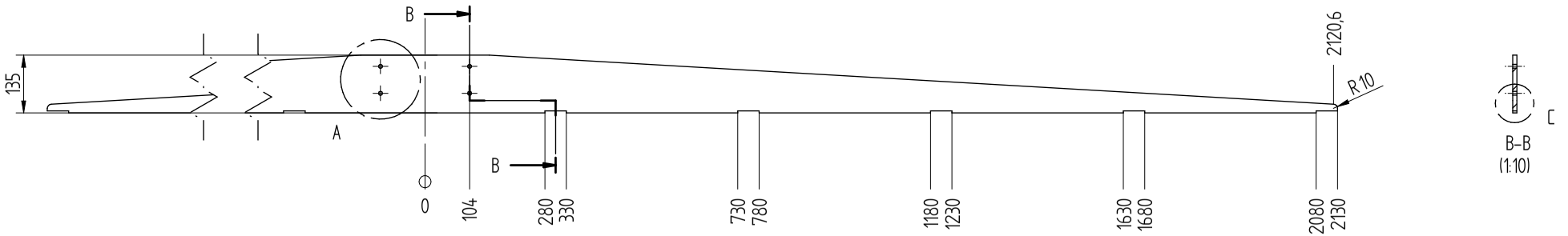
SIMILAR A *SIMILAR TO*

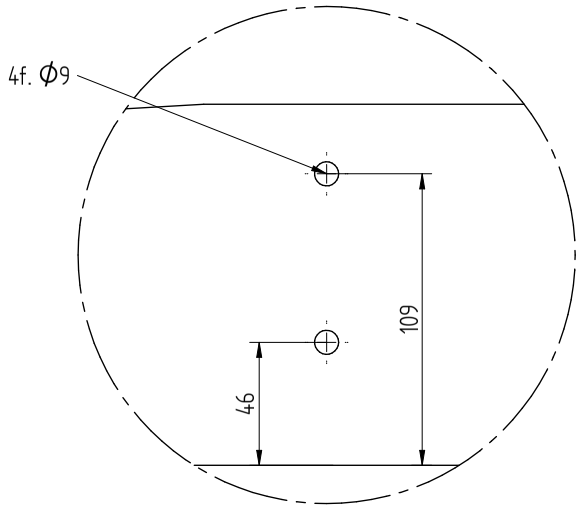
FOLHAS *SHEET*: 1/1

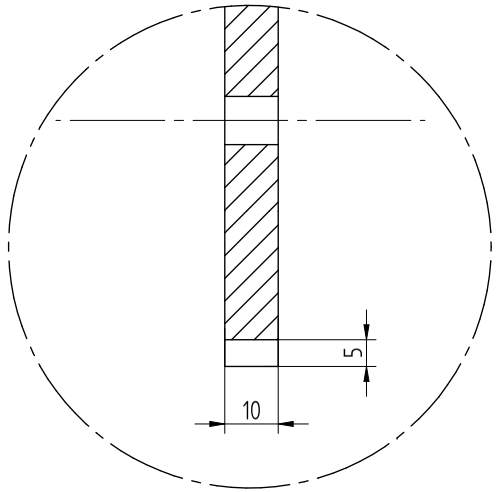
Este documento contem informação propriedade da ADIRA Metal Forming Solutions SA que não pode ser reproduzida, divulgada ou utilizada para fins de fabricação sem a autorização escrita da ADIRA Metal Forming Solutions SA. *This document contains proprietary information of ADIRA Metal Forming Solutions SA that cannot be reproduced, disclosed to others or used for manufacturing purposes without written permission from ADIRA Metal Forming Solutions SA.*

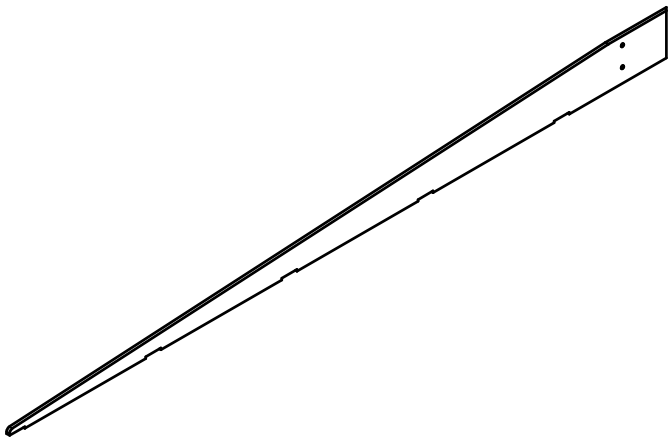
ISO - E

ADIRA / CAD - 2003
Solid Edge









139

Notas:

Algumas cotas de corte ou maquinagem podem estar omitidas propositadamente.

Geometria definida no ficheiro com formato DXF e/ou STEP e com revisão equivalente.

Toleranciamento ISO 8015 | ISO 2768-mK-E			ESCALA: 1:10
S235JR	MASSA *Mass* 27,0 kg		CORTE Ra 25
MATERIAL *MATERIAL*	Natural TRAT. TERM. / DUREZA *HEAT TREATMENT / HARDNESS*	COR *COLOUR*	ACABAMENTO *SURFACE FINISH*

	DATA *DATE*	RÚBRICA *SIGN*
PROJECTOU *DESIGNED BY*	17/04/2024	Gonçalo Martins
DESENHOU *DRAWN BY*	29/05/2024	Gonçalo Martins
APROVOU *APPROVED BY*	17/04/2024	Gonçalo Martins

DES. Nº *DWG NR*: Reforço_Estrutural

adira

Reforço_Estrutural
Structural_Reinforcement

Nº ARTIGO *ITEM NR.*

VERSÃO *REVISION*: A

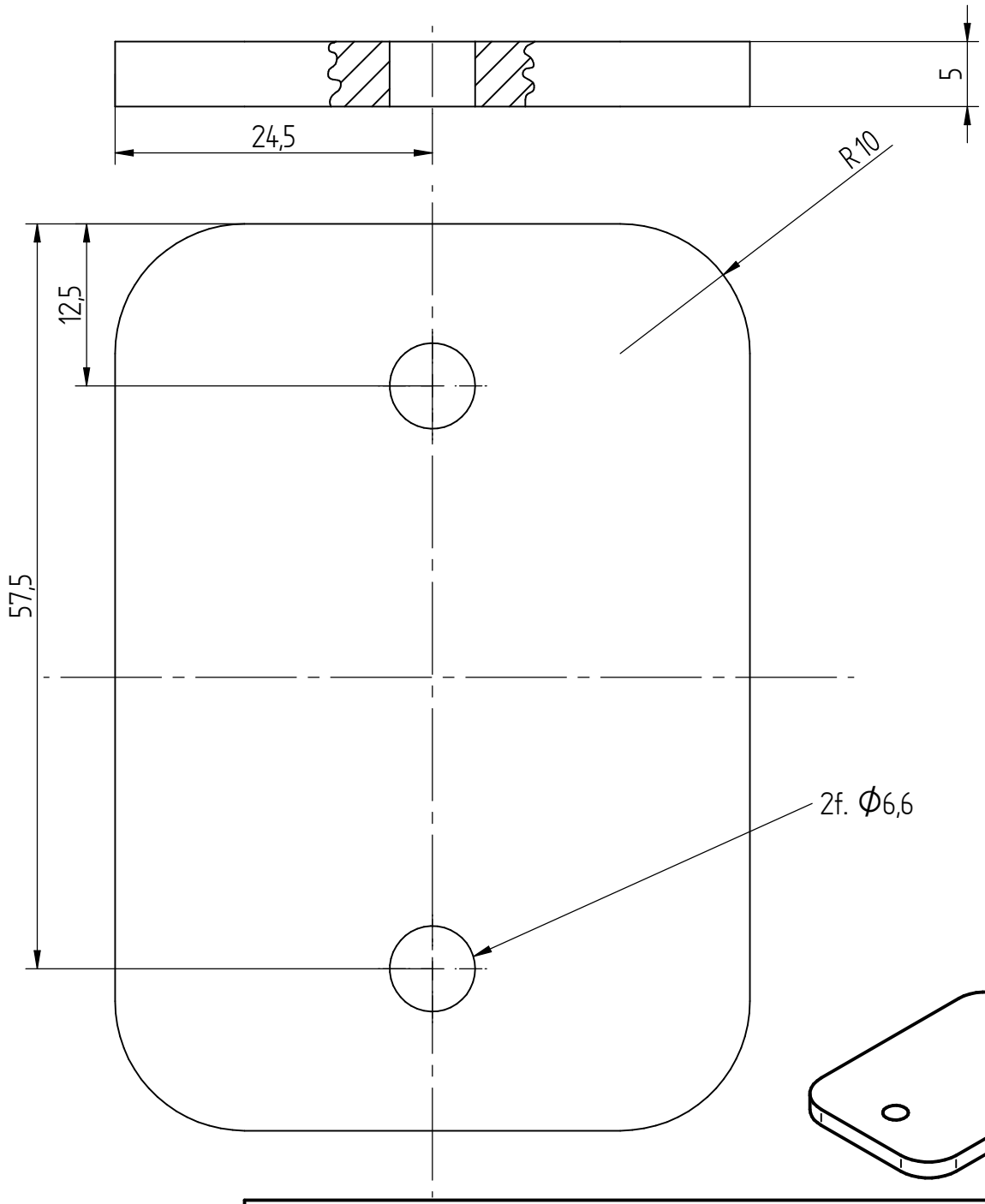
SIMILAR A *SIMILAR TO*

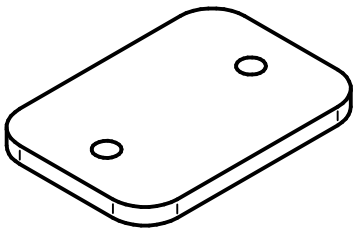
FOLHAS *SHEET*: 1/1

Este documento contem informação propriedade da ADIRA Metal Forming Solutions SA que não pode ser reproduzida, divulgada ou utilizada para fins de fabricação sem a autorização escrita da ADIRA Metal Forming Solutions SA. *This document contains proprietary information of ADIRA Metal Forming Solutions SA that cannot be reproduced, disclosed to others or used for manufacturing purposes without written permission from ADIRA Metal Forming Solutions SA.*

ISO - E

ADIRA / CAD - 2003
Solid Edge





Notas:

Algumas cotas de corte ou maquinagem podem estar omitidas propositadamente.

Geometria definida no ficheiro com formato DXF e/ou STEP e com revisão equivalente.

Tolerancimento ISO 8015 | ISO 2768-mK-E			ESCALA: 2:1
S235JR	MASSA: *Mass:* 0,1 kg		CORTE Ra 25
	Natural		
MATERIAL *MATERIAL*	TRAT. TERM. / DUREZA *HEAT TREATMENT / HARDNESS*	COR *COLOUR*	ACABAMENTO *SURFACE FINISH*

	DATA *DATE*	RÚBRICA *SIGN.*
PROJECTOU *DESIGNED BY*	18/04/2024	Gonçalo Martins
DESENHOU *DRAWN BY*	29/05/2024	Gonçalo Martins
APROVOU *APROVED BY*	18/04/2024	Gonçalo Martins

DES. Nº *DWG NR*: Reforço_chapa

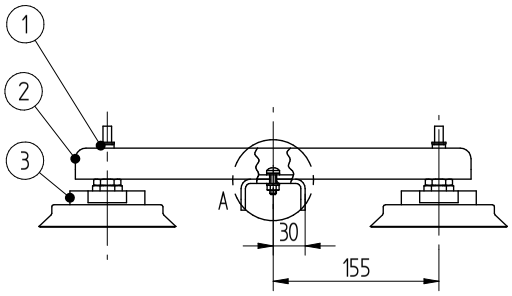
Reforço_chapa Reinforcement_plate	Nº ARTIGO *ITEM NR.*	VERSÃO *REVISION* A
	SIMILAR A *SIMILAR TO*	FOLHAS *SHEET* 1/1

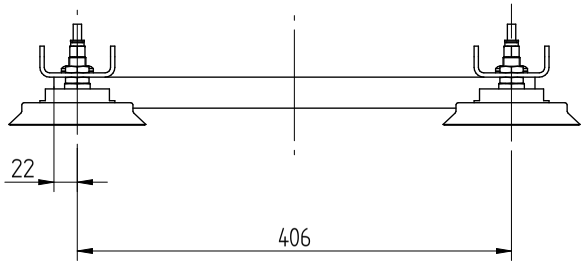
Este documento contem informação propriedade da ADIRA Metal Forming Solutions SA que não pode ser reproduzida, divulgada ou utilizada para fins de fabricação sem a autorização escrita da ADIRA Metal Forming Solutions SA. *This document contains proprietary information of ADIRA Metal Forming Solutions SA that cannot not be reproduced, disclosed to others or used for manufacturing purposes without written permission from ADIRA Metal Forming Solutions SA.*

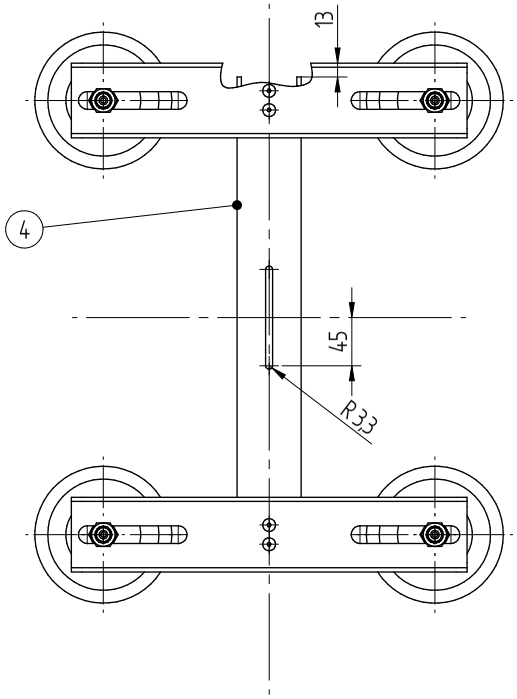
ISO - E

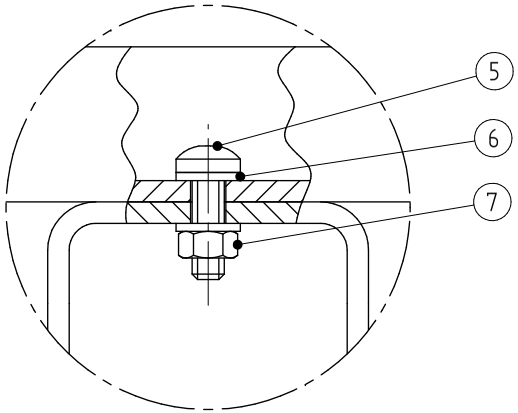
160

ADIRA / CAD - 2003
Solid Edge

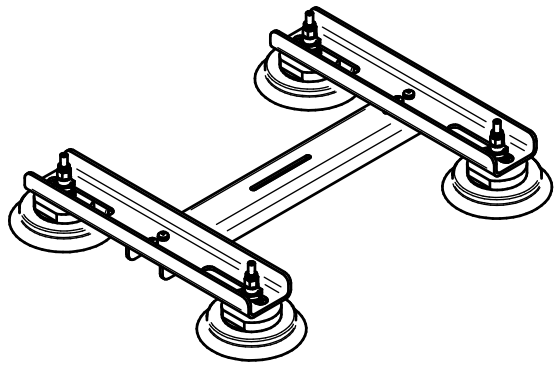








A
(1:1)



Quantity	Title	Item Number	Comments
4	Racor 8 1/8	1	SMC KQ2H08-01AS
2	Profile-C 2	2	
4	Vacuum cup	3	SMC ZPT125HN-A16
1	Profile-C 1	4	
4	Hexagon socket button head screw	5	ISO 7380-1 - M6x20 - 10.9
8	Plain washer	6	ISO 7091 - 6 - 100 HV
4	Hexagon nut	7	DIN934 - M6 - 8

Toleranciamento ISO 8015 | ISO 2768-mK-E

ESCALA: 1:5

MASSA *Mass* 5,4 kg

MATERIAL *MATERIAL*

TRAT. TERM. / DUREZA *HEAT TREATMENT / HARDNESS*

COR *COLOUR*

ACABAMENTO *SURFACE FINISH*

	DATA *DATE*	RÚBRICA *SIGN*
PROJECTOU *DESIGNED BY*	16/04/2024	Gonçalo Martins
DESENHOU *DRAWN BY*	03/06/2024	Gonçalo Martins
APROVOU *APPROVED BY*	16/04/2024	Gonçalo Martins

DES. Nº *DWG NR*: SubAssembly - Vacuum Cups 310

Subassembly Ventosas 310
Vacuum cups subassembly 310

Nº ARTIGO *ITEM NR.*

VERSÃO *REVISION* A

SIMILAR A *SIMILAR TO*

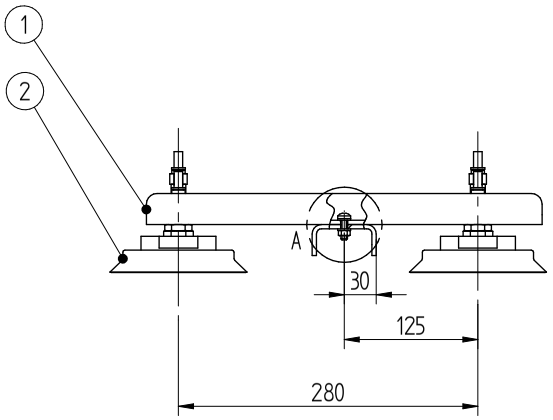
FOLHAS *SHEET* 1/1

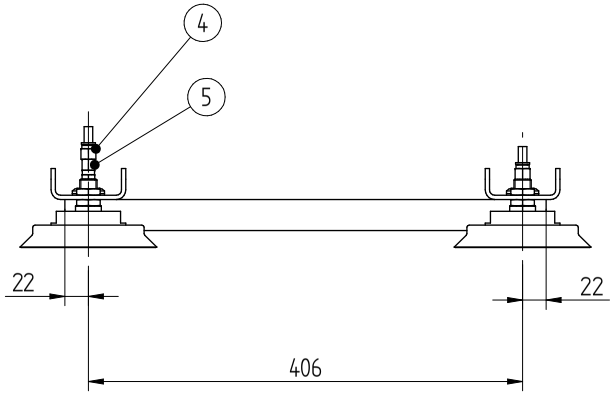
Este documento contem informação propriedade da ADIRA Metal Forming Solutions SA que não pode ser reproduzida, divulgada ou utilizada para fins de fabricação sem a autorização escrita da ADIRA Metal Forming Solutions SA. *This document contains proprietary information of ADIRA Metal Forming Solutions SA that cannot be reproduced, disclosed to others or used for manufacturing purposes without written permission from ADIRA Metal Forming Solutions SA.*

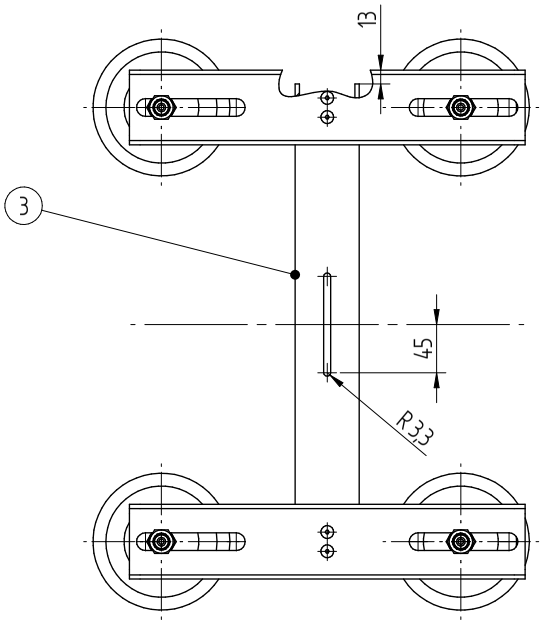
161

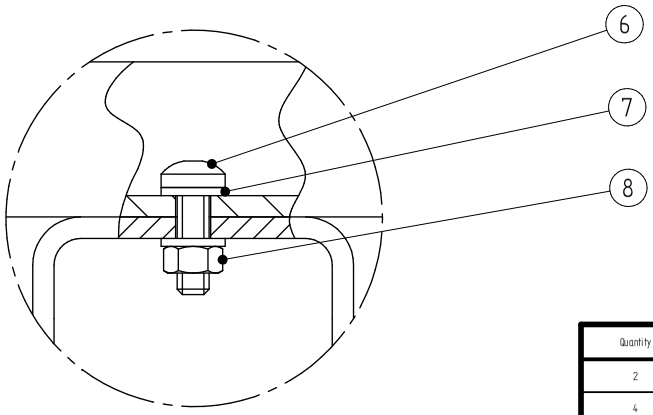
ISO - E

162

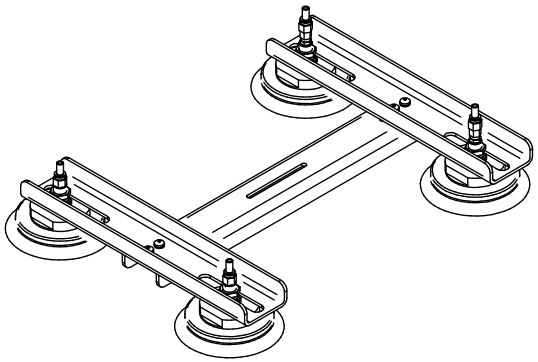








A
(1:1)



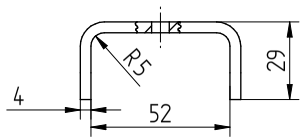
Quantity	Title	Item Number	Comments
2	Profile-E 2	1	
4	Vacuum cup	2	SMC ZPT125HN-A16
1	Profile-E 1	3	
4	Racor 8 1/8	4	SMC KQ2H08-01AS
2	Vacuum saving valve	5	SMC ZP2V-A01-10
4	Hexagon socket button head screw	6	ISO 7380-1 - M6x20 - 10.9
8	Plain washer	7	ISO 7091 - 6 - 100 HV
4	Hexagon nut	8	DIN934 - M6 - 8

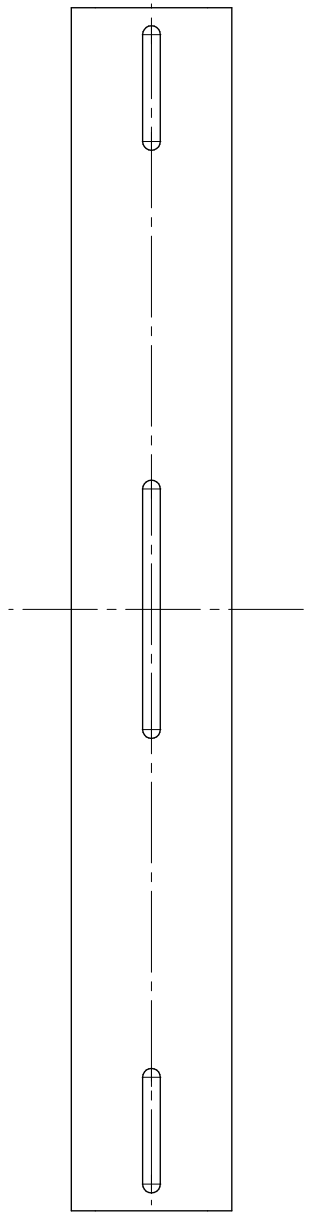
Toleranciamento ISO 8015 | ISO 2768-mK-E			ESCALA: 1:5
	MASSA *Mass* 5,4 kg		
MATERIAL *MATERIAL*	TRAT. TERM. / DUREZA *HEAT TREATMENT / HARDNESS*	COR *COLOUR*	ACABAMENTO *SURFACE FINISH*
	DATA *DATE* / RÚBRICA *SIGN*	DES. Nº *DWG NR*	
PROJECTOU *DESIGNED BY*	24/05/2024 Gonçalo Martins	SubAssembly -Vacuum Cups 280	
DESENHOU *DRAWN BY*	03/06/2024 Gonçalo Martins		
APROVOU *APPROVED BY*	24/05/2024 Gonçalo Martins		
Ventosas subassembly 280 Subassembly vacuum cup 280		Nº ARTIGO *ITEM NR.*	VERSÃO *REVISION* A
		SIMILAR A *SIMILAR TO*	FOLHAS *SHEET* 1/1

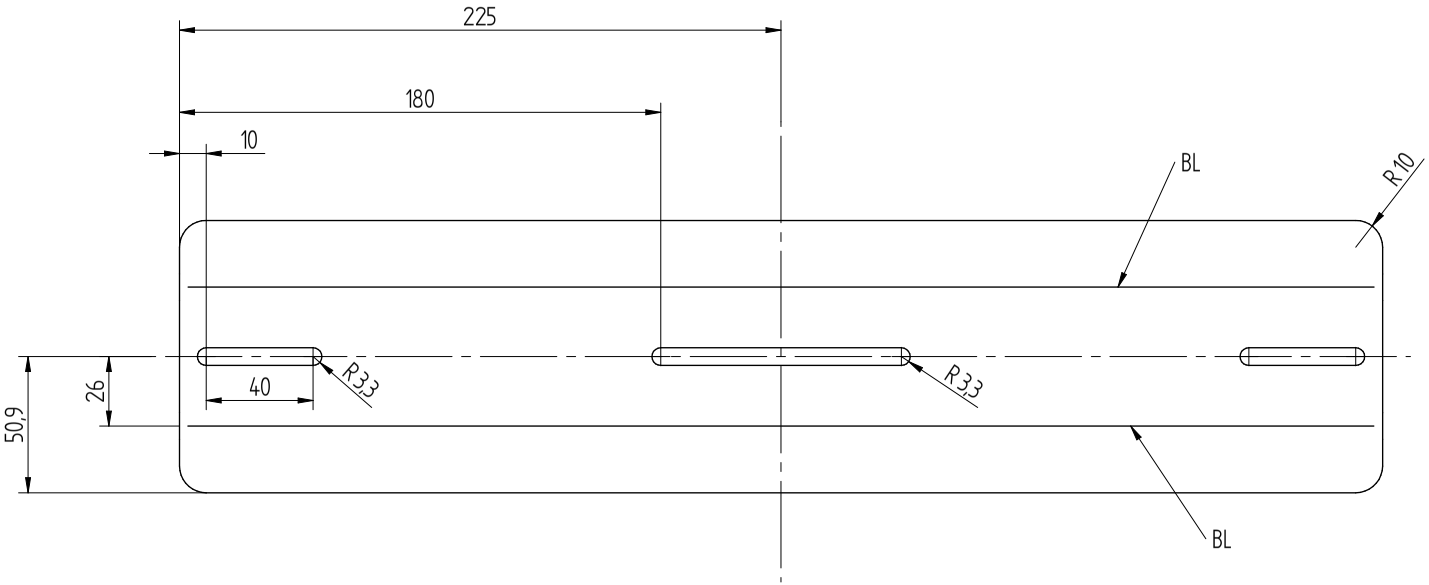
Este documento contem informação propriedade da ADIRA Metal Forming Solutions SA que não pode ser reproduzida, divulgada ou utilizada para fins de fabricação sem a autorização escrita da ADIRA Metal Forming Solutions SA. *This document contains proprietary information of ADIRA Metal Forming Solutions SA that cannot be reproduced, disclosed to others or used for manufacturing purposes without written permission from ADIRA Metal Forming Solutions SA.*

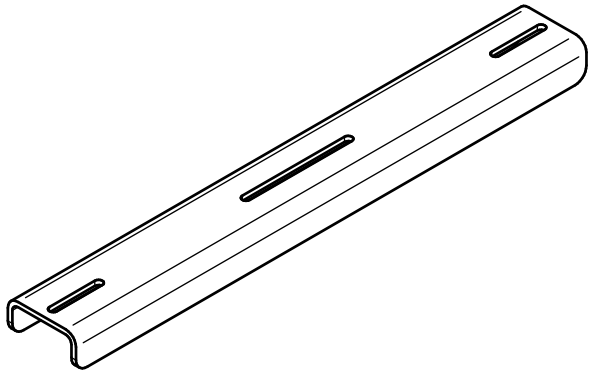
ISO - E

ADIRA / CAD - 2003
Solid Edge









PLANIFICAÇÃO:
RAIO DE QUINAGEM/Bend Radius 5,00 mm
ESPESSURA/Thickness 4,00 mm

Notas:
Algumas cotas de corte ou maquinagem podem estar omitidas propositadamente.
Geometria definida no ficheiro com formato DXF e/ou STEP e com revisão equivalente.

Tolerancimento ISO 8015 | ISO 2768-mK-E			ESCALA: 1:2
S235JR	MASSA *Mass* 1,4 kg Zinc finish 5µm		CORTE Ra 25
MATERIAL *MATERIAL*	TRAT. TERM. / DUREZA *HEAT TREATMENT / HARDNESS*	COR *COLOUR*	ACABAMENTO *SURFACE FINISH*

	DATA *DATE*	RÚBRICA *SIGN*
PROJECTOU *DESIGNED BY*	16/04/2024	Gonçalo Martins
DESENHOU *DRAWN BY*	29/05/2024	Gonçalo Martins
APROVOU *APPROVED BY*	16/04/2024	Gonçalo Martins

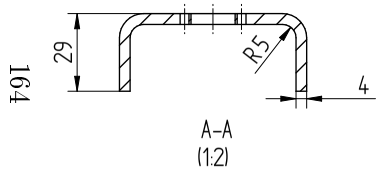
DES. Nº *DWG NR*: Chapa_Ventosa_1

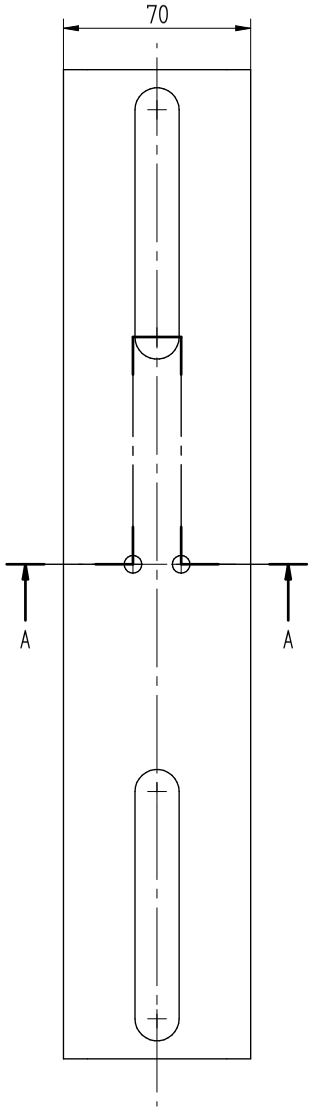
Perfil_C_1 Profile_C_1	Nº ARTIGO *ITEM NR.*	VERSÃO *REVISION* A
SIMILAR A *SIMILAR TO*		FOLHAS *SHEET* 1/1

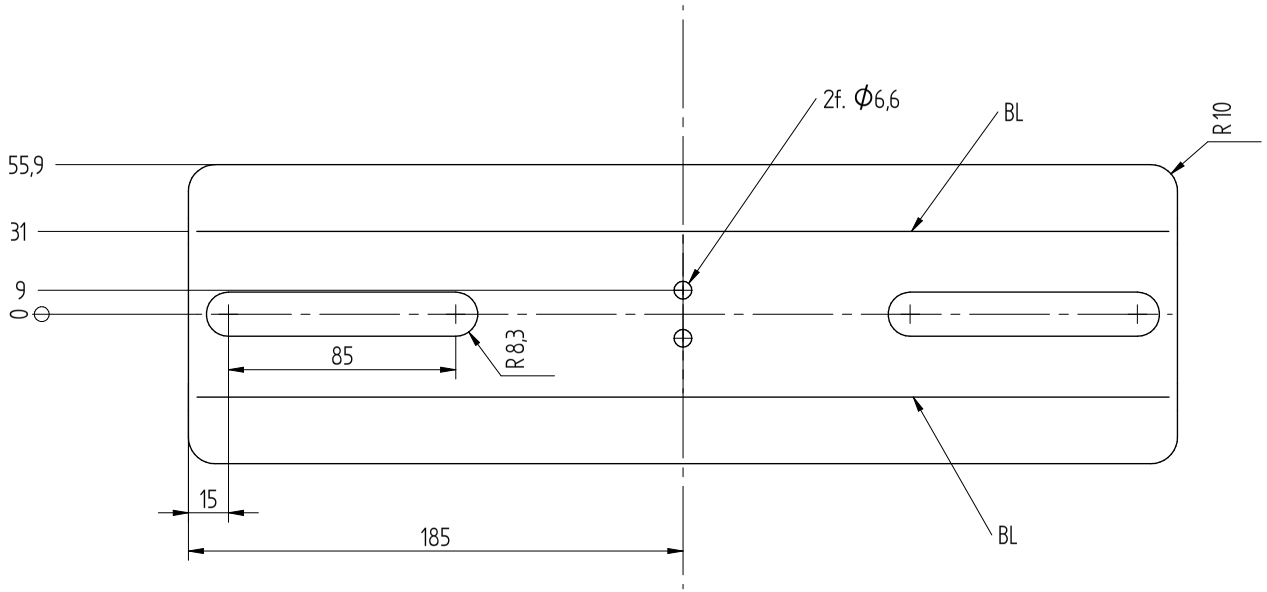
Este documento contem informação propriedade da ADIRA Metal Forming Solutions SA que não pode ser reproduzida, divulgada ou utilizada para fins de fabricação sem a autorização escrita da ADIRA Metal Forming Solutions SA. *This document contains proprietary information of ADIRA Metal Forming Solutions SA that cannot be reproduced, disclosed to others or used for manufacturing purposes without written permission from ADIRA Metal Forming Solutions SA.*

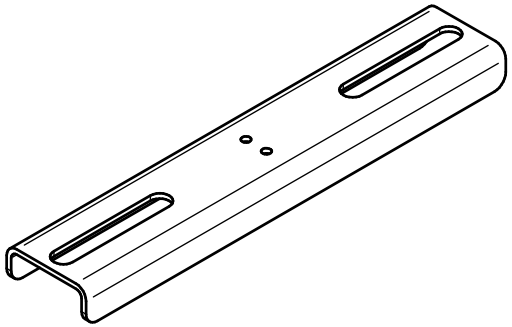
ISO - E

ADIRA / CAD - 2003
Solid Edge









PLANIFICAÇÃO:
RAIO DE QUINAGEM/Bend Radius 5,00 mm
ESPESSURA/Thickness 5,00 mm

Notas:
Algumas cotas de corte ou maquinagem podem estar omitidas propositadamente.
Geometria definida no ficheiro com formato DXF e/ou STEP e com revisão equivalente.

Tolerancimento ISO 8015 | ISO 2768-mK-E			ESCALA: 1:2
S235JR	MASSA *Mass* 1,2 kg Zinc finish 5µm		CORTE Ra 25
MATERIAL *MATERIAL*	TRAT. TERM. / DUREZA *HEAT TREATMENT / HARDNESS*	COR *COLOUR*	ACABAMENTO *SURFACE FINISH*

	DATA *DATE*	RÚBRICA *SIGN*
PROJECTOU *DESIGNED BY*	16/04/2024	Gonçalo Martins
DESENHOU *DRAWN BY*	29/05/2024	Gonçalo Martins
APROVOU *APPROVED BY*	16/04/2024	Gonçalo Martins

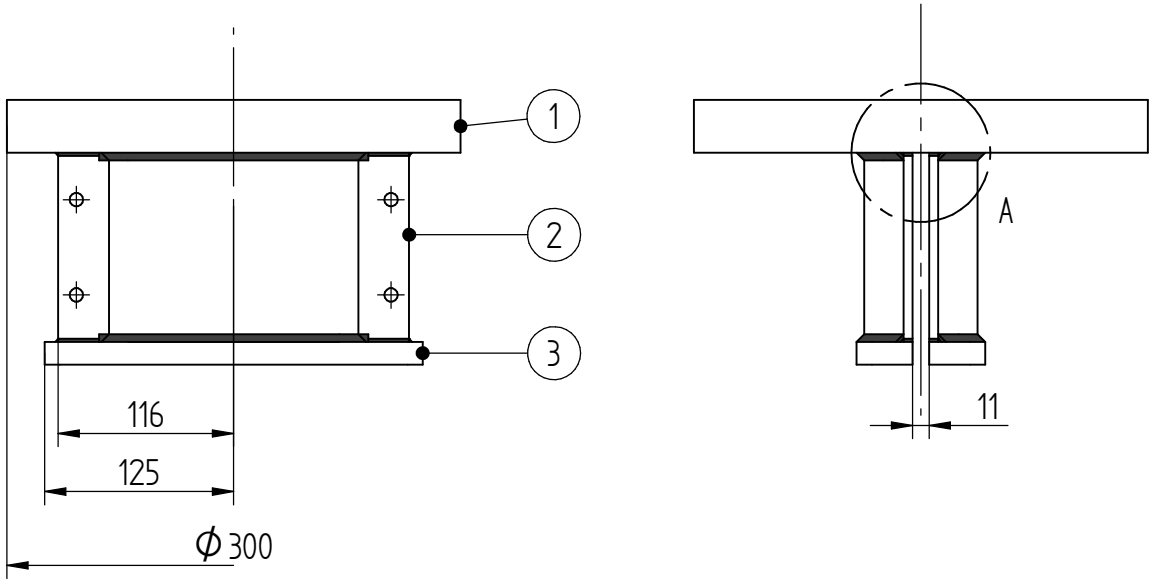
DES. Nº *DWG NR*: Chapa_ventosa_2

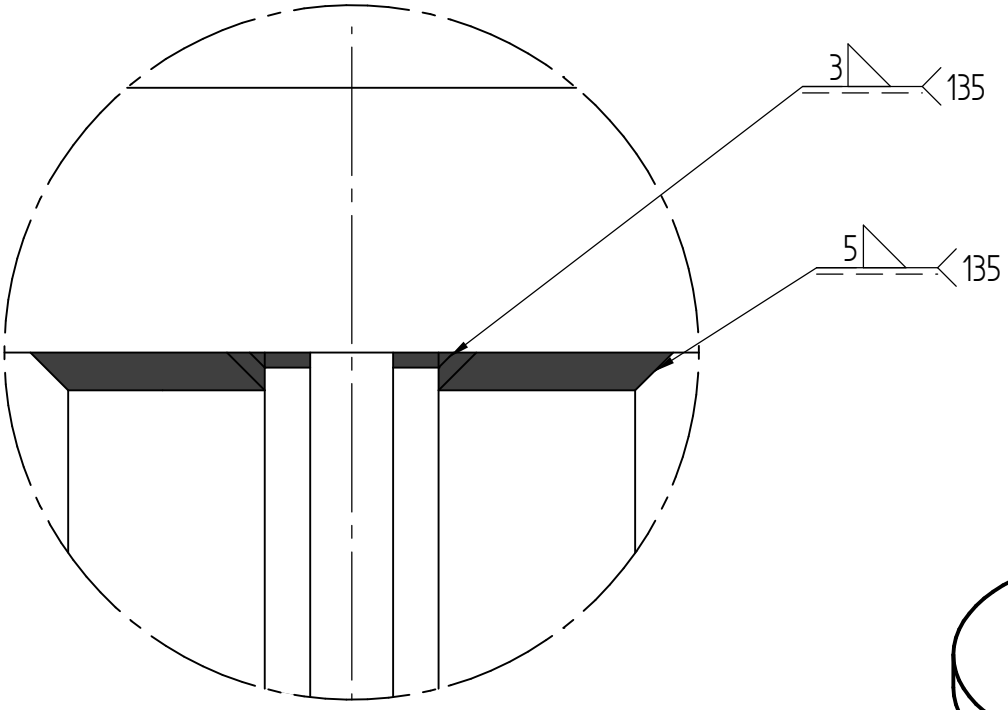
adira

Perfil_C_2 Profile_C_2	Nº ARTIGO *ITEM NR.*	VERSÃO *REVISION* A
	SIMILAR A *SIMILAR TO*	FOLHAS *SHEET* 1/1

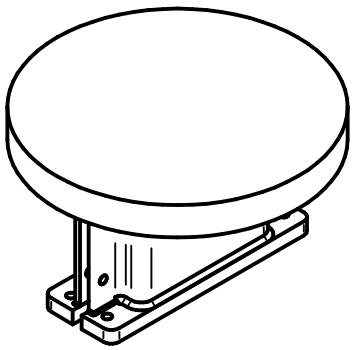
Este documento contem informação propriedade da ADIRA Metal Forming Solutions SA que não pode ser reproduzida, divulgada ou utilizada para fins de fabricação sem a autorização escrita da ADIRA Metal Forming Solutions SA. *This document contains proprietary information of ADIRA Metal Forming Solutions SA that cannot be reproduced, disclosed to others or used for manufacturing purposes without written permission from ADIRA Metal Forming Solutions SA.*

ISO - E





A
(1:1)



Quantity	Title	Item Number	Comments
1	Interface Solid Disc	1	Ramada F10 Steel 300
2	Interface_estrutura_U	2	
2	Interface_gripper	3	

Tolerancimento ISO 8015 I ISO 2768-mK-E			ESCALA: 1:5
	MASSA: *Mass:* 24,7 kg		
	Natural		
MATERIAL *MATERIAL*	TRAT. TERM. / DUREZA *HEAT TREATMENT / HARDNESS*	COR *COLOUR*	ACABAMENTO *SURFACE FINISH*

	DATA *DATE*	RÚBRICA *SIGN.*
PROJECTOU *DESIGNED BY*	03/06/2024	Gonçalo Martins
DESENHOU *DRAWN BY*	03/06/2024	Gonçalo Martins
APROVOU *APROVED BY*	03/06/2024	Gonçalo Martins

DES. Nº *DWG NR*
Subsassembly interfaces Soldadura/Welding

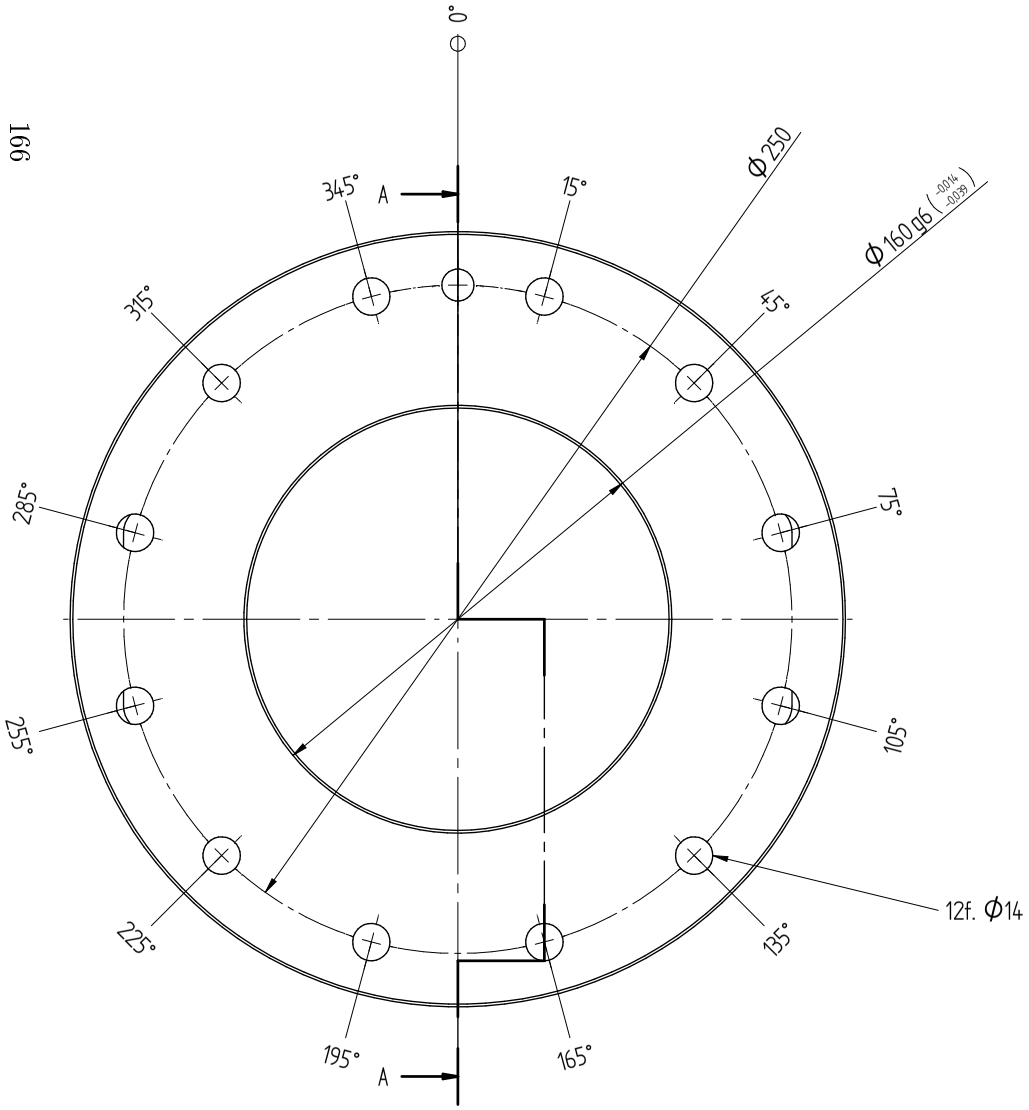
adira
165

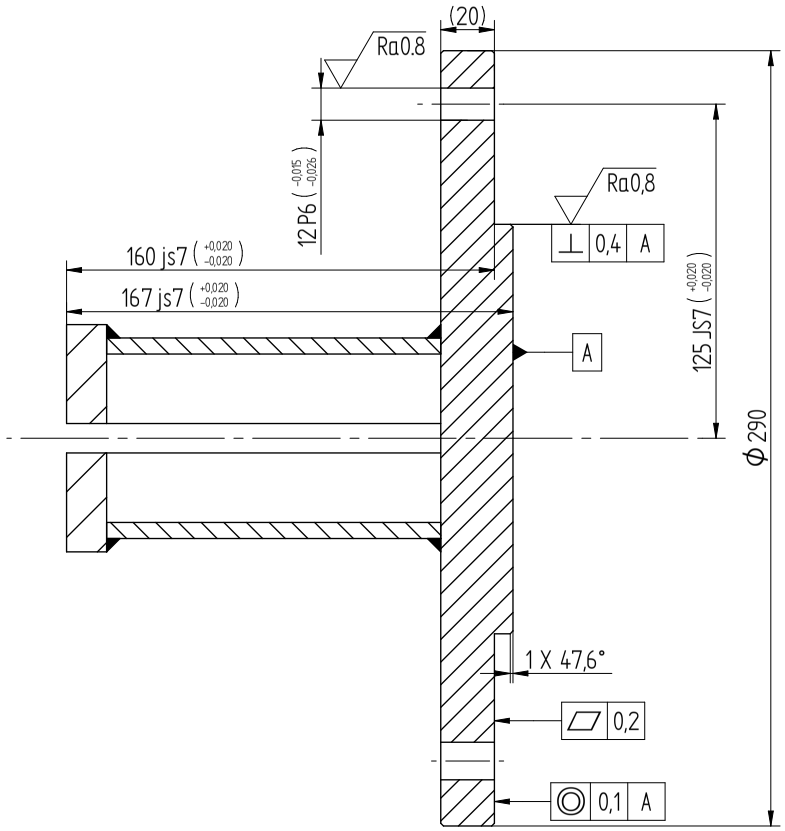
Interfaces subassembly Subassembly interfaces	Nº ARTIGO *ITEM NR.*	VERSÃO *REVISION* A
	SIMILAR A *SIMILAR TO*	FOLHAS *SHEET* 1/1

Este documento contem informação propriedade da ADIRA Metal Forming Solutions SA que não pode ser reproduzida, divulgada ou utilizada para fins de fabricação sem a autorização escrita da ADIRA Metal Forming Solutions SA. *This document contains proprietary information of ADIRA Metal Forming Solutions SA that cannot not be reproduced, disclosed to others or used for manufacturing purposes without written permission from ADIRA Metal Forming Solutions SA.*

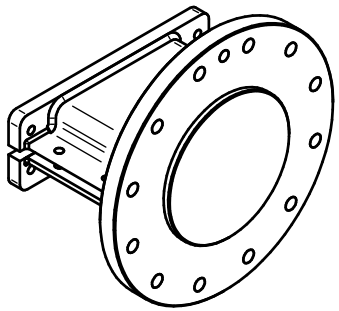
ISO - E

ADIRA / CAD - 2003
Solid Edge





A–A

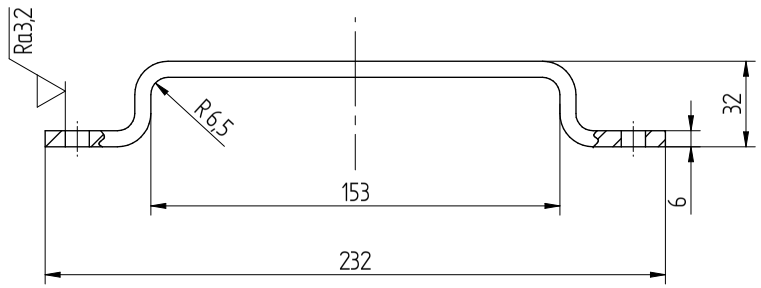


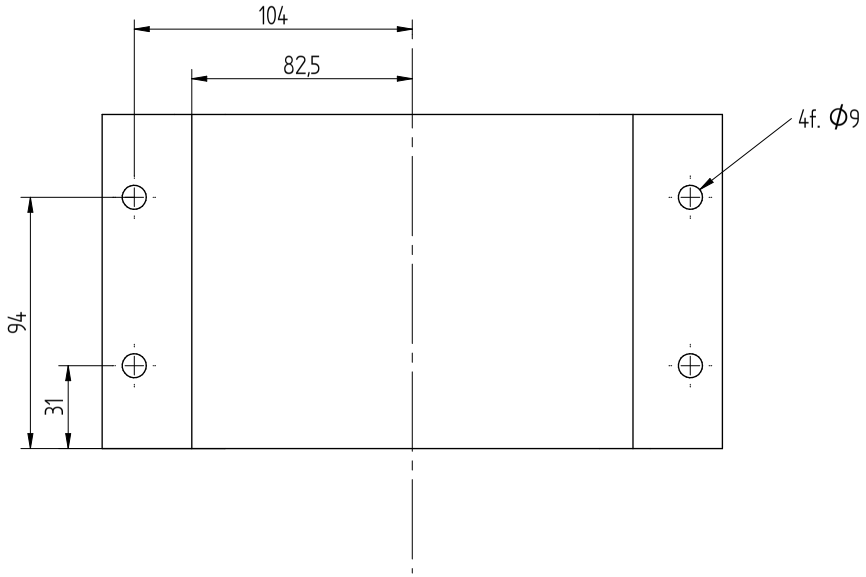
Toleranciamento ISO 8015 | ISO 2768-mK-E				ESCALA: 1:2
			MASSA *Mass* 43,6 kg Zinc finish 10µm	Ra1,6 (Ra 0,8)
MATERIAL *MATERIAL*			TRAT. TERM. / DUREZA *HEAT TREATMENT / HARDNESS*	COR *COLOUR* / ACABAMENTO *SURFACE FINISH*
	DATA *DATE*	RÚBRICA *SIGN*	DES. Nº *DWG NR*	
PROJECTOU *DESIGNED BY*	17/04/2024	Gonçalo Martins	Interfaces subassembly Maquinagem/Machining	adira
DESENHOU *DRAWN BY*	13/06/2024	Gonçalo Martins		
APROVOU *APPROVED BY*	17/04/2024	Gonçalo Martins		
Interfaces subassembly Subassembly interfaces			Nº ARTIGO *ITEM NR.*	VERSÃO *REVISION* A
			SIMILAR A *SIMILAR TO*	FOLHAS *SHEET* 1/1

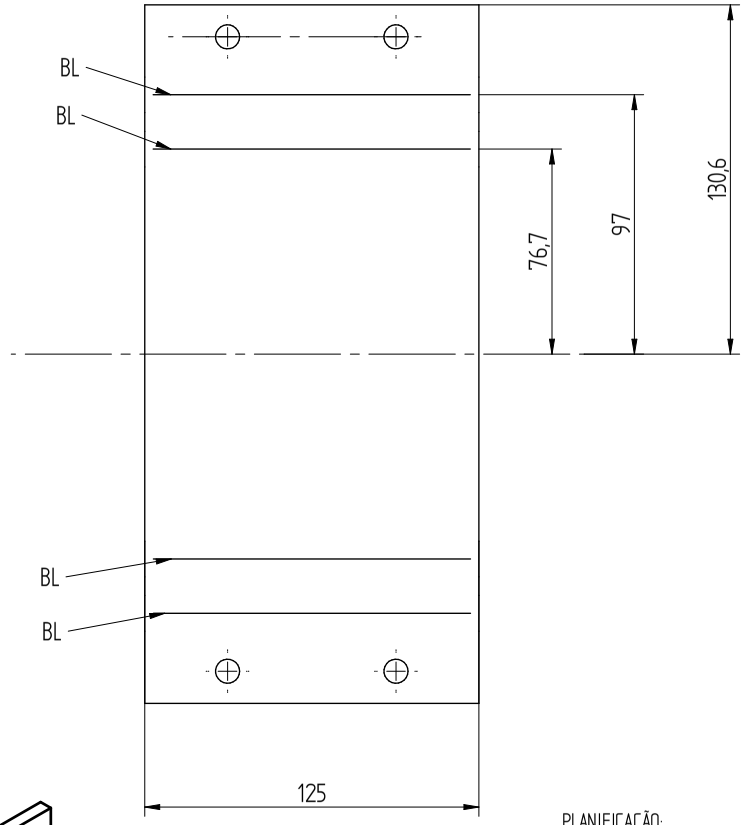
Este documento contem informação propriedade da ADIRA Metal Forming Solutions SA que não pode ser reproduzida, divulgada ou utilizada para fins de fabricação sem a autorização escrita da ADIRA Metal Forming Solutions SA. *This document contains proprietary information of ADIRA Metal Forming Solutions SA that cannot be reproduced, disclosed to others or used for manufacturing purposes without written permission from ADIRA Metal Forming Solutions SA.*

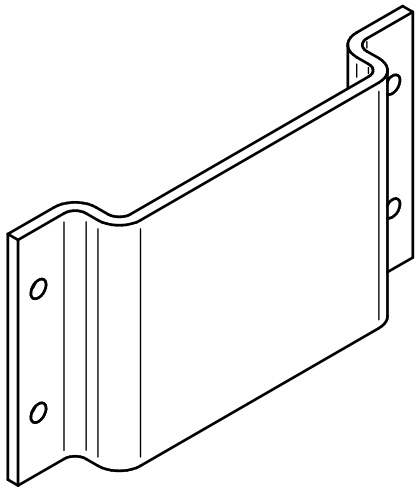
ISO - E

ADIRA / CAD - 2003
Solid Edge









PLANIFICAÇÃO:
RAIO DE QUINAGEM/Bend Radius 6,50 mm
ESPESSURA/Thickness 6,00 mm

Notas:
Algumas cotas de corte ou maquinagem podem estar omitidas propositadamente.
Geometria definida no ficheiro com formato DXF e/ou STEP e com revisão equivalente.

Toleranciamento ISO 8015 | ISO 2768-mK-E			ESCALA: 1:2
S235JR	MASSA / Mass 1,6 kg		CORTE Ra 25 (Ra 3,2)
MATERIAL / MATERIAL	TRAT. TERM. / DUREZA / HEAT TREATMENT / HARDNESS	COR / COLOUR	ACABAMENTO / SURFACE FINISH
	Natural		

	DATA / DATE	RÚBRICA / SIGN
PROJECTOU / DESIGNED BY	17/04/2024	Gonçalo Martins
DESENHOU / DRAWN BY	29/05/2024	Gonçalo Martins
APROVOU / APPROVED BY	17/04/2024	Gonçalo Martins

DES. Nº / DWG NR: Interface_Estrutura_U

Interface_estrutura_U
U_profile_interfaces

Nº ARTIGO / ITEM NR.

VERSÃO / REVISION: A

SIMILAR A / SIMILAR TO

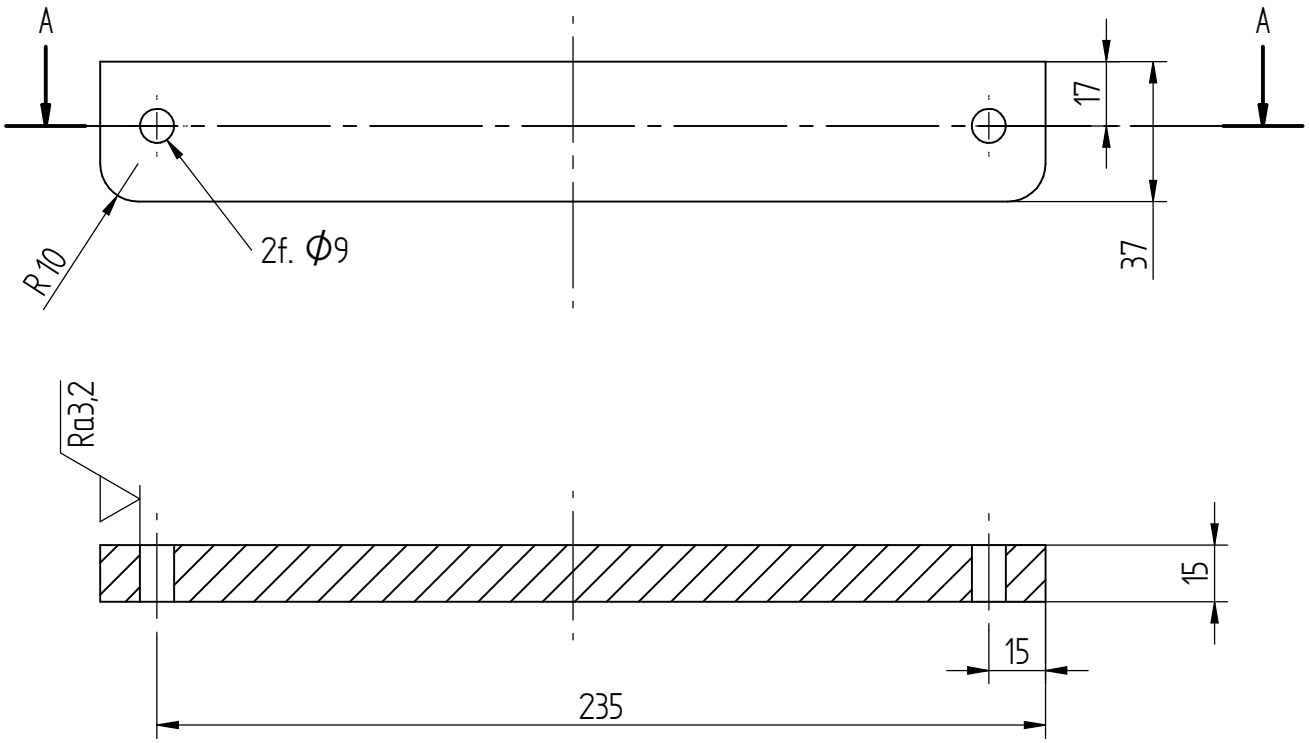
FOLHAS / SHEET: 1/1

Este documento contem informação propriedade da ADIRA Metal Forming Solutions SA que não pode ser reproduzida, divulgada ou utilizada para fins de fabricação sem a autorização escrita da ADIRA Metal Forming Solutions SA. This document contains proprietary information of ADIRA Metal Forming Solutions SA that cannot be reproduced, disclosed to others or used for manufacturing purposes without written permission from ADIRA Metal Forming Solutions SA.

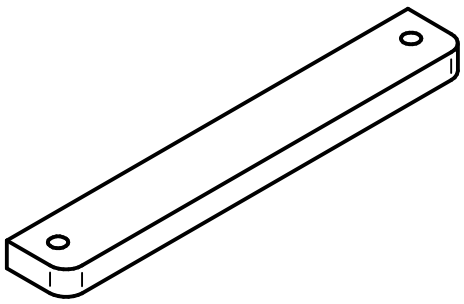
167

ISO - E

ADIRA / CAD - 2003
Solid Edge



A-A



Notas:

Algumas cotas de corte ou maquinagem podem estar omitidas propositadamente.

Geometria definida no ficheiro com formato DXF e/ou STEP e com revisão equivalente.

Tolerancimento ISO 8015 | ISO 2768-mK-E			ESCALA: 1:2
S235JR	MASSA: *Mass:* 1,1 kg		CORTE Ra 25 (Ra 3,2)
	Natural		
MATERIAL *MATERIAL*	TRAT. TERM. / DUREZA *HEAT TREATMENT / HARDNESS*	COR *COLOUR*	ACABAMENTO *SURFACE FINISH*

	DATA *DATE*	RÚBRICA *SIGN.*
PROJECTOU *DESIGNED BY*	17/04/2024	Gonçalo Martins
DESENHOU *DRAWN BY*	29/05/2024	Gonçalo Martins
APROVOU *APROVED BY*	17/04/2024	Gonçalo Martins

DES. Nº *DWG NR*: Interface_Gripper

Interface_gripper
Gripper_interface

Nº ARTIGO *ITEM NR.*	VERSÃO *REVISION* A
SIMILAR A *SIMILAR TO*	FOLHAS *SHEET* 1/2

Este documento contem informação propriedade da ADIRA Metal Forming Solutions SA que não pode ser reproduzida, divulgada ou utilizada para fins de fabricação sem a autorização escrita da ADIRA Metal Forming Solutions SA. *This document contains proprietary information of ADIRA Metal Forming Solutions SA that cannot not be reproduced, disclosed to others or used for manufacturing purposes without written permission from ADIRA Metal Forming Solutions SA.*

ISO - E

168